COCRYSTALLIZATION TO IMPROVE THE DISSOLUTION AND PHARMACOKINETICS OF A POORLY SOLUBLE DRUG

BY

C2010
Mary Stanton

Submitted to the graduate degree program in
Pharmaceutical Chemistry and the Graduate Faculty
of the University of Kansas in partial fulfillment of the
requirements for the degree of Master's of Science

Chairperson _____
Eric J. Munson

Committee Members* _____ *
Ron C. Kelly

_____ *
Valentino J. Stella

_____ *
John F. Stobaugh

Date defended: _____

The Thesis Committee for Mary Stanton certifies

that this is the approved version of the following thesis:

COCRYSTALLIZATION TO IMPROVE THE DISSOLUTION AND PHARMACOKINETICS OF A POORLY SOLUBLE DRUG

Chairperson: _____

Eric J. Munson

_____

Date

:

Acknowledgments

I would first and foremost like to thank Dr. Ron C. Kelly for his enthusiastic support and guidance throughout this research as my advisor in the Pharmaceutics Department at Amgen Inc. I am also appreciative of the learning, feedback and advice from the University of Kansas Pharmaceutical Chemistry Department faculty, especially my advisor, Dr. Eric Munson. The cooperation and support received throughout Amgen is greatly apprecitaed including but not limited to Dr. Mary Wells for her detailed teaching of bioanalytical methods and Dr. Adria Colletti, John Roberts and Meghan Langley for patient teachings and performing *in vivo* pharmacokinetic investigations and to management, especially my supervisors Dr. Annette Bak and Dr. Matthew Peterson for encouraging and supporting my involvement in the Distance Masters Program. Lastly, I must thank my loving, supportive and patient family and friends; your words of encouragement moved mountains.

Table of Contents

Chapter 1. Introduction

Form Selection in Small Molecule Drug Development

Small molecule drug development relies on the ability to achieve efficacious exposure levels of the drug with a desired dosage form. Many active pharmaceutical ingredients (APIs) have poor solubility in an aqueous environment rendering them susceptible to solubility limited absorption. Pharmaceutical strategies for overcoming absorption limited by solubility have been restricted to salt formation or formulation techniques such as amorphous dispersions and nanosizing or a combination thereof.[1] In recent years cocrystallization of an API with a cocrystal former has been shown to be a complimentary pharmaceutical strategy to change the physical properties of the API including dissolution rate and solubility.[2,3]

Form selection of an API in discovery research classically requires the comparison of two or more forms (i.e. polymorphs, salts, solvates) of the API *in vivo* to illustrate acceptable preclinical pharmacokinetics for further development of the drug.[4-6] At the outset, physical property filters such as stability, hygroscopicity and crystallinity of the forms are used to narrow down the field. Predictive methods such as solubility and dissolution are also incorporated into the form selection decision tree to eliminate forms that are likely to perform poorly *in vivo*.[7-9] The directly proportional relationship of dissolution rate to exposure of a poorly soluble API and its different salts, polymorphs or formulations has been well established and therefore remains engrained in the form selection process.[10-14] Crystal surface properties and crystal morphology either measured or calculated may also be used to predict or confirm the results.[15,16]

Pharmaceutical cocrystals are molecular complexes of an API and one or more cocrystal formers, which are solids at room temperature, interacting through hydrogen bonding, π-stacking or van der Waals forces.[17] Under this definition pure salts, solvates and hydrates are excluded although have been shown to co-exist within the same complex.[18] In recent years interest in cocrystallization has gained momentum as noted by the increased frequency of occurrence of organic molecular complexes in the Cambridge Structural Database[19]. A cursory search of the literature in 2009 alone found reports of novel cocrystals of APIs[20-22], cocrystal screening methods[23,24], cocrystal phase diagrams[25,26], prediction of cocrystal formation[27] and physicochemical properties of corystals[3,28]. Inclusion of cocrystals in the form selection process of an API is destined to become, if it has not already, common practice in pharmaceutical reasearch, not only due to the possibility of improving physical properties of an API, but also to protect its intellectual property[29].

Introduction to AMG 517

AMG 517, a potent and selective transient receptor potential vanilliod 1 (TRPV1) antagonist for the treatment of chronic pain, is an anhydrous free base form A (**FBA**) with poor aqueous solubility which is not amenable to stable salt formation due to its low pKa of -0.52 (ACD/pKa DB v12.0, Advanced Chemistry Development, Inc). A second anhydrous form, form B (**FBB**), and a monohydrate (**FBC**) also have poor solubility in aqueous media which rendered them undesirable for development.[30] This API has many known cocrystal forms, 22 of which have been published with powder dissolution data in FaSIF. Almost all of the cocrystals (15/22) have shown improvements over the free form

based on solution concentration maximum during the dissolution experiments.[31,32] One of these cocrystals, the sorbic acid cocrystal (**SRA**), has also shown improvement in the exposure of AMG 517 where a 30 mg/kg dose of the cocrystal was comparable to a 500 mg/kg dose of **FBA** in rats when dosed as a suspension in 10% Pluronic® F108 in OraPlus®.[30]

Further research was conducted here with sixteen cocrystals of AMG 517 to investigate correlations in dissolution with pharmacokinetics of cocrystal forms of a poorly soluble API. The main intention of the research is to show that cocrystals with a higher dissolution rate than the free form will also provide higher exposure in rat pharmacokinetic studies. This would allow the pharmaceutical scientist to use dissolution rate as a filter for selecting not only salts or polymorphs of an API, but also cocrystal forms for further study *in vivo*. The relatively large selection was chosen to include **SRA** as a positive control, two pairs of cocrystals (carboxylic acid with corresponding amide) and eleven other carboxylic acid cocrystals elected to represent a range of dissolution rates. With an additional hydrogen bond donor in comparison to the acids the amides are likely to form a unique hydrogen bonding network resulting in changes to the crystal packing and in turn the physicochemical properties of the compound. The crystal structures of one pair of these cocrystals are analyzed in comparison with **FBA** to elucidate the possible factors responsible for changes in dissolution. Single crystal structure analysis may be another useful filter in selecting API forms for further study.

References

1. Meanwell NA. 2008. The emerging utility of co-crystals in drug discovery and development. In Macor JE, editor Annu Rep Med Chem, ed.: Elsevier Inc. p 373-404.
2. Vishweshwar P, McMahon JA, Bis JA, Zaworotko MJ 2006. Pharmaceutical co-crystals. J Pharm Sci 95(3):499-516.
3. Schultheiss N, Newman A 2009. Pharmaceutical cocrystals and their physicochemical properties. Cryst Growth Des 9(6):2950-2967.
4. Engel GL, Farid NA, Faul MM, Richardson LA, Winneroski LL 2000. Salt form selection and characterization of LY333531 mesylate monohydrate. Int J Pharm 198:239-247.
5. Hirsch CA, Messenger RJ, Brannon JL 1978. Fenoprofen: drug form selection and preformulation stability studies. J Pharm Sci 67(2):231-236.
6. Bowker MJ. 2002. A procedure for salt selection and optimization. In Stahl HP, Wermuth CG, editors. Handbook of Pharmaceutical Salts Properties, Selection, and Use, ed., Zürich: Verlag Helvetica Chimica Acta. p 161-189.
7. Saxena V, Panicucci R, Joshi Y, Garad S 2009. Developability assessment in pharmaceutical industry: an integrated group approach for selecting developable candidates. J Pharm Sci 98(6):1962-1979.
8. Morris KR, Fakes MG, Thakur AB, Newman AW, Singh AK, Venit JJ, Spagnuolo CJ, Serajuddin ATM 1994. An integrated approach to the selection of optimal salt form for a new drug candidate. Int J Pharm 105:209-217.
9. Serajuddin ATM, Pudipeddi M. 2002. Salt selection strategies. In Stahl HP, Wermuth CG, editors. Handbook of Pharmaceutical Salts Properties, Selection, and Use, ed., Zürich: Verlag Helvetica Chimica Acta. p 135-160.
10. Guzmán HR, Tawa M, Zhang Z, Ratanabanangkoon P, Shaw P, Gardner CR, Chen H, Moreau J-P, Almarsson Ö, Remenar JF 2007. Combined use of crystalline salt forms and precipitation inhibitors to improve oral absorption of celecoxib from solid oral formulations. J Pharm Sci 96(10):2686-2700.
11. Sandburg A, Abrahamsson B, Sjögren J 1991. Influence of dissolution rate on the extent and rate of bioavailability of metoprolol. Int J Pharm 68:167-177.
12. Meyer MC, Straughn AB, Mhatre RM, Shah VP, Williams RL, Lesko LJ 1998. The relative bioavailability and *in vivo-in vitro* correlations for four marketed carbamazepine tablets. Pharm Res 15(11):1787-1791.
13. Dressman JB, Amidon GL, Reppas C, Shah VP 1998. Dissolution testing as a prognostic tool for oral drug absorption: immediate release dosage forms. Pharm Res 15(1):11-22.
14. Hörter D, Dressman JB 2001. Influence of physicochemical properties on dissolution of drugs in the gastrointestinal tract. Adv Drug Delivery Rev 46:75-87.
15. Kiang Y-H, Shi HG, Mathre DJ, Xu W, Zhang D, Panmai S 2004. Crystal structure and surface properties of an investigational drug-a case study. Int J Pharm 280:17-26.

16. Muster TH, Prestidge CA 2002. Face specific surface properties of pharmaceutical crystals. J Pharm Sci 91(6):1432-1444.
17. Peterson ML, Hickey MB, Zaworotko MJ, Almarsson Ö 2006. Expanding the scope of crystal form evaluation in pharmaceutical science. J Pharm Pharmaceut Sci 9(3):317-326.
18. Chen AM, Ellison ME, Peresypkin A, Wenslow RM, Variankaval N, Savarin CG, Natishan TK, Mathre DJ, Dormer PG, Euler DH, Ball RG, Ye Z, Wanga Y, Santos I 2007. Development of a pharmaceutical cocrystal of a monophosphate salt with phosphoric acid. Chem Commun:419-421.
19. Childs SL, Zaworotko MJ 2009. The reemergence of cocrystals: The crystal clear writing is on the wall. Introduction to virtual special issue on phramaceutical cocrystals. Cryst Growth Des 9:4208-4211.
20. Aitipamula S, Chow PS, Tan RBH 2009. Trimorphs of a pharmaceutical cocrystal involving two active pharmaceutical ingredients: potential relevance to combination drugs. Cryst Eng Comm 11(9):1823-1827.
21. Lu J, Rohani S 2009. Preparation and characterization of theophylline-nicotnamide cocrystal. Org Process Res Dev 13(6):1269-1275.
22. Bhatt PM, Azim Y, Thakur TS, Desiraju GR 2009. Co-crystals of the anti-HIV drugs lamivudine and zidovudine. Cryst Growth Des 9(2):951-957.
23. Noriyuki T 2009. Cocrystal screening and its application in improvement of physicochemical properties of APIs. Pharm Tech Japan 25(12):2543-2554.
24. Li Z, Yang B-S, Jiang M, Eriksson M, Spinelli E, Yee N, Sensnayake C 2009. A practical solid form screen approach to identify a pharmaceutical glutaric acid cocrystal for development. Org Process Res Dev 13(6):1307-1314.
25. Gagniere e, Mangin D, Puel F, Bebon C, Klein J-P, Monnier O, Garcia E 2009. Cocrystal formation in solution: In situ solute concentration monitoring of the two components and kinetic pathways. Cryst Growth Des 9(8):3376-3383.
26. Ainouz A, Authelin J-R, Billot P, Lieberman H 2009. Modeling and prediction of cocrystal phase diagrams. Int J Pharm 374(1-2):82-89.
27. He G, Chow PS, Tan RBH 2009. Predicting multicomponent crystal formation: The interplay between homomeric and heteromeric interactions. Cryst Growth Des 9(10):4529-4532.
28. Cassidy AMC, Gardner CE, Jones W 2009. Following the surface response of caffeine cocrystals to controlled humidity storage by atomic force microscopy. Int J Pharm 379(1):59-66.
29. Trask AV 2007. An overview of pharmaceutical cocrystals as intellectual property. Mol Pharm 4(3):301-309.
30. Bak A, Gore A, Yanez E, Stanton M, Tufekcic S, Syed R, Akrami A, Rose M, Surapaneni S, Bostick T, King A, Neervannan S, Ostovic D, Koparkar A 2008. The co-crystal approach to improve the exposure of a water-insoluble compound: AMG 517 sorbic acid co-crystal characterization and pharmacokinetics. J Pharm Sci 97(9):3942-3956.
31. Stanton MK, Bak A 2008. Physicochemical properties of pharmaceutical co-crystals: A case study of ten AMG 517 co-crystals. Cryst Growth Des 8(10):3856-3862.

32. Stanton MK, Tufekcic S, Morgan C, Bak A 2009. Drug substance and former structure property relationships in 15 diverse pharmaceutical co-crystals. Cryst Growth Des 9(3):1344-1352.

Chapter 2. Cocrystal Background

History of Cocrystals

Cocrystals have been discussed in the literature since 1844 when Wöhler first described quinhydrone (molecular complex of quinone and hydroquinone) and Ling further investigated halogen derivatives of quinhydrone in 1893.[1] Cocrystals of antipyrine, an analgesic, were described in *Modern Materia Medica* published in 1895.[2,3] Some of these antipyrine cocrystals among many other cocrystals were published in Pfeifer's book *Organische Molekulver-bindungen* (Organic Molecular Compounds) in 1922.[3,4] Around that time Kofler began publishing extensively on forming cocrystals through thermal microscopy techniques.[3] Then, in the 1940's McIntosh et al described a sulfathiazole and 3,6-diaminacridine complex which was used as an antibacterial and theophylline complexes with glycine or phenobarbital were described by Higgins and Krantz respectively.[5-8] Extensive reviews on these cocrystals and many others have been published in the last few years by Zaworotko et al[9], Schultheiss and Newman[10], Meanwell[7] and Stahly.[3]

Terminology used to describe cocrystals has been diverse including phrases such as "molecular complexes", "addition compounds" or "solid-state complexes" to name a few.[9] The definition of cocrystals given in Chapter 1 is one of many proposed in the literature which requires the components of the crystal to be solids at ambient temperatures. Other definitions are more encompassing such as the one proposed by Stahly "unique crystalline solids containing multiple components" where a component is described as "an atom, ionic compound or molecule".[3,11] This definition would also

incorporate hydrates, clathrates and solvates under the same umbrella. As noted by Stahly, the term used to define a solid selected for development of an API is of little concern as long as the components are pharmaceutically acceptable from a safety standpoint,[11] however the classification may prove to be valuable to protect the intellectual property of the API forms and simply removing the ambiguity that exists today.

Utility of Cocrystals

The recent popularity of cocrystals in the literature is centered on pharmaceutical cocrystals, but there are many other areas where cocrystals (in the broader sense) have been identified which were covered in detail in the 2009 perspective by Staley[3] including the adenine:thymine and guanine:cytosine base pairs in DNA, nucleotides and aminocarboxylic acids cocrystallized in sun screens, hair dyes containing polyhydric phenols and aromatic diamines and urea: sugar cocrystals for finishing of fabric in the textile industry. Purification with cocrystals was also described by Stahly[3] where chiral or enantiomeric selectivity of the cocrystal was exploited.

The spotlight in current years has been on pharmaceutical cocrystals and the ability to address many familiar tribulations encountered in drug development such as polymorph control, stability, crystallinity, dissolution rate, solubility and bioavailability. Two examples of polymorph control in the literature are cocrystals of the pharmaceuticals caffeine and piracetam. Selective crystallization of two polymorphs of a caffeine and glutaric acid cocrystal were conducted through grinding techniques.[12] Grinding of caffeine and glutaric acid in a grinding jar with four drops of a non-polar solvent or no solvent resulted primarily in cocrystal form I. When polar solvents were

added in place of the non-polar solvents cocrystal form II was the prevalent form. In a similar study the polymorphic drug piracetam was cocrystallized with two polymorphic cocrystal formers, gentisic acid or p-hydroxybenzoic acid by slow evaporation from acetonitrile.[13] These cocrystals were then produced via solvent drop grinding with 23 different solvents or by slurry in water. Neither piracetam cocrystal exhibited polymorphism in these studies.

Theophylline and caffeine are two structurally similar pharmaceutical compounds which are susceptible to conversion between anhydrate and hydrate as a function of relative humidity (RH). Investigations were conducted by Trask, Motherwell and Jones to form cocrystals of these compounds with the intent of stabilizing the drugs to humidity changes.[14,15] In both cases multiple anhydrous cocrystals were formed and one (oxalic acid cocrystal in both cases) was found to be stable from 0-98% RH throughout the time frame tested of 7 weeks.

Co-crystalization of an API with a cocrystal former has been demonstrated to be a successful method for altering the dissolution rate of an API as covered in recent reviews.[7,9,10] Improvements to the dissolution of the API of interest were found for the drugs indomethacin, fluoxetine and itraconazole. The indomethacin cocrystal with saccharin was found to dissolve instantaneously in 60 or 200 mM phosphate buffer at pH 7.4 reaching solution concentrations of ~3.0-3.7 mg/mL as compared to the γ-form of indomethacin which required 250 min to reach a lower maximum solution concentration of 0.72 – 1.3 mg/mL in the two buffers respectively.[16] Fluoxetine hydrochloride cocrystallized with benzoic acid, succinic acid or fumaric acid presented variable behavior in intrinsic dissolution studies where two of the cocrystals dissolved more

slowly than the API alone while the third cocrystal (succinic acid) displayed a faster dissolution rate than the API in water.[17] Itraconazole, an insoluble antifungal drug, is marketed as in the amorphous form to attain oral bioavailability. Three cocrystals of itraconazole were compared to crystalline and amorphous forms of the free API in a dissolution study in 0.1N HCl.[18] All three cocrystals were superior to the crystalline itraconazole and the malic acid cocrystal was found to behave similarly to the marketed form.

Few examples exist in the literature where dissolution of the cocrystal is correlated with exposure. Theophylline tablets from different manufacturers were suspected to perform differently in the clinic partially due to complexation of the theophylline with phenobarbital during tablet processing.[19] Dissolution studies of theophylline and the theophylline-phenobarbital complex were conducted in water, 0.02% polysorbate 80 and simulated gastric fluid. In all media the complex slowed the dissolution of theophylline. This correlated well to the pharmacokinetics in humans where seven of nine subjects produced high serum levels of theophylline quicker when dosed with theophylline alone than when dosed with the complex. One subject was also dosed with a physical mixture of theophylline and phenobarbital which performed similarly to theophylline alone indicating that any pharmacodynamic properties of phenobarbital were not responsible for the decrease.[19] A sodium channel blocker with low solubility when co-crystallized with glutaric acid was shown to have an intrinsic dissolution rate in water 18 times that of the free base. When dosed as neat solids in a gelatin capsule at 5 and 50 mg/kg to dogs a 3 fold improvement of AUC was achieved at both dose levels with the cocrystal.[20] The poorly soluble anti-epileptic agent

carbamazepine co-crystallized with saccharin was shown to be a feasible option, in terms of exposure in dogs, to the marketed Tegretol® tablets which contain an anhydrous polymorph of carbamazepine.[21] The cocrystal, dosed as a blend with lactose in an HPMC capsule at 200 mg (carbamazepine equivalents), maintained consistently higher exposure levels than the Tegretol® tablet however the pharmacokinetic parameters were not found to be statistically different. In a separate study L-883555, a phosphodiesterase IV inhibitor with poor bioavailability, was cocrystallized with L-tartaric acid. The cocrystal improved the aqueous solubility of the free base from 7.5 to 23.7 μg/mL which corresponded to improved plasma concentrations from a 3 mg/kg dose in rhesus monkey achieving an AUC (μg/mL*h) 0.24 for the free base and 5.5 for the cocrystal.[22] In a recent investigation into the dissolution and bioavailability of lamotrigine crystal forms a 10 mg/kg dose in rats formulated as a suspension in 5% polyethylene glycol 400 and 95% methyl cellulose aqueous solution resulted in lower exposures for two lamotrigine nicotinamide cocrystals (anhydrous and monohydrate forms) compared to the pure drug ($AUC_{0\text{-}24h}$ 37, 26 and 60 μg/mL respectively).[23] The drug concentrations over time in water or at pH 1 do not appear to correlate with the AUC. In water the anhydrous cocrystal achieves a higher solubility than the pure drug while at pH 1 both cocrystals maintain a higher concentration than the pure drug.

Conclusions

Regardless of terminology or definition, cocrystals have been investigated since the 1840's for various functionalities across industries. The interest has been amplified over recent years in the pharmaceutical industry as more literature is produced

exemplifying the ability to overcome physical property liabilities in an API. Cocrystal screening will likely become (if it is not already) as inherent a pharmaceutical technique as salt screening in the search for developable forms of a novel API.

References

1. Ling AR, Baker JL 1893. Halogen derivatives of quinone. Part III. Derivatives of quinhydrone. J Chem Soc Trans 63(1314-1327).
2. Helbing H. 1895. Modern Materia Medica, 4th edition. ed., New York.
3. Stahly GP 2009. A survey of cocrystals reported prior to 2000. Cryst Growth Des 9(10):4212-4229.
4. Pfeiffer P. 1922. Organische Molekulverbindungen. ed., Stuttgart.
5. Higgins WM, Dunker MFW 1944. A study of the reaction of theophylline with barbiturates. J Am Pharm Assoc 33(9):310-314.
6. Mcintosh J, Robinson RHM, Selbie FR, Reidy JP, Blake HE, Guttmann L 1945. Acridine-sulphonamide compounds as wound antiseptics clinical trials of flavazole. Lancet 246(6361):97-99.
7. Meanwell NA. 2008. The emerging utility of co-crystals in drug discovery and development. In Macor JE, editor Annu Rep Med Chem, ed.: Elsevier Inc. p 373-404.
8. Krantz JC, Holbert JM, Iwamoto HK, Carr CJ 1946. Sodium theophylline glycinate. J Am Pharm Assoc 36(8):248-250.
9. Vishweshwar P, McMahon JA, Bis JA, Zaworotko MJ 2006. Pharmaceutical co-crystals. J Pharm Sci 95(3):499-516.
10. Schultheiss N, Newman A 2009. Pharmaceutical cocrystals and their physicochemical properties. Cryst Growth Des 9(6):2950-2967.
11. Stahly GP 2007. Diversity in single- and multiple-component crystals. The search for and prevalence of polymorphs and cocrsytals. Cryst Growth Des 7(6):1007-1026.
12. Trask AV, Motherwell WDS, Jones W 2004. Solvent-drop grinding: green polymorph control of cocrystatallisation. Chem Commun:890-891.
13. Vishweshwar P, McMahon JA, Peterson ML, Hickey MB, Shattock TR, Zaworotko MJ 2005. Crystal engineering of pharmaceutical co-crystals from polymorphic active pharmaceutical ingredients. Chem Commun:4601-4603.
14. Trask AV, Motherwell WDS, Jones W 2006. Physical staiblity enhancement of theophylline via cocrystallization. Int J Pharm 320:114-123.
15. Trask AV, Motherwell WDS, Jones W 2005. Pharmaceutical cocrystallization: Engineering a remedy for caffeine hydration. Cryst Growth Des 5(3):1013-1021.
16. Basavoju S, Bostrom D, Velaga SP 2008. Indomethacin-saccharin cocrystal: Design, synthesis and preliminary pharmaceutical characterization. Pharm Res 25(3):530-541.

17. Childs SL, Chyall LJ, Dunlap JT, Smolenskaya VN, Stahly BC, Stahly GP 2004. Crystal engineering approach to forming cocrystals of amine hydrochlorides with organic acids. Molecular complexes of fluoxetine hydrochloride with benzoic, succinic, and fumaric acids. J Am Chem Soc 126(41):13335-13342.
18. Remenar JF, Morissette SL, Peterson ML, Moulton B, MacPhee JM, Guzman HR, Almarsson O 2003. Crystal engineering of novel cocrystals of a triazole drug with 1,4-dicarboxylic acids. J Am Chem Soc 125(28):8456-8457.
19. Bettis JW, Lach JL, Hood J 1973. Effect of complexation with phenobarbital on the biologic availability of theophylline from three tablet formulations. Amer J Hosp Pharm 30:240-243.
20. McNamara DP, Childs SL, Giordano J, Iarriccio A, Cassidy J, Shet MS, Mannion R, O'Donnell E, Park A 2006. Use of a glutaric acid cocrystal to improve oral bioavailability of a low solubility API. Pharm Res 23(8):1888-1897.
21. Hickey MB, Peterson ML, Scoppettuolo LA, Morrisette SL, Vetter A, Guzmán HR, Remenar JF, Zhang Z, Tawa MD, Haley S, Zaworotko MJ, Almarsson Ö 2007. Performance comparison of a co-crystal of carbamazepine with marketed product. Eur J Pharm Biopharm 67:112-119.
22. Variankaval N, Wenslow R, Murry J, Hartman R, Helmy R, Kwong E, Clas S-D, Dalton C, Santos I 2006. Preparation and solid-state characterization of nonstoichiometric cocrystals of a phosphodiesterase-IV inhibitor and L-tartaric acid. Cryst Growth Des 6(3):690-700.
23. Cheney ML, Shan N, Healey ER, Hanna M, Wojtas L, Zaworotko MJ, Sava V, Song S, Sanchez-Ramos JR 2010. Effects of crystal form on solubility and pharmacokinetics: A crystal engineering case study of lamotrigine. Cryst Growth Des 10(1):394-405.

Chapter 3. Preparation and Characterization of AMG 517 Cocrystals

Introduction

Cocrystals have been produced through a variety of different methods including grinding of dry components alone or with a drop of solvent in a mortar and pestle or ballmill, crystallization from the melt of the components, moisture generated cocrystals as well as the more traditional crystallization techniques such as solution or slurry crystallizations.[1-7] All of these techniques have their benefits and drawbacks such as small material requirements for cocrystal screening, scalability of the process for manufacture of drug substance, polymorph control and "green" chemistry reducing solvent usage.[1,6] Although there are a variety of cocrystallization methods available to the pharmaceutical scientist all processes may not be successful at producing a particular cocrystal of interest, therefore it is useful when screening for new crystal forms to utilize multiple techniques.

Characterization of cocrystals has been similar to that of a salt or solvate of an active pharmaceutical ingredient (API). Initially, the crystal form was determined to be distinctive from that of the starting crystal form (and not simply a mixture of the two starting materials) by a variety of available methods such as X-ray powder diffraction (XRPD), thermal gravimetric analysis (TGA), differential scanning calorimetry (DSC) or Raman spectroscopy. Once the uniqueness of the crystal form was confirmed analytical methods such as nuclear magnetic resonance (NMR) or high pressure liquid chromatography coupled with ultraviolet (HPLC-UV) or mass spectroscopy (LC-MS) should be utilized to determine that the API and cocrystal former are both present in the new material and that neither has degraded into a new molecule. Distinguishing a

complex as a salt or a cocrystal has been defined by calculating differences in pKa values (ΔpKa) between the acid and base in the complex. In the case of a basic drug the pKa of the drug minus the pKa of the acid cocrystal former resulting in a $\Delta pKa < 0$ is said to result in a cocrystal and $\Delta pKa > 3$ in a salt.[8] The area between ΔpKa of 0 and 3 however requires a secondary technique to determine if proton transfer has occurred. Single crystal structure determination and solid state NMR are two techniques that have been used in this capacity.[9,10]

Single crystal structure analysis has been applied broadly within the pharmaceutical industry. Crystal structures of APIs are frequently determined in pharmaceutical research to confirm the molecular structure of a single molecule. Complexes, such as hydrates, solvates and salts or combinations thereof may also be confirmed by solving the single crystal structure. Determining the location of the guest molecule within the crystal lattice of a complex, i.e. in a channel or occupying a specific site within the crystal, and how they bind to the API can elucidate issues with physical and chemical stability and possibly provide insight on how to improve the form. When it comes to cocrystals, crystal engineering has utilized crystal structure analysis to identify common hydrogen bonding synthons that can be exploited to design new crystal forms of an API.[11-13] Single crystal structures have also been used to distinguishing between a salt and cocrystal. When carboxylic acids are involved, the distances of the C-O bonds in the carboxylic acid in the single crystal structure have been measured. A neutral carboxyl group will have two distinctively different distances ($\Delta D_{C-O} > 0.08$) where the carboxyl anion will have two similar distances ($\Delta D_{C-O} < 0.03$).[8]

Cocrystals of AMG 517 were prepared here through tradition solution or slurry crystallizations to produce the bulk powders. These powders were than characterized by XRPD, TGA, DSC, HPLC-UV, laser diffraction, microscopy and ^{1}H NMR to confirm their identity, purity, potency, crystallinity and particle size. Single crystals were also grown from solution crystallization methods including vapor diffusion, evaporation and slow cooling procedures. Crystal structures were determined and analyzed to confirm that the complexes were cocrystals rather than salts and to explore the hydrogen bonding heterosynthons. The structures of AMG 517 and the cocrystal formers selected for investigation are shown in figure 3.1 along with a letter designation which will be used to identify each compound, after its first mention here, for clarity throughout this manuscript.

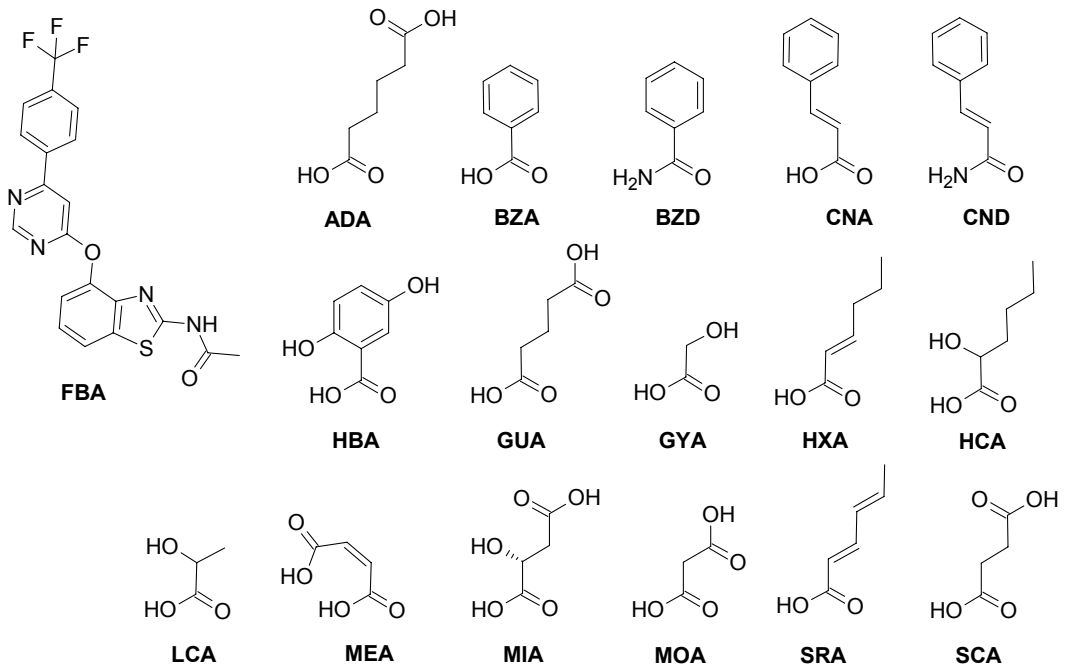

Figure 3.1. Chemical structures of **FBA)** AMG 517 free base, **ADA)** adipic acid, **BZA)** benzoic acid, **BZD)** benzamide, **CNA)** *trans*-cinnamic acid, **CND)** cinnamamide, **HBA)** 2,5-dihydroxybenzoic, **GUA)** glutaric acid, **GYA)** glycolic acid, **HXA)** *trans*-2-hexanoic acid, **HCA)** 2-hydroxycaproic acid, **LCA)** L(+)-lactic acid, **MEA)** maleic acid, **MIA)** L-malic acid, **MOA)** malonic acid, **SRA)** sorbic acid and **SCA)** succinic acid.

Experimental

X-Ray Powder Diffractometry

X-ray diffraction (XRPD) patterns were obtained on a PANalytical X'Pert PRO X-ray diffraction system (Almelo, the Netherlands). Samples were scanned in continuous mode from 5-45 º (2θ) with step size of 0.0334 º on a spinning stage at 45 kV and 40 mA with CuKα radiation (1.54 Å). The incident beam path was equipped with a 0.02 rad soller slit, 15mm mask, 4 º fixed anti-scatter slit and a programmable divergence slit. The diffracted beam was equipped with a 0.02 rad soller slit, programmable anti-scatter slit and a 0.02 mm nickel filter. Detection was accomplished with an RTMS detector (X'Celerator). Data analysis was conducted with PANalytical X'Pert Data Viewer software.

Thermal Analysis

Differential scanning calorimetry was performed on a TA Instruments Q100 calorimeter (New Castle, DE) at 10 ºC/min from 30 to 300 ºC in an open, aluminum pan. Thermal gravimetric analysis was performed on a TA Instruments Q500 analyzer at 10 ºC/min from 30 to 300 ºC in a platinum pan. Data analysis was accomplished with TA Instruments Universal Analysis 2000 software v4.4A.

Proton Nuclear Magnetic Resonance

^{1}H Nuclear Magnetic Resonance analysis was performed on a Bruker 400 MHz NMR (Germany) in DMSO-d_6 at 25 ºC. Data analysis conducted with ACD/SpecManager software v12.01 (Toronto, Canada).

High Pressure Liquid Chromatography

HPLC-UV was performed on an Agilent 1100 series HPLC (Palo Alto, CA) equipped with a binary pump (G1312A), DAD detector (G1315B), auto sampler (G1329A) and a 4.5 x 150 mm, 8 nm pore size, 5μm particle size, Eclipse XDB C18 column. Elution was achieved by a gradient method from 10 to 95% of solvent B (98% acetonitrile, 2% water, 0.1% triflouroacetic acid) in solvent A (98% water, 2% acetonitrile, 0.1% triflouracetic acid) at 1 mL/min for 8.0 min, isocratic 8.0 to 10.0 min then equilibrate at 10% solvent B 10.5 – 15.0 min. AMG 517 standards were prepared in methanol at 0.05 mg/mL and injected at 0.5, 1, 5, 10 and 15 μL (R^2 1.000). Detection was accomplished at 280 nm. Data analysis was conducted with Dionex Corporation Chromeleon Client v6.8 (Sunnyvale, CA) software.

Particle Size Analysis

Particle size of dry powders was determined by laser diffraction on the Sympatec HELOS/BF with a RODOS/M disperser equipped with the ASPIROS powder feeder (Clausthal-Zellerfeld). The powder (10-50mg) was delivered at 50 mm/s with a primary pressure of 1 bar and analyzed for 2 s on the R1 or R3 lens in triplicate.

Microscopy

Polarized light microscopy photomicrographs were acquired on a Nikon Eclipse E600 POL microscope (Melville, NY) at 200x magnification with a Nikon Digital Sight DS-5M camera and Media Cybernetics Image Pro Plus v5.1 (Bethesda, MD) software.

Bulk Powder: Crystallization Methods

Drug substances, AMG 517 free base form A (**FBA)** and the AMG 517 sorbic acid cocrsytal (**SRA**) were synthesized by Amgen, Inc.[14,15] The AMG 517 adipic acid (**ADA**), AMG 517 benzoic acid (**BZA**), AMG 517 benzamide (**BZD**), AMG 517 *trans*-

cinnamic acid (**CNA**), AMG 517 cinnamamide (**CND**), AMG 517 2,5-dihydroxybenzoic acid (**HBA**), AMG 517 glutaric acid (**GUA**), AMG 517 glycolic acid (**GYA**), AMG 517 *trans*-2-hexanoic acid (**HXA**), AMG 517 2-hydroxycaproic acid (**HCA**), AMG 517 L(+)-lactic acid (**LCA**), AMG 517 maleic acid (**MEA**), AMG 517 L-malic acid (**MIA**), AMG 517 malonic acid (**MOA**) and AMG 517 succinic acid (**SCA**) cocrystals were prepared by slurry or solution crystallization. **FBA** (1.0 g - 3.2 g) and the cocrystal former (0.2 g - 2.0 g) were weighed into a 50 mL glass vial in a 1:1 or 2:1 molar ratio (**FBA** to former). Ethyl acetate (15-46 mL) was then added and stirred at 50 – 55 ºC for 1hr. Solutions were allowed to cool to room temperature. Slurries or precipitate from cooled solutions were isolated by filtration through a 0.22µm nylon membrane filter and air dried for 24hr.

Single Crystal: Crystallization Methods

ADA: **FBA** was dissolved at 10.0 mg/mL in ethyl acetate at room temperature. A 10.0 mg/mL suspension of adipic acid in ethyl acetate was prepared at room temperature. The **FBA** solution and the adipic acid suspension were filtered through 0.22 µm nylon syringe filters into separate clean glass vials. The two filtrates were mixed 1:1 into a new clean glass vial, capped and left at room temperature.

BZA: **FBA** was dissolved at 10.0 mg/mL in ethyl acetate at room temperature. Benzoic acid was dissolved at 8.6 mg/mL in ethyl acetate at room temperature. The **FBA** and benzoic acid solutions were filtered through 0.22 µm nylon syringe filters into separate clean glass vials. The two filtrates were mixed 1:1 into a plastic eppendorf tube, capped stored at 50 ºC.

CND: A solution of cocrystal **CND** (21.8 mg in 2 mL) in ethyl acetate was prepared. The solution was filtered through a 0.22 µm nylon syringe filter into a clean

glass vial. An aliquot (0.5 mL) of this solution was added to a 1 mL glass tube which was placed inside an 8.0 mL glass vial containing 1mL hexane. The 8.0 mL vial was capped and left at room temperature.

GUA: A solution of cocrystal **GUA** (22.6 mg in 2 mL) in ethyl acetate was prepared. The solution was filtered through a 0.22 μm nylon syringe filter into a clean glass vial. An aliquot (0.5 mL) of this solution was added to a 1 mL glass tube which was placed inside an 8 mL glass vial containing 1mL hexane. The 8 mL vial was capped and left at room temperature.

GYA: A solution of cocrystal **GYA** (6.2 mg in 1.0 mL) was prepared in butyl acetate saturated with polyvinylpyrrolidone (PVP) K25 in a glass vial. The vial was capped and stored at 50 ºC for 3 days. The sample was then slow cooled at 2 ºC/hr to room temperature, then left at room temperature.

HCA: **FBA** was dissolved at 10.0 mg/mL in ethyl acetate at room temperature. 2-Hydroxycaproic acid was dissolved at 9.0 mg/mL in ethyl acetate at room temperature. The **FBA** and 2-hydroxycaproic acid solutions were filtered through 0.22 μm nylon syringe filters into separate clean glass vials. The two filtrates were mixed 1:1 into a clean glass vial, capped and stored at 50 ºC for 38 days at which time 1 drop of benzene was added, a pin hole was poked through the cap and the sample was left at room temperature.

LCA: **FBA** was dissolved at 10.0 mg/mL in ethyl acetate at room temperature. L(+)-Lactic acid was dissolved at 6.2 mg/mL in ethyl acetate at room temperature. The **FBA** and L(+)-lactic acid solutions were filtered through 0.22 μm nylon syringe filters

into separate clean glass vials. The two filtrates were mixed 1:1 into a clean glass vial, capped and stored at room temperature.

MEA: A solution of cocrystal **MEA** (4.6 mg in 1.0 mL) was prepared in ethyl acetate saturated with PVP K25 in a glass vial. The vial was capped and stored at 50 ºC for 3 days. The sample was then slow cooled at 2 ºC/hr to room temperature, then left at room temperature.

Single Crystal: X-Ray Structure Determination Method

Single crystal structures for **FBA, SRA, CNA** and **HXA** were reported previously.[15,16] Single crystal structures for all other co-crystals with suitable single crystals were determined by Dr. Richard J. Staples of Michigan State University and Crystallographic Resources Inc. (Dewitt, MI). Data were collected using a Bruker CCD (charge coupled device) based diffractometer equipped with an Oxford Cryostream low-temperature apparatus operating at 173 K. Data were measured using omega and phi scans of 0.5° per frame for 30 s. The total number of images was based on results from the program COSMO1 where redundancy was expected to be 4.0 and completeness to 100% out to 0.83 Å. Cell parameters were retrieved using APEX II software and refined using SAINT on all observed reflections. Data reduction was performed using the SAINT software which corrects for Lp. Scaling and absorption corrections were applied using SADABS multi-scan technique, supplied by George Sheldrick. The structures are solved by the direct method using the SHELXS-97 program and refined by least squares method on F^2, SHELXL- 97, which are incorporated in SHELXTL-PC V 6.10[17].

Results and Discussion

Preparation and Solid State Characterization

Fifteen cocrystals were successfully prepared through solution or slurry crystallization techniques. A total of 29 crystallizations of approximately 1-2.5 g scale were conducted to produce 1-2 g per cocrystal (table 3.1). Crystallization conditions were not optimized and therefore low yields were encountered in some cases requiring 2-3 batches to be combined to reach the target amount. The desired powders were then hand ground in a mortar and pestle to reduce particle size and blend multiple crystallizations into one homogeneous batch. Particle size reduction was conducted in order to harmonize the mean particle size of the cocrystals with the **FBA** and **SRA** material available in house which had already been micronized. Mortar and pestle hand grinding technique was chosen over other available methods such as ball milling and jet milling because it produces less mechanical stress. Mechanical stress can introduce defects to the crystal faces, produce amorphous content or other changes to the solid form which may influence the dissolution of the powder[18,19].

Table 3.1. Summary of crystallization conditions to produce each cocrystal

Cocrystal	AMG 517 (mg)	Former (mg)	EtOAc (mL)	Sol/Slurry	Evaporation	Recovery (mg)
ADA	1024	350	15	Slurry	NO	1004
ADA	1293	224	18	Slurry	NO	1074
BZD	2579	730	26	Slurry	NO	1594
BZA	1003	283	40	Slurry	NO	926
BZA	1424	403	46	Slurry	NO	1172
CND	2548	860	26	Slurry	NO	2152
CNA	1035	362	40	Slurry	NO	1012
CNA	1251	441	40	Slurry	NO	1299
HBA	1021	360	40	Slurry	NO	871
HBA	1452	512	40	Slurry	NO	613
HBA	1040	376	20	Slurry	NO	~940
GUA	1004	300	20	Solution	YES	104
GUA	2074	621	35	Solution	NO	578
GUA	1766	537	22	Solution	NO	~780
GYA	2126	775	21	Solution	NO	~1720
HXA	1253	346	20	Solution	NO	<1g
HXA	2085	556	26	Solution	NO	986
HCA	3134	1988	43	Solution	YES	>2g
LCA	2232	977	21	Solution	NO	1590
LCA	1393	640	16	Solution	NO	739
MEA	1036	327	15	Slurry	NO	712
MEA	1816	276	16	Slurry	NO	791
MEA	1044	174	16	Slurry	NO	~681
MIA	1037	282	15	Slurry	NO	930
MIA	1661	230	18	Slurry	NO	1006
MOA	1019	247	15	Slurry	NO	816
MOA	1675	397	16	Slurry	NO	1341
SCA	1045	294	15	Slurry	NO	754
SCA	2485	338	32	Slurry	NO	1361

Particle sizes of all powders measured by laser diffraction are listed in table 3.2. Mean particle sizes range from 1.73-6.24 μm (d_{50}). The full particle size distributions are located in the appendix. All powders were analyzed by X-ray powder diffraction (XRPD), differential scanning calorimetry (DSC), thermogravimetric analysis (TGA), proton nuclear magnetic resonance (^{1}H NMR), near-infrared spectroscopy (NIR) and high pressure liquid chromatography (HPLC). All XRPD patterns (figure 3.2) and DSC/TGA thermograms indicate crystalline material matching the powder patterns and thermograms of historical data indicating that the desired form was produced. Melting

onsets determined by DSC and weight loss % on TGA are listed in table 3.2 while complete spectral data and thermograms are compiled in the appendix.

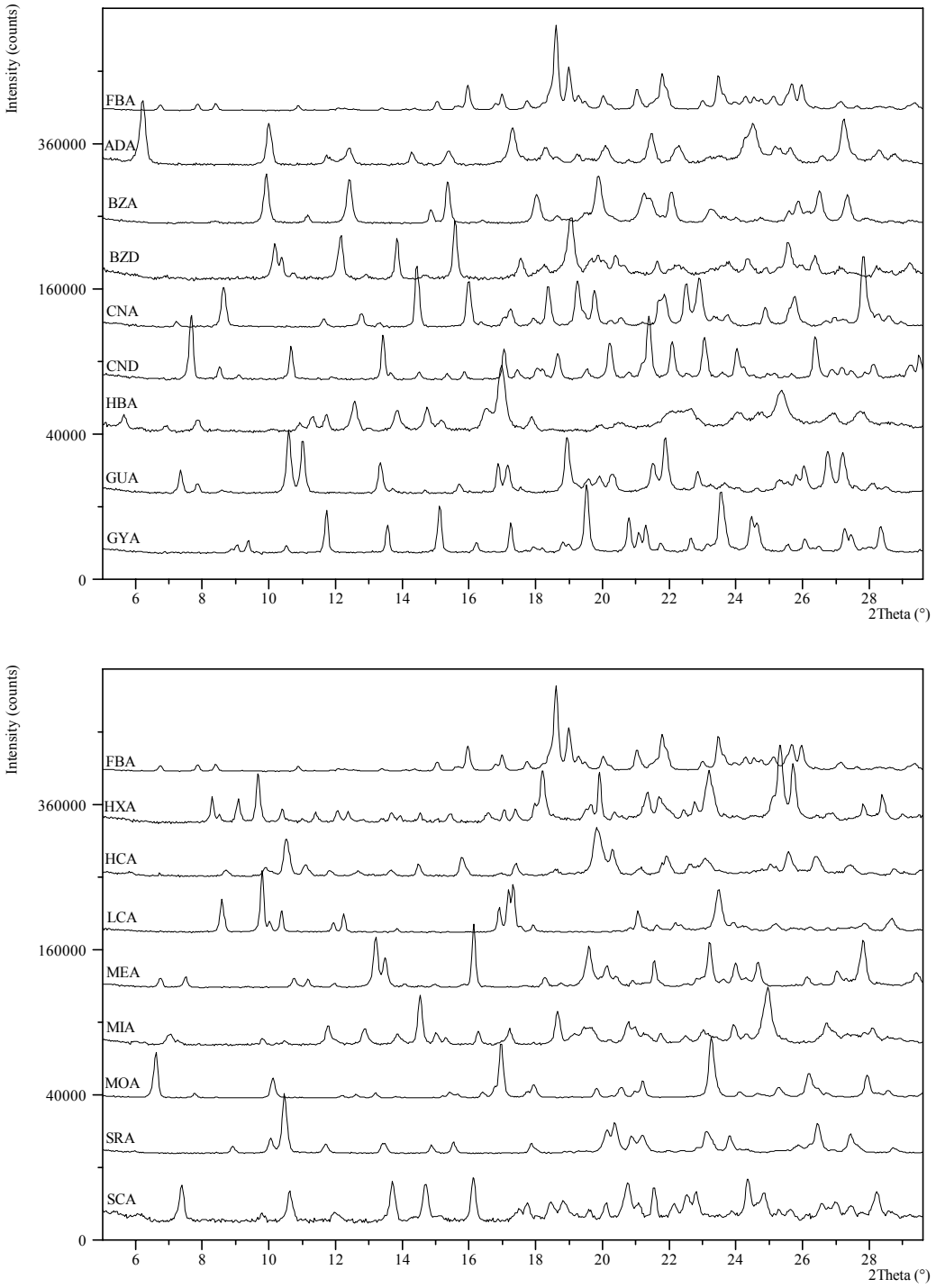

Figure 3.2. Original X-ray powder diffraction patterns for FBA and the sixteen cocrystals.

Table 3.2. Summary of characterization of **FBA** and sixteen cocrystals.

compound	molar ratio[a]	melting onset[b]	weight loss[c]	target potency[d]	particle size (μm)[e]		
	base:acid	(ºC)	%	%	d_{10}	d_{50}	d_{90}
FBA	NA	228	0.7	NA	0.44	1.73	4.58
ADA	2:1	205	14.9	102.0%	0.64	2.46	7.45
BZA	1:1	174	21.9	101.9%	0.53	1.85	6.89
BZD	1:1	177	22.3	101.8%	0.57	2.15	7.8
CNA	1:1	214	25.8	102.2%	0.83	4.59	22.02
CND	1:1	184	26.0	102.2%	0.75	2.92	8.79
HBA	2:1	226	19.0	100.0%	0.89	4.35	47.33
GUA	1:1	149	23.8	100.0%	0.91	4.06	22.19
GYA	1:1	137	14.1	101.5%	0.62	3.52	16.09
HXA	1:1	128	21.0	104.0%	0.87	4.00	20.80
HCA	1:1	133	20.5	104.2%	1.02	6.24	33.28
LCA	1:1	118	18.1	102.3%	0.73	3.31	17.89
MEA	2:1	192	12.3	104.0%	0.59	3.05	12.46
MIA	2:1	218	15.8	100.3%	0.60	2.49	7.15
MOA	1:1	186	20.0	102.4%	0.53	2.04	5.44
SRA	1:1	159	20.8	101.3%	0.53	1.91	5.00
SCA	2:1	206	13.3	101.2%	0.89	4.45	14.96

(a) molar ratio of base to acid determined by ^{1}H NMR (b) melting onset temperature determined by DSC (c) weight loss % due to heating determined by TGA (d) target potency determined by HPLC (e) particle size of original powder determined by laser diffraction (f) dehydration onset temperature. NA = not applicable

^{1}H NMR and HPLC were used to confirm the purity and content of the materials. Molar ratios of AMG 517 to cocrystal former determined by integration of the ^{1}H NMR (table 3.2) were used to calculate the AMG 517 content (potency) within each cocrystal. Experimental potencies determined by HPLC ranged from 100 – 104% of the calculated value (table 3.2). Purity of each compound, also quantified by HPLC, was greater than 98%.

Single Crystal Structures

Crystal structures for **FBA** and cocrystals **CNA, HXA** and **SRA** have been previously reported.[15,16] Crystallographic data for these and eight new crystal structures solved for single crystals produced during this work, **ADA**, **BZA**, **CND**, **GUA**, **GYA**, **HCA**, **LCA** and **MEA** are reported in table 3.3.

Table 3.3. Crystallographic data of **FBA** and eleven cocrystals

	FBA[15]	**ADA**	**BZA**	**CNA**[16]
formula	$C_{20}H_{13}F_3N_4O_2S$	$C_{46}H_{36}F_6N_8O_8S_2$	$C_{27}H_{19}F_3N_4O_4S$	$C_{29}H_{21}F_3N_4O_4S$
stoichiometry	1	2:1	1:1	1:1
formula weight	430.40	1006.95	552.52	578.56
crystal system	triclinic	triclinic	triclinic	triclinic
space group	$P\bar{1}$	$P\bar{1}$	$P\bar{1}$	$P\bar{1}$
a (Å)	12.861(2)	5.113(5)	4.784(3)	9.536(17)
b (Å)	14.956(2)	15.131(5)	10.819(6)	11.326(2)
c (Å)	11.612(3)	15.413(5)	24.403(14)	13.502(2)
α (deg)	100.76(1)	108.414(5)	77.435(4)	65.312(3)
β (deg)	106.00(1)	94.125(5)	88.542(4)	88.844(3)
γ (deg)	111.387(8)	96.846(5)	82.950(4)	87.819(3)
volume ($Å^3$)	1893.5(5)	1115.7(12)	1223.5(12)	1324.1(4)
calc density (g cm^{-3})	1.51	1.50	1.50	1.45
Z	4	1	2	2
T (K)	293(2)	173(2)	173(2)	193(2)
R1	0.0540	0.1998	0.1307	0.0773
wR2	0.0620	0.3390	0.2332	0.1170

	CND	GUA	GYA	HXA[16]
formula	$C_{29}H_{22}F_3N_5O_3S$	$C_{25}H_{21}F_3N_4O_6S$	$C_{22}H_{17}F_3N_4O_5S$	$C_{26}H_{23}F_3N_4O_4S$
stoichiometry	1:1	1:1	1:1	1:1
formula weight	577.58	562.52	506.46	544.54
crystal system	monoclinic	triclinic	monoclinic	monoclinic
space group	*C*2/c	*P*$\bar{1}$	*P* 2_1	*C*2/c
a (Å)	44.876(5)	4.629(10)	10.050(2)	62.498(18)
b (Å)	5.102(10)	11.297(3)	5.688(2)	8.116(2)
c (Å)	26.401(3)	24.152(7)	19.356(4)	19.870(6)
α (deg)	90.000	89.900(2)	90.000	90.000
β (deg)	120.012(10)	86.295(10)	97.058(2)	94.141(9)
γ (deg)	90.000	81.042(2)	90.000	90.000
volume ($Å^3$)	5234.0(13)	1245.1(6)	1098.2(5)	10052(5)
calc density (g cm^{-3})	1.47	1.50	1.53	1.44
Z	8	2	2	16
T (K)	173(2)	173(2)	173(2)	193(2)
R1	0.0717	0.0853	0.0419	0.0903
wR2	0.1589	0.1649	0.0954	0.0792
	HCA	**LCA**	**MEA**	**SRA[15]**
formula	$C_{26}H_{25}F_3N_4O_5S$	$C_{23}H_{19}F_3N_4O_5S$	$C_{44}H_{29}F_6N_8O_8S_2$	$C_{26}H_{21}F_3N_4O_4S$
stoichiometry	1:1	1:1	2:1	1:1
formula weight	562.56	520.48	975.87	542.53
crystal system	triclinic	triclinic	triclinic	triclinic
space group	*P*$\bar{1}$	*P*$\bar{1}$	*P*$\bar{1}$	*P*$\bar{1}$
a (Å)	4.729(11)	4.26530(10)	9.396(6)	4.720
b (Å)	9.139(19)	10.5529(4)	13.535(8)	8.812
c (Å)	30.731(6)	26.0208(7)	17.036(10)	29.640
α (deg)	93.847(14)	79.685(3)	104.757(8)	89.694
β (deg)	94.068(15)	86.626(3)	91.076(7)	85.565
γ (deg)	98.881(14)	85.887(3)	90.354(8)	81.898
volume (Å3)	1304.7(5)	1148.1(6)	2094(2)	1216.7
calc density (g cm-3)	1.43	1.51	1.55	1.48
Z	2	2	2	2
T (K)	173(2)	173(2)	173(2)	113(2)
R1	0.1900	0.0685	0.2087	0.0410
wR2	0.3340	0.1544	0.2929	0.0580

ADA This crystal was small, twined and had poor diffraction quality but confirms identity of the crystal[17]; **GUA** There is a 50% disorder in the acid, two orientations for the chain of carbon atoms[17]; **HCA** This was a very small crystal and the data is poor but it confirms the identity of the crystal[17]. Suitable single crystals of the polymorph representative of the powder of **BZD**, **HBA**, **MIA**, **MOA** and **SCA** were not obtained.

Crystal structures for cocrystals **BZD**, **HBA**, **MIA**, **MOA** and **SCA** remain unavailable at this time. Calculated powder patterns from the single crystal structures were confirmed to match the experimental X-ray powder pattern of the bulk powders used herein confirming that the single crystals are representative of the bulk powder. The calculated pKa for AMG 517 (ACD/pKa DB v12.0, Advanced Chemistry Development,

Inc) is -0.52 while the lowest pKa of each carboxylic acids ranges from 2.39 - 4.80. This results in a minimum ΔpKa of -2.91 indicating that all of the complexes are indeed cocrystals and not salts. Analysis of the C-O distances in the carboxylic acids also confirms that the acids remain neutral with ΔD_{C-O} values ranging from 0.09 to 0.14 indicating that proton transfer has not occurred.

All of the AMG 517 cocrystals with carboxylic acids reported to date hydrogen bond through heterosynthon 1 as illustrated by **BZA** in figure 3.3 where the amide proton on AMG 517 hydrogen bonds to the carbonyl group on the acid and the hydroxyl group on the acid hydrogen bonds to the benzothiozole nitrogen on AMG 517. Of the seven new AMG 517 carboxylic acid cocrystal single crystal structures disclosed here five (**ADA**, **BZA**, **GUA**, **HCA** and **LCA)** also hydrogen bond through heterosynthon 1, though **GUA** also contains the common COOH--COOH homosynthon while **HCA** and **LCA** form chains through a hydrogen bond with the additional hydroxyl group on the acid and the nitrogen on the AMG 517 pyrimidine ring (figure 3.4). It is important to note that cocrystals which hydrogen bond solely through this widespread heterosynthon 1 still lead to unpredictable crystal packing (figure 3.5).

The first reported AMG 517 carboxylic acid cocrystals which do not bind through heterosynthon 1 are cocrystals **GYA** and **MEA**. The NH--O hydrogen bond of heterosynthon 1 for both **GYA** and **MEA** is maintained, but in **MEA** an intramolecular OH--O hydrogen bond within maleic acid and in **GYA** an intermolecular OH--O hydrogen bond between glycolic acid molecules occupies the hydroxyl group of the COOH. Cocrystal **GYA** forms heterosynthon 2 through an OH--N hydrogen bond between the additional hydroxyl group on the acid and the benzothiazole nitrogen on

AMG 517 as shown in figure 3.4. Based on a search of Cambridge Structural Database (version 5.30 with updates through Sept 2009) heterosynthon 2 is novel for multi-component organic complexes and could be exploited in future cocrystal screening efforts with molecules containing similar functionalities.

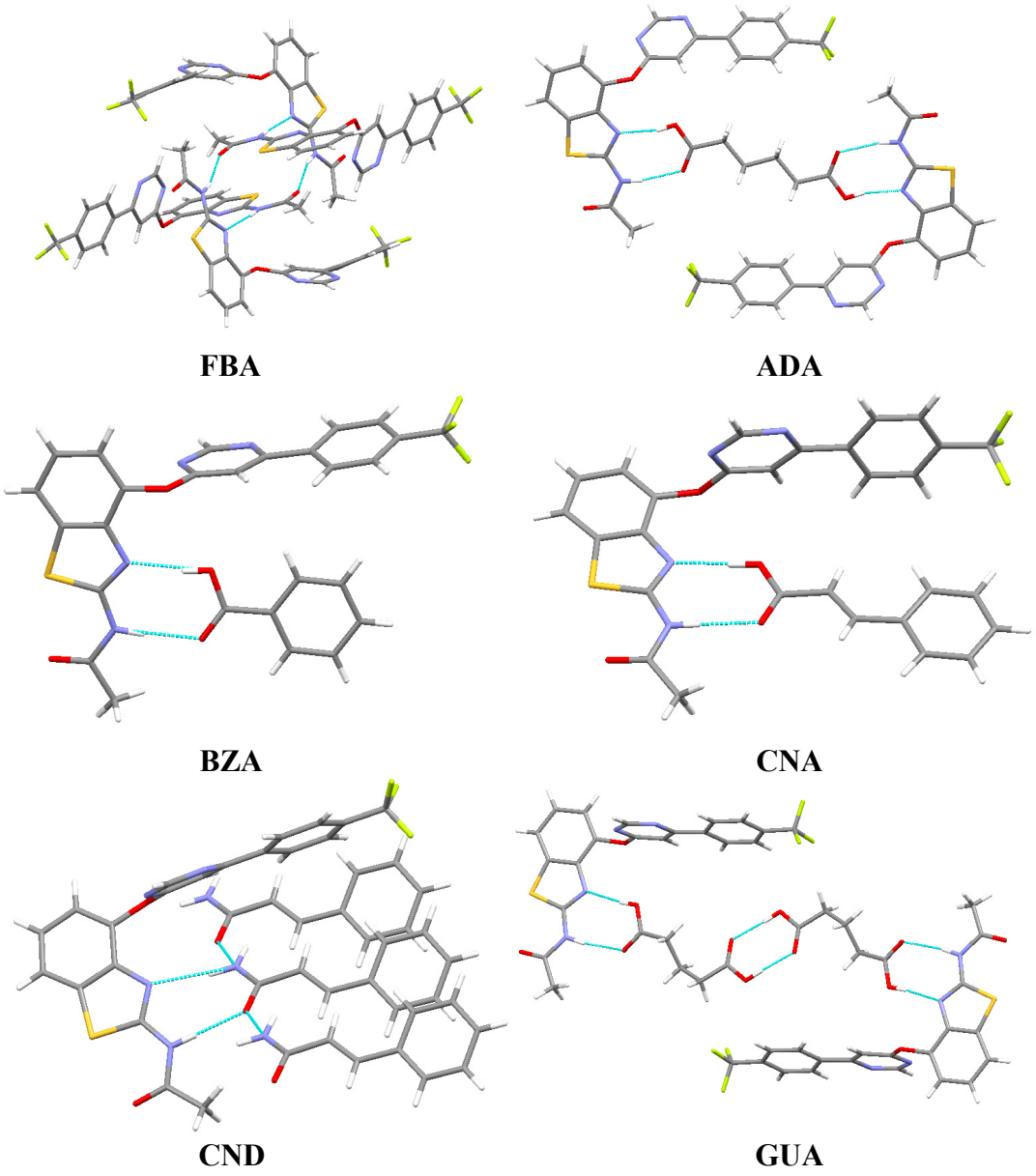

Figure 3.3. Hydrogen bonding (aqua) in **FBA**, **ADA, BZA, CNA, CND** and **GUA** (view chosen to highlight hydrogen bonds; grey = carbon, blue = nitrogen, red = oxygen, yellow = sulfur, green = fluorine, white = hydrogen).

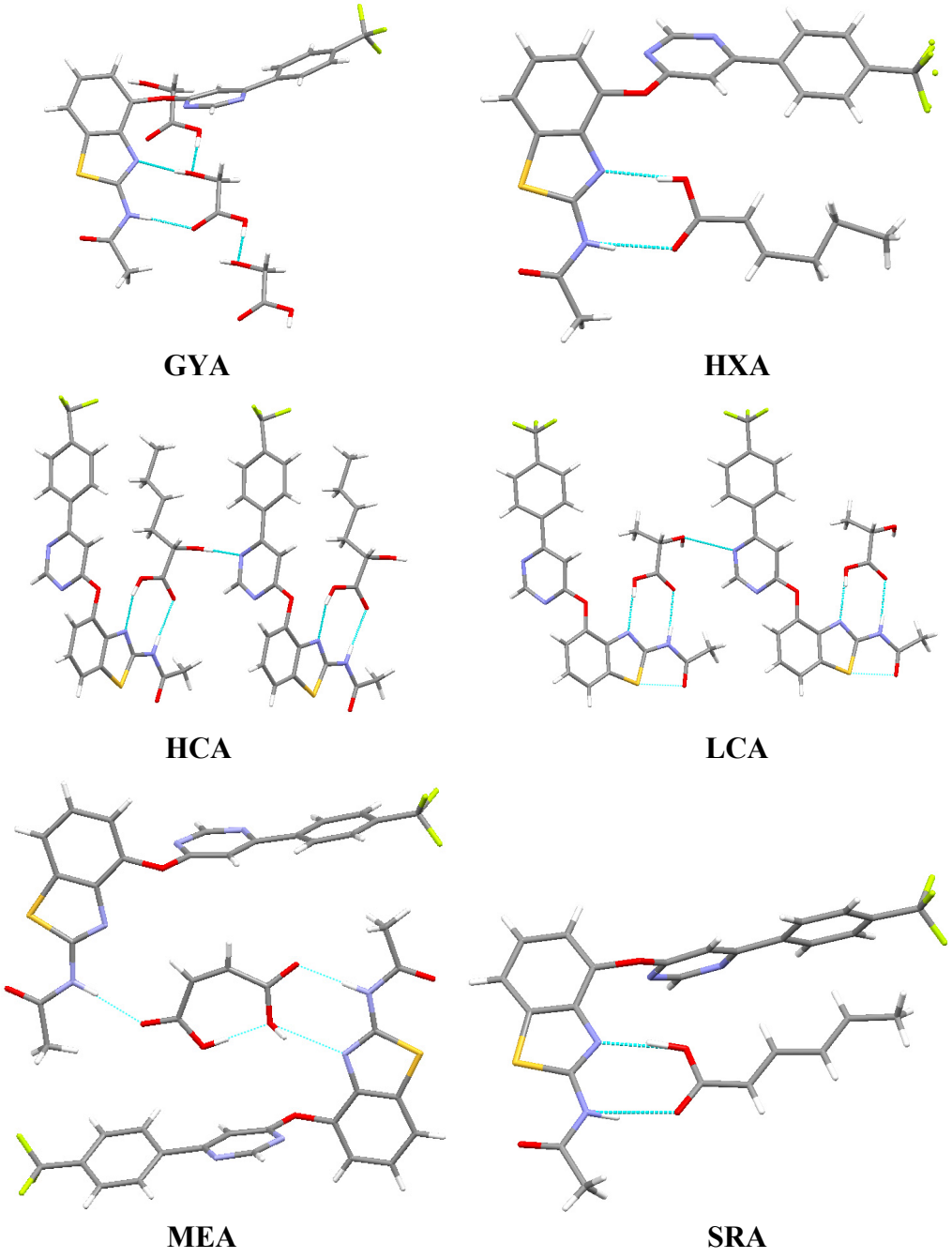

Figure 3.4. Hydrogen bonding (aqua) in **GYA, HXA, HCA, LCA, MEA** and **SRA** (view chosen to highlight hydrogen bonds; grey = carbon, blue = nitrogen, red = oxygen, yellow = sulfur, green = fluorine, white = hydrogen).

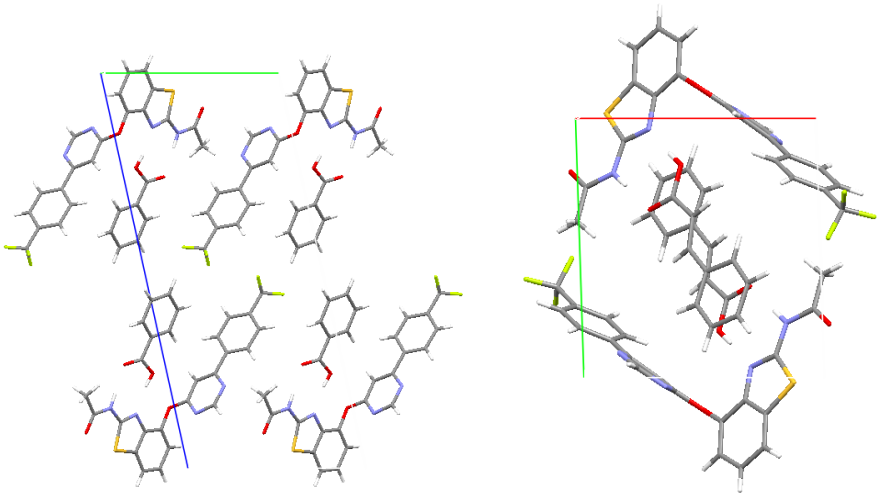

BZA (a-axis) **CNA** (c-axis)

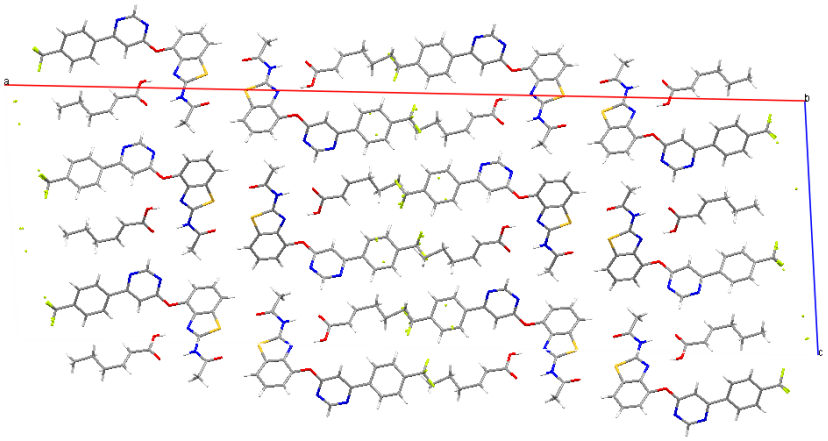

HXA (b-axis)

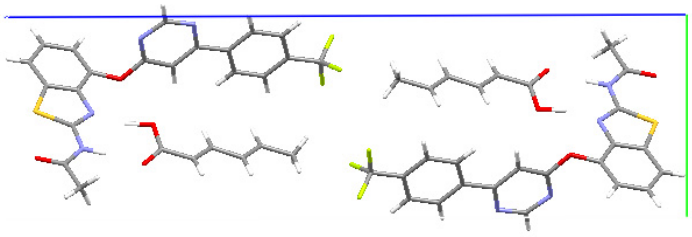

SRA (a-axis)

Figure 3.5. Crystal packing diagrams of four AMG 517 cocrystals which hydrogen bond solely through heterosynthon 1.

The only amide cocrystal crystal structure **CND** consists of heterosynthon 3 as shown in figure 3.3 which consists of a hydrogen bond from the amide proton on the API to the carbonyl group on cinnamamide and from the amide proton on cinnamamide to the benzothiazole nitrogen on the API. The additional amide proton forms a hydrogen bond with a neighboring cinnamamide carbonyl group forming a chain similar to that of **GYA**.

Conclusions

The fifteen cocrystals prepared from solution or slurry crystallization were determined to be crystalline, pure complexes of AMG 517 and cocrystal former in either a 1:1 or 2:1 molar ratio. The X-ray powder diffraction patterns and thermal properties were determined to be unique to those of **FBA** and the mean particle sizes were all less then 10 μm.

Even though the ΔpKa values were significant enough to argue that all of the complexes formed are cocrystals and not salts, analysis of the C-O distances in the carboxylic acids verifying that they are in the neutral form was still valuable information obtained from the single crystals structures. The most pertinent finding from the single crystal structures was that the presence of both API and cocrystal former in the complex is confirmed as well as the molar ratio. Also, heterosynthon 1 was seemingly robust based on its presence in the majority of cocrystals and could be valuable in future cocrystal design.

References

1. Trask AV, Motherwell WDS, Jones W 2004. Solvent-drop grinding: green polymorph control of cocrystatallisation. Chem Commun:890-891.
2. Lu E, Rodríguez-Hornedo N, Suryanarayanan R 2008. A rapid thermal method for cocrystal screening. Cryst Eng Comm 10:665-668.
3. Trask AV, Haynes DA, Motherwell WDS, Jones W 2006. Screening for crystalline salts *via* mechanochemistry. Chem Commun:51-53.
4. Bucar D-K, Henry RF, Lou X, Borchardt TB, Zhang GGZ 2007. A "hidden" co-crystal of caffeine and adipic acid. Chem Commun:525-527.
5. Trask AV, Motherwell WDS, Jones W 2005. Pharmaceutical cocrystallization: Engineering a remedy for caffeine hydration. Cryst Growth Des 5(3):1013-1021.
6. Vishweshwar P, McMahon JA, Bis JA, Zaworotko MJ 2006. Pharmaceutical co-crystals. J Pharm Sci 95(3):499-516.
7. Jayasankar A, Somwangthanaroj A, Shao ZJ, Rodriguez-Hornedo N 2006. Cocrystal formation during cogrinding and storage is mediated by amorphous phase. Pharm Res 23(10):2381-2392.
8. Childs SL, Stahly GP, Park A 2007. The salt-cocrystal continuum: The influence of crystal structure on ionization state. Mol Pharm 4(3):323-338.
9. Schultheiss N, Newman A 2009. Pharmaceutical cocrystals and their physicochemical properties. Cryst Growth Des 9(6):2950-2967.
10. Li JZ, Abramov Y, Bordner J, Leonard J, Medek A, Trask AV 2006. Solid-state acid-base interactions in complexes of heterocyclic bases with dicarboxylic acids: crystallography, hydrogen bond analysis, ^{15}N NMR spectroscopy. J Am Chem Soc 128:8199-8210.
11. Remenar JF, Morissette SL, Peterson ML, Moulton B, MacPhee JM, Guzman HR, Almarsson O 2003. Crystal engineering of novel cocrystals of a triazole drug with 1,4-dicarboxylic acids. J Am Chem Soc 125(28):8456-8457.
12. Vishweshwar P, McMahon JA, Peterson ML, Hickey MB, Shattock TR, Zaworotko MJ 2005. Crystal engineering of pharmaceutical co-crystals from polymorphic active pharmaceutical ingredients. Chem Commun:4601-4603.
13. Childs SL, Chyall LJ, Dunlap JT, Smolenskaya VN, Stahly BC, Stahly GP 2004. Crystal engineering approach to forming cocrystals of amine hydrochlorides with organic acids. Molecular complexes of fluoxetine hydrochloride with benzoic, succinic, and fumaric acids. J Am Chem Soc 126(41):13335-13342.
14. Doherty EM, Fotsch C, Bannon AW, Bo Y, Chen N, Dominguez C, Falsey J, Gavva NR, Katon J, Nixey T, Ognyanov VI, Pettus L, Rzasa R, Stec M, Surapaneni S, Tamir R, Zhu J, Treanor JJS, Norman MH 2007. Novel vanilloid receptor-1 antagonists: 2. Structure-activity relationships of 4-oxopyrimidines leading to the selection of a clinical candidate. J Med Chem 50(15):3515-3527.
15. Bak A, Gore A, Yanez E, Stanton M, Tufekcic S, Syed R, Akrami A, Rose M, Surapaneni S, Bostick T, King A, Neervannan S, Ostovic D, Koparkar A 2008. The co-crystal approach to improve the exposure of a water-insoluble compound: AMG

517 sorbic acid co-crystal characterization and pharmacokinetics. J Pharm Sci 97(9):3942-3956.
16. Stanton MK, Bak A 2008. Physicochemical properties of pharmaceutical co-crystals: A case study of ten AMG 517 co-crystals. Cryst Growth Des 8(10):3856-3862.
17. Staples R. 2009. Structure Report. ed., Dewitt, MI: Crystallographic Resources Inc.
18. Chamarthy SP, Pinal R 2008. The nature of crystal disorder in milled pharmaceutical materials Colloids Surf, A 331(1-2):68-75.
19. Longuemard P, Jbilou M, Guyot-Hermann A-M, Guyot J-C 1998. Ground and native crystals: comparison of compression capacity and dissolution rate. Int J Pharm 170:51-61.

Chapter 4. Dissolution and Pharmacokinetics of AMG 517 Cocrystals

Introduction

AMG 517 was a poorly soluble small molecule drug afflicted with dissolution and solubility limited absorption in preclinical pharmacokinetic investigations.[1] The traditional method to improve dissolution and solubility of an API, such as salt formation, proved difficult due to the low basic pKa of the molecule leading to rapid dissociation of salts in an aqueous environment. Cocrystallization of AMG 517 with sorbic acid has been proven to improve the initial dissolution rate of AMG 517 which resulted in an improvement in pharmacokinetics in the rat over **FBA** when dosed as suspensions in 10% Pluronic F108 in OraPlus®.[1] Further study with AMG 517 from this lab produced a series of AMG 517 cocrystals, most of which have been shown to improve the dissolution rate of AMG 517 in fasted simulated intestinal fluid (FaSIF).[2,3]

Deciding which form(s) of an API to develop as the final drug substance for the clinic will undoubtedly include pharmacokinetic studies to ensure proper coverage of the drug target *in vivo*.[4-7] Ethically the number of *in vivo* studies conducted has been minimized and therefore filters prior to pharmacokinetic investigations have been utilized to predict and remove from consideration forms that were likely to perform poorly *in vivo* or that were not developable due to unrelated reasons such as processability or stability. Dissolution rates and solubility of the API form in a biologically relevant system have been relied upon heavily to make this prediction due to its proven correlation for salts, polymorphs and formulations of a drug substance. Cocrystals, having resurged only recently in the literature, do not have the same comprehensive research correlating

dissolution to pharmacokinetics. Therefore the focus of this research is to analyze the dissolution rate and behavior of sixteen AMG 517 cocrystals and associate that to the exposure seen in rat pharmacokinetic studies. Both powder and intrinsic dissolution methods are investigated and contrasted to one another and the fate of the remaining solids in each study are determined.

Experimental

X-Ray Powder Diffractometry

X-ray diffraction (XRPD) patterns were obtained on a PANalytical X'Pert PRO X-ray diffraction system (Almelo, the Netherlands). Samples were scanned in continuous mode from 5-45 º (2θ) with step size of 0.0334 º on a spinning stage at 45 kV and 40 mA with CuKα radiation (1.54 Å). The incident beam path was equipped with a 0.02 rad soller slit, 15mm mask, 4 º fixed anti-scatter slit and a programmable divergence slit. The diffracted beam was equipped with a 0.02 rad soller slit, programmable anti-scatter slit and a 0.02 mm nickel filter. Detection was accomplished with an RTMS detector (X'Celerator). Data analysis was conducted with PANalytical X'Pert Data Viewer software.

Thermal Analysis

Differential scanning calorimetry was performed on a TA Instruments Q100 calorimeter (New Castle, DE) at 10 ºC/min from 30 to 300 ºC in an open, aluminum pan. Thermal gravimetric analysis was performed on a TA Instruments Q500 analyzer at 10

ºC/min from 30 to 300 ºC in a platinum pan. Data analysis was accomplished with TA Instruments Universal Analysis 2000 software v4.4A.

Near-Infrared Spectroscopy

NIR was performed on a FOSS NIRSystems XDS^{TM} near-infrared rapid content analyzer (Laurel, MD) and the data was analyzed with Vision 3.30 software. Absorbance was measured from 400 – 2500 nm. Powders were analyzed in 20 mL clear glass scintillation vials with 1-2 g of compound per vial. Compacts prepared for intrinsic dissolution were analyzed directly pre and post dissolution. Compacts were allowed to dry at room conditions for 24 hr before analysis post dissolution.

High Pressure Liquid Chromatography

HPLC-UV was performed on an Agilent 1100 series HPLC (Palo Alto, CA) equipped with a binary pump (G1312A), DAD detector (G1315B), auto sampler (G1329A) and a 4.5 x 150 mm, 8 nm pore size, 5µm particle size, Eclipse XDB C18 column. Elution was achieved by a gradient method from 10 to 95% of solvent B (98% acetonitrile, 2% water, 0.1% triflouroacetic acid) in solvent A (98% water, 2% acetonitrile, 0.1% triflouracetic acid) at 1 mL/min for 8.0 min, isocratic 8.0 to 10.0 min then equilibrate at 10% solvent B 10.5 – 15.0 min. AMG 517 standards for all studies except intrinsic dissolution were prepared in methanol at 0.05 mg/mL and injected at 0.5, 1, 5, 10 and 15 µL (R^2 1.000). AMG 517 standards for intrinsic dissolution were prepared at 1.56 µg/mL in methanol and injected at 0.1, 0.5, 1, 5 and 10 µL (R^2 1.000). Cocrystal former standards were prepared at 0.1 mg/mL in water. Injections were made at 1, 5 and 10 µL (**SRA** R^2 0.998), or 1, 5, 10, 15 and 20 µL (**BZA**, **BZD** and **HBA** R^2 1.000) or 1, 5, 10 and 15 µL (**CNA** and **CND** R^2 0.987). Detection was accomplished at

280 nm. Data analysis was conducted with Dionex Corporation Chromeleon Client v6.8 (Sunnyvale, CA) software. Representative chromatograms are shown in figure 4.1. Standard curves bracketed all concentration ranges for unknowns.

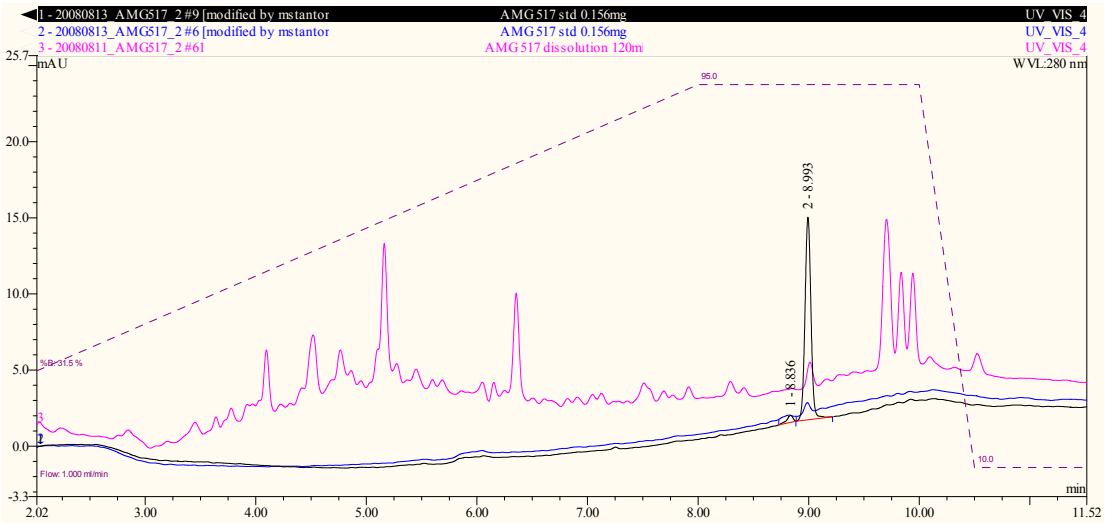

Figure 4.1. Representative HPLC-UV chromatograms of high and low standards in methanol and **FBA** in FaSIF.

Particle Size Analysis

Particle size of the suspension formulations for PK studies and the suspensions in FaSIF from powder dissolution studies were determined by laser diffraction on the Sympatec HELOS/BF with a CUVETTE disperser (Clausthal-Zellerfeld). The suspension was added drop-wise to the 6mL cuvette containing 5mL vehicle (1% PVP K25 in water or FaSIF) until a 10-45% optical concentration was achieved. Measurements were taken for 10 s using R1 or R3 lens in triplicate.

Microscopy

Polarized light microscopy photomicrographs were acquired on a Nikon Eclipse E600 POL microscope (Melville, NY) at 200x magnification with a Nikon Digital Sight DS-5M camera and Media Cybernetics Image Pro Plus v5.1 (Bethesda, MD) software.

Filter Binding Investigation

Loss of sample due to binding to surfaces has been a common issue with small molecules. Filter binding has been of significant importance especially when sample concentrations are very low when minute losses become significant. Due to the expectedly low concentrations of AMG 517 in the dissolution and formulation samples and investigation into the appropriate filters was conducted. Different filter materials, sizes and styles were compared (table 4.1). The recovery of AMG 517 in FaSIF was best when a PTFE membrane was used for filtration. Complete recovery was achieved when the first few drops of FaSIF were left to waste before collecting the sample. Nylon and cellulose acetate recoveries were low, while the steel frit likely allowed small particles to pass through the filter resulting in high recoveries. Recovery of AMG 517 from the 1% PVP K25 in water formulations was very low for both nylon and PTFE filters therefore double centrifugation (2 x 13,000 rpm for 20 min, pipette supernatant to a new vial before second centrifugation) was utilized as the sample preparation technique before HPLC analysis of the dosing formulations.

Table 4.1. Summary of filter binding studies

Compound	Media	Volume (mL)	Treatment	Peak Area	Recovery
FBA	FaSSIF	0.5	Centrifuge	0.594	control
FBA	FaSSIF	0.5	PTFE, 0.45m, miniprep	0.590	99%
FBA	FaSSIF	0.5	PTFE, 0.45m, acrodisc, 13mm	0.516	87%
FBA	FaSSIF	0.5	Nylon, 0.45m, acrodisc, 13mm	0.316	53%
FBA	FaSSIF	1	Centrifuge	0.270	control
FBA	FaSSIF	1	PTFE, 0.2m, nalgene, 25mm	0.261	97%
FBA	FaSSIF	1	CA, 0.2m, whatman, 25mm	0.000	0%
FBA	FaSSIF	1	Nylon, 0.2m, acrodisc, 25mm	0.055	21%
SRA	FaSSIF	0.5	Centrifuge	5.884	control
SRA	FaSSIF	0.5	PTFE, 0.45m, miniprep	4.524	77%
SRA	FaSSIF	0.5	PTFE, 0.45m, acrodisc, 13mm	4.536	77%
SRA	FaSSIF	0.5	Nylon, 0.45m, acrodisc, 13mm	1.497	25%
SRA	FaSSIF	1	Centrifuge	2.887	control
SRA	FaSSIF	1	PTFE, 0.2m, nalgene, 25mm	2.319	80%
SRA	FaSSIF	1	CA, 0.2m, whatman, 25mm	0.091	3%
SRA	FaSSIF	1	Nylon, 0.2m, acrodisc, 25mm	0.114	4%
SRA	FaSSIF	0.5	Centrifuge	4.651	control
SRA	FaSSIF	0.5	Steel, 0.5m, 1/8", vial 1	6.527	140%
SRA	FaSSIF	0.5	Steel, 0.5m, 1/8", vial 2	5.848	126%
SRA	FaSSIF	0.5	Steel, 0.5m, 1/8", vial 3	5.404	116%
SRA	FaSSIF	0.5	Steel, 0.5m, 1/8", vial 4	5.517	119%
SRA	FaSSIF	0.5	Steel, 0.5m, 1/8", vial 5	5.483	118%
SRA	FaSSIF	0.5	Centrifuge	7.026	control
SRA	FaSSIF	0.5	PTFE, 0.45m, acrodisc, 13mm, Vial 1	6.993	100%
SRA	FaSSIF	0.5	PTFE, 0.45m, acrodisc, 13mm, Vial 2	7.307	104%
SRA	FaSSIF	0.5	PTFE, 0.45m, acrodisc, 13mm, Vial 3	7.321	104%
SRA	FaSSIF	0.5	PTFE, 0.45m, acrodisc, 13mm, Vial 4	7.368	105%
SRA	FaSSIF	0.5	PTFE, 0.45m, acrodisc, 13mm, Vial 5	7.374	105%
SRA	FaSSIF	0.5	Centrifuge	7.026	control
SRA	FaSSIF	0.5	PTFE, 0.45m, acrodisc, 13mm, Vial 1*	7.216	103%
SRA	FaSSIF	0.5	PTFE, 0.45m, acrodisc, 13mm, Vial 2	7.318	104%
SRA	FaSSIF	0.5	PTFE, 0.45m, acrodisc, 13mm, Vial 3	7.311	104%
SRA	FaSSIF	0.5	PTFE, 0.45m, acrodisc, 13mm, Vial 4	7.314	104%
SRA	1% PVP K25	0.5	Centrifuge	8.746	control
SRA	1% PVP K25	0.5	PTFE, 0.45m, acrodisc, 13mm	0.646	7%
SRA	1% PVP K25	0.5	Nylon, 0.45m, acrodisc, 13mm	0.917	10%

*Three drops of FaSIF went to waste prior to collection in vial 1.

Powder Dissolution Method

Approximately 30mg of compound was weighed into 20mL glass scintillation vials in triplicate. Then, 10mL of FaSIF (5mM taurocholic acid sodium salt and 1.5 mM lecithin in pH 6.8 phosphate buffer) was added and continually stirred on a magnetic stirrer at room temperature (20-25˚C). At each time point (1, 15, 30, 45, 60, 90, 120, 240 and 1440 min) 0.6 mL was filtered through a 0.45 μ, 13 mm, PTFE syringe filter into an HPLC vial (leaving the first 4 drops to waste). Samples were diluted 3 fold with DMSO to prevent precipitation if needed. Analysis was conducted by HPLC-UV to determine the AMG 517 and cocrystal former (where possible) concentration in solution. After the final time point the suspension was analyzed by laser diffraction and microscopy for particle size determination and then centrifuged 10 min at 13,000 rpm. The surpernatent was discarded and the pellet was air dried for 24 hr then analyzed by XRPD, DSC and TGA to determine the form.

Intrinsic Dissolution Method

Intrinsic dissolution was conducted in a Varian VK 7025 dissolution apparatus (Palo Alto, CA) using a rotating disk apparatus at 37 ˚C at 100 rpm in 500 mL FaSIF for 2 hr (n = 1) and 4 hr (n = 2). Compacts were produced by compressing 100 mg of compound into a die at 2000 psi (3000 psi for cocrystal **HCA**) for 2 min in a carver press (surface area 0.5 cm^2). Compacts were analyzed by NIR pre dissolution to assess form. FaSIF samples (0.7 mL) were withdrawn manually at each time point and filtered through 0.45 μm PTFE syringe filter, leaving 8 drops to waste before collection into an HPLC vial, then analyzed by HPLC-UV at 280 nm for AMG 517 content. Compacts were dried

at room temperature for at least 24 hr then analyzed by NIR and XRPD to assess the form.

Dose Analysis Method

The formulations dosed in the PK studies were analyzed pre-dose for total AMG 517 content and pH and within 2 hr post-dose for particle size, solid form and AMG 517 concentration in solution. Total AMG 517 content was analyzed by HPLC-UV of a 10 µL aliquot diluted 100x with methanol to dissolve (n=3 dilutions). AMG 517 concentration in solution was measured with HPLC-UV by direct injection of the supernatant after double centrifugation at 13,000 rpm for 20 min (n=3 injections). The pellet was dried at room conditions over night then analyzed by XRPD to determine form.

Pharmacokinetic Investigation Methods

The animal procedures were conducted under a protocol approved by the Amgen, Inc (Cambridge, MA) Institutional Animal Care and Use Committee. Male Sprague Dawley rats, 300-325 g, were obtained from Charles River Laboratories (Wilmington, MA) with catheters implanted in the femoral artery and vein; the surgical procedures were conducted under aseptic conditions. The rats were housed in a temperature- and humidity-controlled environment subject to a 12 h light:12 h dark cycle and had access to water and a standard laboratory rodent diet *ad libitum*. Animals were allowed to acclimate for one week prior to use. Rats (n=3) were administered a single dose of test material (100 mg/kg) formulated as suspensions in 1% PVP K25 in water by oral gavage. Blood samples were collected from the femoral artery catheter at 0.25, 0.5 1, 2, 4, 6, 8,

and 24 h post-dose. Plasma was separated by centrifugation and stored at -80° C until analyzed.

Plasma standards were prepared by serial dilution in male Sprague-Dawley rat plasma with K_2EDTA (Bioreclamation) at 25,000, 12,500, 6,250, 3,125, 1,562, 781, 391, 195 and 98 ng/mL AMG 517. Plasma standards and samples were extracted with a 4x dilution of an internal standard (ISTD) solution (acetonitrile with 0.1 % formic acid and 200 ng/mL AMG 831664[3]) and centrifuged for 20 min at 4 ˚C.

LC/MS-MS analysis of plasma extracts was conducted on an Agilent HPLC-MSD Trap equipped with an APCI probe, Varian Pursuit C18, 30 x 2 mm, 5 µ column and ChemStation software in multiple reaction monitoring (431.1 m/z and 445.1 m/z) mode. The chromatographic method was isocratic at 45 % acetonitrile in water with 0.1% formic acid at 0.75 mL/min. Integration of the smoothed, extracted ion chromatogram at 389.1 m/z was used for quantitation against the standard curve corrected with the ISTD concentration. Integration of the smoothed, extracted ion chromatogram at 389.1 m/z with the Bruker Daltonics DataAnalysis for LC/MSD Trap software v3.3 was used for quantitation against the standard curve corrected with the ISTD concentration. Retention time of AMG 517 is 1.4-1.5 min and the ISTD retention time is 2.2-2.3 min (figure 4.2).

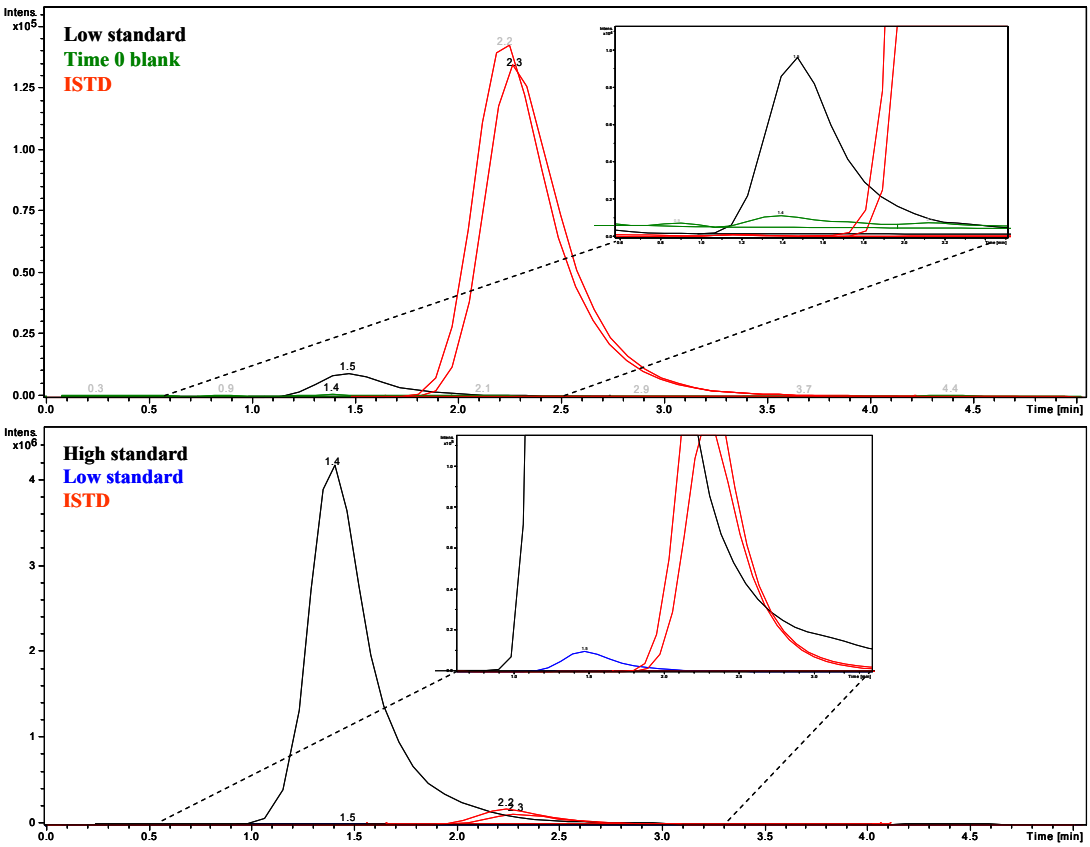

Figure 4.2. Representative mass spectroscopy chromatograms; low standard in plasma matrix and blank matrix (top), high standard and low standard in plasma matrix (bottom).

According to the U.S Department of Health and Human Services Food and Drug Administration (FDA) accuracy of a bioanalytical method should be measured with a minimum of three concentrations and five determinations per concentration.[8] The mean value should be within 15% of the target concentration except at the lower limit of quantification (LLOQ) where 20% is acceptable. Due to the wide concentration range a second order polynomial regression equation and 1/x weighting was used to fit the curve. The goodness of fit (R^2) ranges from 0.9945 – 0.9976. With this method the mean accuracy of the nine concentrations which make up the standard curve, which were each freshly prepared and injected on eight different days, ranges from 93 – 106%. The FDA guidance also suggests that the lowest standard on the calibration curve is acceptable as

the LLOQ if the analyte response is at least 5 times that of the blank and should be accurate within 80 – 120%. The mean response of the 97.7 ng/mL standard and the mean response of the time zero plasma samples from each animal across all days are 334302 and 16523 peak areas respectively. The 97.7 ng/mL standard has a 20 times higher response than the blank response and a mean accuracy of 93% qualifying it as the LLOQ. All samples (mean of n = 3 injections) lie within the range of the standard curve and the lowest sample concentration (291 ng/mL) is 3.0 times higher than the LLOQ.

Statistical Calculation Methods

Statistical differences between groups were calculated using SigmaStat for Windows version 3.0.1 (SPSS Inc., Chicago, IL) applying a Kruskal-Wallis[9] one-way analysis of variance on ranks (ANOVA) followed by a multiple comparison procedure versus **FBA** (Holm-Sidak method, p value must be lower than the critical value to be considered significant). Student's t-test was used to determine statistical significance between two groups.

Results and Discussion

Powder Dissolution

The powder dissolution profiles of **FBA** and the sixteen cocrystals in FaSIF at room temperature have been reported previously from this laboratory.[2,3] The studies were repeated here to eliminate any variation between lots of compound, especially due to the large differences in particle size (historical data was produced with lots containing 30-640 μm mean particle sizes). FaSIF, besides being representative of *in vivo*

conditions[10], was chosen over pure water or gastric media due to the low solubility of AMG 517 in water and its instability at low pH. The powder dissolution profiles for all compounds are shown in figure 4.3 and associated data to be discussed below is summarized in table 4.2. The dissolution profiles of the cocrystals are typical of an API that was not in its most stable form under these conditions and therefore crystallizes to a more stable form producing a decrease in solubility over time (i.e. dissociation of a salt to free form, amorphous to crystalline material or anhydrous to hydrate conformation). The remaining solids for all compounds after 24 hr were isolated and analyzed by XRPD, DSC, TGA and laser diffraction to determine if any form changes occurred (example figure 4.4, all others appendix). No form alteration or change in particle size of **FBA** was detected while the cocrystals all show total (**HBA**, **GUA**, **GYA**, **HXA**, **HCA**, **LCA**, **MEA**, **MIA**, **MOA**, and **SCA**) or partial (**ADA, BZA, BZD, CNA, CND** and **SRA)** crystallization to either **FBA**, AMG 517 free base form B (**FBB**), AMG 517 free base hydrate form C **(FBC)** or a mixture as well as an increased mean particle size 1.4 – 2.9x. A rough estimate of the % conversion of the solids from cocrystal to free form was made from the weight loss on TGA associated with the melt of the cocrystal and coinciding release of the cocrystal former. By this technique cocrystals **ADA, BZA**, **BZD**, **CNA**, **CND** and **SRA** maintained approximately 38, 20, 35, 82, 87 and 65% of the cocrystal form respectively at 24 h.

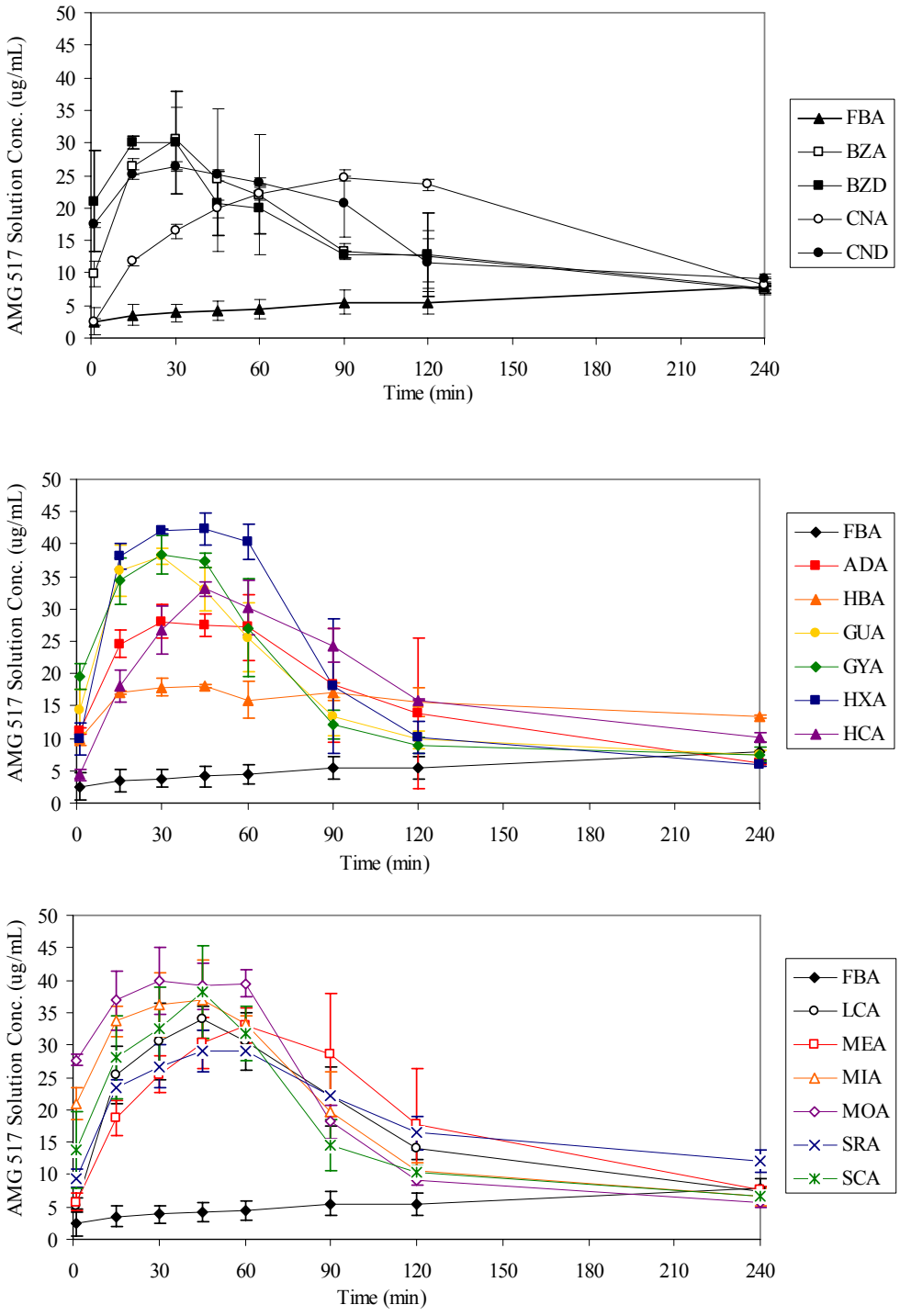

Figure 4.3. Powder dissolution profiles to 240min of **FBA** and the cocrystals. **FBA** is represented in each graph for reference.

Table 4.2. Summary of powder dissolution analysis.

initial form	pre-dissolution particle size[a] d_{50} (μm)	post-dissolution particle size[b] d_{50} (μm)	sol. conc. 15 min[c] (μg/mL)	final form[d]
FBA	1.73	1.85 ± 0.02	3.5 ± 1.6	**FBA**
ADA	2.46	7.84 ± 0.11	24.6 ± 2.0	~38% **ADA**, **FBB/FBC**
BZA	1.85	7.44 ± 0.90	26.4 ± 1.2	~20% **BZA**, **FBB/FBC**
BZD	2.15	5.94 ± 0.68	30.1 ± 0.9	~35% **BZD**, **FBB/FBC**
CNA	4.59	5.35 ± 0.05	11.8 ± 0.6	~82% **CNA**, **FBB**
CND	2.92	3.92 ± 0.00	25.1 ± 0.8	~87% **CND**, **FBB**
HBA	4.35	12.83 ± 0.11	17.2 ± 0.2	**FBB/FBC**
GUA	4.06	7.73 ± 0.12	35.8 ± 4.0	**FBC**
GYA	3.52	5.30 ± 0.12	34.3 ± 3.6	**FBC**
HXA	4.00	10.26 ± 0.04	38.2 ± 2.0	**FBC**
HCA	6.24	4.02 ± 0.05	18.1 ± 2.5	**FBC/FBA**
LCA	3.31	4.98 ± 0.12	25.4 ± 4.4	**FBC**
MEA	3.05	6.06 ± 0.01	18.7 ± 2.6	**FBB/FBC**
MIA	2.49	5.99 ± 0.03	33.7 ± 2.3	**FBB/FBC**
MOA	2.04	5.10 ± 0.15	36.8 ± 4.6	**FBB/FBC**
SRA	1.91	1.99 ± 0.02	23.5 ± 1.0	~65% **SRA**, **FBB**
SCA	4.45	6.37 ± 0.02	28.1 ± 6.3	**FBB/FBC**
Control **FBA**	1.73	1.85 ± 0.02	1.7 ± 0.5	**FBA**

(a) Mean particle size of dry powder, (b) mean particle size of solids in suspension after 24hr in FaSIF (c) concentration of AMG 517 in solution in FaSIF at 15 min and (d) solid form of solids isolated from FaSIF after 24 hr. Control **FBA**; sorbic acid added to the dissolution media.

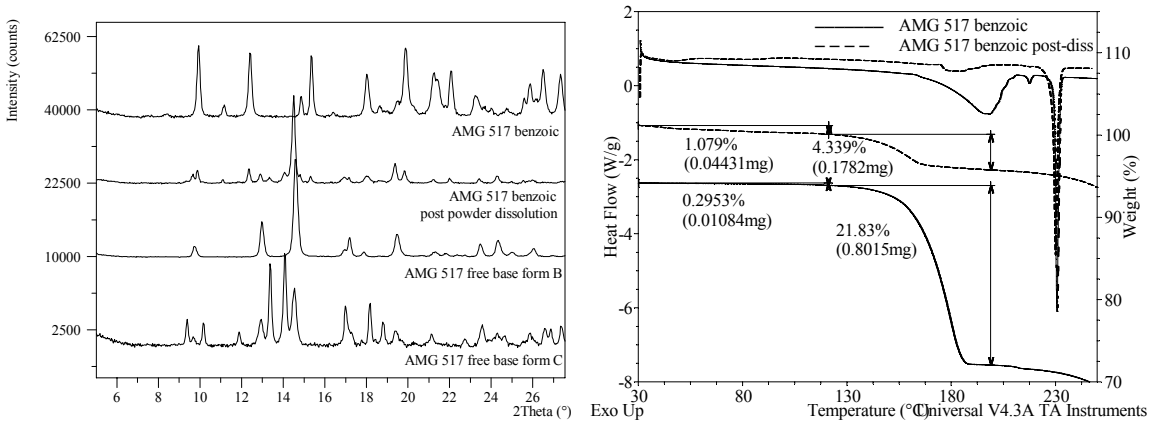

Figure 4.4. XRPD (left), DSC and TGA (right) of BZA pre and post powder dissolution.

Another possible measurement of conversion to free form from cocrystal is the concentration of cocrystal former found in solution in the FaSIF assuming the former is freely soluble in the dissolution media. Based on published solubility in water of benzoic acid, benzamide, cinnamic acid, cinnamamide, 2-hydroxybenzoic acid and sorbic acid (2.9[11], 13.5[11], 0.5[11], 1.3[12], 5.0[11] and 2.5[11] mg/mL respectively) and the amount of these cocrystal formers present in the powder dissolution study (0.45 – 0.76 mg/mL) all of the cocrystal formers would likely be completely solubilized in FaSIF with the exception of cinnamic acid which would be about 67% solubilized. Figure 4.5 shows the concentration of formers in solution during the same experiment as measured by HPLC through 240 min for clarity. Adipic acid was not detectable by the HPLC method utilized and is therefore not included in this analysis. After 24 hr the concentration of former for cocrystals **BZA, BZD, CNA**, **CND, HBA** and **SRA** was 616 ± 20, 421 ± 27, 182 ± 19, 120 ± 8, 423 ± 36 and 467 ± 49 µg/mL respectively. This indicates approximately 7, 36, 76, 84, 7 and 24% of the total former added to the dissolution experiment in cocrystal form is *not* in solution presumably remaining as part of the cocrystal. There is good

agreement between the TGA and HPLC determination of % cocrystal remaining for **BZD** (35% and 36% respectively), **CNA** (82% and 76%), **CND** (87% and 84%) and **HBA** (0% and 7%) however **BZA** (20% and 7%) and **SRA** (65% and 24%) do not agree. During the dissolution experiment solids are removed due to sampling (both inside and outside of the syringe) which decreases the amount of cocrystal or converted free base form within the dissolution experiment to an unknown degree. This may account for the variability between the TGA and HPLC methods.

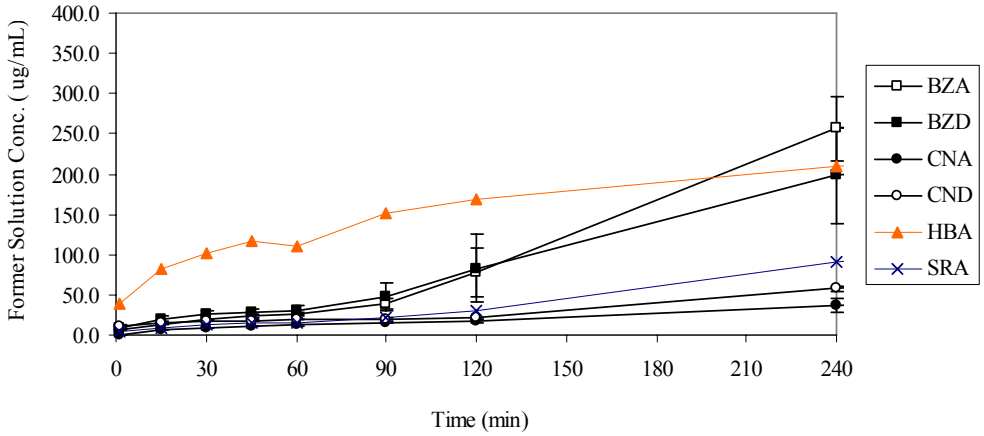

Figure 4.5. Cocrystal former solution concentrations in FaSIF over time

Due to the unexpected crystallization of **FBB** rather than **FBA** in the dissolution experiment a brief side discussion of the relationship between these free forms seems necessary. The free forms **FBB** and **FBC**, when tested under the same powder dissolution conditions as **FBA**, maintain FaSIF solubility lower than that of **FBA** even up to 10 days (5 ± 3, 5 ± 2 and 25 ± 1 µg/mL respectively, figure 4.6).

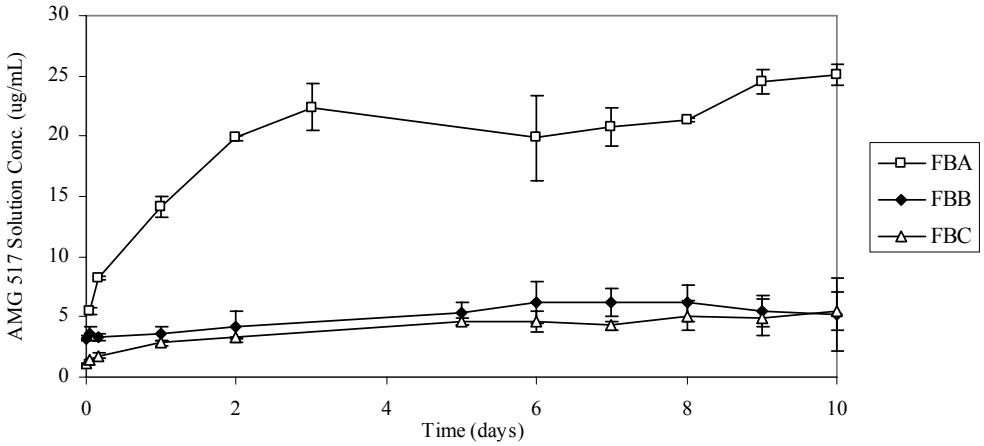

Figure 4.6. AMG 517 solution concentration in FaSIF over ten days.

Also, **FBA** and **FBB** samples remain their original solid form as determined by XRPD of the isolated solids. **FBC**, which appears to be a mixture of **FBC** and **FBB** to start, converts purely to **FBC** after 10 days in FaSIF (see appendix for XRPD spectra). Based on solubility alone crystallization of the cocrystals to the least soluble forms, **FBB** and **FBC**, would be expected however, **FBB** has been shown to be the thermodynamically *less* stable form and *monotropically* related to **FBA** by slurry conversion experiments, van't Hoff plot of solubility at different temperatures and modulated DSC**.** Co-slurry of **FBA** and **FBB** in acetonitrlie at 30˚C or ethanol and toluene at 30˚C and 50˚C all crystallize to **FBA**. Surry of **FBB** alone at 30, 40 and 50˚C in toluene also crystallized to **FBA**. Solubility of the two forms in toluene plotted against 1/T results in parallel lines (figure 4.7) with **FBA** preserving lower solubility.

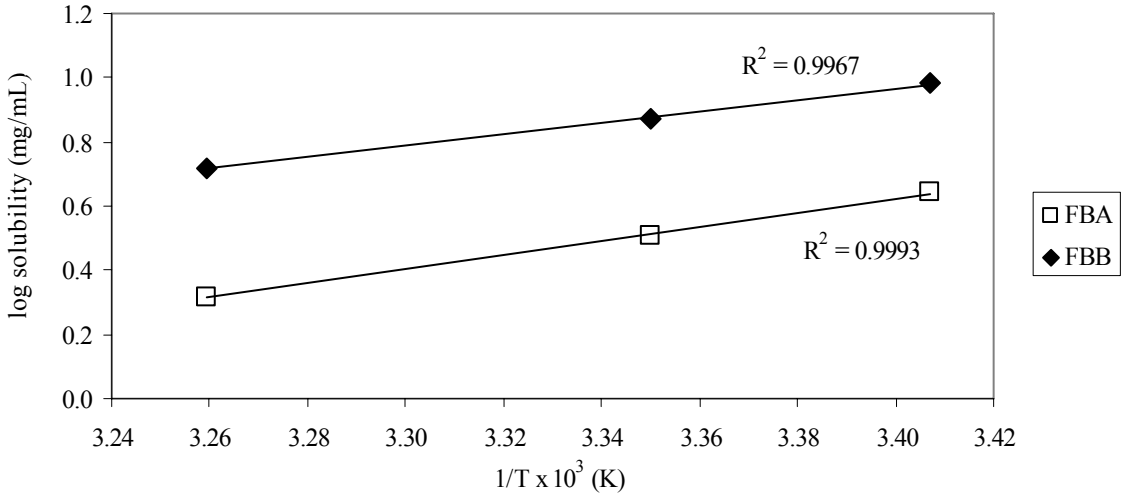

Figure 4.7. van't Hoff plot of **FBA** and **FBB** solubility in toluene.

On DSC **FBC** dehydrates and then recrystallizes to **FBB** when heated to ~175˚C. **FBB** has a broad melt and recrystallization (185-191˚C) to **FBA** which melts at 228˚C on DSC. Modulated DSC was used to determine the heat of fusion of **FBA** (110 J/g) and **FBB** (3 J/g). Based on the definition of a monotropic system the less soluble form on the van't Hoff plot when lines are parallel and the form on DSC with both the highest melt and heat of fusion is the stable form at all temperatures.[13] **FBA** should be more stable than **FBB** at all temperatures as determined by these methods, however in FaSIF at room temperature **FBB** did not convert to **FBA** after ten days and the cocrystals tend to crystallize to **FBB** or **FBC** rather than **FBA**. Based on the Ostwald Rule of Stages the appearance of the thermodynamically less stable form from solution would be expected to appear first, however recrystallization to the thermodynamically stable form should follow.[14] The crystallization of **FBB** was likely a kinetic event and presents an interesting twist to the interpretation of the pharmacokinetic data as there is no way of knowing if the same occurs *in vivo* in the study design used here. Further study utilizing

techniques to measure real time transformation of the phases in a variety of media or a flow through dissolution system may provide more insight as to why **FBB** is present and if this is what occurs *in vivo*.

A linear regression analysis to determine the slope of the initial dissolution rate proved ineffective due to the limited number of data points (2-3) before the C_{max} is reached, therefore the concentration of AMG 517 in solution at 15 min is utilized as a point of comparison. All of the cocrystals provide an increase in dissolution ranging from 3.4-11.0 fold over the free base (table 4.2). This increase is statistically significant for all cocrystals ($p < 0.001$). Cocrystals **BZD**, **GUA**, **GYA**, **HXA**, **MOA** and **MIA** rapidly approach and maintain a high concentration of AMG 517 from 15-45 min while the other cocrystals are either slow to reach a similar C_{max} (**ADA, BZA, CND, HCA, LCA, MEA, SRA, SCA**) or maintain a low C_{max} throughout the 24 h experiment (**CNA**, **HBA**). After 4 hr the AMG 517 solution concentration is similar for all samples (6 - 13 μg/mL) including **FBA** at 8 μg/mL, however after 24 hr **FBA** continues to dissolve reaching 19 μg/mL while the cocrystals remain at 5-11 μg/mL (with the exception of **HCA** at 16 μg/mL which is the only cocrystal to show evidence of crystallization to **FBA** form).

To ensure that the improved dissolution was due to the complex and not simply due to the presence of the carboxylic acid or amide a single control experiment was conducted. A side by side dissolution study with the free base in FaSIF or in FaSIF with 1 mg/mL sorbic acid added to the media was performed. The concentration of sorbic acid added to the FaSIF media was chosen to be in excess of the concentration of sorbic acid which would have resulted if all of the cocrystal **SRA** were to dissolve in the dissolution

experiment. The dissolution profiles of the free base in either media were approximately identical (figure 4.8) indicating that the fast dissolution of cocrystal **SRA** is due to the properties of the solid complex.

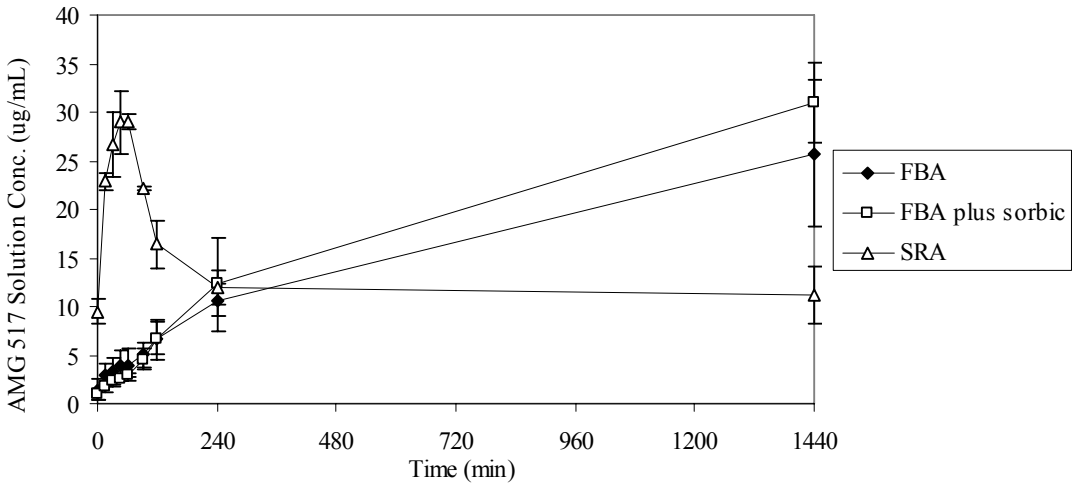

Figure 4.8. AMG 517 solution concentration in FaSIF with or without sorbic acid additive compared to **SRA**.

Cocrystallization of AMG 517 with the carboxylic acids or amides resulted in a significant increase in the initial dissolution rate of the powders compared to **FBA** in FaSIF for all cocrystals. Even though the increase is transient ending in lower solution concentrations after 24 hr as compared to **FBA**, the high initial solution concentrations may provide the desired increase in exposure in the rat pharmacokinetic studies.

Intrinsic Dissolution

As a compliment to the powder dissolution studies, intrinsic dissolution was also conducted in FaSIF. Intrinsic dissolution was a more controlled study in that the temperature is held constant, particle size is no longer considered a major influential factor due to the consistent surface area of the compact when using the woods apparatus

and the amount of solution removed through sampling over time is accounted for in the calculations. This method however may be less representative of the suspension formulation *in vivo* due to the difference in surface area.

The amount dissolved at time t (S_t) was calculated as follows:

$$S_t = (C_t V_t) + D_t$$

where C_t is the solution concentration at time t, V_t is the total volume of FaSIF remaining at time t and D_t is the cumulative amount of drug removed from the system at time t.

Table 4.3. Summary of intrinsic dissolution analysis for **FBA** and the cocrystals.

initial form	IDR[a] (mg/cm^2/min)	final form[b]
FBA	0.0006 ± 0.0002	**FBA**
ADA	0.0007 ± 0.0003	**ADA**
BZA	0.0012 ± 0.0002	**BZA**, minor **FBA**
BZD	0.0014 ± 0.0002	**BZD**, minor **FBA**
CNA	0.0010 ± 0.0002	**CNA**
CND	0.0013 ± 0.0002	**CND**
HBA	0.0010 ± 0.0002	**HBA**
GUA	0.0016 ± 0.0001	**GUA**, minor **FBA**
GYA	0.0014 ± 0.0001	**GYA**
HXA	0.0015 ± 0.0002	**HXA**
HCA	0.0017 ± 0.0003	**HCA**[c], minor **FBA**
LCA	0.0010 ± 0.0002	**LCA**
MEA	0.0013 ± 0.0001	**MEA**
MIA	0.0014 ± 0.0002	**MIA**, minor **FBA**
MOA	0.0016 ± 0.0002	**MOA**
SRA	0.0011 ± 0.0003	**SRA**, minor **FBA**
SCA	0.0011 ± 0.0003	**SCA**

a) IDR determined from 0-30min if FaSIF b) analysis of the compact surface by XRPD and NIR post intrinsic dissolution c) differences noted in NIR of **HCA** post compaction, pre dissolution.

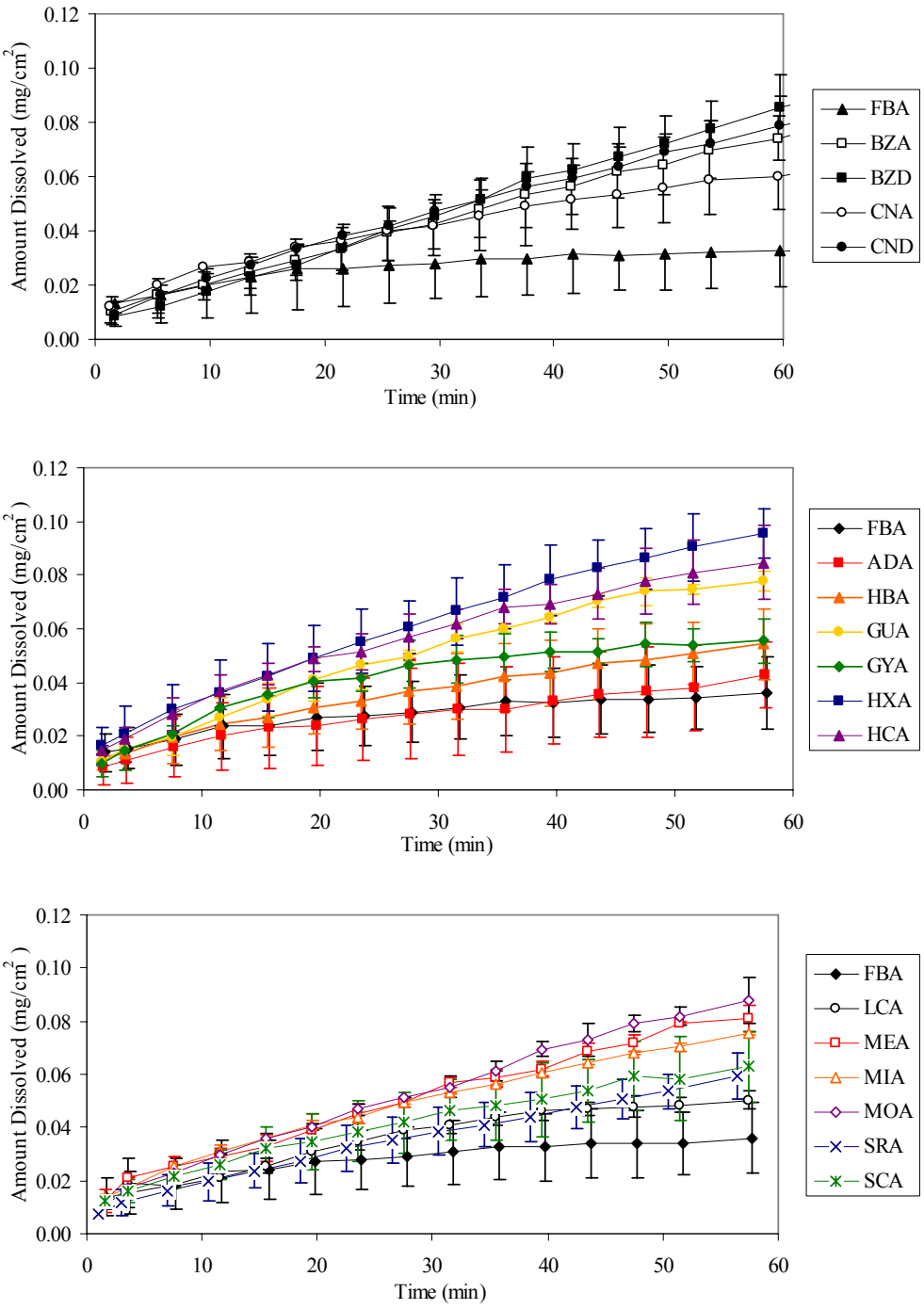

Figure 4.9. Intrinsic dissolution profiles at 60 min of **FBA** and the cocrystals.

The intrinsic dissolution rate in mg/cm^2/min (IDR) was determined from the slope of the linear regression line when S_t divided by the surface area was plotted against time t from

0-30min. The IDR of **FBA** and the cocrystals are listed in table 4.3 and the dissolution profiles are shown in figure 4.9. All cocrystals except **ADA** significantly ($p \leq 0.013$) improve the IDR of **FBA** by 1.7 – 2.9 fold.

The IDR is expected to correlate well with the powder dissolution data assuming that particle sizes between forms were similar and early time points were used to avoid the effects from phase transformation over time. The graph in figure 4.10 comparing the two methods indicates that the correlation of the powder and intrinsic dissolution by linear regression was very poor ($R^2 = 0.390$).

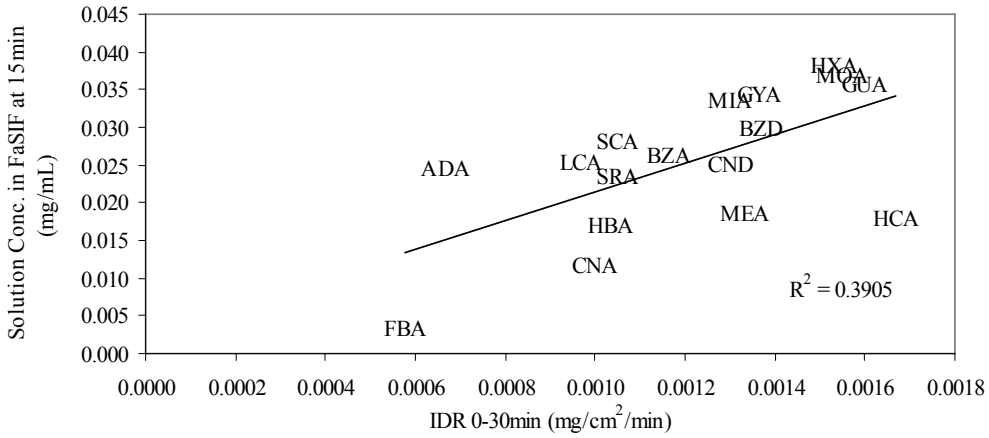

Figure 4.10. Correlation analysis of powder and intrinsic dissolution data

Cocrystal **HCA** stands out as having a very high IDR, but a very low concentration in solution at 15 min in the powder dissolution study. This may be partially due to the larger particle size of this cocrystal which would decrease the surface area exposed to the media in the powder dissolution study therefore slowing the initial dissolution rate. The particle size would not affect the intrinsic dissolution study since the woods apparatus maintains a constant surface area of 0.5 cm^2. More realistically the difference between powder and intrinsic dissolution rates for **HCA** is likely due to compaction. **HCA** was

the only cocrystal which required a higher compression pressure (3000psi instead of 2000psi) in order to produce a smooth surface in the woods apparatus for the IDR study. The surface of the compacts were analyzed by NIR after compaction and compared to the original powder. A clear change in form was detected by NIR of the 1901 and 2220nm peaks due to compaction (appendix). This form change may have influenced the intrinsic dissolution rate of this cocrystal. If **HCA** is removed from the correlation between the two dissolution methods the relationship greatly improves ($R^2 = 0.598$) but is still not remarkable. **ADA** also stands out in the correlation although due to a low intrinsic dissolution rate as compared to its behavior in the powder dissolution study. There is no evidence of any phase transformations of **ADA** due to compaction or even post intrinsic dissolution by XRPD and NIR and its particle size distribution does not stand out from any of the other cocrystal forms as being particularly small. Therefore any explanation of the inconsistency would be conjecture, although it is worth mentioning that the relationship between powder and intrinsic dissolution for the remaining cocrystals and **FBA** is far superior ($R^2 = 0.7289$). Nonetheless, the overall discrepancies between the two methods in general likely arose due to the dissimilarity in exposed surface area to the media and the kinetics of phase transformations occurring in both conditions.

The intrinsic dissolution curves became non-linear after only ~30-60 min when a maximum of 0.1% of the total weight has dissolved. Form conversion to a crystalline material with slower dissolution may have taken place on the surface of the compact causing the diminished dissolution rate. Analysis of the compact surface post dissolution by XRPD and NIR indicate cocrystals **BZA**, **BZD, GUA**, **MIA**, **MOA** and **SRA** crystallize minor **FBA** on the surface. **FBA** has a characteristic N-H combination region

peak at 2064 nm on NIR (appendix). Based on the available single crystal structures this NH-N hydrogen bond between molecules of **FBA** is replaced by an OH-N hydrogen bond with the carboxylic acid of cocrystals **BZA**, **GUA** and **SRA**. Therefore the growth of this characteristic peak in the analysis of the compact surfaces post dissolution indicates crystallization of the **FBA** on the surface. Crystal structure of **MIA** and **MOA** were not available, however the same changes occur on NIR indicating similar circumstances are possible. For the **BZD** cocrystal the NIR also points toward a slight change in the 2064 nm region although not as dramatic as the carboxylic acids. The crystal structure was not available but based on the **CND** crystal structure (and other published amide cocrystals[3] with AMG 517) it is likely that one of the amine protons forms a hydrogen bond with the benzothiazole nitrogen of AMG 517. This slight change combined with characteristic peaks of **FBA** in the X-ray powder pattern provide evidence of minor **FBA** on the surface of this compact at the end of the dissolution study. For all other cocrystals a phase change was not apparent. Based on experience in the *powder* dissolution experiments where crystallization of free form was identified for all cocrystals, it was possible that form conversion was also occurring here but the extent is below the limits of detection for the methods utilized. Another possible rationalization for the decreased dissolution rate over time was that the tests were not performed under sink conditions where the total volume of dissolution media should exceed that required to dissolve all of the test material or be continuously replenished. In nonsink conditions dissolution would be slowed as the drug is not efficiently removed from the receptor phase. Nonsink conditions were likely more representative of *in vivo* conditions in the rat

based on a gut volume of only 11.3mL[15] and is thus a more appropriate environment for the *in vitro* testing to build a correlation.

Similar to the powder dissolution results the intrinsic dissolution rates of all cocrystals (except ADA) were significantly improved over **FBA**. The linear correlation between the two methods is only moderate. Though, if intrinsic dissolution were the only method utilized to filter the cocrystals to be tested *in vivo* in a drug development paradigm (as opposed to powder dissolution), the selection would have likely been similar. **HCA** is the only cocrystal with a high IDR that would have been eliminated based on slow powder dissolution, however due to the changes in form during processing in preparation for the intrinsic dissolution study; **HCA** would likely have been removed from further consideration at any rate. The decision to use one or the other technique (or both) would likely be made based on its similarity to the dosage form or simply the available supply.

Pharmacokinetics

Formulation Development

As mentioned in the introduction, **FBA** and **SRA** were previously dosed in rats using a formulation containing OraPlus®. The same formulation could not be used for the pharmacokinetic evaluation here for multiple reasons. OraPlus® contains sorbic acid as a preservative. Therefore some of the free form (and possibly other cocrystals) will convert to the **SRA** with the existing sorbic acid in the formulation which would influence the exposure of the dose due to the higher dissolution rate of the **SRA** over the

FBA. OraPlus® is also a suspension itself. The solids in this suspension would greatly interfere with the interpretation of the analysis of the stability of the solid form of **FBA** and the cocrystals in the formulation. For these main reasons a new formulation was desired. A simple powder in capsule formulation was considered, but concerns about the poor wetability of the powders leading to very slow dissolution *in vivo*, reduced absorption and possibly undetectable levels of AMG 517 in the plasma lead to the design of a suspension formulation. The suspending vehicle was designed for dual purpose; to stabilize the cocrystal form from conversion or changes in particle size for 24 hr (to allow for preparation of the dose the day before dosing) and to maintain consistent solubility across all compounds, if possible. High solubility was not a goal of the formulation since the intent of this study was not to affect exposure through formulation, but through co-crystallization. Also, in order to physically stabilize the cocrystals in the suspension they need to have a lower solubility than the free forms in the vehicle.

From previous experience with **SRA**, a 2% Pluronic® F108 in water formulation stabilized the cocrystal in suspension, therefore all other cocrystals were tested in this vehicle at 10 mg/mL. Seven of the cocrystals were not physically stable after only one hour as determined by XRPD of the isolated solids (table 4.4).

Table 4.4 Formulation development summary

Compound	Vehicle	pH	solution concentration (μg/mL)	physical stability
FBA	2% Pluronic F108 in water	6.00	8.4	stable 1hr
ADA	2% Pluronic F108 in water	4.28	1.4	stable 1hr
HBA	2% Pluronic F108 in water	3.17	2.2	stable 1hr
GUA	2% Pluronic F108 in water	2.98	13.5	not stable 1hr
GYA	2% Pluronic F108 in water	2.76	2.9	not stable 1hr
HXA	2% Pluronic F108 in water	4.06	0.7	stable 1hr
HCA	2% Pluronic F108 in water	2.98	12.8	not stable 1hr
LCA	2% Pluronic F108 in water	2.83	6.5	not stable 1hr
MEA	2% Pluronic F108 in water	2.48	3.1	not stable 1hr
MIA	2% Pluronic F108 in water	2.90	4.0	not stable 1hr
MOA	2% Pluronic F108 in water	2.36	2.7	not stable 1hr
SRA	2% Pluronic F108 in water	4.38	2.3	stable 1hr
SCA	2% Pluronic F108 in water	3.60	0.3	stable 1hr
HCA	2% Pluronic F108 in 100mM PB pH 6.8	6.67	63.6	not stable 1hr
HCA	1% HPMC 1% Pluronic 50mM PB pH 6.8	6.68	69.7	amorphous 1hr
HCA	2% HPMC 1% Pluronic 20% HP-β-CD	3.99	217.5	amorphous 1hr
HCA	2% HPMC 1% polysorbate 80 in water	2.98	95.1	not stable 1hr
HCA	2% HPMC in water	3.35	41.4	not stable 1hr
HCA	10% HP-β-CD in water	3.66	355.9	stable 24hr
HCA	20% HP-β-CD in water	4.18	1132.0	stable 24hr
HCA	1% Methylcellulose in water	3.57	5.1	stable 24hr
HCA	0.5% MC 1% polysorbate 80 in water	2.93	85.8	not stable 1hr
FBA	1% PVP K25 in water	4.67	7.2	stable 24 hr
ADA	1% PVP K25 in water	4.42	3.2	stable 24 hr
BZA	1% PVP K25 in water	4.57	1.3	stable 24 hr
BZD	1% PVP K25 in water	4.70	3.3	stable 24 hr
CNA	1% PVP K25 in water	4.53	0.9	stable 24 hr
CND	1% PVP K25 in water	4.96	1.4	stable 24 hr
HBA	1% PVP K25 in water	3.36	0.6	stable 24 hr
GUA	1% PVP K25 in water	3.74	1.3	stable 24 hr
GYA	1% PVP K25 in water	3.13	1.4	not stable 24 hr
HXA	1% PVP K25 in water	4.49	1.7	stable 24 hr
HCA	1% PVP K25 in water	3.53	1.2	stable 24 hr
LCA	1% PVP K25 in water	3.52	1.0	stable 24 hr
MEA	1% PVP K25 in water	3.56	1.8	stable 24 hr
MIA	1% PVP K25 in water	3.70	1.5	stable 24 hr
MOA	1% PVP K25 in water	3.47	1.1	stable 24 hr
SRA	1% PVP K25 in water	4.48	1.7	stable 24 hr
SCA	1% PVP K25 in water	3.92	1.7	stable 24 hr

Solution concentrations of AMG 517 for the stable cocrystals in this vehicle ranged from 0.3 – 2.3 μg/mL which was lower than the solution concentration of **FBA** at 8.4 μg/mL

after one hour. Solution concentrations of the unstable cocrystals ranged from 2.7 – 13.5 μg/mL. Since an unknown amount of dissociation to the free form had occurred these values may not be directly interpreted. Instability was also accompanied by a drop in the pH to below 3 indicating dissociation of the carboxylic acid into the solution. To investigate if the dissociation could be slowed by maintaining the pH above 3 **HCA** and **LCA** were tested for stability in 2% Pluronic® F108 in 100 mM phosphate buffer pH 6.8. Within one hour, although the pH was stable, both cocrystals dissociated indicating that the drop in pH was a consequence of the physical instability rather than the cause of instability.

The **HCA** cocrystal was then tested in a series of other vehicles containing hydroxypropyl methylcellulose (HPMC), methylcellulose (MC), hydroxypropyl-β-cyclodextrin (HP-β-CD), polysorbate 80, polyvinylpyrrolidone (PVP) K25 and combinations thereof (table 4). The cocrystal was found to be physically stabilized by 10% or 20% HP-β-CD in water; however the solution concentration after 24 hr was very high at 0.355 and 1.132 mg/mL respectively. **HCA** was also physically stable in 1% MC after 24 hr with a solution concentration of only 4 μg/mL although the formulation proved difficult to prepare due to the hydrophobicity of the powder rendering it very difficult to wet. In order to improve the wetting of the powder a 0.5% MC and 1% polysorbate 80 in water vehicle was tested. The powder was indeed easier to wet but **HCA** was no longer physically stable with an increased solution concentration to 77 μg/mL.

The vehicle 1% PVP K25 in water provided physical stability and a low solution concentration of **HCA** after 24 hr and also made it easier to wet the powder than the 1%

MC vehicle. Therefore the remaining cocrystals and the **FBA** were then tested in this vehicle. All cocrystals were found to be physically stable by XRPD for 24 hr with the exception of **GYA** which showed some minor dissociation to **FBA** after 24 hr. This cocrystal was formulated within two hours of dosing to minimize the conversion. Solution concentrations after three hours of AMG 517 in the 1% PVP K25 in water formulations ranged from 0.6-3.3 µg/mL for the cocrystals while FBA was higher at 7.2 µg/mL (table 4.4). 1% PVP K25 in water was therefore selected as the formulation vehicle for *in vivo* studies because it provided a formulation with physical stability, a narrow range of solubilities across all compounds and wettability.

In Vivo Study: Formulation Preparation and Analysis

The cocrystals and **FBA** were formulated as suspensions in 1% PVP K25 in water at 100 mg/kg (10 mg/mL) the day prior to dosing (except **GLY** which was prepared within 2 hr of dosing). The dosing suspensions were all analyzed within 2 hr post dose to ensure consistency of the solids in form and particle size and to measure the solution concentration of AMG 517 (data summarized in table 4.5, XRPD data compiled in the appendix). A few outliers were seen in the data. Cocrystal **MEA** is the only formulation which has higher solubility than the free base in this vehicle. This may have increased the plasma concentrations of this cocrystal in the animals (see discussion below) however no overall correlation with solution concentration of AMG 517 in the vehicle and exposure is seen.

Table 4.5. Formulation analysis of AMG 517 and cocrystals.

initial form	pH [a]	total conc. [b] (mg/mL)	sol. conc. [c] (μg/mL)	particle size [d] d_{50} (μm)	final form
FBA	4.3	9.7 ± 0.2	14.8 ± 0.0	1.49 ± 0.01	**FBA**
ADA	4.1	11.7 ± 0.0	0.6 ± 0.1	2.55 ± 0.09	**ADA**
BZA	4.0	11.0 ± 0.5	1.2 ± 0.2	1.85 ± 0.05	**BZA**
BZD	4.2	10.2 ± 0.1	5.7 ± 0.3	1.96 ± 0.05	**BZD**
CNA	4.2	9.9 ± 0.5	0.5 ± 0.1	7.96 ± 0.10	**CNA**
CND	4.0	9.9 ± 0.1	2.4 ± 0.3	2.70 ± 0.03	**CND**
HBA	3.4	10.2 ± 0.0	3.4 ± 0.0	2.52 ± 0.23	**HBA**
GUA	4.1	9.6 ± 0.3	3.0 ± 0.2	3.65 ± 0.21	**GUA**, minor **FBC**
GYA	3.3	10.0 ± 0.2	4.0 ± 0.4	3.05 ± 0.07	**GYA**
HXA	4.0	9.8 ± 0.1	1.5 ± 0.2	4.20 ± 0.11	**HXA**
HCA	3.5	10.3 ± 0.1	6.4 ± 0.5	4.16 ± 0.06	**HCA**
LCA	3.0	9.7 ± 0.1	1.6 ± 0.5	19.95 ± 0.11	**LCA**, significant amorphous
MEA	3.3	10.1 ± 0.2	24.3 ± 0.6	3.29 ± 0.01	**MEA**
MIA	3.5	9.5 ± 0.2	9.3 ± 0.3	2.25 ± 0.02	**MIA**
MOA	3.3	9.9 ± 0.1	4.8 ± 0.3	2.65 ± 0.03	**MOA**
SRA	4.4	9.9 ± 0.1	5.8 ± 0.1	1.75 ± 0.01	**SRA**
SCA	3.8	9.9 ± 0.0	0.7 ± 0.1	2.85 ± 0.03	**SCA**

(a) pH measured pre-dose, (b) total concentration of AMG 517 measure pre-dose, (c) solution concentration of AMG 517 measured within 2 hr post dose and (d) mean particle size of formulation measured within 2 hr post dose.

Cocrystal **LCA** possesses an unexpectedly large mean particle size based on the particle size of the starting powder. The particle size increase is due to partial conversion of this cocrystal to an amorphous form, as seen by a halo and broadened peaks in the XRPD and loss of birefringence in polarized light microscopy, which then agglomerated in the formulation (see appendix). The pH of this formulation was also low which is an indication that the cocrystal has partially dissociated. The formulations were also

analyzed pre-dose for total AMG 517 concentration to insure that the suspensions were homogeneous and accurately prepared. All formulations were within the target concentration of 10 mg/mL ± 10% with the exception of cocrystal **ADA** which was 17% above the target concentration (table 4.5). Therefore the dose-normalized AUC (DNAUC) was used for all compounds in the data correlations to correct for the actual concentration of AMG 517.

In Vivo Study: Results and Correlations with Dissolution

The pharmacokinetic parameters are listed in table 4.6 and the plasma concentration over time curves are shown in figure 4.11. The plasma concentrations measured for cocrystal **SRA** in this investigation are consistent with historical data when dosed as suspensions in 10% Pluronic® F108 in OraPlus® (C_{max} 13,400 ng/mL and $AUC_{0\text{-}24h}$ 320,000 ng*h/mL[1]) indicating that the 1% PVP K25 in water vehicle did not have a considerable effect on the exposure as intended. The DNAUC is listed in table 9 for both 0-6 hr and 0-24 hr in table 9 since groups **CNA** and **CND** both have one animal for which the time points after 6 or 8 hr are not available. The linear regression analysis of the two DNAUC values correlates very well with R^2 0.9069, the only outlier being **CND** whose $DNAUC_{0\text{-}24\ hr}$ for two animals is high compared to its $DNAUC_{0\text{-}6\ hr}$ for all 3 animals. Due to this discrepancy, the $DNAUC_{0\text{-}6\ hr}$ is used for statistical analysis. All of the cocrystals increased the $DNAUC_{0\text{-}6\ hr}$ 2.3 – 8.1 fold over the free base with 10 out of the 16 (**BZD**, **CND**, **GUA**, **GYA**, **HXA**, **MEA**, **MIA**, **MOA**, **SRA** and **SCA)** resulting in statistically significant increases ($p \leq 0.003$). The cocrystals also reach a higher C_{max} than **FBA** with the same 10 cocrystals above as well as **BZA** qualify as significant increases ($p \leq 0.008$).

Table 4.6. Pharmacokinetic parameters of AMG 517 and cocrystals.

Compound	T_{max}[a] (hr)	C_{max}[b] (ng/mL)	$DNAUC_{0-6hr}$[c] (hr*ng/mL per mg/kg)	$DNAUC_{0-24hr}$[d] (hr*ng/mL per mg/kg)
FBA	4-6	2553 ± 875	116 ± 38	462 ± 169
ADA	6-8	8638 ± 2257	329 ± 101	1454 ± 390
BZA	1-4	13237 ± 5341	543 ± 213	1988 ± 799
BZD	2	16900 ± 3995	789 ± 178	3000 ± 305
CNA	2, 8	5270	268 ± 87	1072
CND	8, 24	16310	623 ± 303	3369
HBA	4-8	11404 ± 3353	485 ± 51	2100 ± 551
GUA	2-8	16167 ± 5864	796 ± 311	2921 ± 848
GYA	1-4	20110 ± 3525	938 ± 190	3444 ± 726
HXA	2-8	13789 ± 4980	606 ± 179	2701 ± 762
HCA	1-2	11618 ± 4827	514 ± 224	1897 ± 775
LCA	2-8	7047 ± 3628	318 ± 155	1311 ± 701
MEA	2-8	18145 ± 5000	810 ± 194	2976 ± 715
MIA	2-8	18416 ± 7053	868 ± 272	3441 ± 1275
MOA	2	19550 ± 6850	894 ± 238	3152 ± 670
SRA	2	19533 ± 1305	882 ± 14	3283 ± 531
SCA	2	16943 ± 2909	777 ± 130	2747 ± 602

(a) Time of plasma maximum concentration, (b) plasma maximum concentration (c) dose normalized plasma area under the curve from 0-6 hr (d) dose normalized plasma area under the curve from 0-24 hr

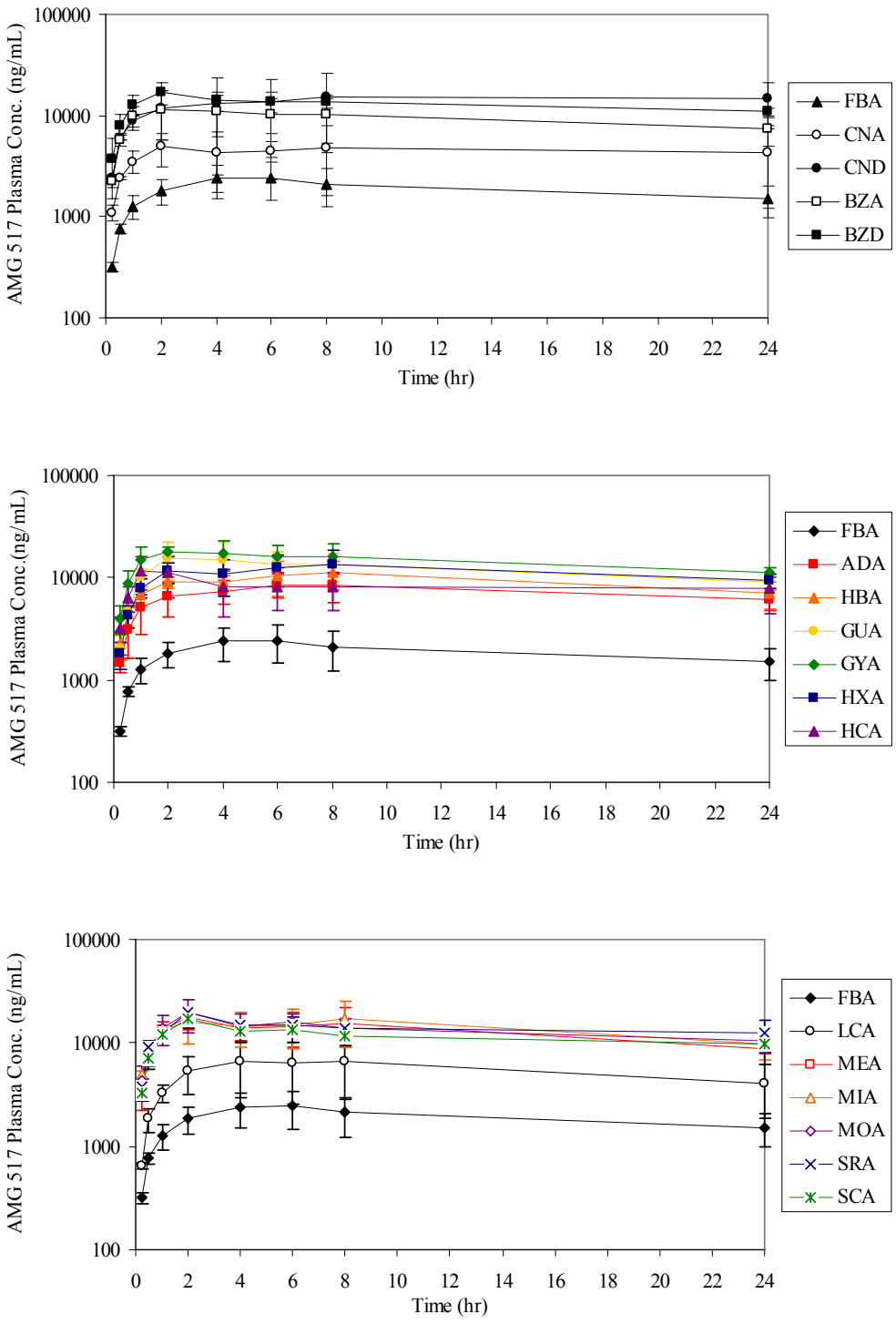

Figure 4.11. AMG 517 plasma concentration over time profiles for **FBA** and the cocrystals.

As discussed in the introduction a correlation between dissolution rate and exposure is expected for the different forms of a poorly soluble molecule such as AMG 517 where faster dissolution, under conditions relevant to the *in vivo* study, provides greater concentrations of drug in the plasma. In general, this holds true here where all AMG 517 cocrystals had a faster IDR and a higher solution concentration at 15 min in FaSIF as well as a higher AUC as compared to **FBA.** **N**evertheless a strong overall linear correlation between powder or intrinsic dissolution rate and exposure was not seen (R^2 0.5065 and 0.4245 respectively). Figure 4.12 shows the linear regression analysis of the two *in vitro* dissolution methods with the $DNAUC_{0\text{-}6hr}$.

Examining the powder dissolution relationship with $DNAUC_{0\text{-}6hr}$, cocrystal **MEA** obtained one of the highest $DNAUC_{0\text{-}6hr}$ even though the concentration at 15min in solution in FaSIF was one of the lowest. As mentioned previously this formulation was the only one with an AMG 517 concentration in solution higher than the free base formulation. This may have provided the higher than expected exposure for this cocrystal. Cocrystal **LCA**, which became partially amorphous and agglomerated in the formulation, has an unexpectedly low $DNAUC_{0\text{-}6hr}$ based on its behavior in the powder dissolution study. The decrease in surface area due to agglomeration may have caused the low $DNAUC_{0\text{-}6hr}$. Deletion of this cocrystal from the correlation as well as cocrystal **MEA** discussed above results in an improved association ($R^2 = 0.6550$).

Examining the intrinsic dissolution relationship with $DNAUC_{0\text{-}6hr}$ it is seen that the IDR of cocrystal **HCA** may be exaggerated as discussed in the intrinsic dissolution section due to excessive compression inducing change to the form as seen by NIR. Elimination of this data point from the IDR and $DNAUC_{0\text{-}6hr}$ comparison greatly

improves the linear relationship (R^2 = 0.5687). Exclusion of cocrystals **LCA** and **MEA** as discussed in relation to the powder dissolution does not have a noteworthy effect on the association of $DNAUC_{0\text{-}6hr}$ with IDR.

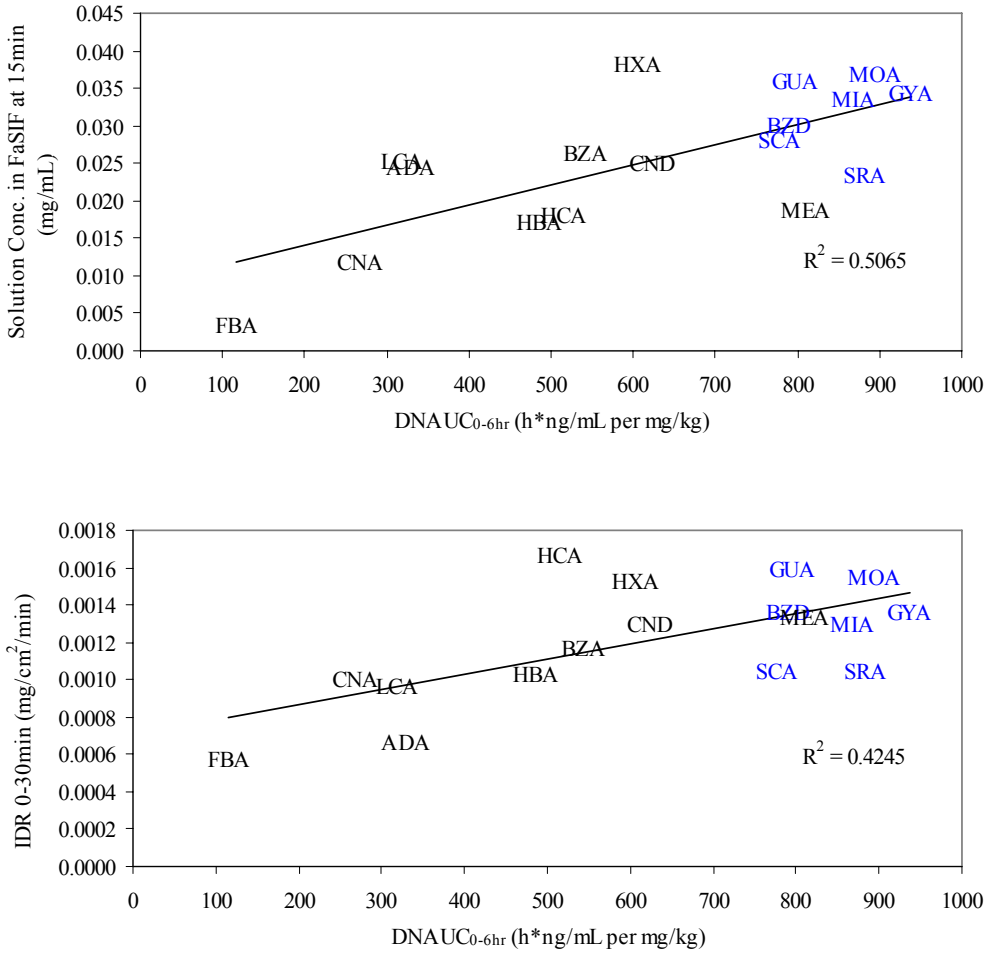

Figure 4.12. Correlation analysis of DNAUC with powder dissolution (top) and intrinsic dissolution (bottom) in FaSIF.

Conclusion

An increase in dissolution rate did lead to improved pharmacokinetics of AMG 517 however a strong *linear* correlation with $DNAUC_{0\text{-}6hr}$ among the 16 cocrystals is not apparent. Even with removing outliers based on the analysis of the formulations only a

moderate correlation was noted with both dissolution techniques although slightly improved for powder dissolution compared to intrinsic dissolution. This was likely due to the similarity of the dosage form (suspension) to the powder dissolution conditions. Other parameters were also investigated in linear regression analysis such as the plasma C_{max} instead of the $DNAUC_{0\text{-}6hr}$ or different time points in the powder dissolution profiles but the correlations were not greatly improved. The lack of a strong *in vitro/in vivo* correlation was not too surprising considering the inherent variability within *in vivo* systems and the power of the study.

What does come from that data and perhaps more relevant in a drug development setting is that one group of seven cocrystals were consistently high performers (highlighted in blue in figure 4.12) with $DNAUC_{0\text{-}6hr} \geq 777$ hr*ng/mL per mg/kg, IDR $\geq$ 0.0011 mg/cm^2/min and powder dissolution solution concentration ≥ 24 µg/mL at 15 min. If the cutoff criteria for a cocrystal to be examined in pharmacokinetic investigations in the rat had been set at a 30 µg/mL solution concentration at 15 min in FaSIF in the powder dissolution study six of the sixteen cocrystals would have continued into PK studies. Three cocrystals with $DNAUC_{0\text{-}6hr} \geq 777$ hr*ng/mL per mg/kg would have been overlooked (**MEA, SRA** and **SCA**), one cocrystal would have performed poorly with a $DNAUC_{0\text{-}6hr}$ of only 606 hr*ng/mL per mg/kg (**HXA**) and five would have performed well as expected with $DNAUC_{0\text{-}6hr} \geq 789$ hr*ng/mL per mg/kg (**BZD, GUA, GYA, MIA** and **MOA**). A similar analysis of the intrinsic dissolution data, dosing the top six cocrystals with IDR $\geq$ 0.0014 mg/cm^2/min in PK studies, would have only encompassed four of the eight cocrystals with high $DNAUC_{0\text{-}6hr} \geq 777$ hr*ng/mL per mg/kg. Most importantly, the two cocrystals with the highest exposures (**GYA** and

MOA) would have been encompassed by both filters thereby allowing for the selection of a single cocrystal form to be developed as a drug product.

References

1. Bak A, Gore A, Yanez E, Stanton M, Tufekcic S, Syed R, Akrami A, Rose M, Surapaneni S, Bostick T, King A, Neervannan S, Ostovic D, Koparkar A 2008. The co-crystal approach to improve the exposure of a water-insoluble compound: AMG 517 sorbic acid co-crystal characterization and pharmacokinetics. J Pharm Sci 97(9):3942-3956.
2. Stanton MK, Bak A 2008. Physicochemical properties of pharmaceutical co-crystals: A case study of ten AMG 517 co-crystals. Cryst Growth Des 8(10):3856-3862.
3. Stanton MK, Tufekcic S, Morgan C, Bak A 2009. Drug substance and former structure property relationships in 15 diverse pharmaceutical co-crystals. Cryst Growth Des 9(3):1344-1352.
4. Morris KR, Fakes MG, Thakur AB, Newman AW, Singh AK, Venit JJ, Spagnuolo CJ, Serajuddin ATM 1994. An integrated approach to the selection of optimal salt form for a new drug candidate. Int J Pharm 105:209-217.
5. Saxena V, Panicucci R, Joshi Y, Garad S 2009. Developability assessment in pharmaceutical industry: an integrated group approach for selecting developable candidates. J Pharm Sci 98(6):1962-1979.
6. Engel GL, Farid NA, Faul MM, Richardson LA, Winneroski LL 2000. Salt form selection and characterization of LY333531 mesylate monohydrate. Int J Pharm 198:239-247.
7. Hirsch CA, Messenger RJ, Brannon JL 1978. Fenoprofen: drug form selection and preformulation stability studies. J Pharm Sci 67(2):231-236.
8. 2001. Guidance for Industry Bioanalytical Method Validation. In USFDA, editor, ed.
9. Kruskal WH, Wallis WA 1952. Use of ranks in one-criterion variance analysis. J Am Stat Assoc 47(260):583-621.
10. Galia E, Nicolaides E, Hörter D, Löbenberg R, Reppas C, Dressman JB 1998. Evaluation of various dissolution media for predicting *in vivo* performance of class I and II drugs. Pharm Res 15(5):698-705.
11. 2006. The Merck Index: An Encyclopedia of Chemicals, Drugs, and Biologicals. fourteenth ed., Whitehouse Station, NJ: Merck & Co., Inc.
12. Cotterill J, Nadian AK, Cowan DP 2004. Improving the persistence of a formulation of the avian repellent cinnamamide, for the protection of autumn-sown oilseed rape. Pest Manag Sci 60(10):1019-1024.
13. Byrn SR, Pfeiffer RR, Stowell JG. 1999. Solid-state chemistry of drugs. second ed., West Lafayette, IN: SSCI, Inc. p 574.
14. Nývlt J 1995. The Ostwald rule of stages. Cryst Res Tech 30(4):443-449.

15. Davies B, Morris T 1993. Physiological parameters in laboratory animals and humans. Pharm Res 10(7):1093-1095.

Chapter 5. Acid and Amide Cocrystal Pairs

Introduction

Screening for pharmaceutical cocrystals of an API in industry is typically restricted to cocrystal formers which have a history of being safe for use in humans (i.e. listed as "generally regarded as safe" by the FDA and found in currently marketed products).[1,2] Due to their known safety profile a product containing these cocrystal formers would be less time consuming and costly to develop. This characteristically leads to a cocrystal screen of only carboxylic acids previously used as salt formers for basic APIs. Arguments have been made that expanding beyond carboxylic acids would provide more variety in hydrogen bonding functional groups to interact with the API resulting in a higher probability of forming a cocrystal as well as more diverse physicochemical properties. An amide in particular, with an additional hydrogen bond donor in comparison to a carboxylic acid, is likely to form a unique hydrogen bonding network resulting in changes to the crystal packing and in turn the physicochemical properties of the compound. A second motivation to screen for a larger variety of cocrystal forms is to protect the intellectual property of an API.

Two case studies of the carboxylic acid cocrystals, **BZA** and **CNA,** and the corresponding amide cocrystals, **BZD** and **CND,** were examined here to see if the differences in crystal packing lead to varied dissolution and pharmacokinetics. Also, the utility of the *in silico* tool of crystal structure analysis as an added layer to form selection in the drug development process is discussed.

Experimental

Powder Dissolution Method

Approximately 30mg of compound was weighed into 20mL glass scintillation vials in triplicate. Then, 10mL of FaSIF (5mM taurocholic acid sodium salt and 1.5 mM lecithin in pH 6.8 phosphate buffer) was added and continually stirred on a magnetic stirrer at room temperature (20-25˚C). At each time point (1, 15, 30, 45, 60, 90, 120, 240 and 1440 min) 0.6 mL was filtered through a 0.45 µ, 13 mm, PTFE syringe filter into an HPLC vial (leaving the first 4 drops to waste). Samples were diluted 3 fold with DMSO to prevent precipitation if needed. Analysis was conducted by HPLC-UV to determine the AMG 517 and cocrystal former (where possible) concentration in solution. After the final time point the suspension was analyzed by laser diffraction and microscopy for particle size determination and then centrifuged 10 min at 13,000 rpm. The surpernatent was discarded and the pellet was air dried for 24 hr then analyzed by XRPD, DSC and TGA to determine the form.

Intrinsic Dissolution Method

Intrinsic dissolution was conducted in a Varian VK 7025 dissolution apparatus (Palo Alto, CA) using a rotating disk apparatus at 37 ˚C at 100 rpm in 500 mL FaSIF for 2 hr (n = 1) and 4 hr (n = 2). Compacts were produced by compressing 100 mg of compound into a die at 2000 psi (3000 psi for cocrystal **HCA**) for 2 min in a carver press (surface area 0.5 cm^2). Compacts were analyzed by NIR pre dissolution to assess form. FaSIF samples (0.7 mL) were withdrawn manually at each time point and filtered through 0.45 µm PTFE syringe filter, leaving 8 drops to waste before collection into an HPLC vial, then analyzed by HPLC-UV at 280 nm for AMG 517 content. Compacts were dried

at room temperature for at least 24 hr then analyzed by NIR and XRPD to assess the form.

Pharmacokinetic Investigation Methods

The animal procedures were conducted under a protocol approved by the Amgen, Inc (Cambridge, MA) Institutional Animal Care and Use Committee. Male Sprague Dawley rats, 300-325 g, were obtained from Charles River Laboratories (Wilmington, MA) with catheters implanted in the femoral artery and vein; the surgical procedures were conducted under aseptic conditions. The rats were housed in a temperature- and humidity-controlled environment subject to a 12 h light:12 h dark cycle and had access to water and a standard laboratory rodent diet *ad libitum*. Animals were allowed to acclimate for one week prior to use. Rats (n=3) were administered a single dose of test material (100 mg/kg) formulated as suspensions in 1% PVP K25 in water by oral gavage. Blood samples were collected from the femoral artery catheter at 0.25, 0.5 1, 2, 4, 6, 8, and 24 h post-dose. Plasma was separated by centrifugation and stored at -80° C until analyzed.

Plasma standards were prepared by serial dilution in male Sprague-Dawley rat plasma with K_2EDTA (Bioreclamation) at 25,000, 12,500, 6,250, 3,125, 1,562, 781, 391, 195 and 98 ng/mL AMG 517. Plasma standards and samples were extracted with a 4x dilution of an internal standard (ISTD) solution (acetonitrile with 0.1 % formic acid and 200 ng/mL AMG 831664[3]) and centrifuged for 20 min at 4 ˚C.

LC/MS-MS analysis of plasma extracts was conducted on an Agilent HPLC-MSD Trap equipped with an APCI probe, Varian Pursuit C18, 30 x 2 mm, 5 µ column and ChemStation software in multiple reaction monitoring (431.1 m/z and 445.1 m/z) mode.

The chromatographic method was isocratic at 45 % acetonitrile in water with 0.1% formic acid at 0.75 mL/min. Integration of the smoothed, extracted ion chromatogram at 389.1 m/z was used for quantitation against the standard curve corrected with the ISTD concentration. Integration of the smoothed, extracted ion chromatogram at 389.1 m/z with the Bruker Daltonics DataAnalysis for LC/MSD Trap software v3.3 was used for quantitation against the standard curve corrected with the ISTD concentration.

Single Crystal: Attachment Energy and Morphology Calculation Methods

Attachment energies and crystal morphologies were calculated using Dreiding force field[4] and Ewald summation[5] with Accelrys Materials Studio® v4.4 (San Diego, CA). The calculated crystal morphology was determined using the attachment energy (AE) method.[6,7] The AE method was based on atom-atom interactions within the crystal. The crystal morphology was determined by calculating the energy released when one layer of the molecular assembly was added to the growing crystal, which was proportional to the growth rate of the crystal face.[7,8] Morphology calculations were compared to the morphology of crystals grown from solution to confirm consistency in crystal shape in order to determine molecular packing within the crystal planes.

Statistical Calculation Methods

Statistical differences between groups were calculated using SigmaStat for Windows version 3.0.1 (SPSS Inc., Chicago, IL) applying a Kruskal-Wallis[9] one-way analysis of variance on ranks (ANOVA) followed by a multiple comparison procedure versus **FBA** (Holm-Sidak method, p value must be lower than the critical value to be considered significant). Student's t-test was used to determine statistical significance between two groups.

Results and Discussion

Powder dissolution profiles of the four cocrystals in FaSIF over time are displayed in figure 5.1. It is clear from this figure that **BZA** and **BZD** have comparable dissolution profiles where both cocrystals reach a similar maximum solution concentration of AMG 517 (S_{max} 30.1 and 30.5 μg/mL respectively) within 15-30 min. In contrast, **CNA** and **CND** have very different dissolution profiles where **CND** reaches S_{max} (26.5 μg/mL) at 30 min and **CNA** dissolves very slowly reaching a similar S_{max} (24.6 μg/mL), but not until 90 min. The spread between the solution concentration of AMG 517 at 15 min between **CNA** and **CND** is statistically significant ($P<0.001$).

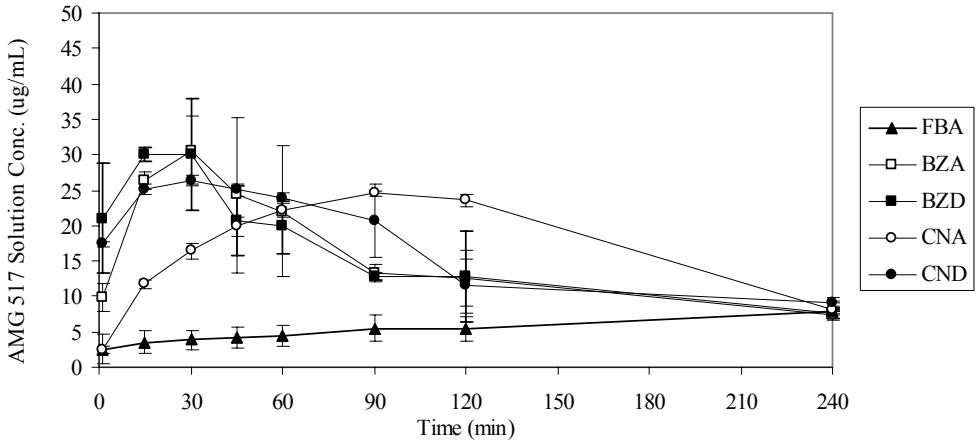

Figure 5.1. Powder dissolution profiles to 240min of **FBA** and the cocrystals.

Intrinsic dissolution rates (IDR) of **BZA**, **BZD**, **CNA** and **CND** (0.0012, 0.0014, 0.0010, 0.0013 mg/cm^2/min respectively) while being significantly higher than the IDR of **FBA** (0.006 mg/cm^2/min, $p \leq 0.012$)), are not significantly different within the acid and amide pairs (**BZA** and **BZD** $p = 0.184$ and **CNA** and **CND** $p = 0.200$). The AMG

517 plasma concentration over time profiles from rat pharmacokinetic investigations are shown in figure 5.2. Visually this data correlates well with the powder dissolution results where the **BZA** and **BZD** cocrystals perform similarly while the **CNA** cocrystal is not absorbed to the same extent as the **CND** cocrystal maintaining a lower plasma concentration throughout the 24 hr study. However no statistical difference exists between the $DNAUC_{0\text{-}6hr}$ of the acid and amide pairs (**BZA** and **BZD** p = 0.291 and **CNA** and **CND** p = 0.123). Over all, the dissolution and pharmacokinetics of **BZA** and **BZD** are very similar while **CND** displays properties superior to those of **CNA** for development of an API.

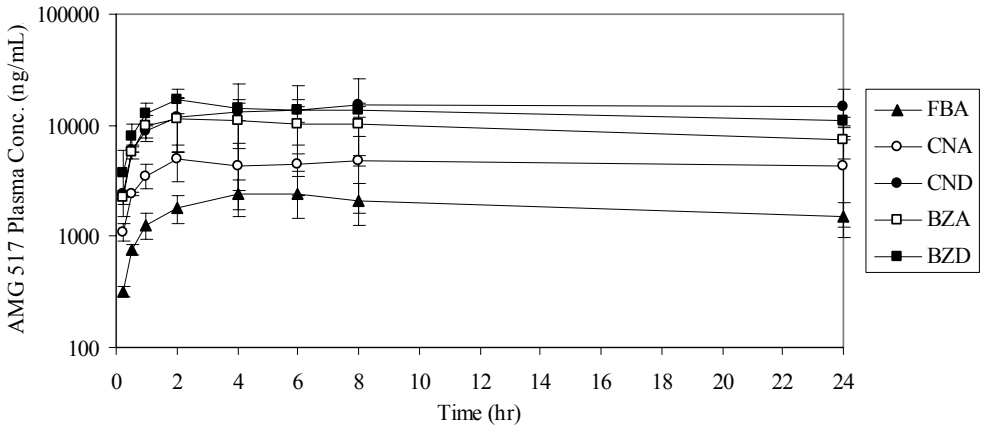

Figure 5.2. AMG 517 plasma concentration over time profiles for **FBA** and the cocrystals.

The crystal structure of **BZD** is unavailable, despite great effort to crystallize a suitable crystal for single crystal structure analysis; consequently the discussion as it relates to crystal structure will utilize only the **CNA** and **CND** acid/amide cocrystal pair with comparisons to **FBA**. The additional hydrogen bond donor on the amide as compared to the carboxylic acid cocrystal former did produce two unique matrices for **CNA** and **CND** as shown in figure 5.3.

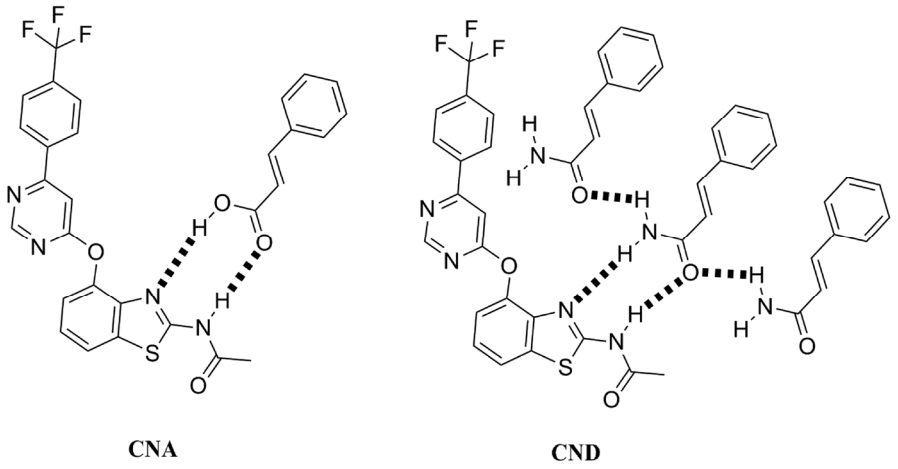

Figure 5.3. Schematic representation of hydrogen bonding in **CNA** and **CND**

The crystal structure of **CNA** consists of hydrogen bonded dimers of AMG 517 and the cocrystal former resulting in a triclinic crystal system and $P\bar{1}$ space group. In contrast to **CNA** the dimers of AMG 517 and cocrystal former in **CND** form continuous chains through the additional hydrogen bond from amide to amide generating a monoclinic crystal system and $C2/c$ space group.

Further *in silico* analysis of the crystal structures may reveal characteristics of the different packing arrangements which could be responsible for the difference in physical properties described above. This type of analysis could be included in the form selection process to predict or explain physical properties of a given crystal form. The attachment energy (E_{att}) or the energy released per mole of layer added to a crystal face is proportional to the growth rate of that face.[10,11] Therefore, crystal faces with a low absolute E_{att} are the slow growing and consequently morphologically significant faces. These crystal faces will have the most contact with the dissolution media and will directly impact the rate at which dissolution occurs depending on the compatibility of the crystal face with the media. The calculated E_{att} of the crystal faces of **FBA**, **CNA** and **CND** are

listed in table 5.1. Overall, the absolute attachment energies of the two faces which make up the most % facet area for **FBA** (1-10 and 001) and **CNA** (011 and 001) are approximately 4 times lower than the faces which make up the largest % facet area for **CND** (200 and 20-2). These two morphologically significant faces comprise 68.6-72.2% of the total surface area of all three crystals, therefore the surface properties of these faces are likely responsible for the bulk physical properties of the powder.

Table 5.1. Calculated attachment energies for **FBA**, **CNA** and **CND**

FBA							
face (hkl)	1 -1 0	0 0 1	1 0 -1	1 0 0	0 1 0	0 1 -1	
% total facet area	46.4%	22.2%	14.0%	10.9%	3.3%	3.2%	
E_{att} total (kcal/mol)	-46.4	-79.7	-89.3	-104.3	-150.7	-116.3	
CNA							
face (hkl)	0 1 1	0 0 1	1 0 1	1 1 1	1 0 0	0 1 0	1 1 0
% total facet area	38.0%	34.2%	17.2%	4.1%	2.5%	2.5%	1.5%
E_{att} total (kcal/mol)	-40.3	-42.9	-70.5	-84.1	-107.2	-70.9	-103.1
CND							
face (hkl)	2 0 0	2 0 -2	0 0 2	1 1 -1	1 1 1	3 1 -1	1 1 -2
% total facet area	37.2%	32.1%	10.7%	10.6%	7.8%	1.5%	0.1%
E_{att} total (kcal/mol)	-169.2	-176.7	-207.4	-397.5	-400.3	-416.7	-412.7

The calculated crystal morphologies of **FBA**, **CNA** and **CND** are shown in figure 5.4 along with photomicrographs of representative crystals of the same polymorph. The calculated morphologies appear to correlate well with the actual crystals. In figure 5.5 a

slice of the two crystal faces with the highest % total facet area for compounds **FBA**, **CNA** and **CND** are shown.

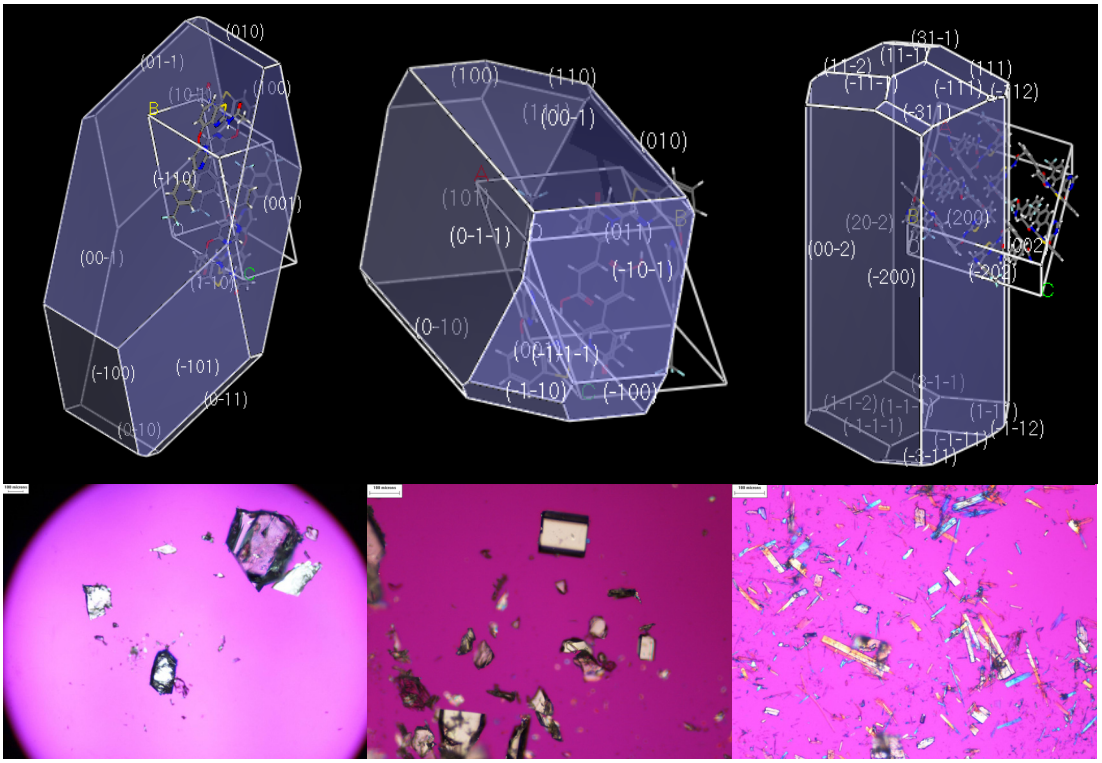

Figure 5.4. Calculated crystal morphology (top) and photomicrographs (bottom) of **FBA** (left), **CNA** (middle) and **CND** (right).

The slice of the (2 0-2) face of **CND** indicates the presence of polar amide groups (green circle in figure 5.5) near the crystal face while the other morphologically significant crystal faces of **FBA**, **CNA** and **CND** contain less polar acetamide, pyrimidine or CF_3 groups. The higher absolute attachment energies of **CND** and the polarity of the significant (2 0-2) face, which would be expected to be more hydrophilic, should provide a stronger interaction with the aqueous environment during the dissolution processes *in vitro* and *in vivo*. This correlates well with the improved dissolution and bioavailability of **CND** over **CNA** and **FBA** seen here.

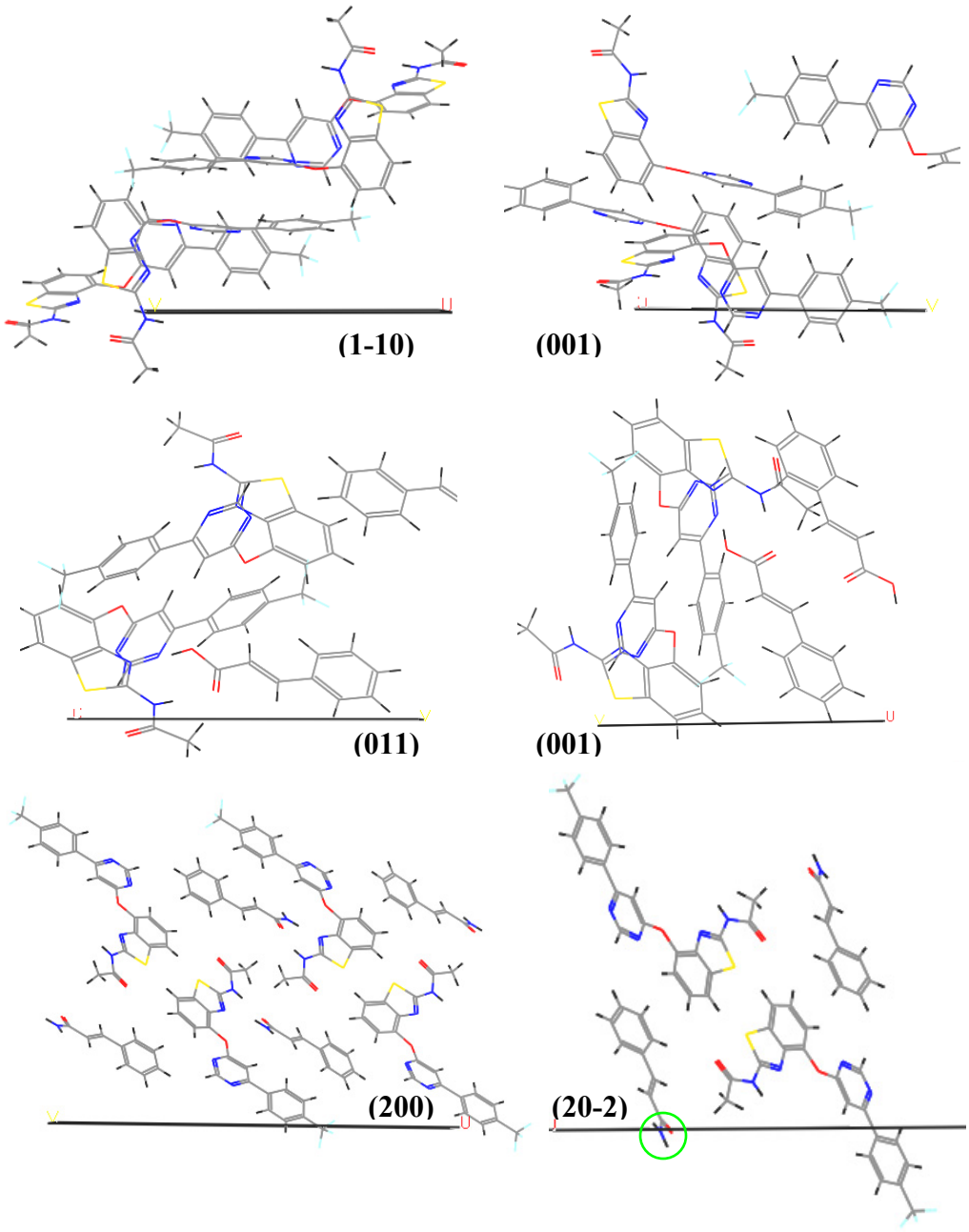

Figure 5.5. Slice through morphologically important crystal faces of **FBA** (top), **CNA** (middle) and **CND** (bottom). Green circle highlighting the amide group on the surface of the (20-2) face of **CND**.

Conclusion

The AMG 517 amide cocrystals displayed unique dissolution and pharmacokinetic properties in only one of the two case studies above. It is clear from the crystal structures of **CNA** and **CND** that the hydrogen bonding of the amide produced a unique packing arrangement to that of the carboxylic acid which has distinctive physical properties. Without the crystal structure of **BZD** it is unknown if a similar difference in hydrogen bonding between **BZD** and **BZA** lead to the opposite result in this case. Although based on the rules derived by Etter[12], all reliable proton donors and acceptors would be used in hydrogen bonding and the amide is classified as a reliable donor. Also, one other AMG 517 amide cocrystal (propionamide)[3] also contained the same hydrogen bonding pattern to that of **CND**. Thus it is likely that the **BZD** hydrogen bonding pattern is at least unique to that of **BZA** if not the same as **CND** and the AMG 517 propionamide cocrystal. If this is the case, the uniqueness of the hydrogen bonding and crystal packing did not produce distinctive dissolution rates for both amide cocrystals. The benefit of expanding the list of cocrystal formers for screening of an API beyond carboxylic acids would likely need to be made on a case by case basis and may way more on protecting intellectual property than improving physical properties.

References

1. Vishweshwar P, McMahon JA, Bis JA, Zaworotko MJ 2006. Pharmaceutical co-crystals. J Pharm Sci 95(3):499-516.
2. Schultheiss N, Newman A 2009. Pharmaceutical cocrystals and their physicochemical properties. Cryst Growth Des 9(6):2950-2967.
3. Stanton MK, Tufekcic S, Morgan C, Bak A 2009. Drug substance and former structure property relationships in 15 diverse pharmaceutical co-crystals. Cryst Growth Des 9(3):1344-1352.

4. Mayo SL, Olafson BD, Goddard III WA 1990. DREIDING: A generic force field for molecular simulations. J Phys Chem 94:8897-8909.
5. Koehl P 2006. Electrostatics calculations: latest methodological advances. Curr Opin Struct Biol 16:142-151.
6. Hartman P, Bennema P 1980. The attachment energy as a habit controlling factor: I. Theoretical considerations. J Cryst Growth 49(1):145-149.
7. Berkovitch-Yellin Z 1985. Toward an ab initio derivation of crystal morphology. J Am Chem Soc 107(26):8239-8253.
8. Hartman P, Bennema P 1980. The attachment energy as a habit controlling factor: I. Theorectical considerations. J Cryst Growth 49(1):145-149.
9. Kruskal WH, Wallis WA 1952. Use of ranks in one-criterion variance analysis. J Am Stat Assoc 47(260):583-621.
10. Davey R, Garside J. 2000. From molecules to crystallizers. ed., New York: Oxford University Press, Inc.
11. Kiang Y-H, Shi HG, Mathre DJ, Xu W, Zhang D, Panmai S 2004. Crystal structure and surface properties of an investigational drug-a case study. Int J Pharm 280:17-26.
12. Etter MC 1990. Encoding and decoding hydrogen-bond patterns of organic compounds. Acc Chem Res 23:120-126.

Chapter 6: Conclusions and Future Considerations

Dissolution testing is a vital and widely accepted *in vitro* tool available to the pharmaceutical chemist when selecting a form of a poorly soluble drug for development in the clinic. Polymorphs or salts with dissolution rates similar to or less than that of the free form are likely not tested further unless they posses some other benefit such as physical stability or processability. The same would hold true here with different cocrystals or polymorphs of cocrystals. The dissolution testing would have likely led to selection of the top 4-6 cocrystals to continue on to *in vivo* studies reducing the number of animal studies required to reach the clinic. As more cocrystal screening for new APIs is conducted and these forms are considered for development dissolution will likely be embedded in the form selection process as it has been for salts, polymorphs or formulations of an API. Other tools utilized in conjunction with *in vitro* studies such as the *in silico* attachment energy calculations conducted here would be a useful addition to the dissolution data especially with single crystal structure determination becoming more accessible, with less expensive bench top X-ray diffractometors and software with more automated analysis.

Having produced a substantial library of crystal structures of AMG 517 hydrates, solvates, cocrystals, polymorphs of these corystals, a cocrystal-hydrate, as well as cocrystals of similar compounds,[36] a detailed look into patterns in crystal packing and conformational energies is essential. Furthermore, any insight these results may reveal into the physical properties such as physical stability, hygroscopicity, dissolution and pharmacokinetics collected thus far is warranted.

The benefit of growing the list of cocrystal formers beyond carboxylic acids to discover a new API form is still up for debate. While an improvement in dissolution and pharmacokinetics was seen here with one amide cocrystal compared to its corresponding acid cocrystal, there were other carboxylic acid cocrystals which performed just as well as the amide cocrystal. Also, it was shown that even cocrystals which hydrogen bond through the same heterosynthon may result in unique crystal packing. Although protecting the intellectual property of an API is clearly vital, what is the utility of a cocrystal produced with a cocrystal former of an unknown or questionable safety profile? It may be that only when no other acceptable salts, polymorphs, cocrystals or formulations of the API can be produced that this option would be considered. Further research and publication of these alternative cocrystals is needed to elucidate the benefit or futility of the effort.

Regardless of the type of cocrystal former, cocrystallization has been shown to be a successful process to improve the dissolution and pharmacokinetics of the poorly soluble API AMG 517. While the overall linear correlation of AUC with dissolution rate of all sixteen AMG 517 cocrystals and the free base form A was only moderate, dissolution testing of the cocrystals, either powder or intrinsic, was also considered valuable in selecting a cocrystal form for study in pharmacokinetic investigations.

Chapter 7. Appendix

The following is a compilation of all X-ray powder diffraction (XRPD), proton nuclear magnetic resonance (^{1}H NMR), differential scanning calorimetry (DSC), thermal gravimetric analysis (TGA), particle size distributions, polarized light microscopy (PLM) and near-infrared spectroscopy (NIR) data for **FBA**, **FBB**, **FBC** and the sixteen cocrystals. XRPD overlay is of the original powder, the solids isolated from powder dissolution, the pellet after intrinsic dissolution and the solids isolated from the formulation. Any changes to the original form post-dissolution or in the formulation are noted. Samples isolated from FaSIF may have a peak at 28.4º 2theta due to the FaSIF component potassium chloride. ^{1}H NMR spectra in DMSO-d_6 of the original powder. DSC and TGA thermograms of the original powder and the solids isolated post-powder dissolution. Any changes to the form are noted. Particle size distributions show an overlay of the original powder, the solids in FaSIF post powder dissolution and the solids in the formulation post dose. Polarized light microscopy photos of the original powder, the solids in FaSIF post powder dissolution and the solids in the formulation post dose. NIR spectra of the original powder in a 20mL glass vial and the compacted powder in the woods apparatus pre and post intrinsic dissolution. Any changes to the original form are noted. The glass vial produced a peak at 1396 nm. **FBB** and **FBC** were not included in all experiments; therefore the data for these forms is limited.

FBA

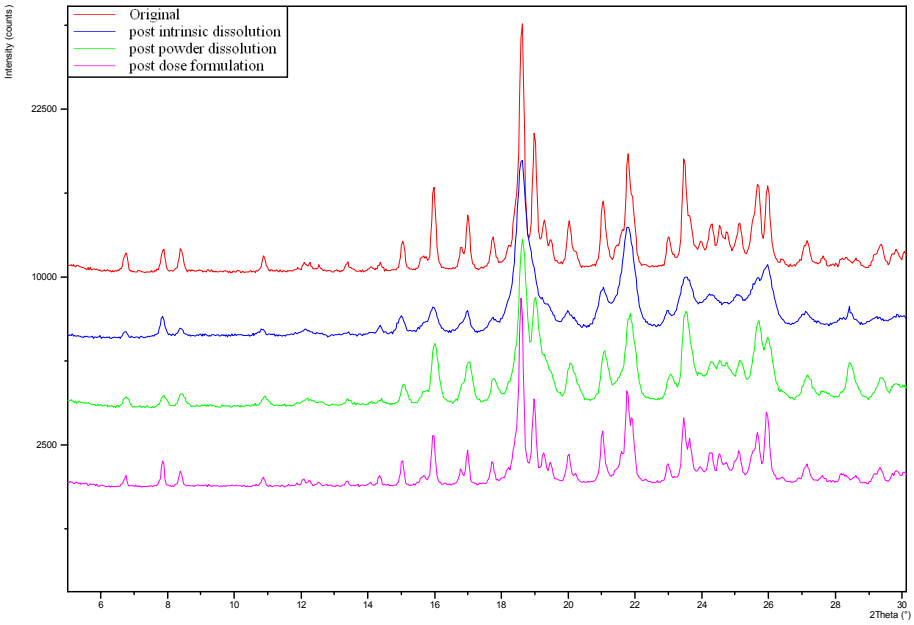

XRPD: No changes to form observed

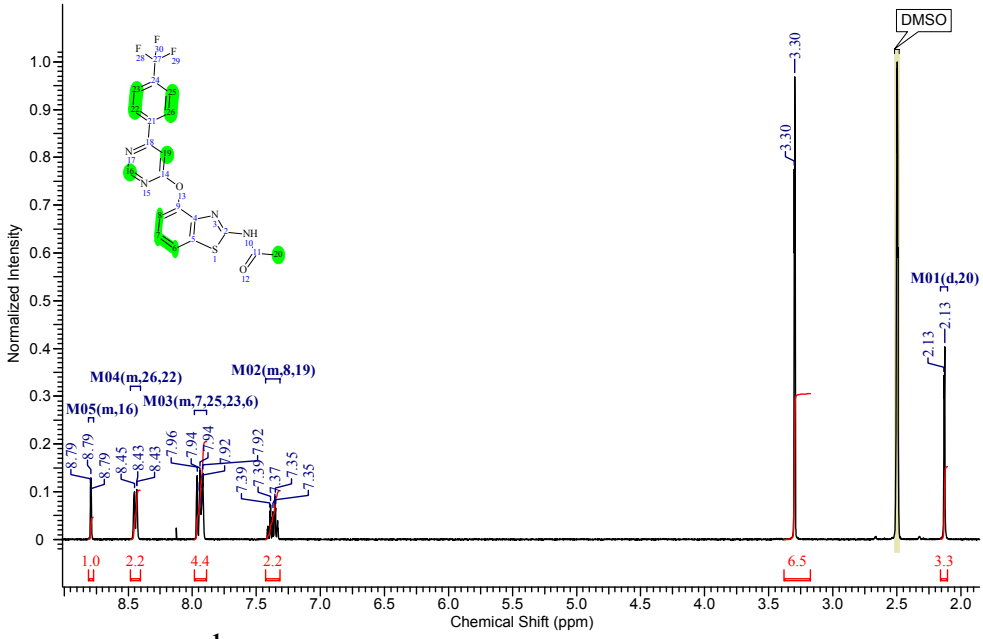

^{1}H NMR: Assignments shown on spectrum

FBA (cont.)

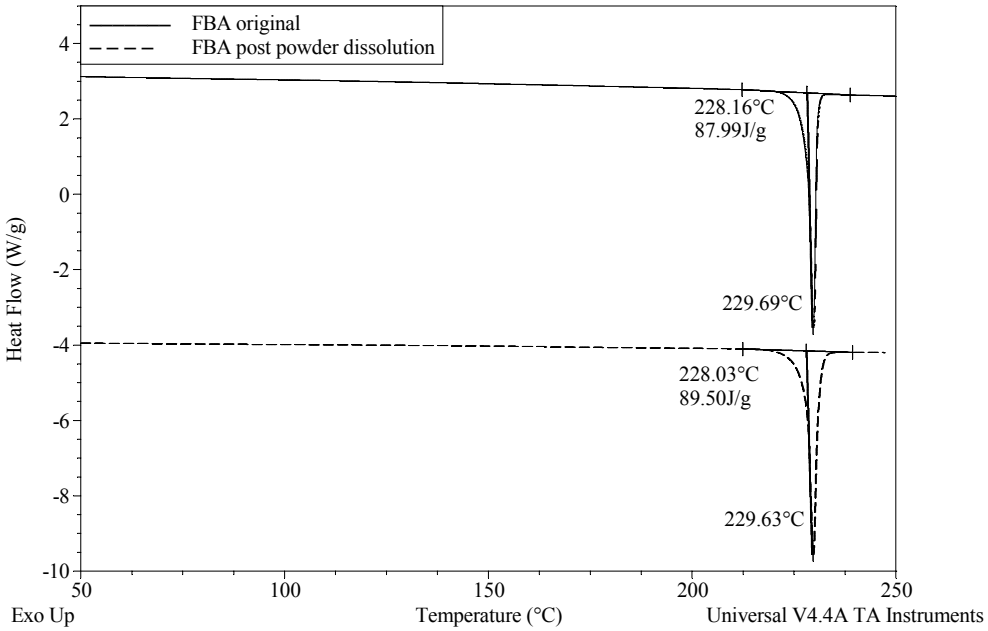

DSC: No changes to form observed

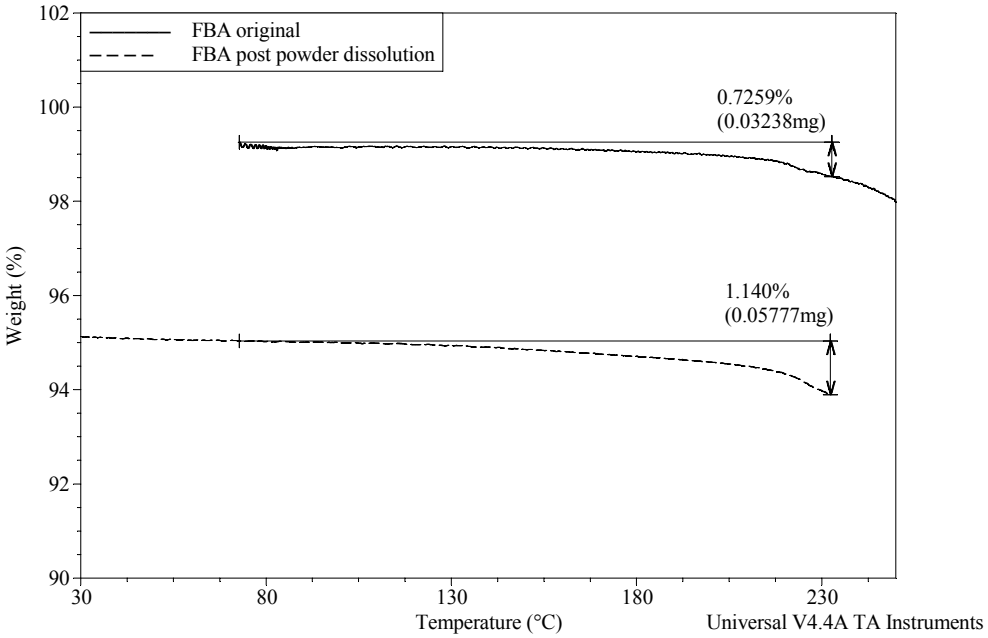

TGA: No changes to form observed

FBA (cont.)

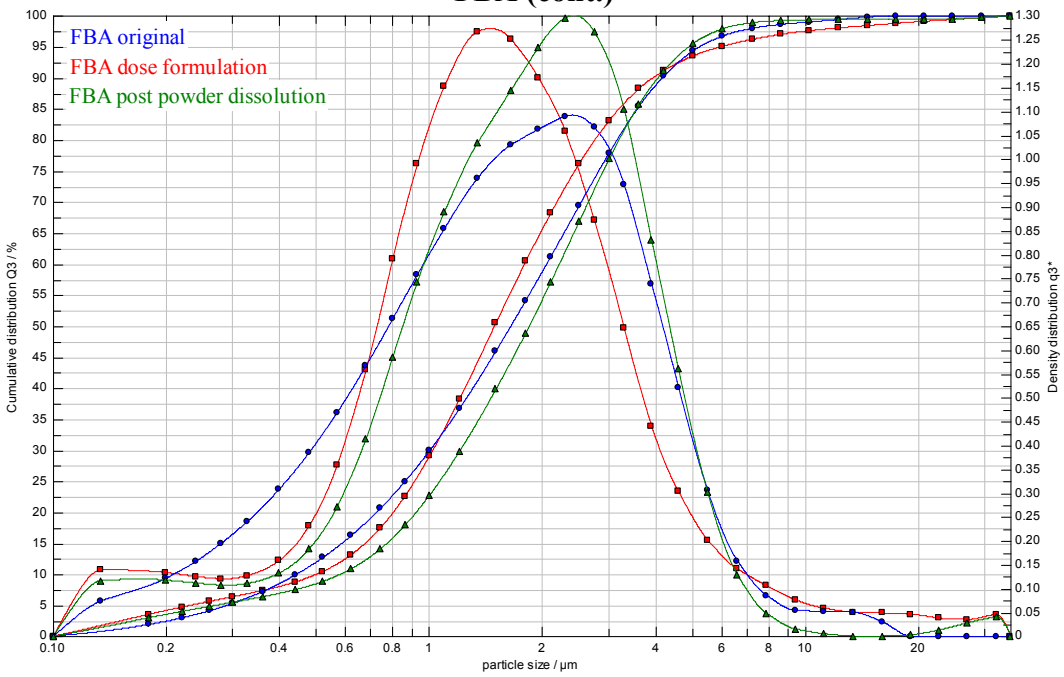

Particle Size Distributions

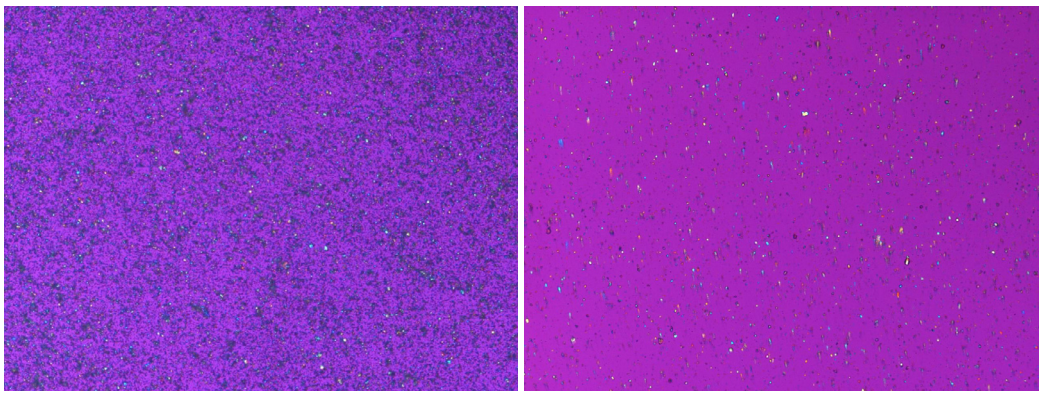

PLM: 200x original powder (left) post powder dissolution (right)

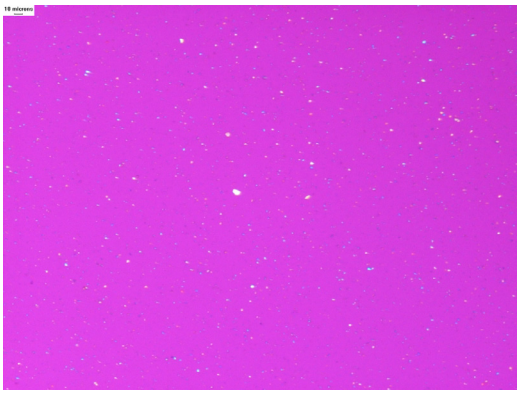

PLM: 200x post dose formulation

FBA (cont.)

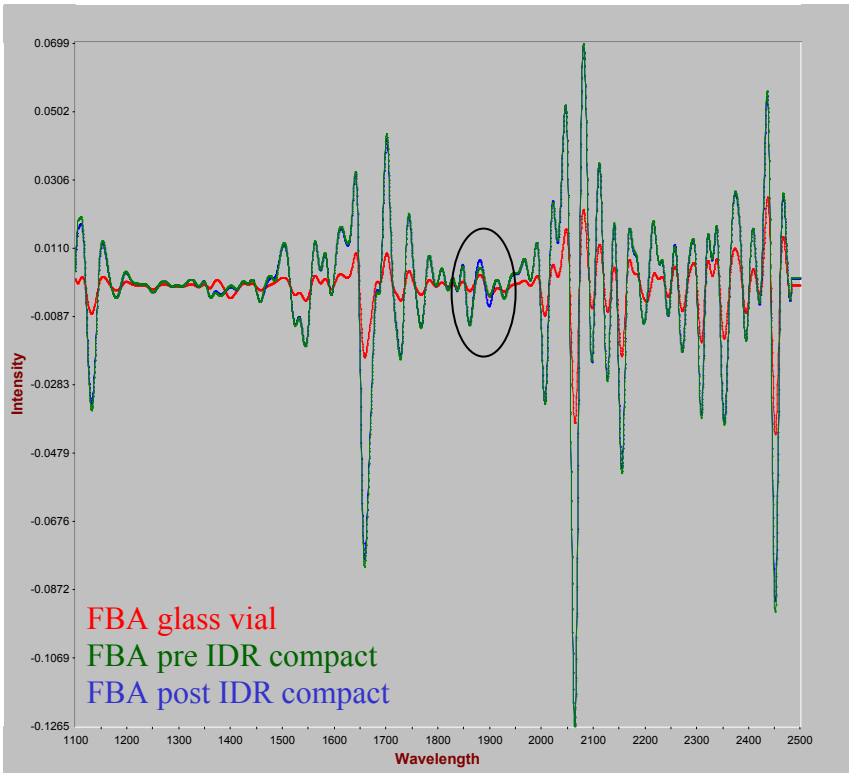

NIR: 1899nm minor change post intrinsic dissolution

FBB

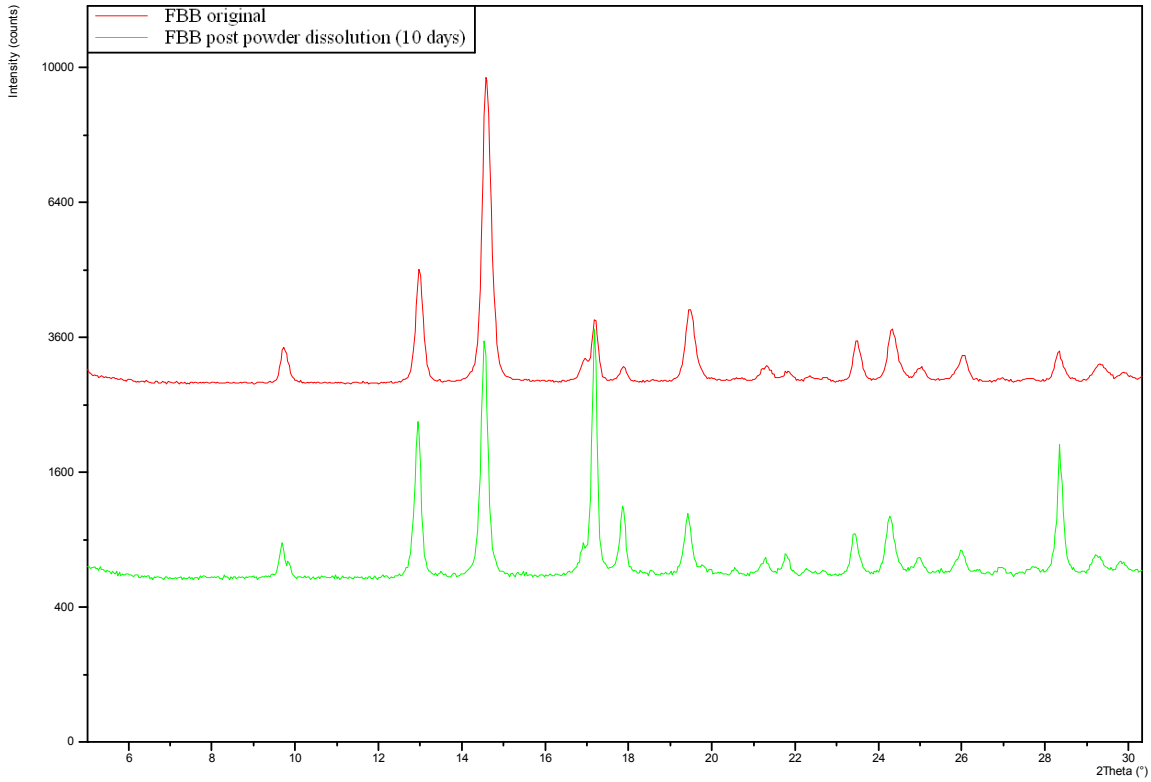

XRPD: No change post powder dissolution

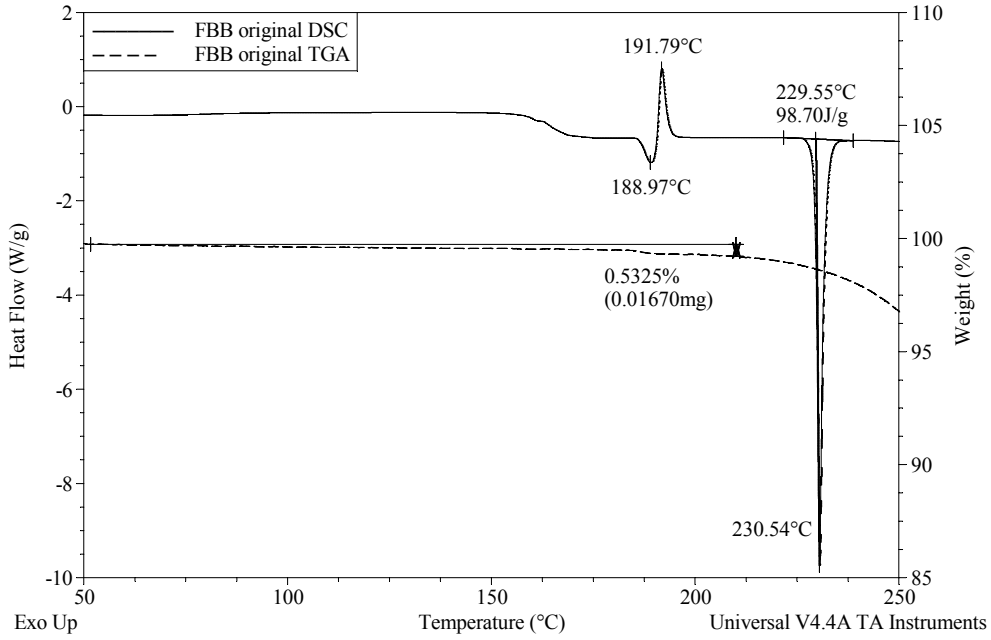

DSC/TGA: Original powder

FBB (cont.)

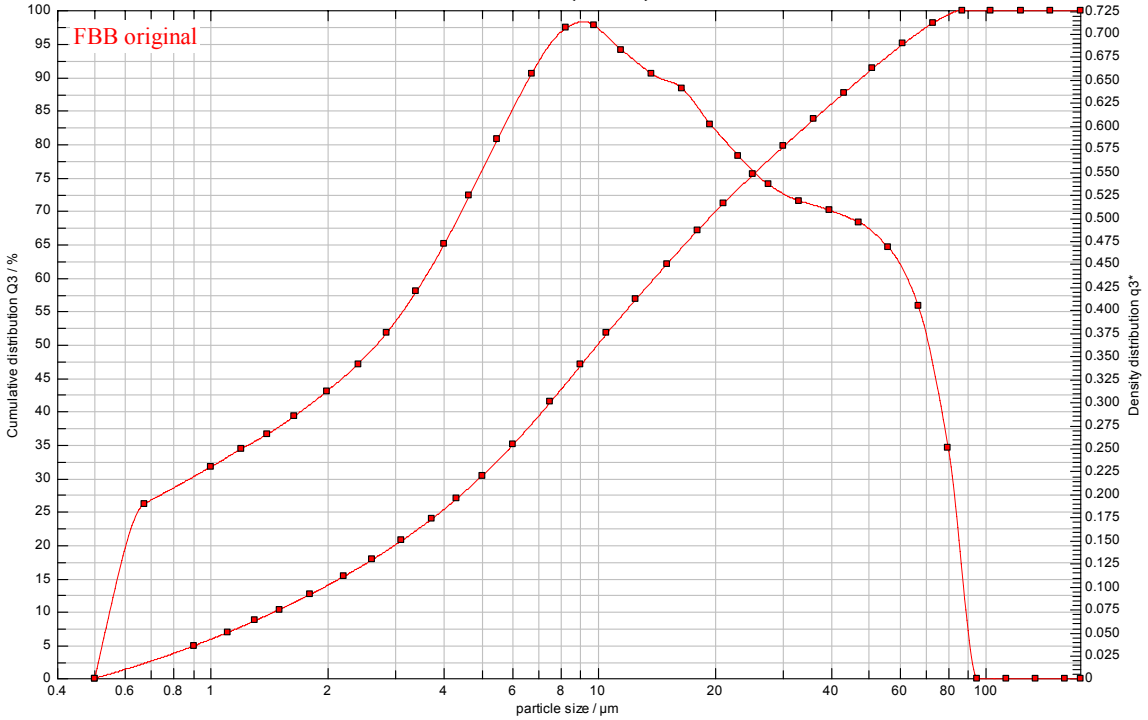

Particle Size Distribution

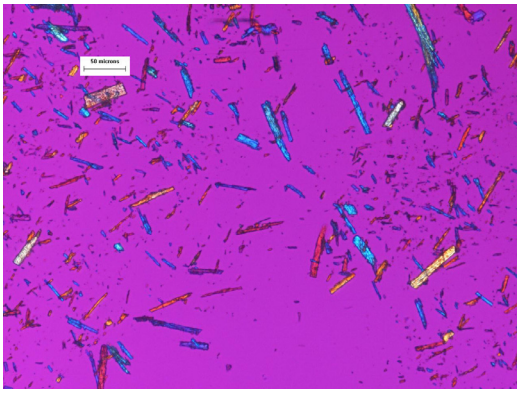

PLM: 200x original powder

FBB (cont.)

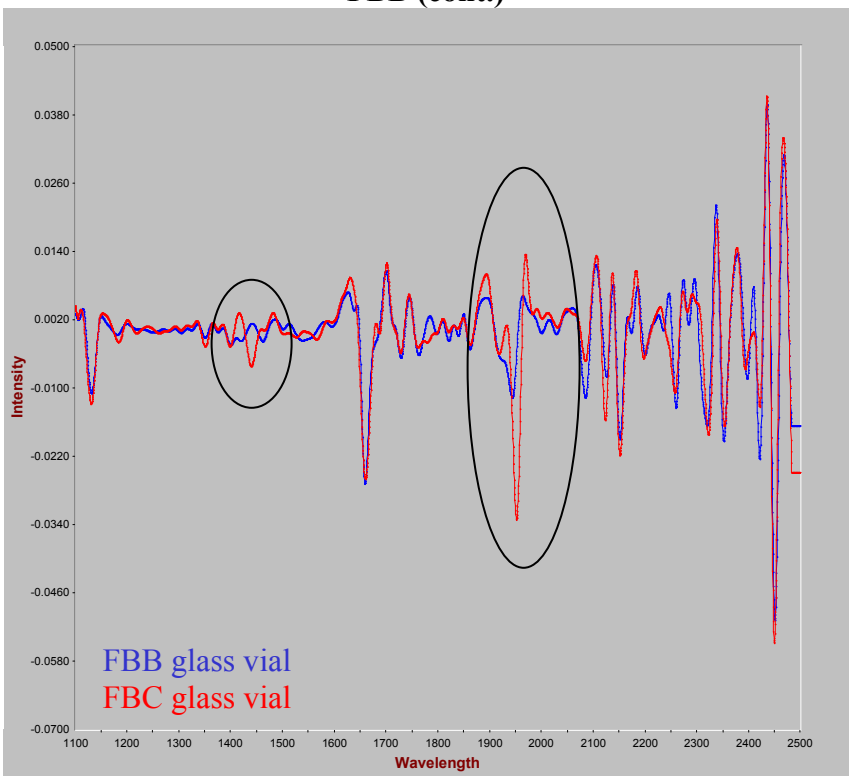

NIR: FBC 1440 and 1953nm (H_2O)

FBC

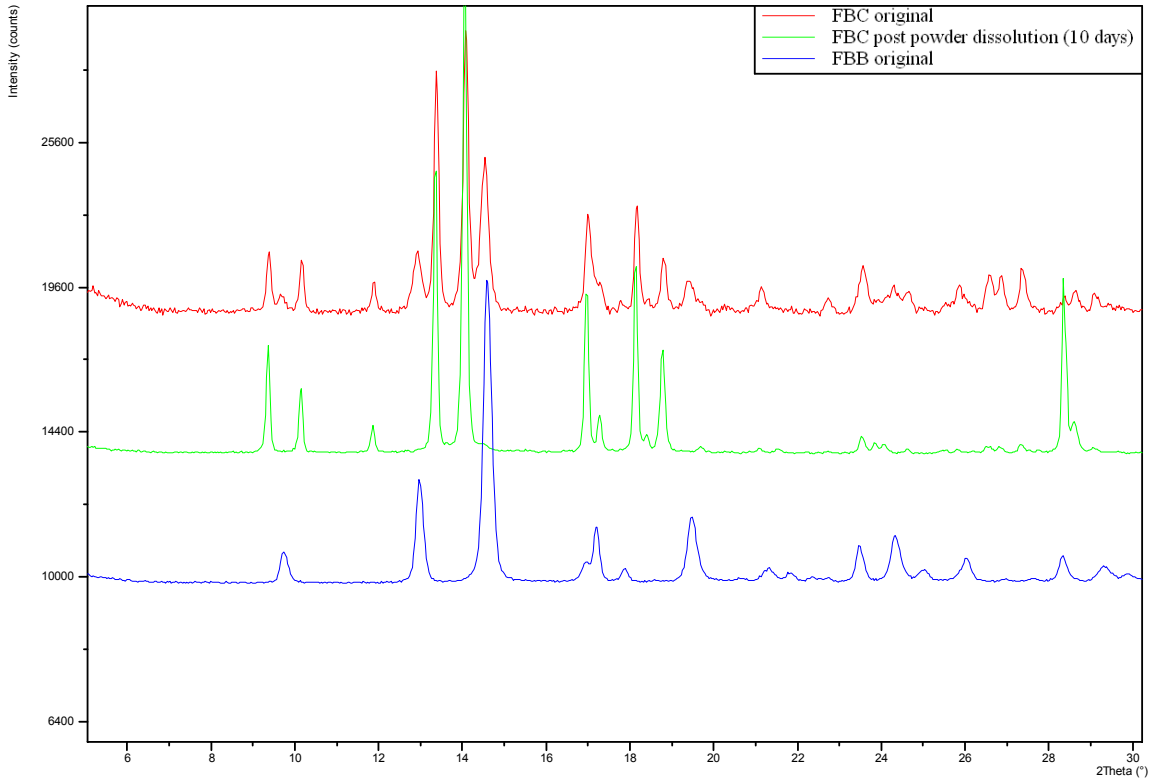

XRPD: FBC of increased purity (no **FBB**) post powder dissolution

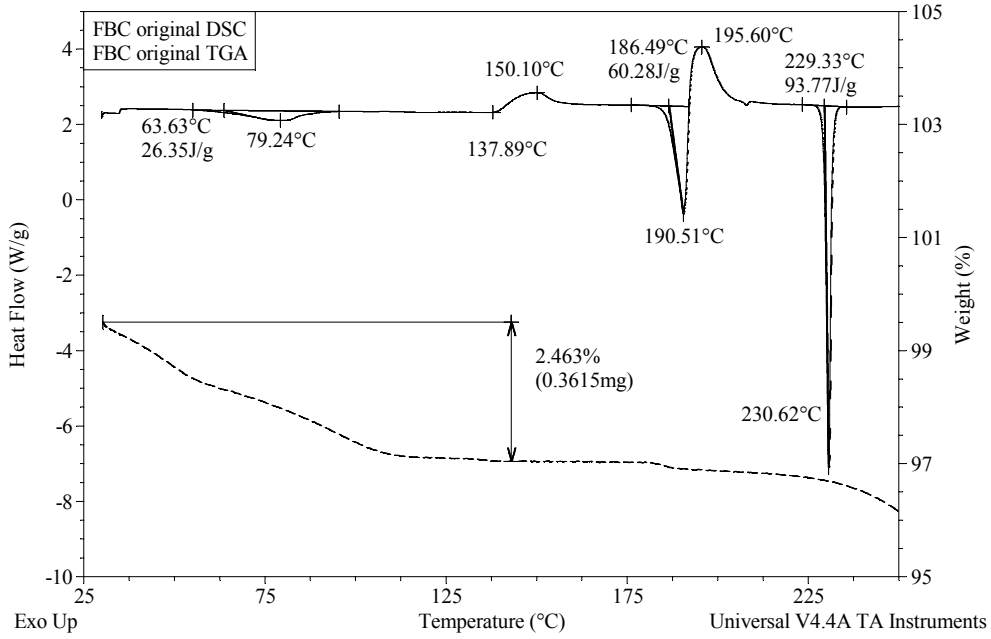

DSC/TGA: Original powder

FBC (cont.)

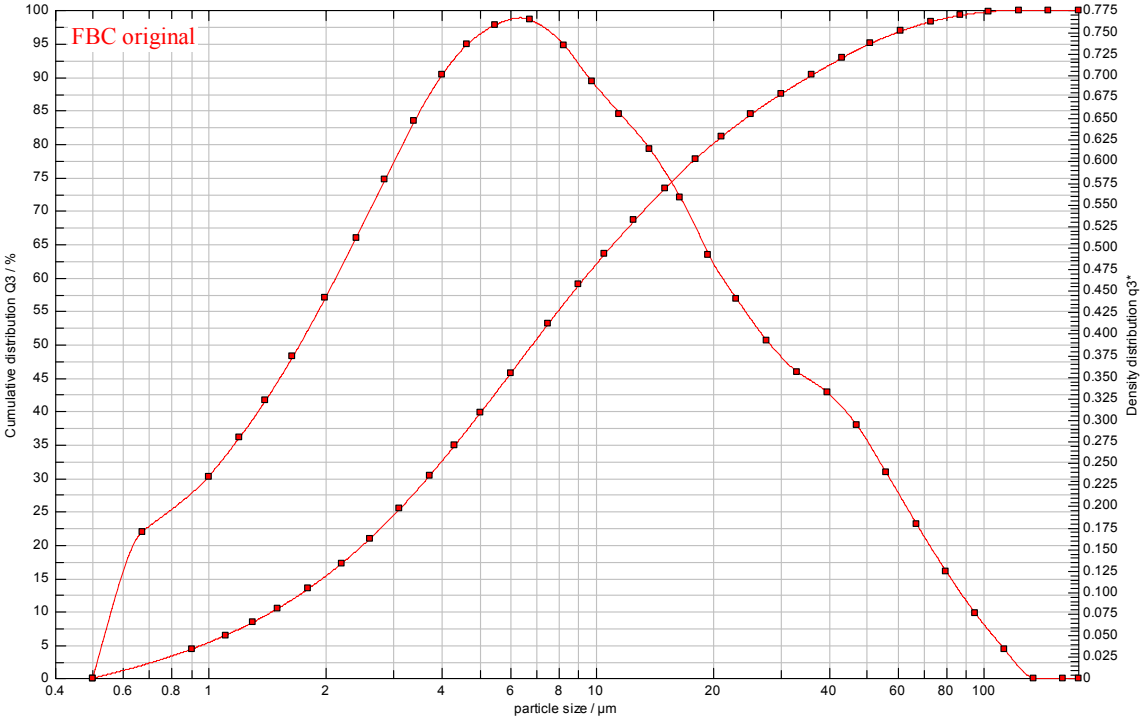

Particle Size Distribution

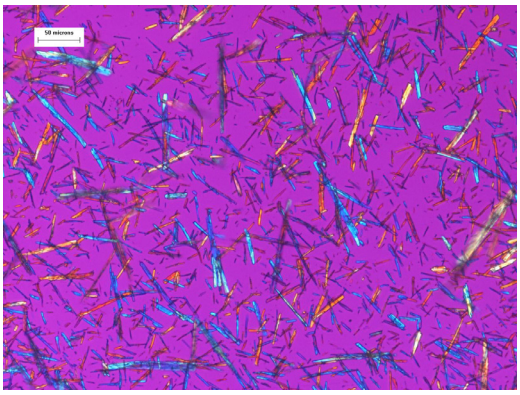

PLM: 200x original powder

FBC (cont.)

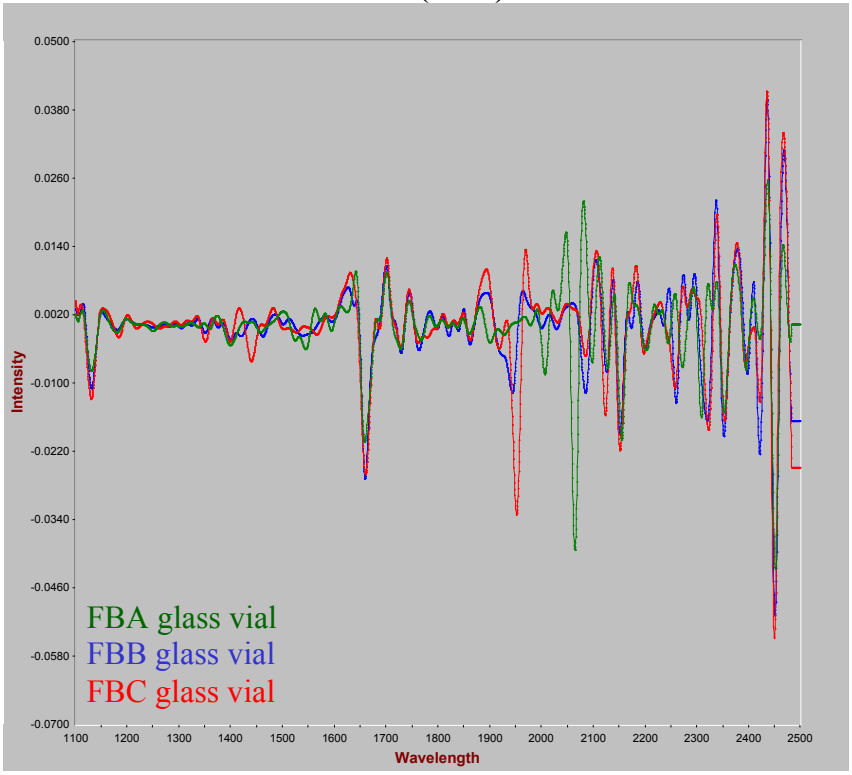

NIR: FBA more unique to **FBB/FBC**

ADA

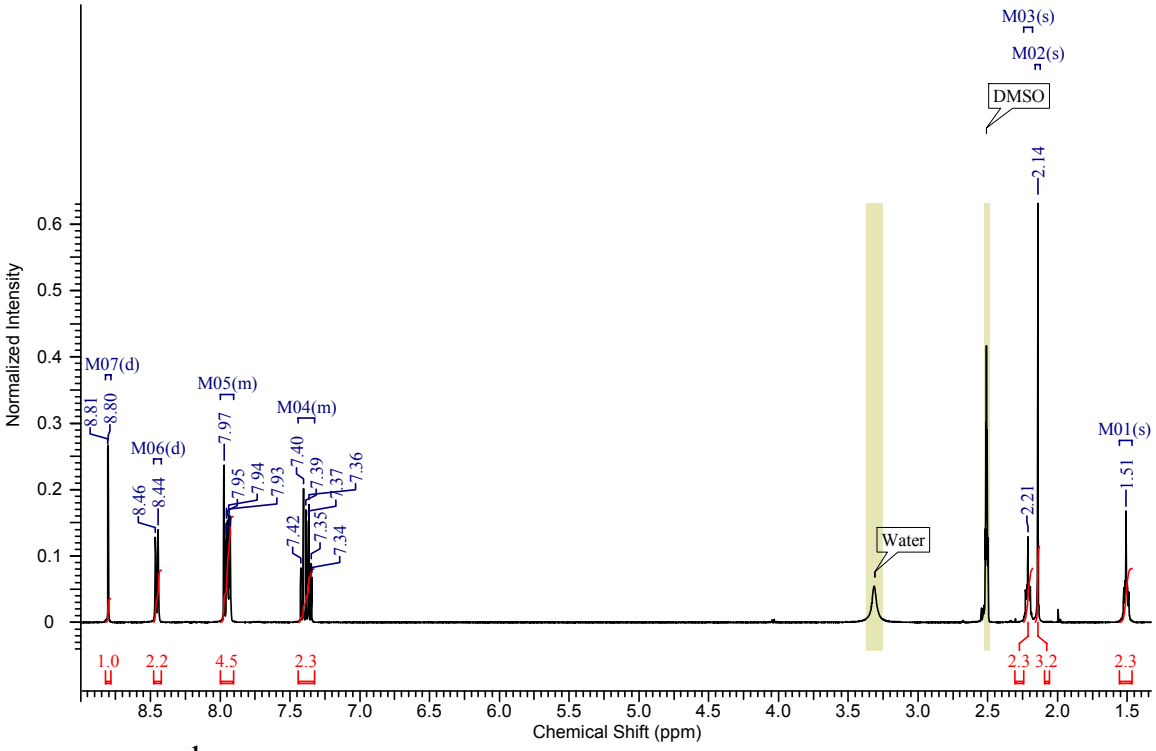

^{1}H NMR: 0.5 eq acid; 2(CH_2) integrate as 1 2.2 and 1.5ppm

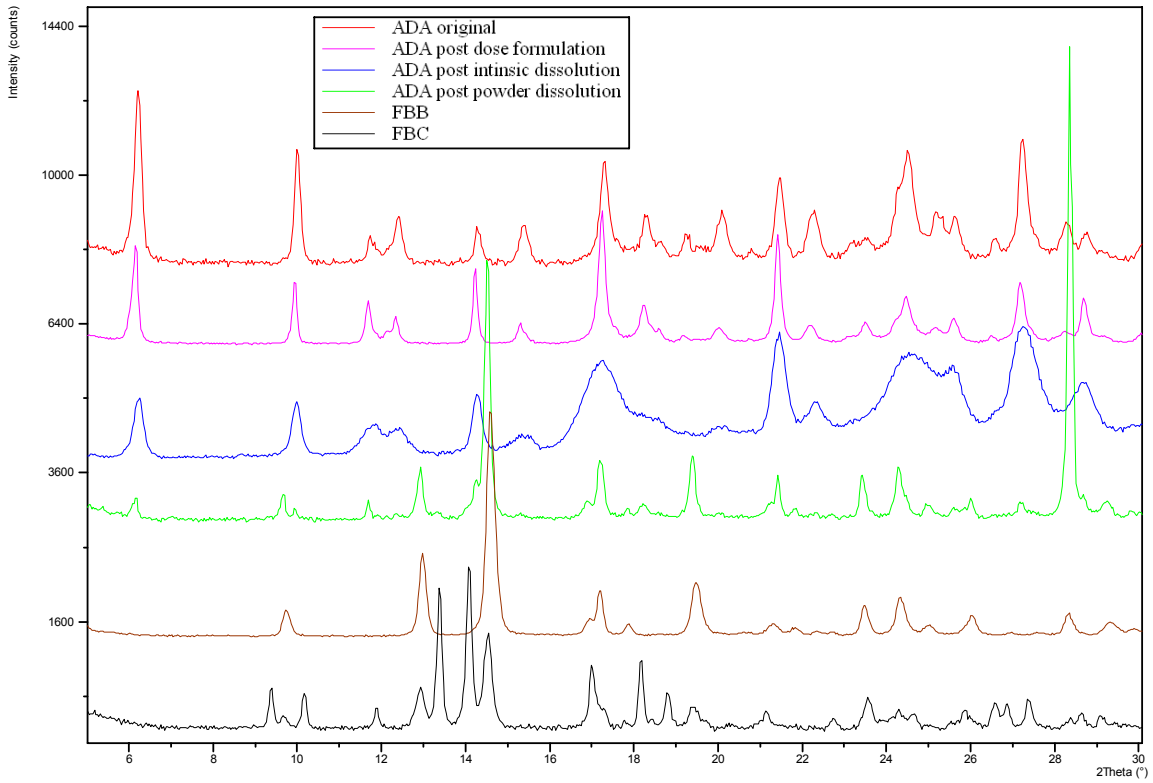

XRPD: FBB/FBC/ADA post powder dissolution

ADA (cont.)

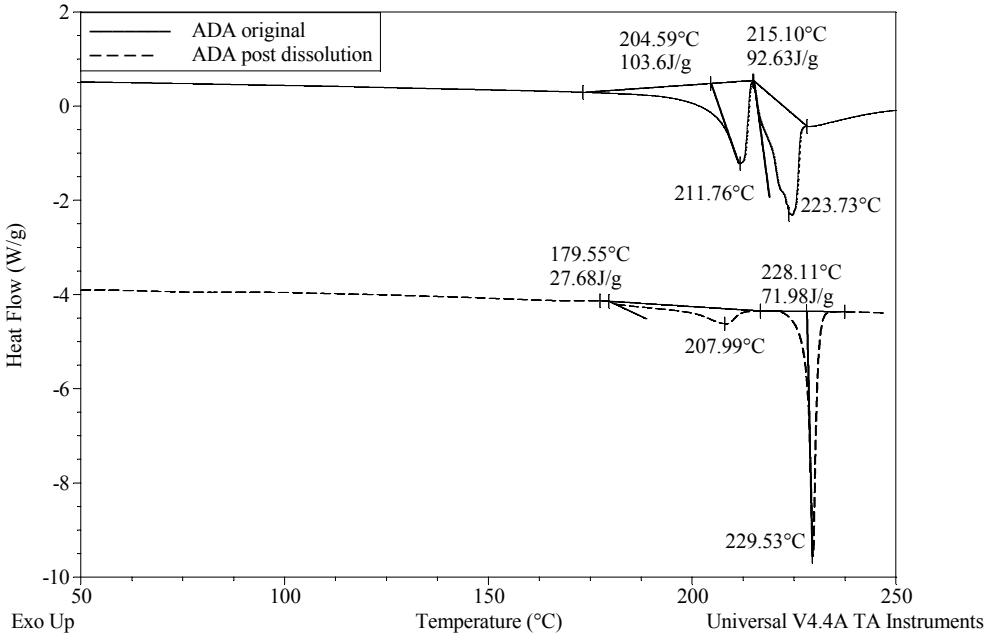

DSC: Some cocrystal remaining

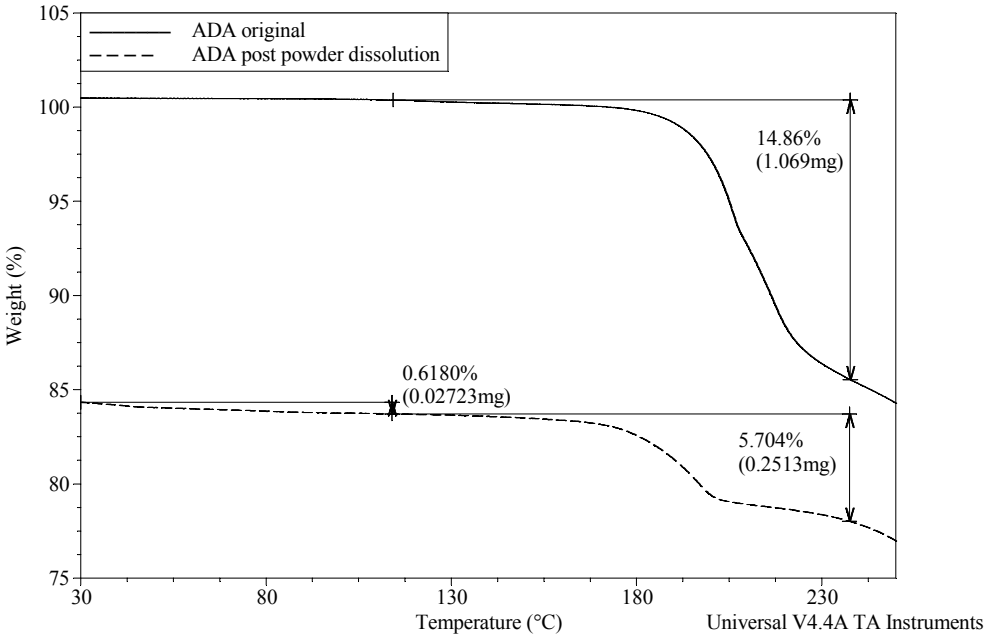

TGA: ~38% cocrystal remaining, 0.6% likely **FBC**

ADA (cont.)

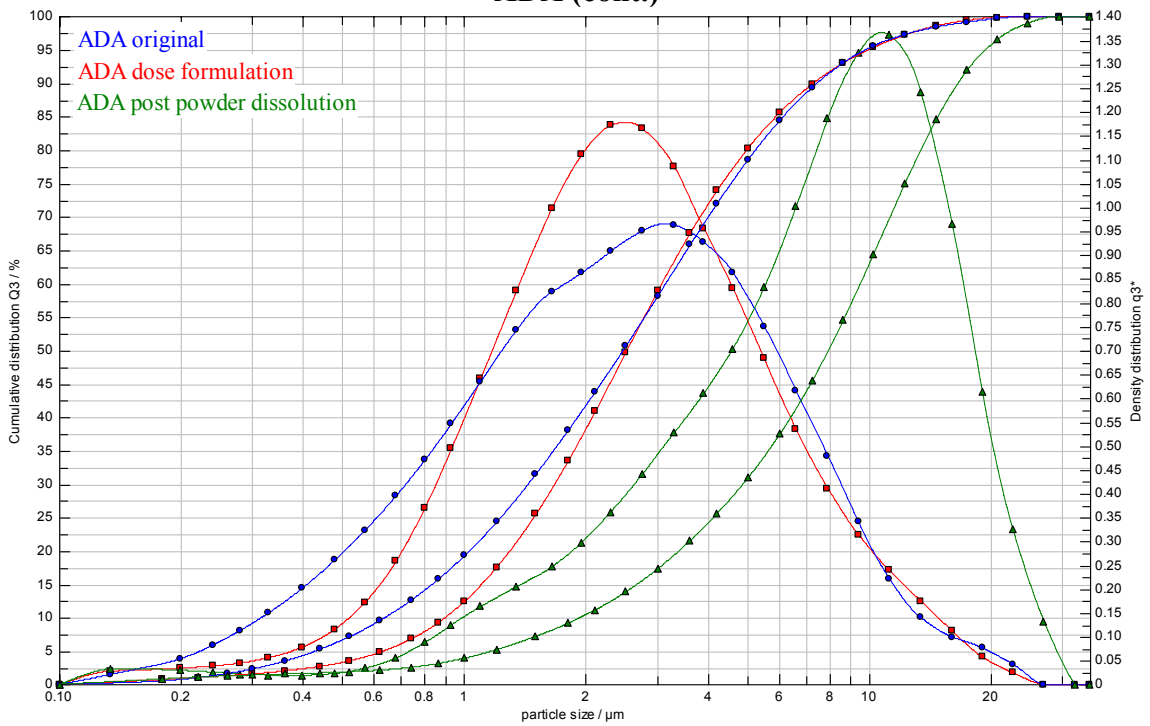

Particle size disributions

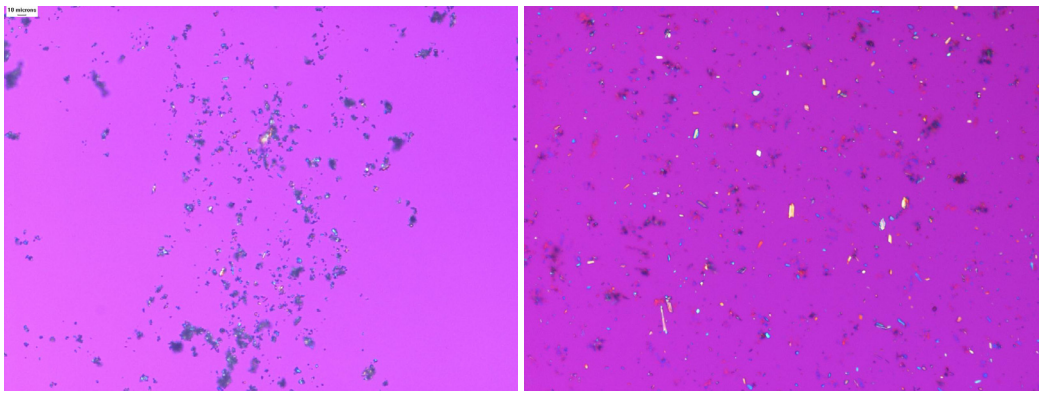

PLM: 200x original powder (left) post powder dissolution (right)

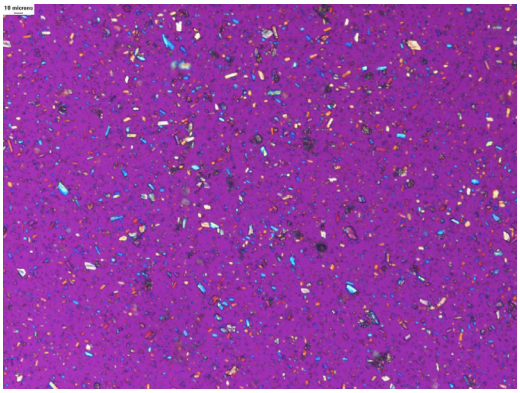

PLM: 200x post dose formulation

ADA (cont.)

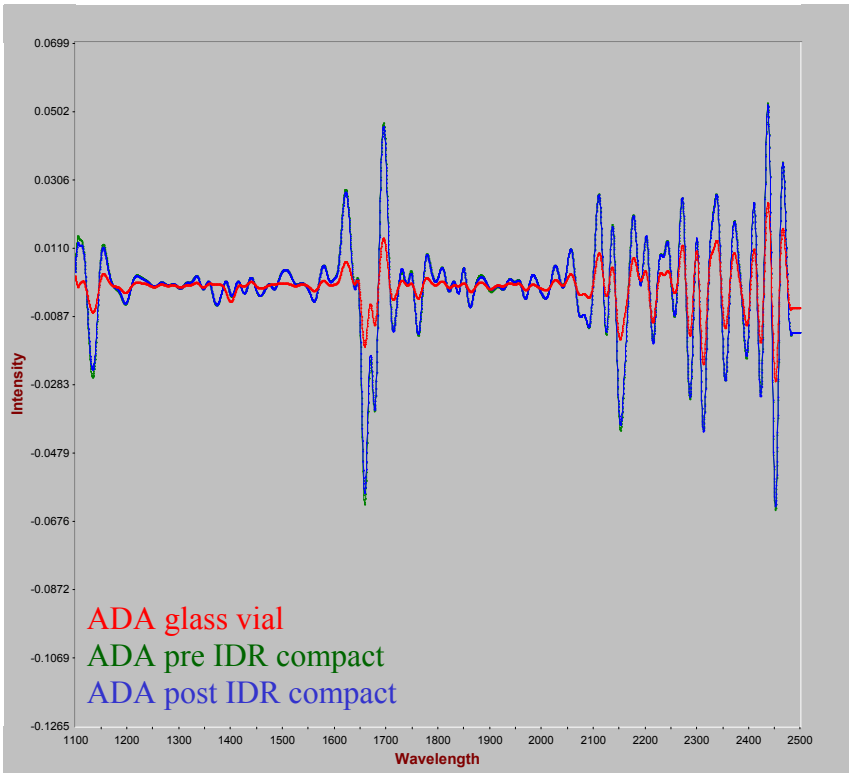

NIR: No change

BZA

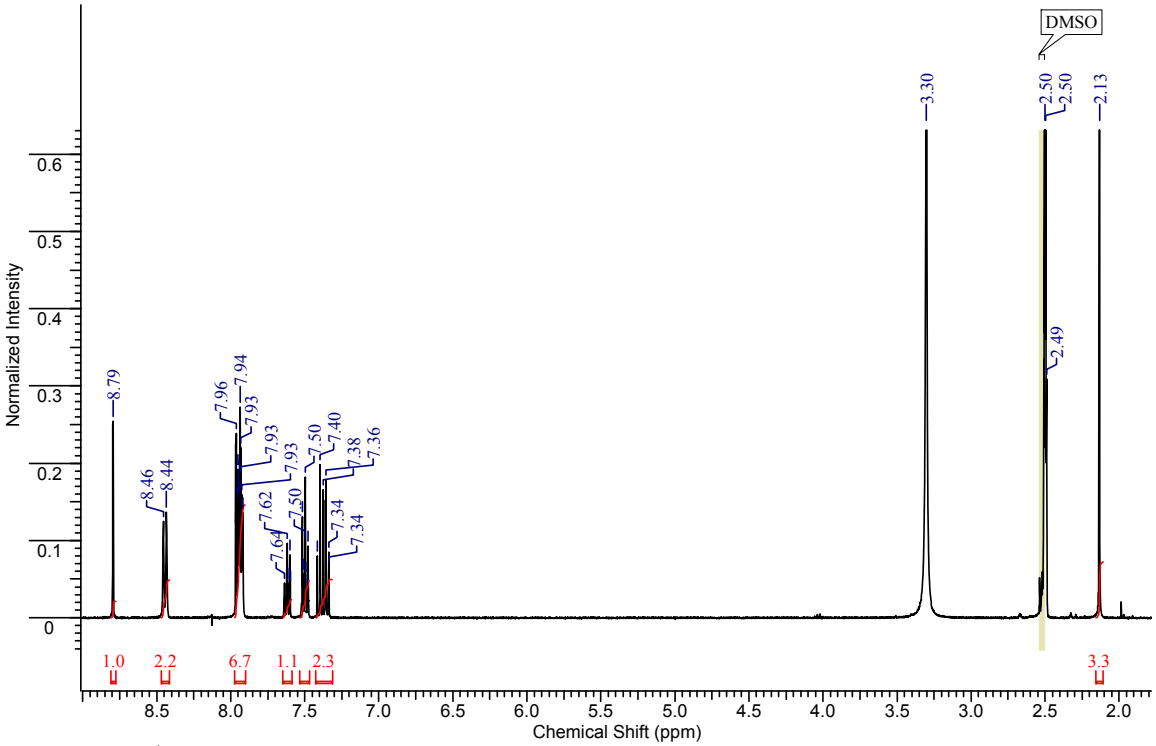

^{1}H NMR: 1.0 eq acid; 2(CH) 7.9ppm, CH 7.6ppm, 2(CH) 7.5ppm

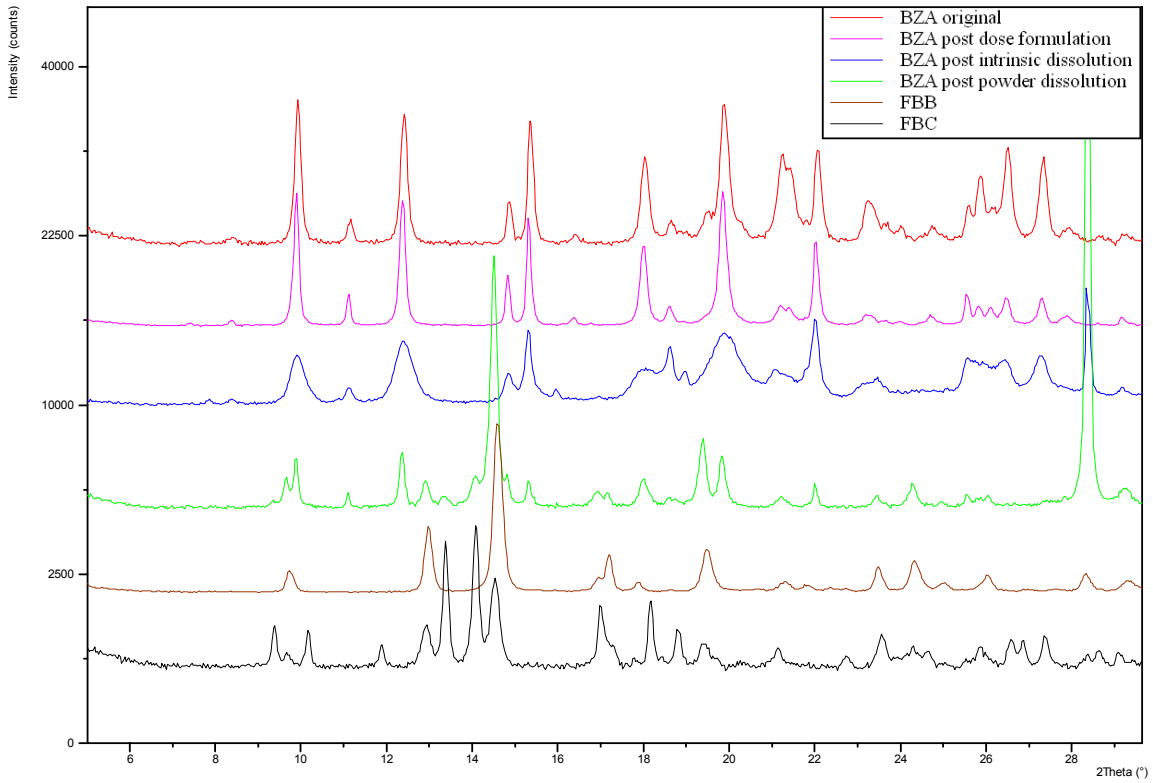

XRPD: FBB/FBC/BZA post powder dissolution

BZA (cont.)

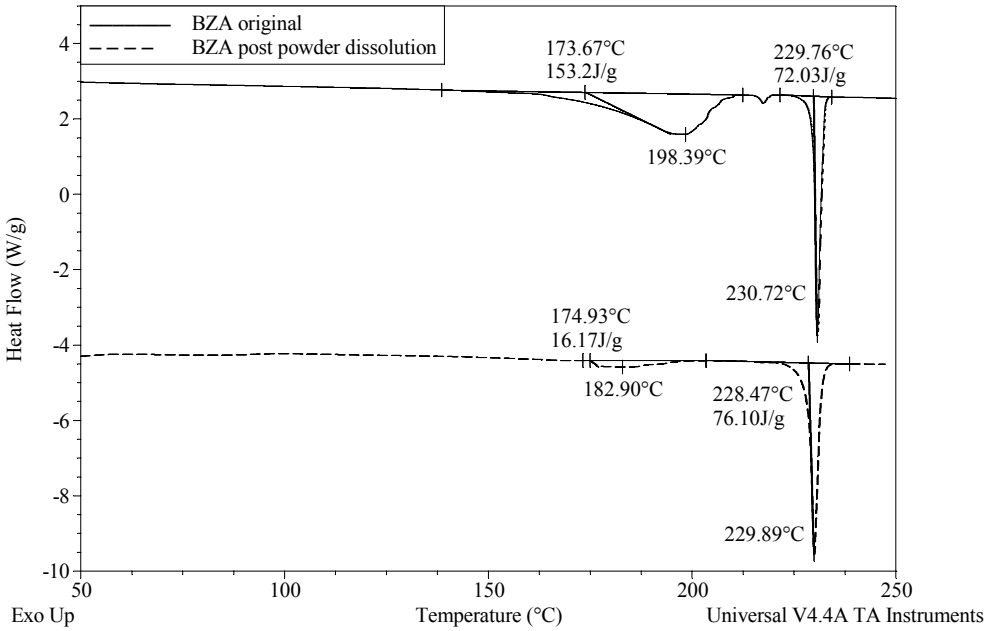

DSC: Some cocrystal remaining

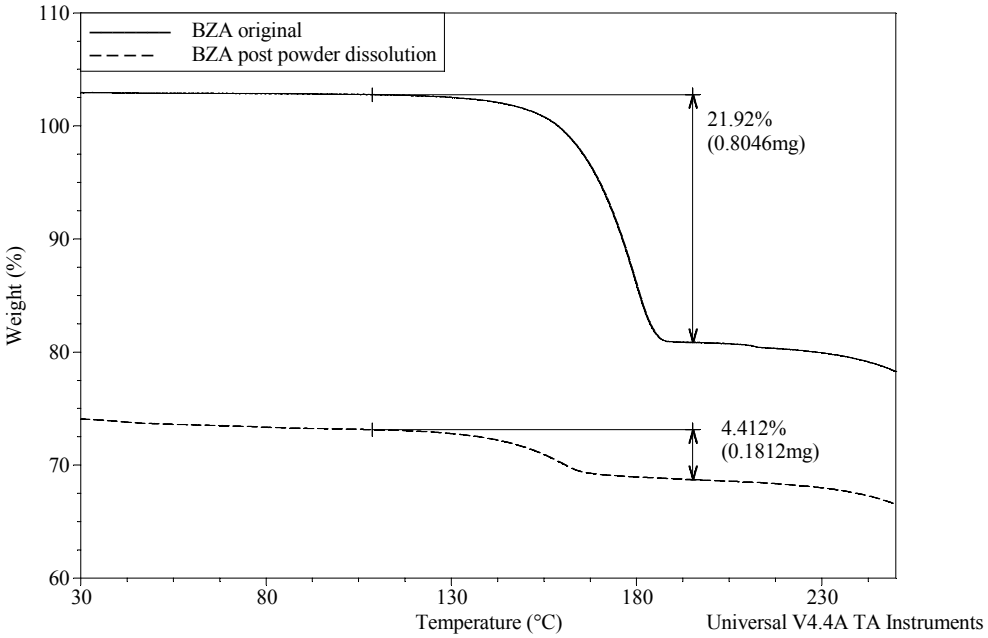

TGA: ~20% cocrystal remaining

BZA (cont.)

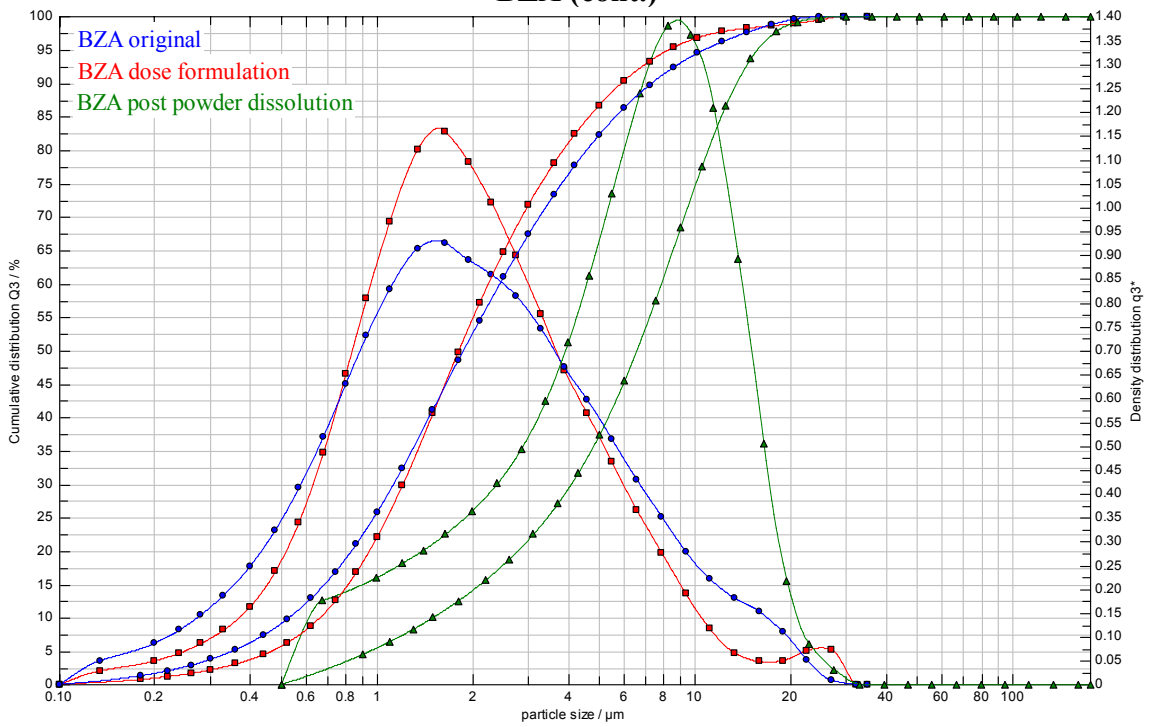

Particle Size Distributions

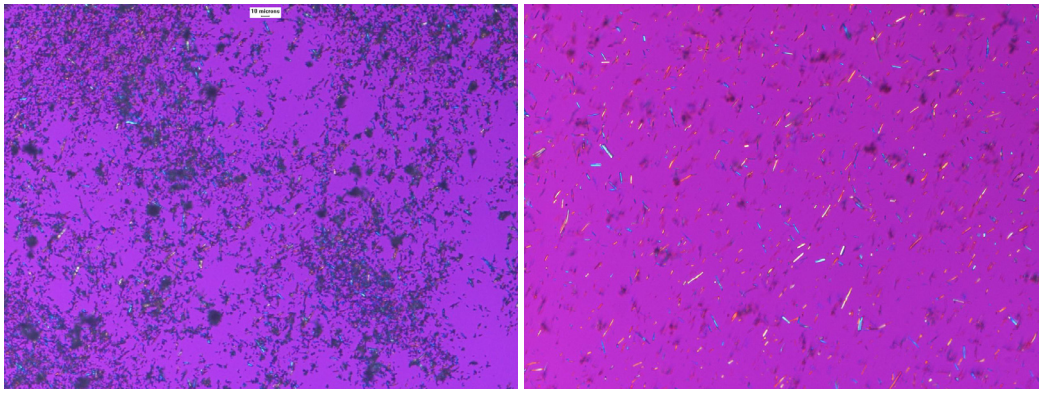

PLM: 200x original powder (left) post powder dissolution (right)

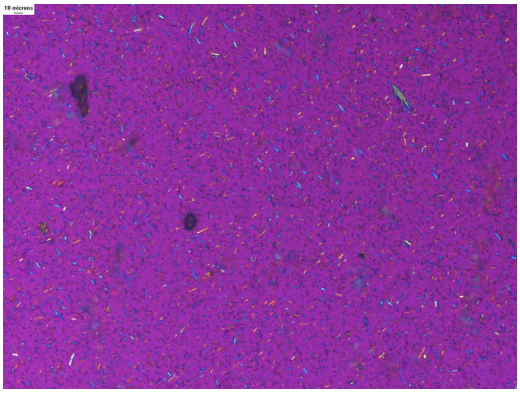

PLM: 200x post dose formulation

BZA (cont.)

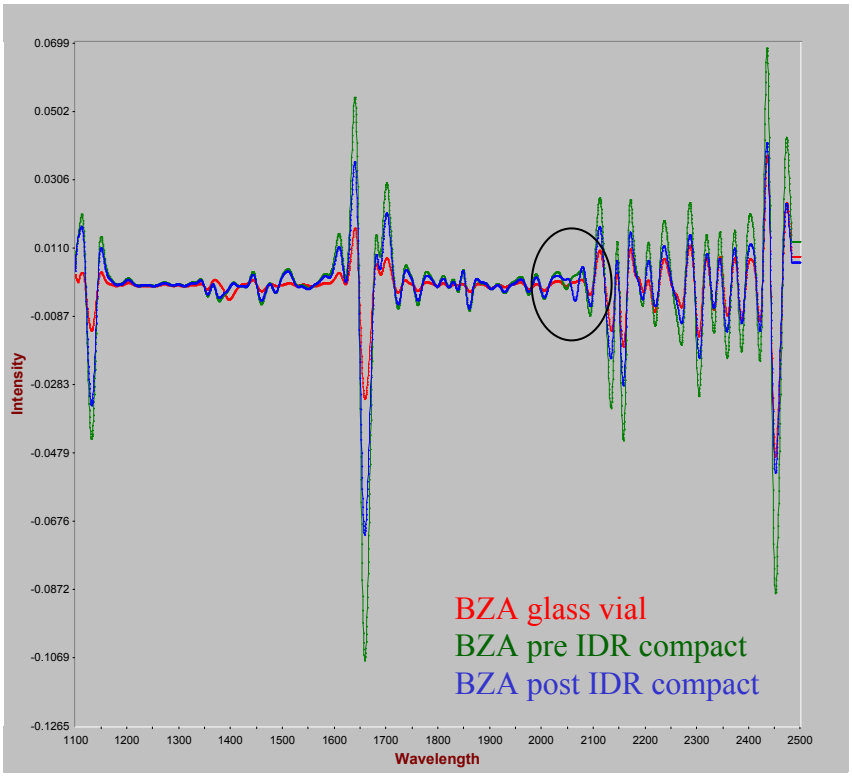

NIR: FBA at 2063nm post intrinsic dissolution

BZD

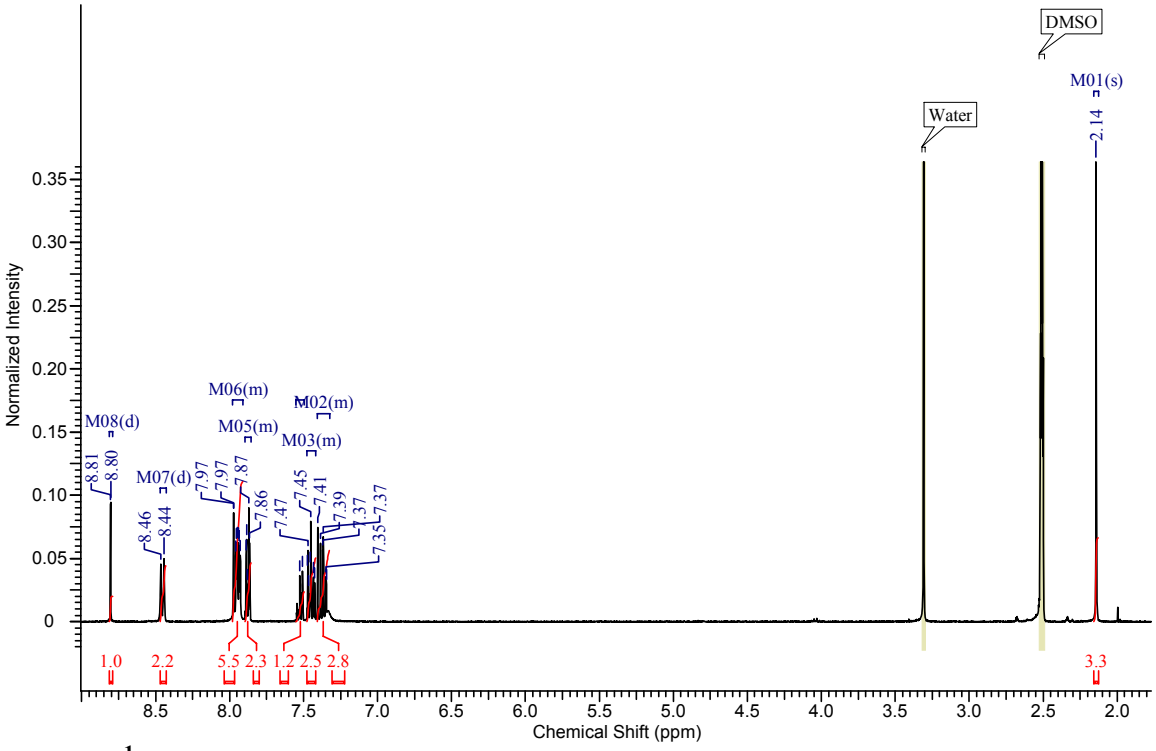

^{1}H NMR: 1.0 eq amide; 2(CH) 7.86ppm, CH 7.6ppm, 2(CH) 7.45ppm

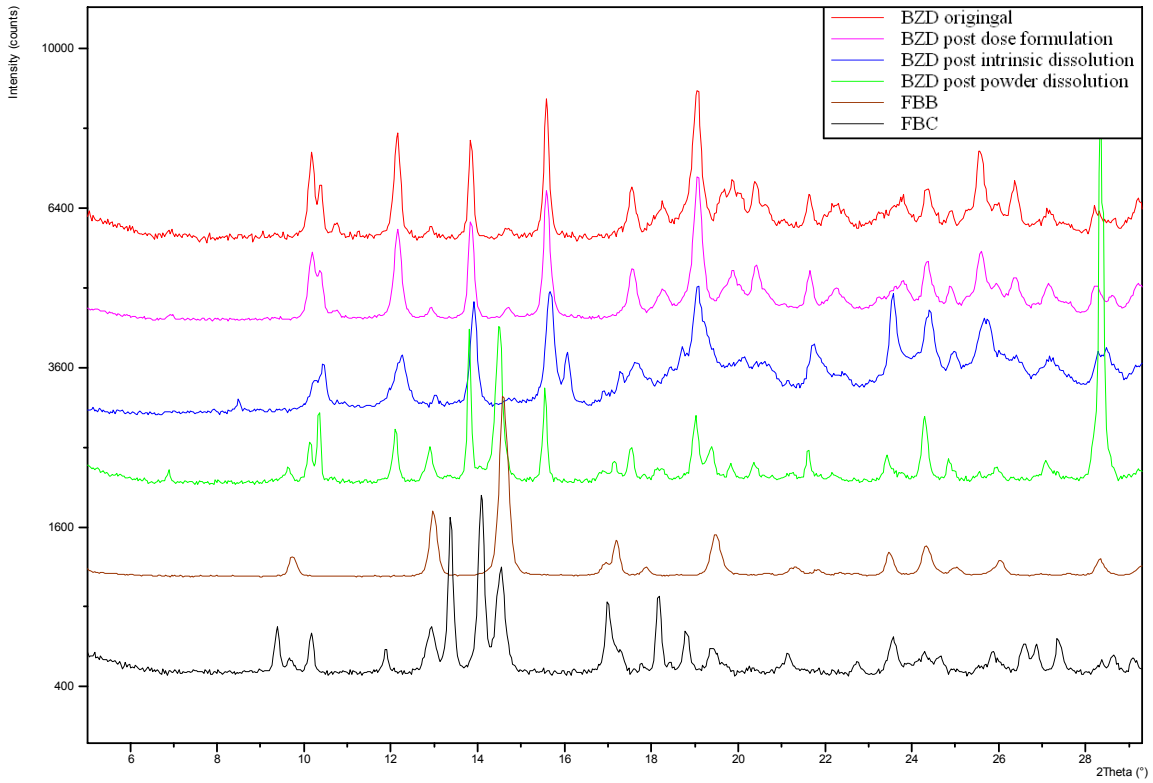

XRPD: FBB/FBC/BZD post powder dissolution

BZD (cont.)

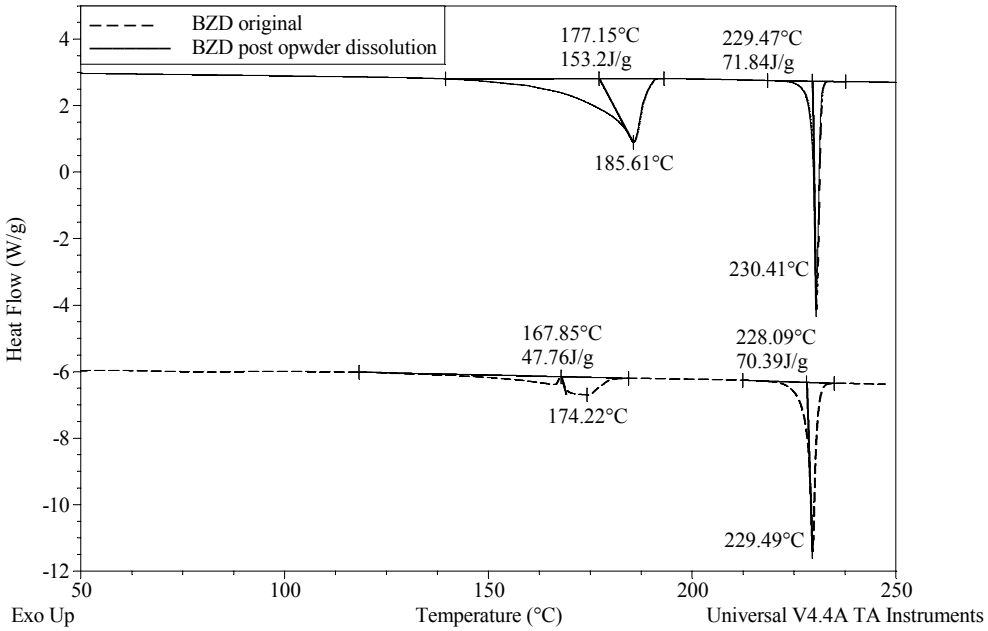

DSC: Some cocrystal remaining

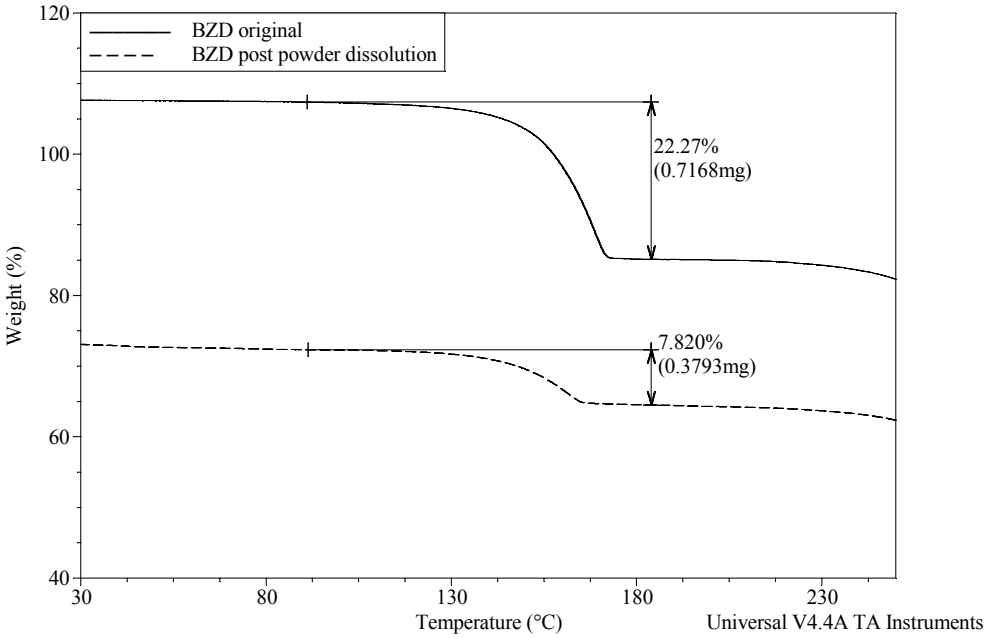

TGA: ~35% cocrystal remaining

BZD (cont.)

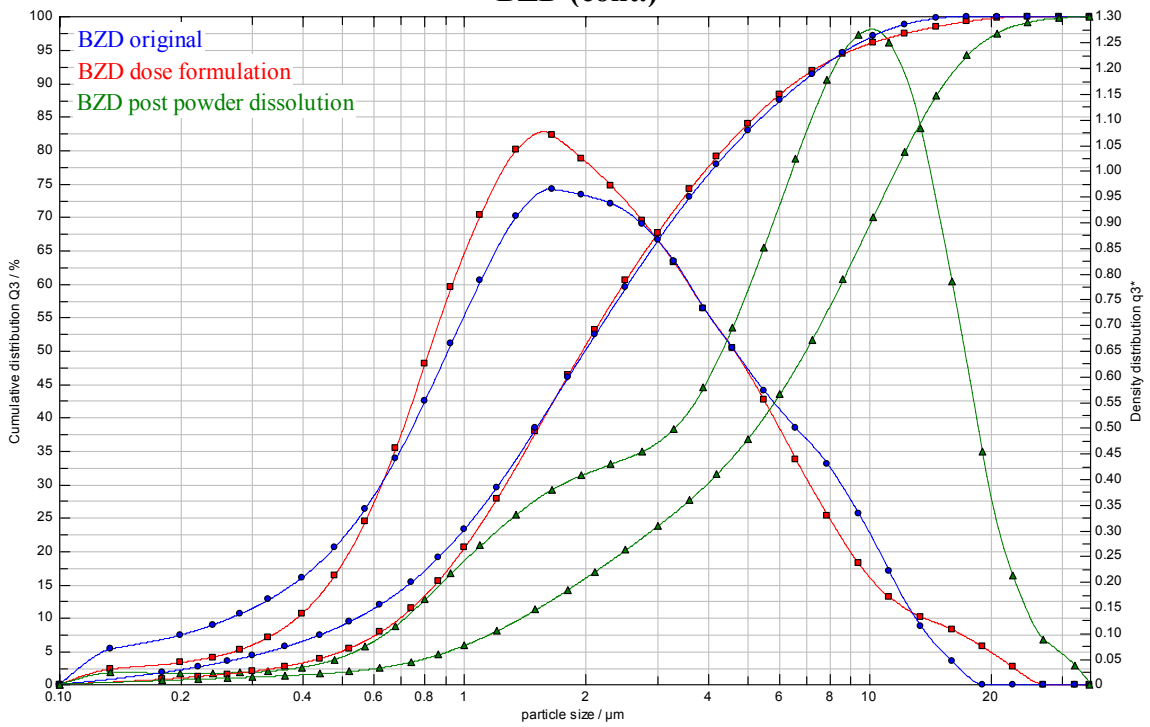

Particle Size Distributions

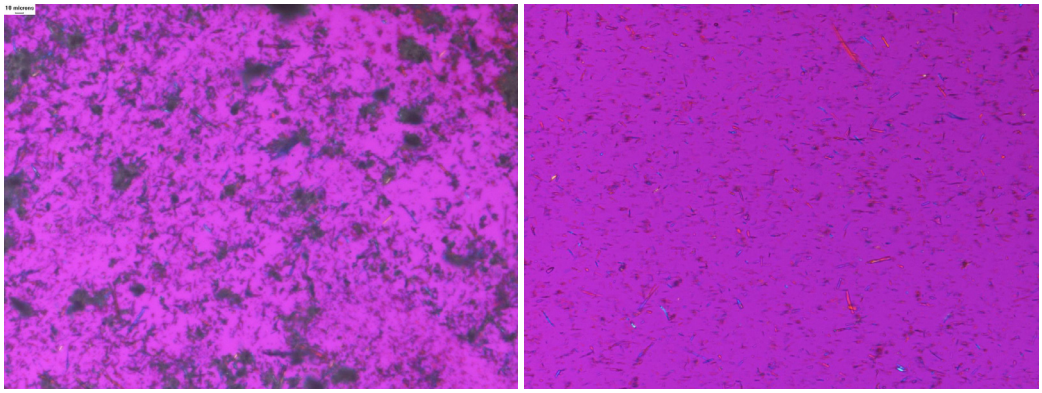

PLM: 200x original powder (left) post powder dissolution (right)

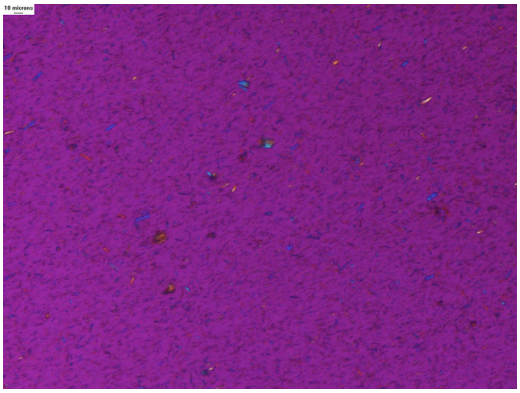

PLM: 200x post dose formulation

BZD (cont.)

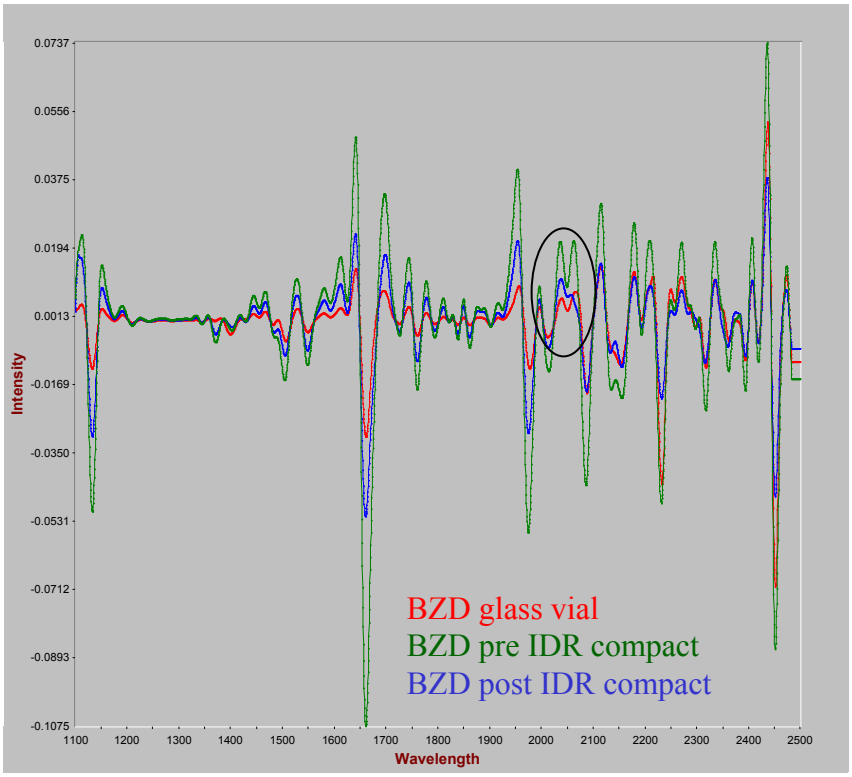

NIR: Minor **FBA** possible at 2066nm post dissolution

CNA

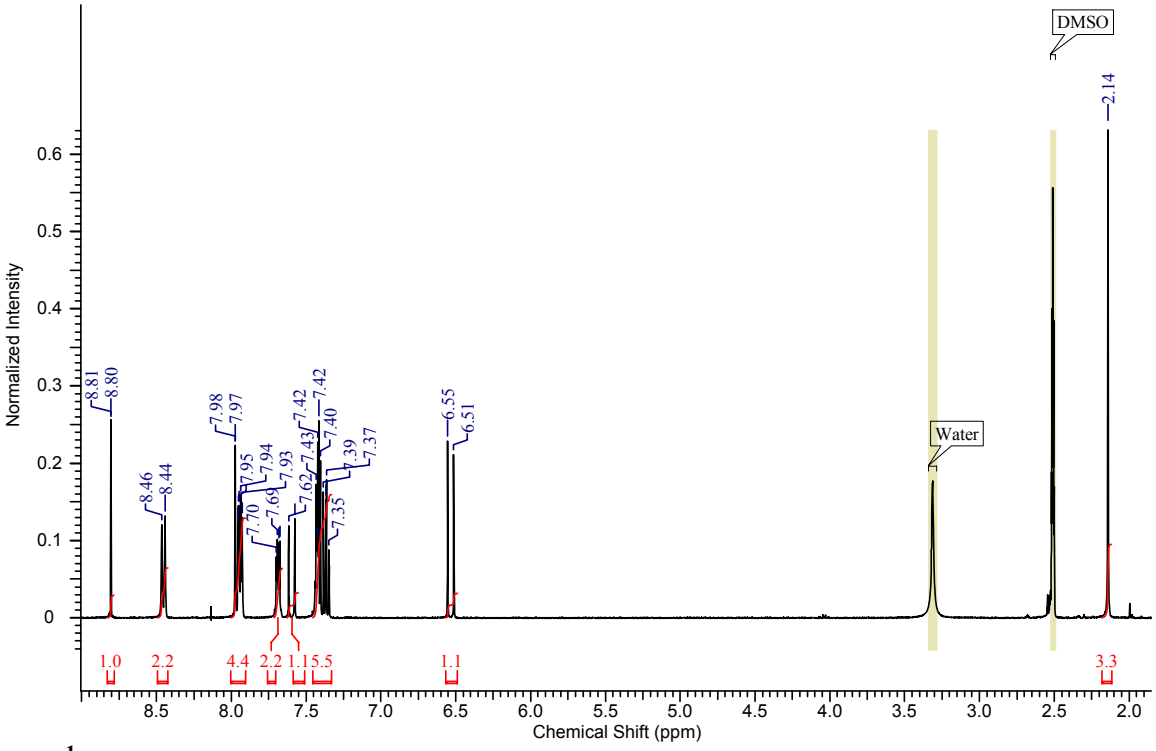

^{1}H NMR: 1.0 eq acid; 2(CH) 7.7ppm, CH 7.6ppm, 3(CH) 7.4ppm, CH 6.5 ppm

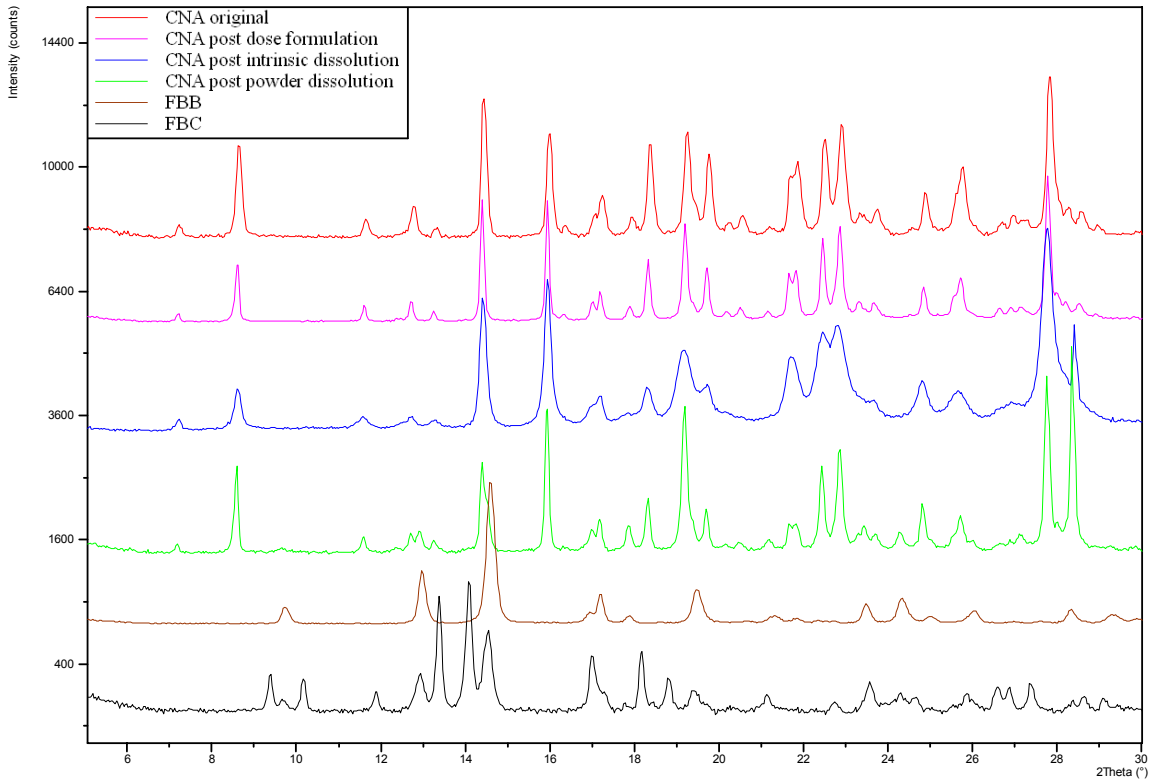

XRPD: CNA/FBB post powder dissolution

CNA (cont.)

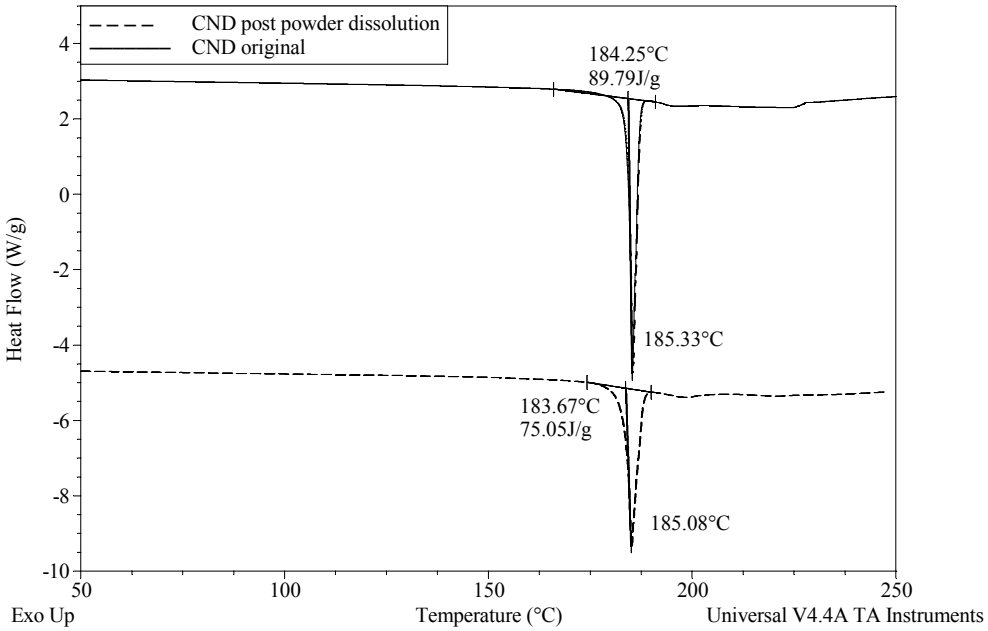

DSC: Mostly cocrystal remaining

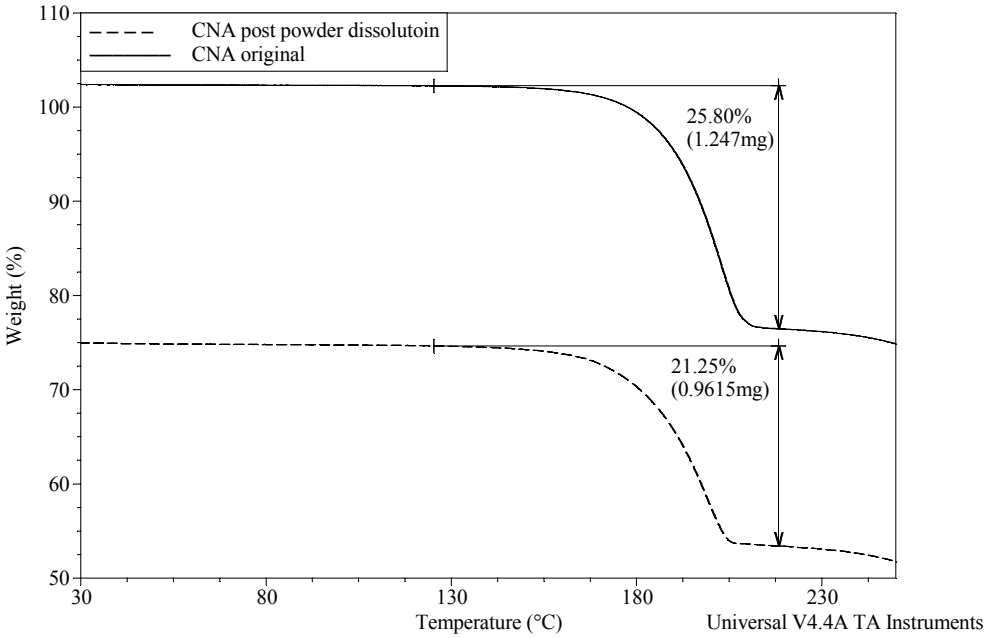

TGA: ~82% cocrystal remaining

CNA (cont.)

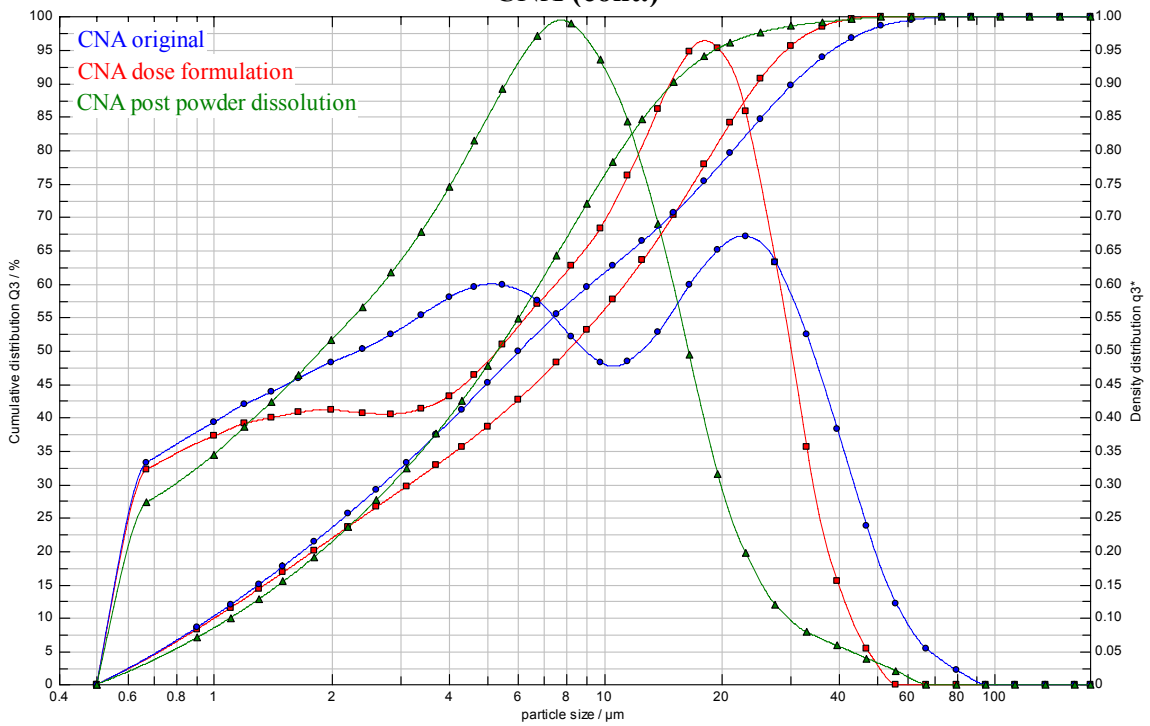

Particle Size Distributions

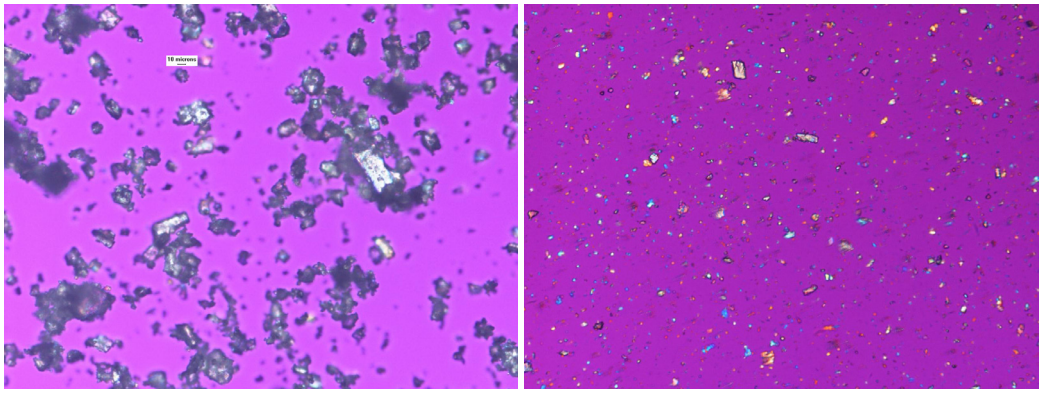

PLM: 200x original powder (left) post powder dissolution (right)

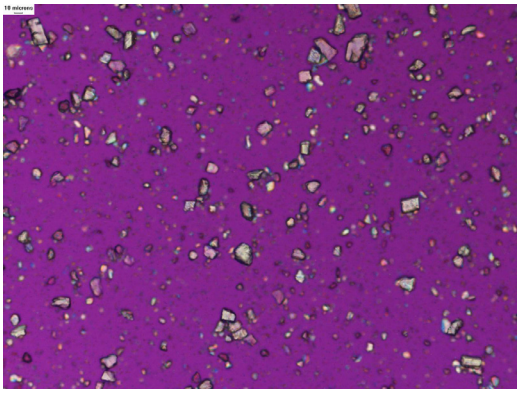

PLM: 200x post dose formulation

CNA (cont.)

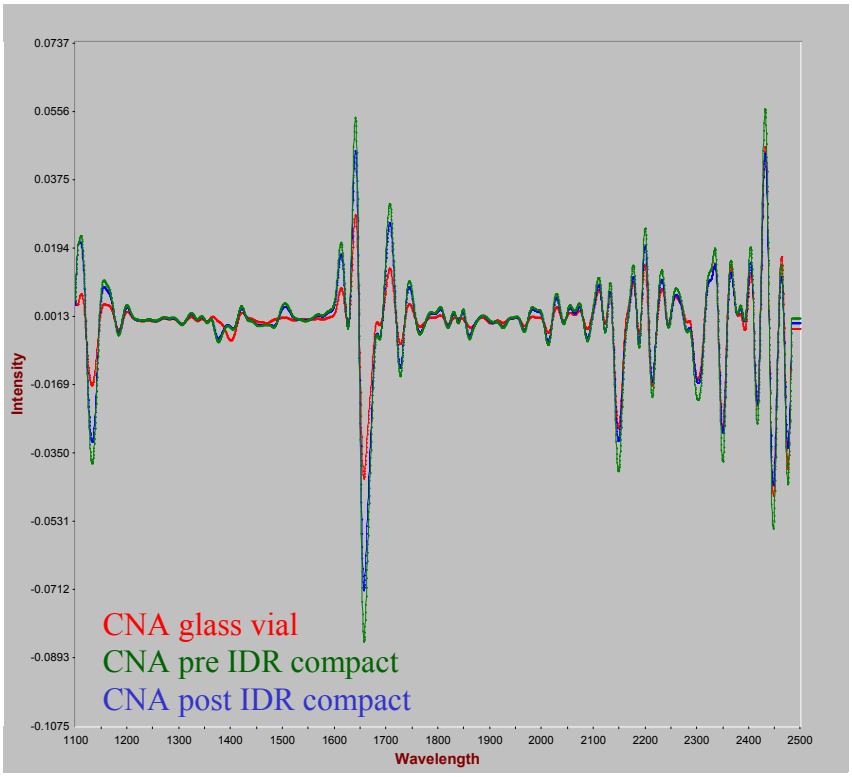

NIR: No change

CND

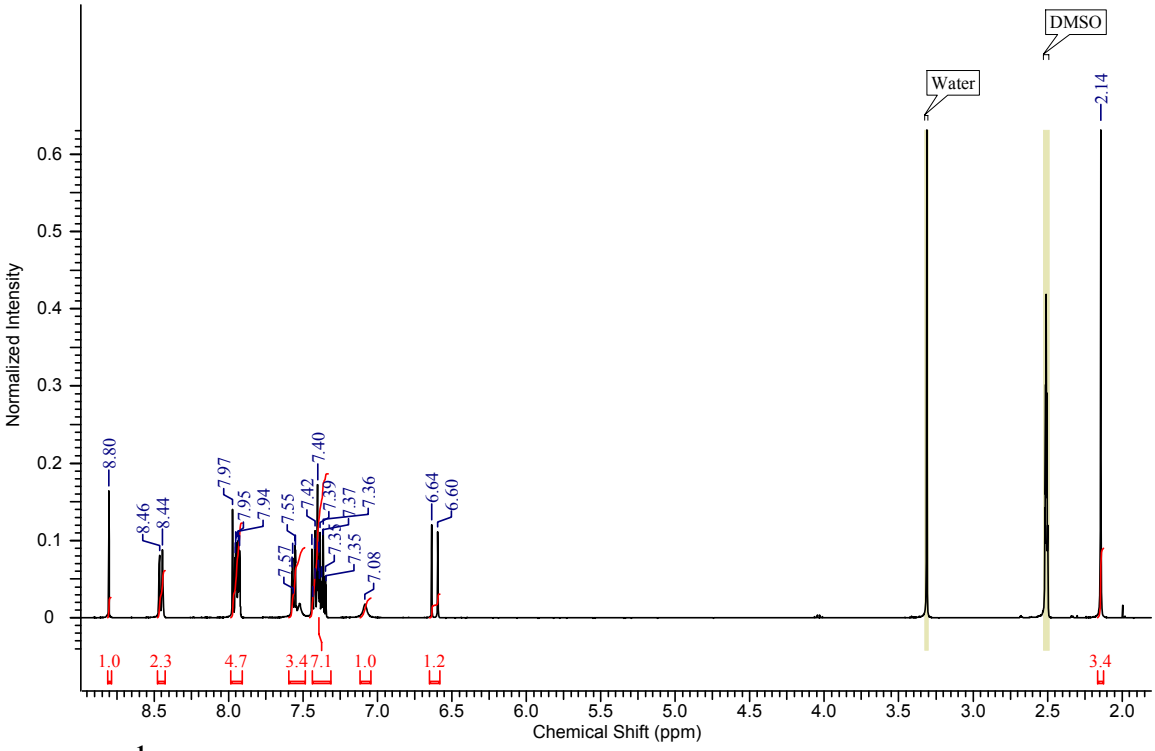

^{1}H NMR: 1.0 eq amide; 2(CH) 7.6ppm, 4(CH) 7.4ppm, CH 6.5 ppm

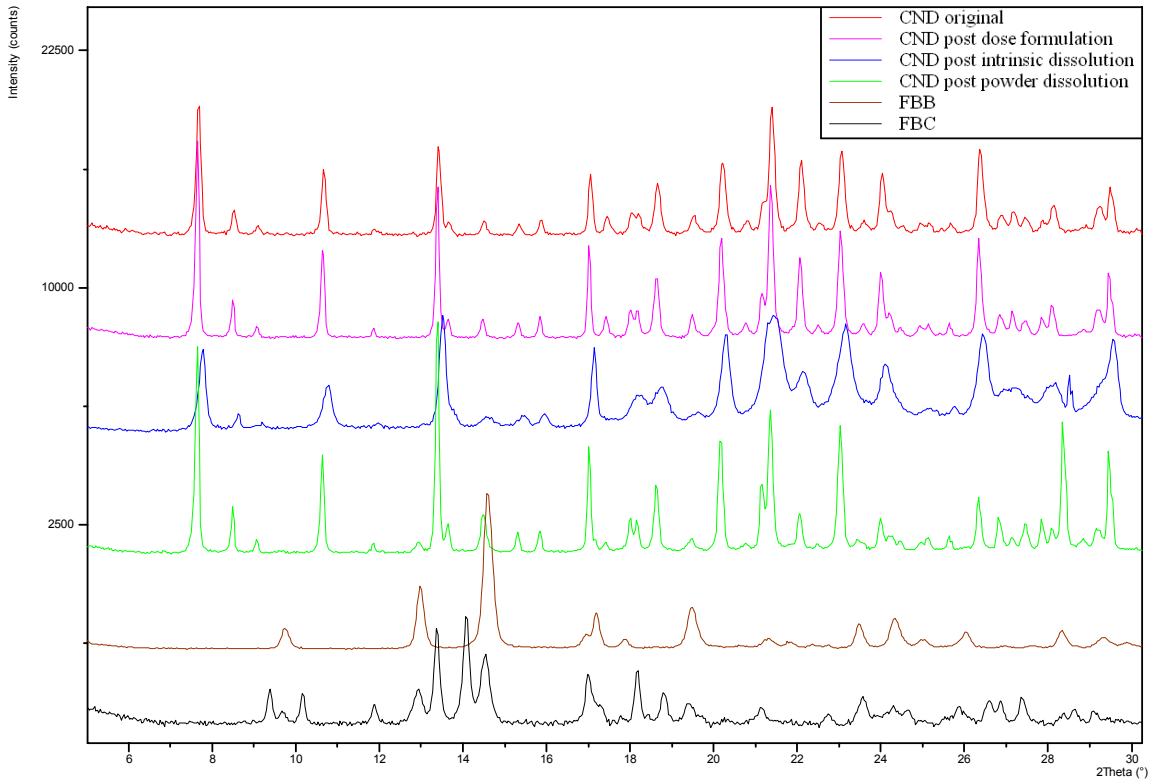

XRPD: CND/FBB post powder dissolution

CND (cont.)

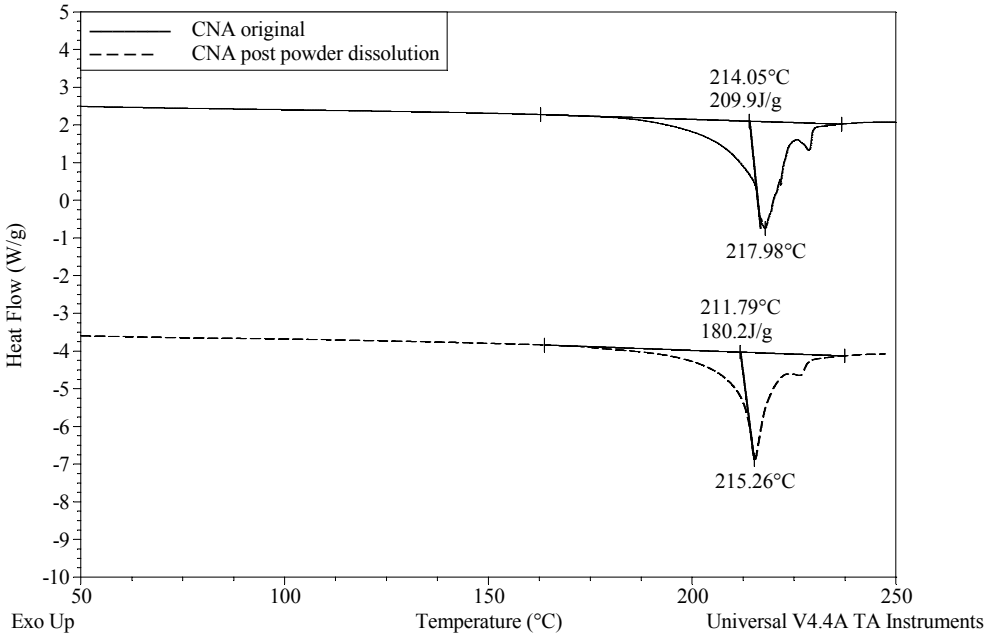

CND: Mostly cocrystal remaining

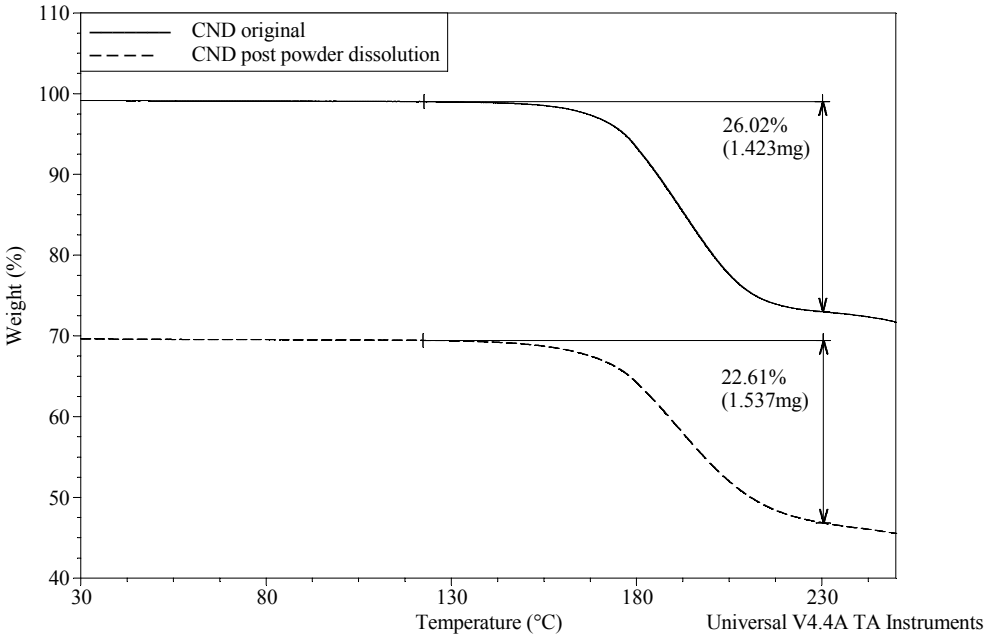

CND: ~87% cocrystal remaining

CND (cont.)

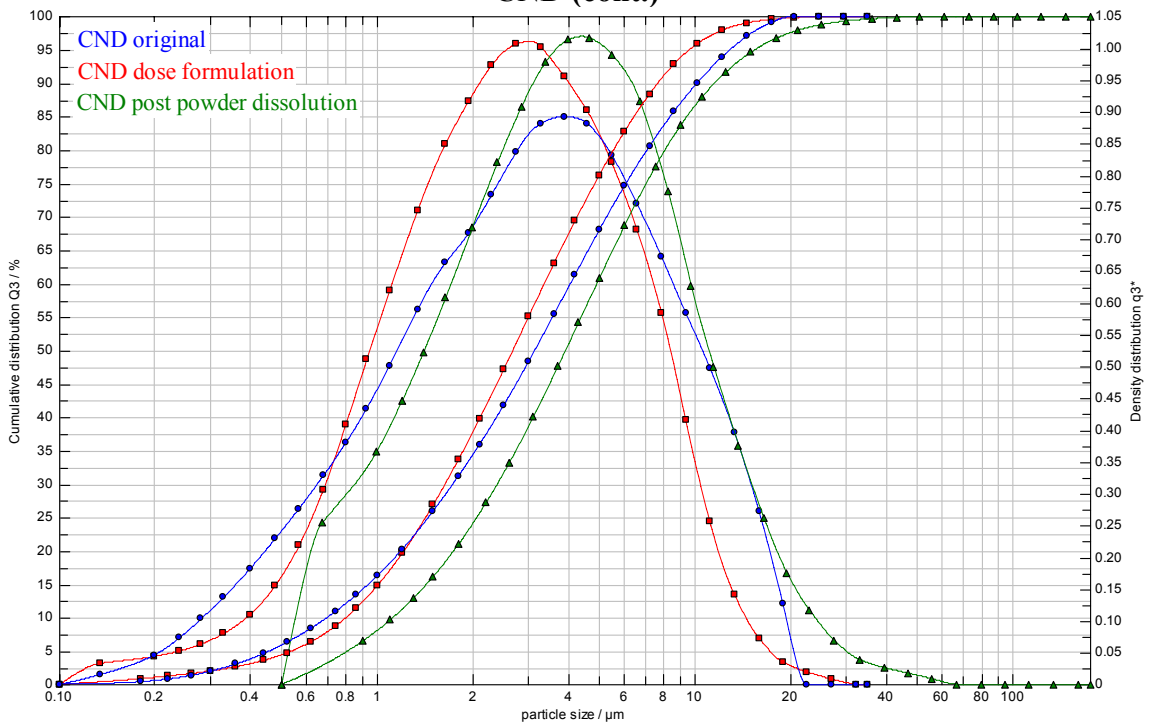

Particle Size Distributions

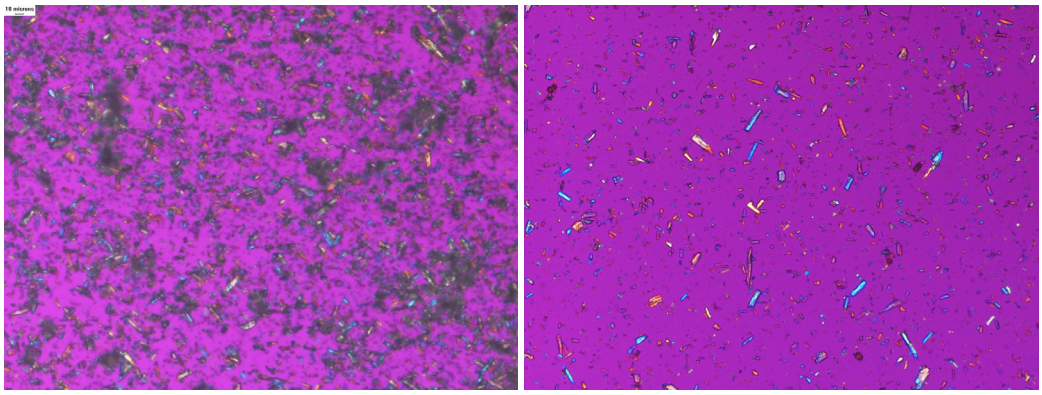

PLM: 200x original powder (left) post powder dissolution (right)

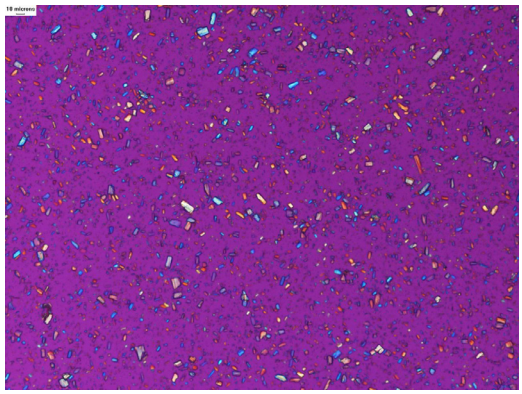

PLM: 200x post dose formulation

CND (cont.)

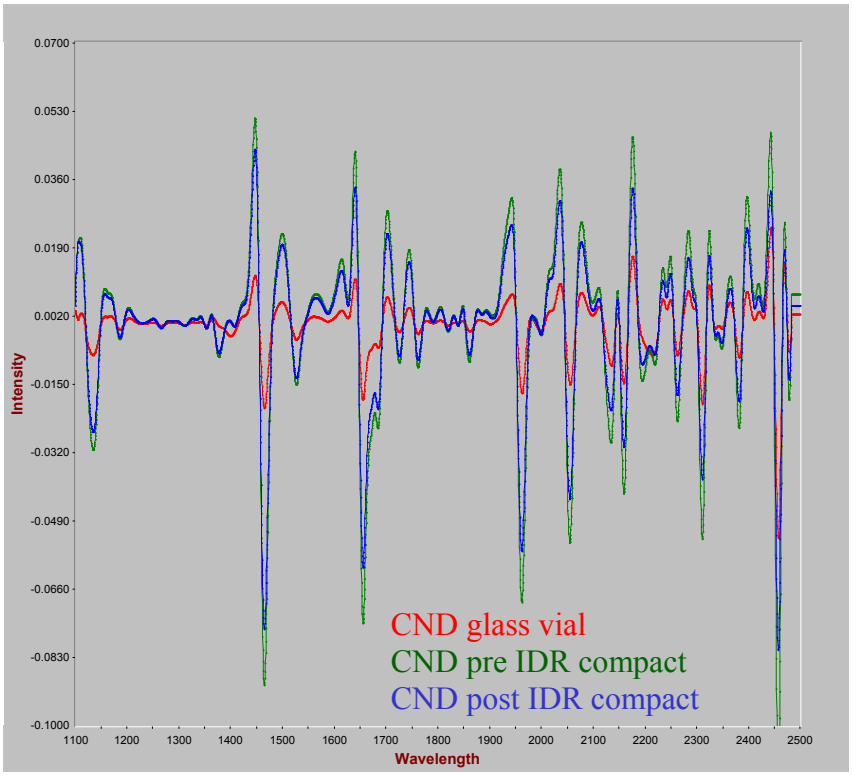

NIR: No change

HBA

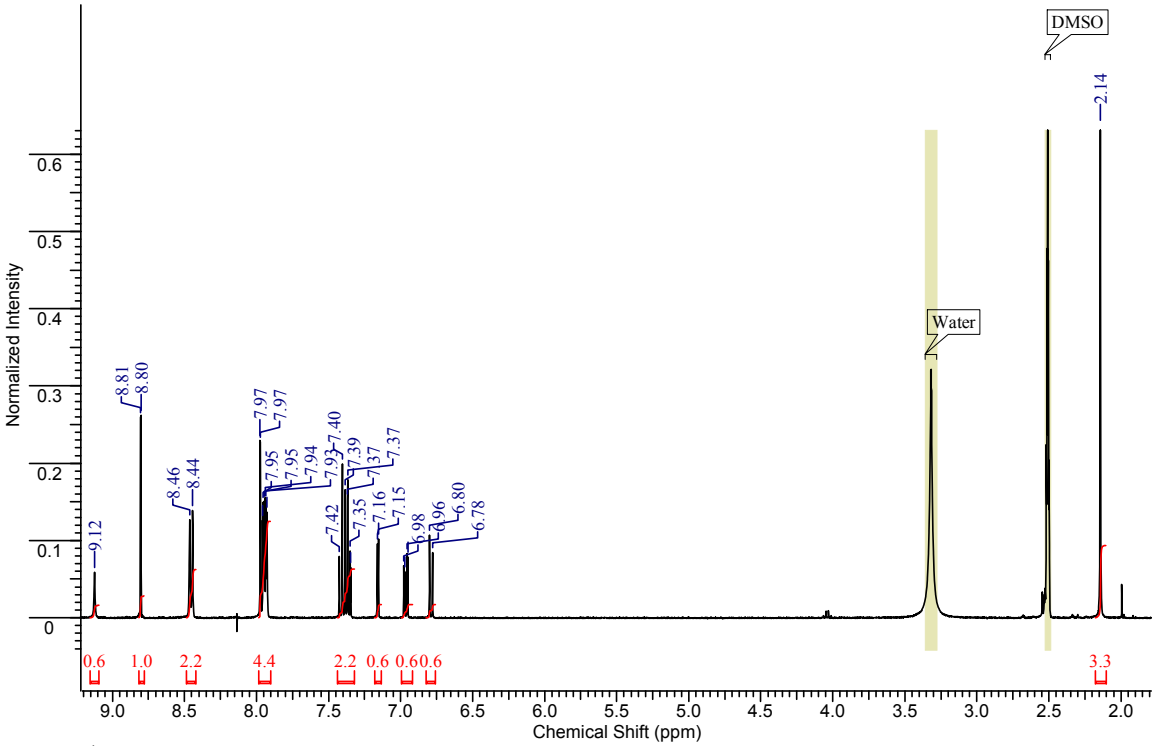

^{1}H NMR: 0.5 eq acid; CH integrates as 0.5 7.16ppm, 6.98ppm and 6.78ppm

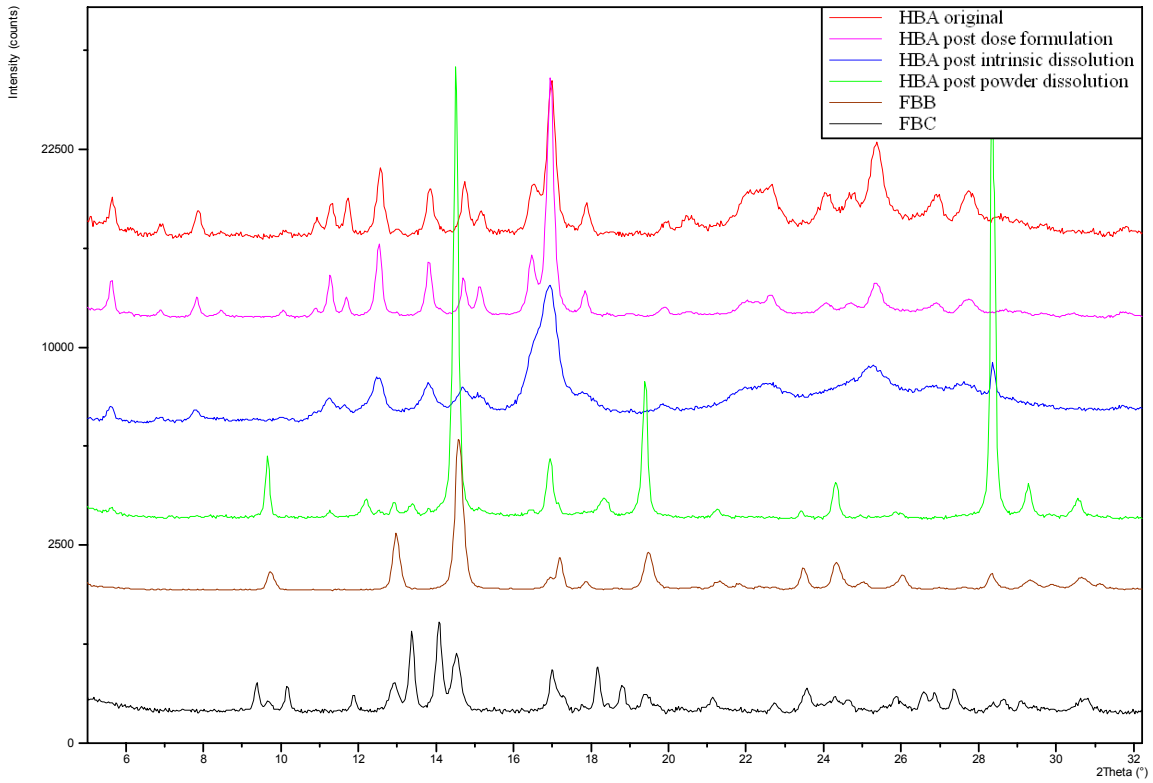

XRPD: FBB/FBC post powder dissolution

HBA (cont.)

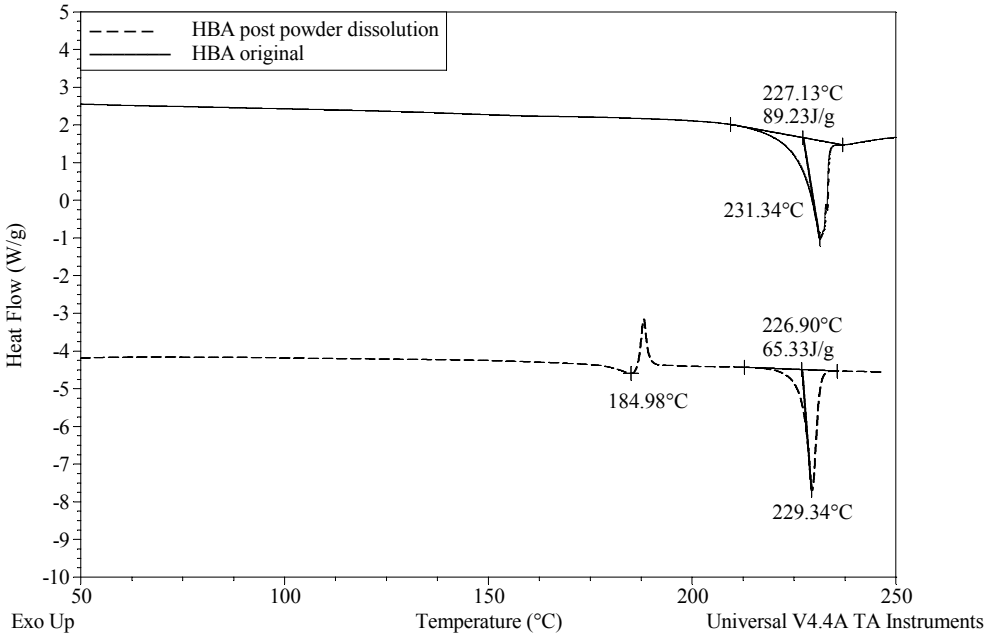

DSC: Likely **FBB**

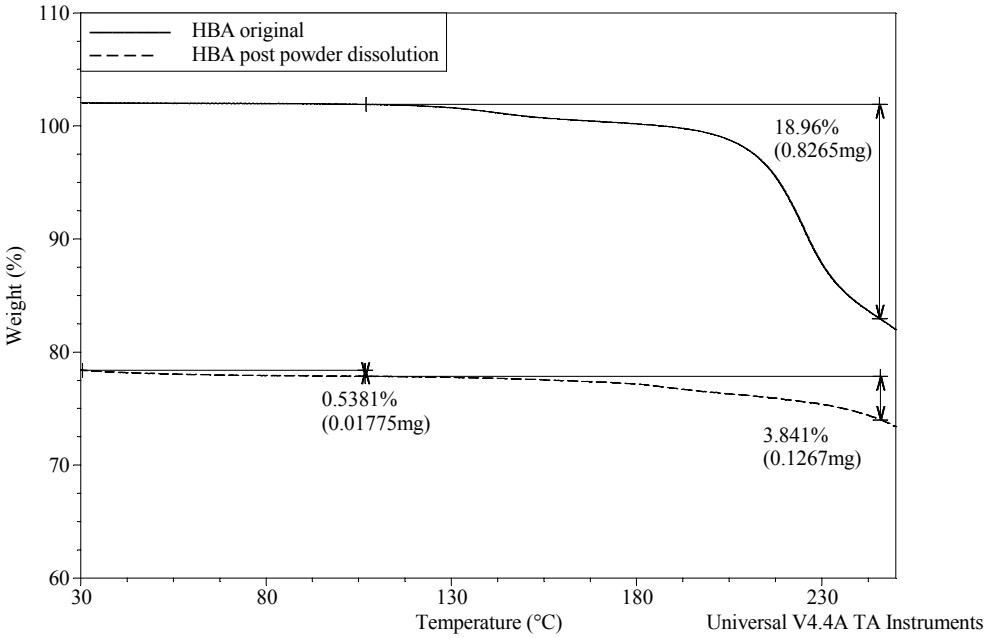

TGA: No cocrystal remaining, 0.5% likely **FBC**

HBA (cont.)

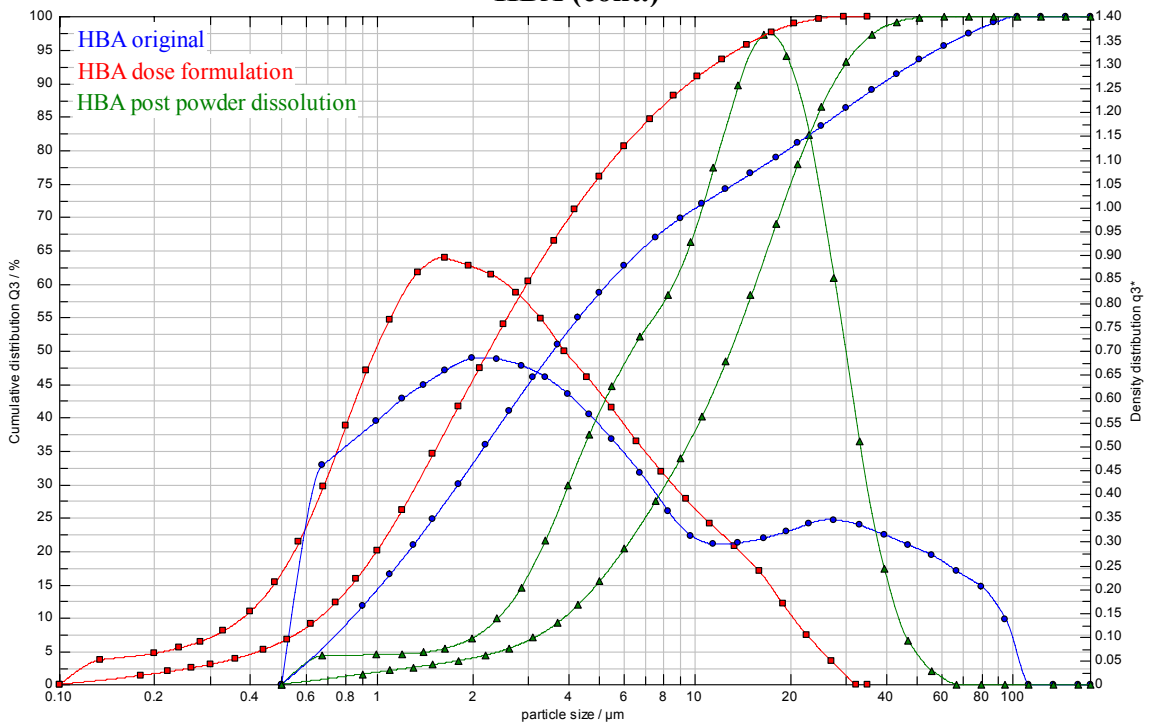

Particle Size Distributions

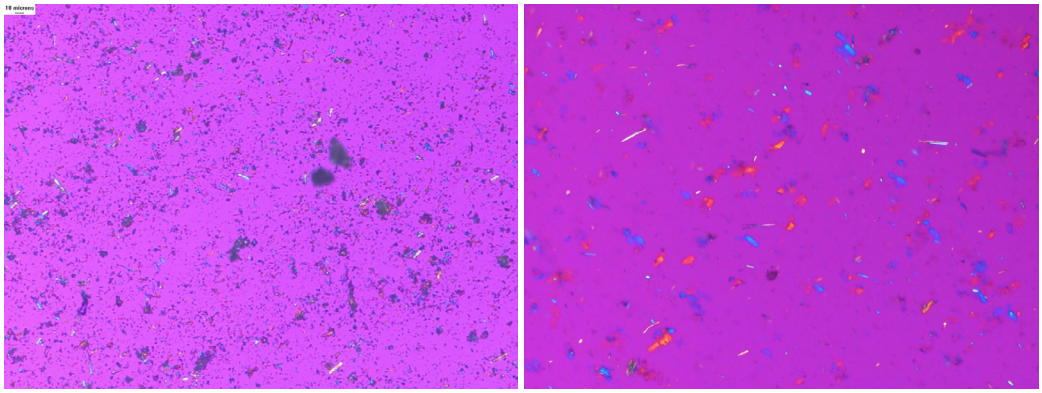

PLM: 200x original powder (left) post powder dissolution (right)

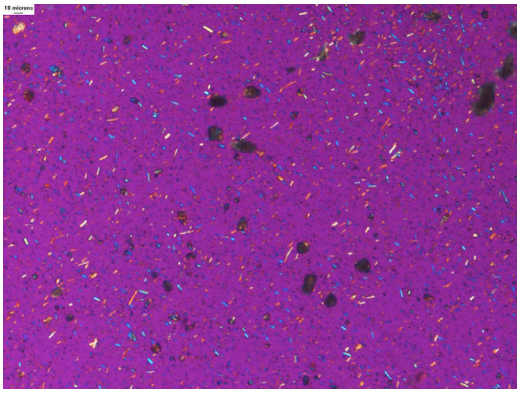

PLM: 200x post dose formulation

HBA (cont.)

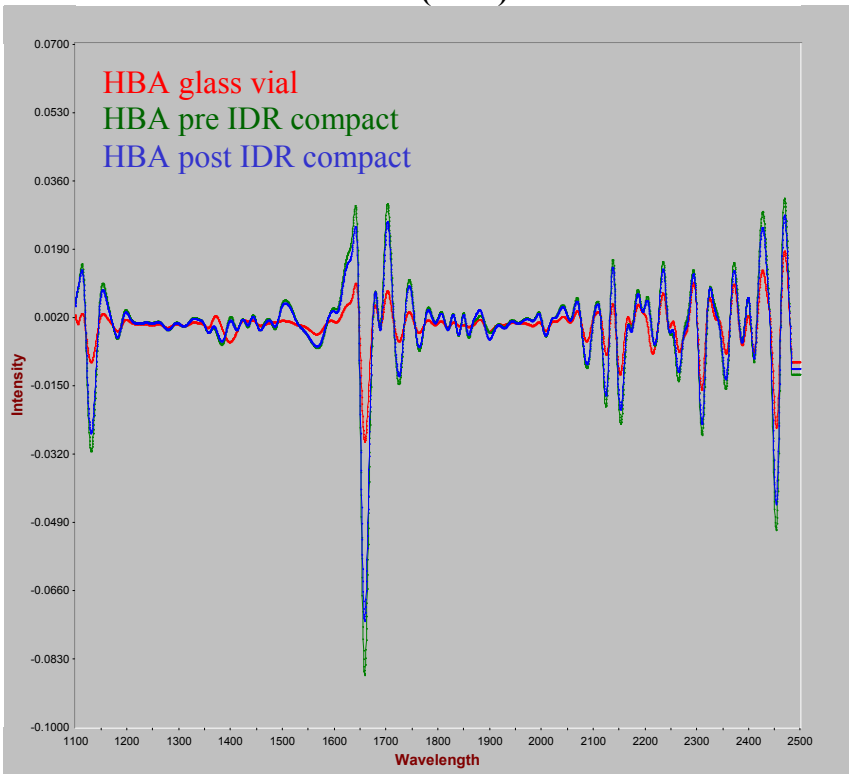

NIR: No change

GUA

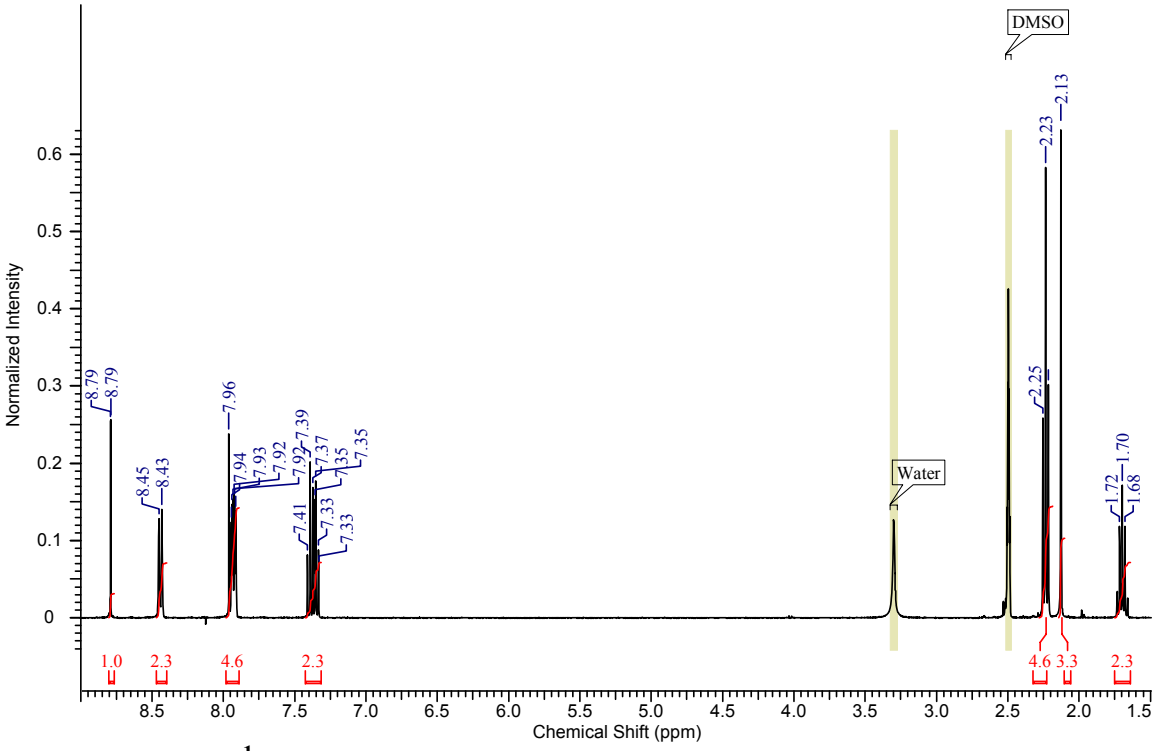

^{1}H NMR: 1.0 eq acid; 2(CH_2) 2.2ppm, CH_2 1.7ppm

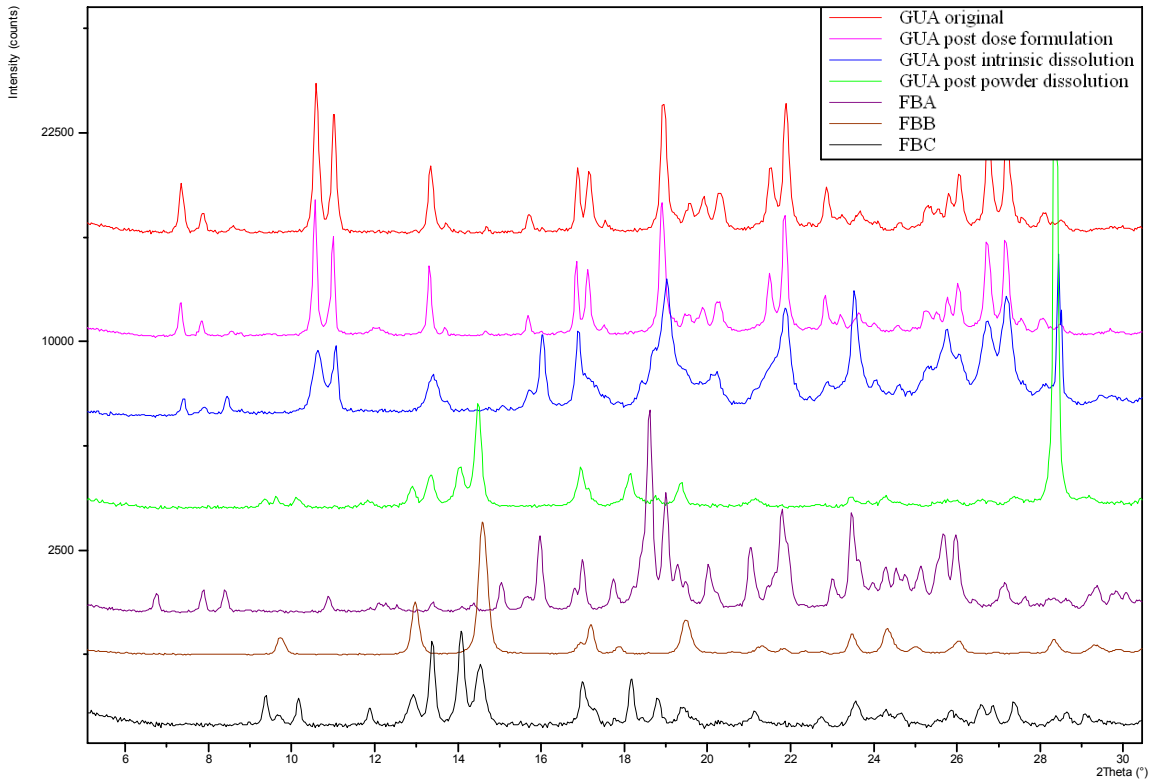

XRPD: FBC post powder dissolution, **GUA/FBA** post intrinsic dissolution

GUA (cont.)

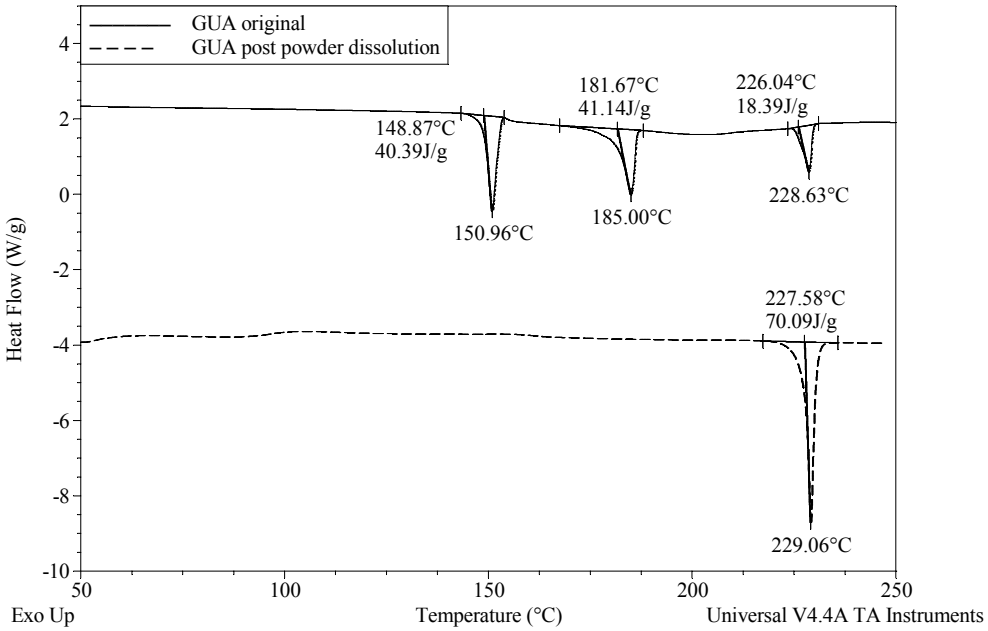

DSC: No cocrystal remaining

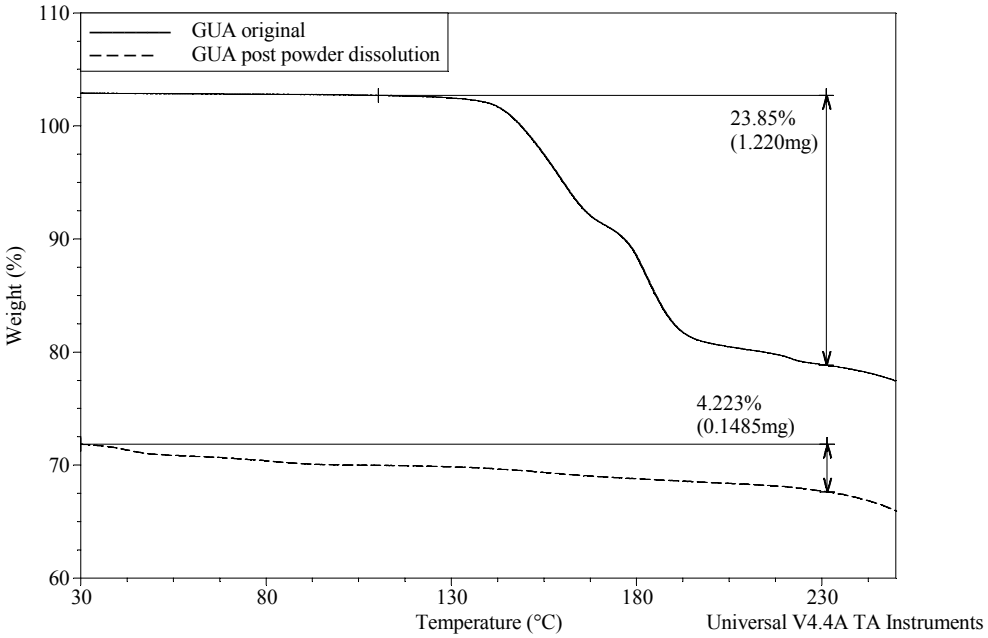

TGA: No cocrystal remaining, 4.2% likely **FBC**

GUA (cont.)

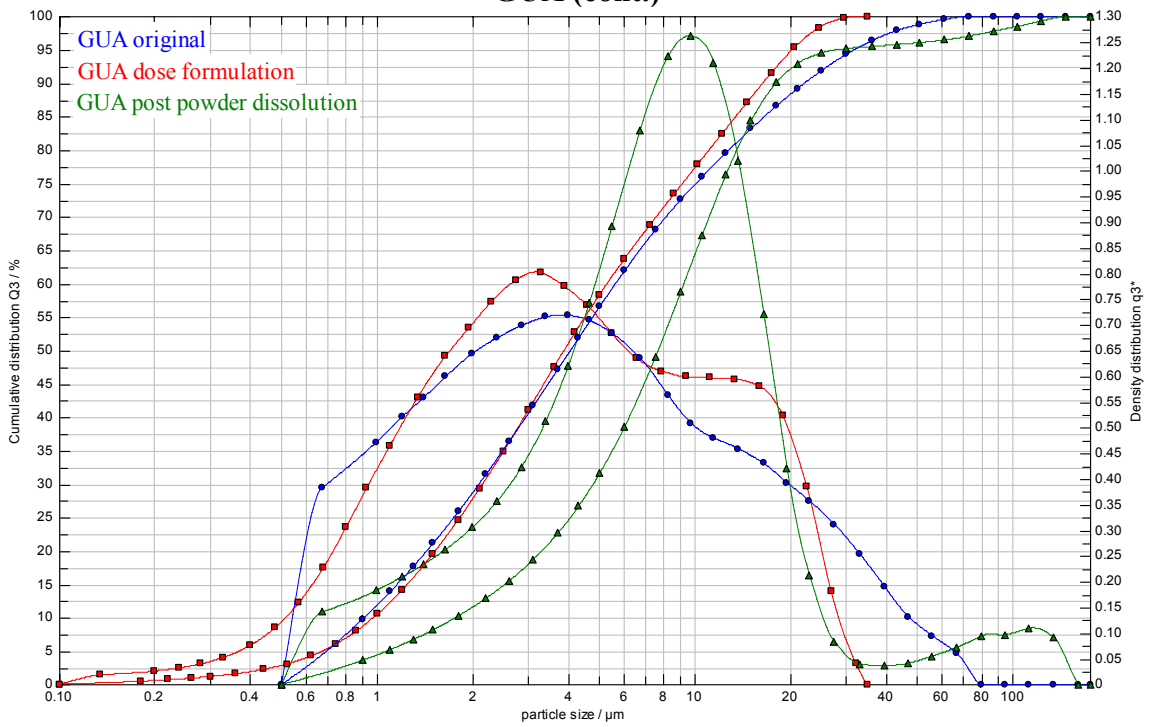

Particle Size Distributions

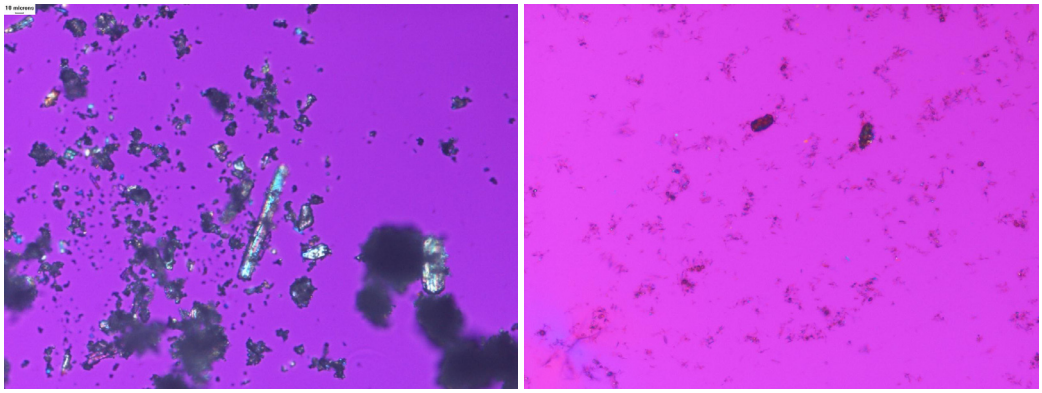

PLM: 200x original powder (left) post powder dissolution (right)

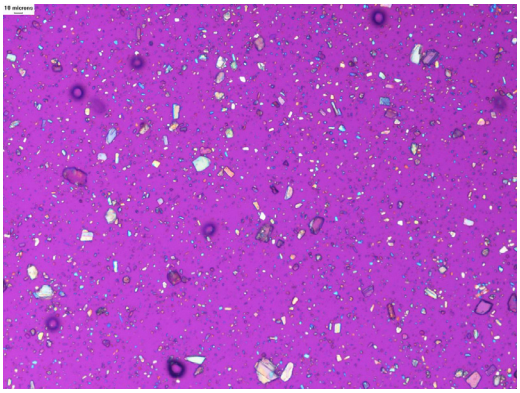

PLM: 200x post dose formulation

GUA (cont.)

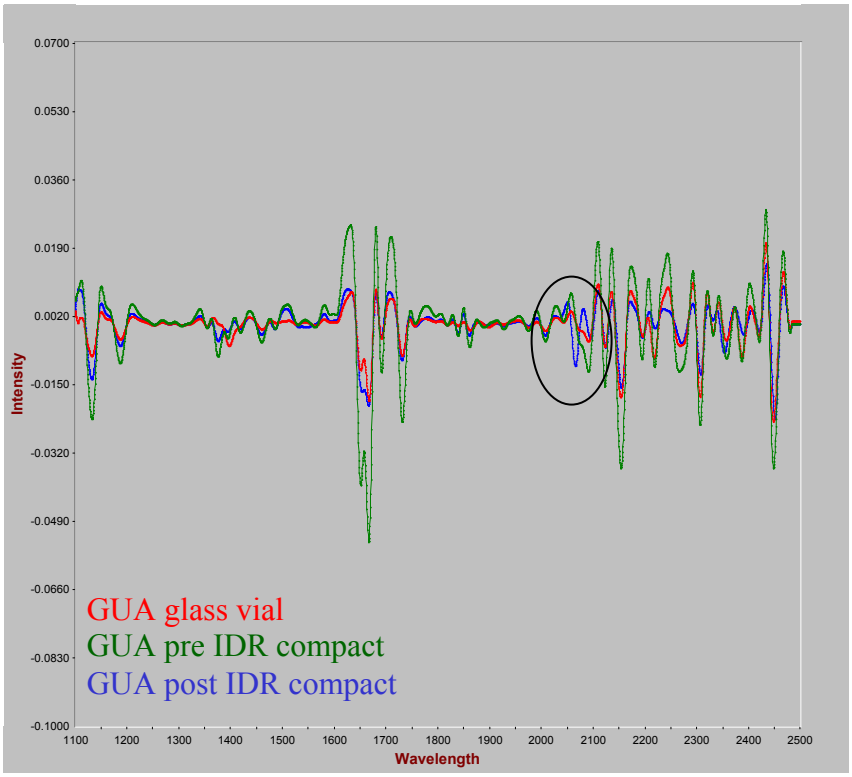

NIR: FBA at 2066nm post intrinsic dissolution

GYA

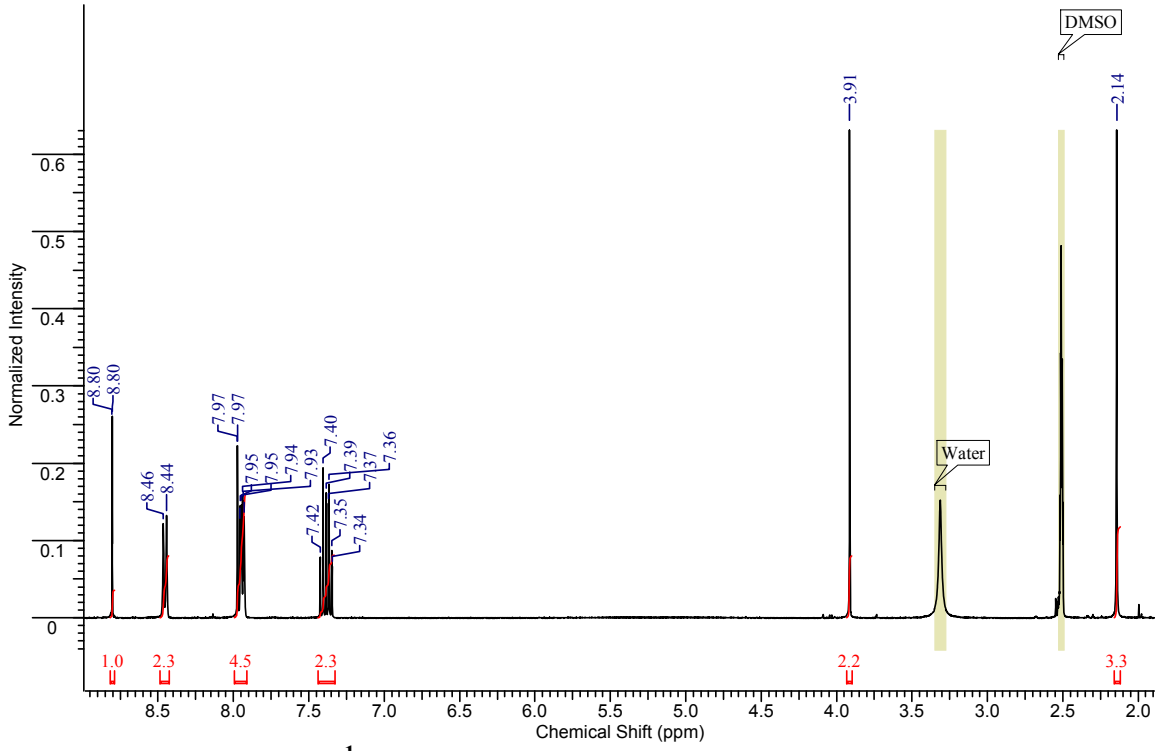

^{1}H NMR: 1.0 eq acid; CH_2 3.91ppm

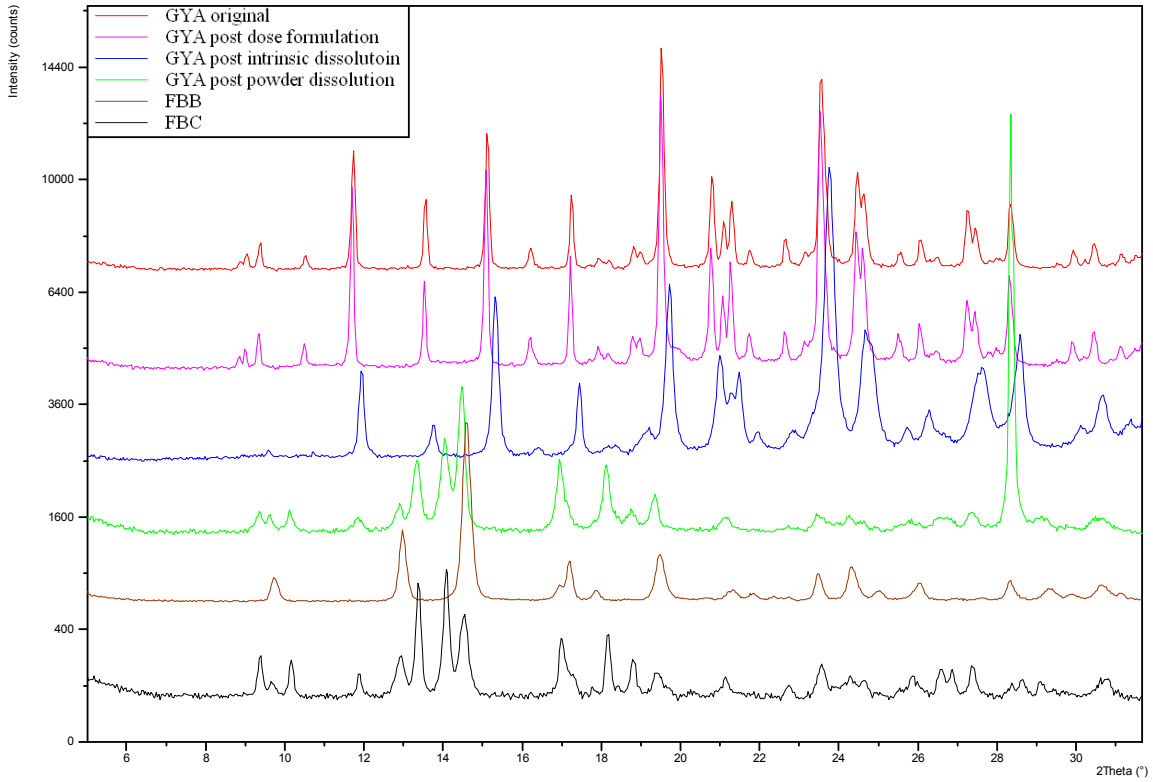

XRPD: FBC post powder dissolution

GYA (cont.)

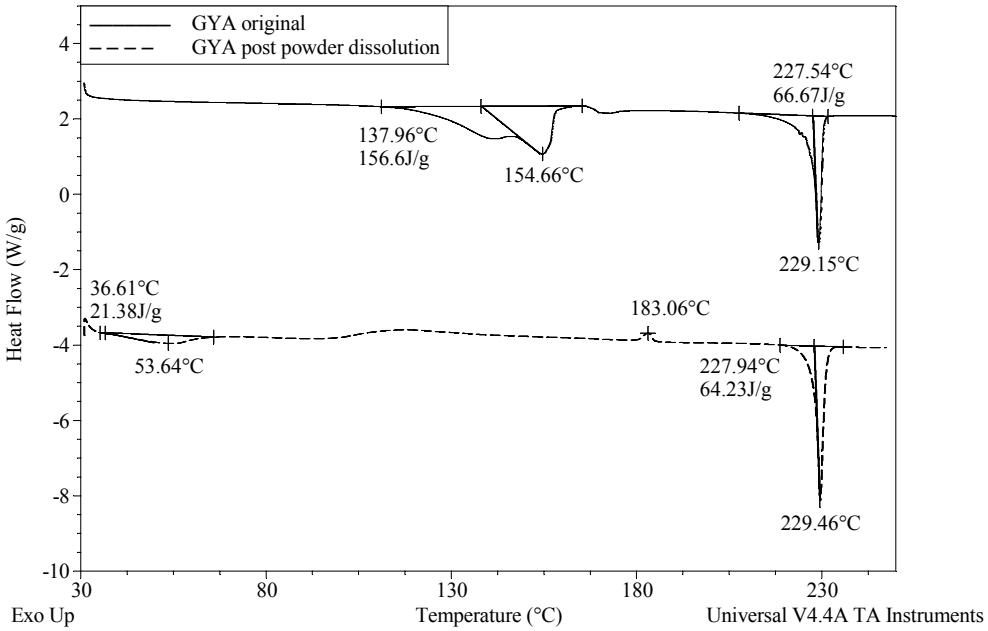

DSC: No cocrystal remaining, early endotherm likely **FBC**

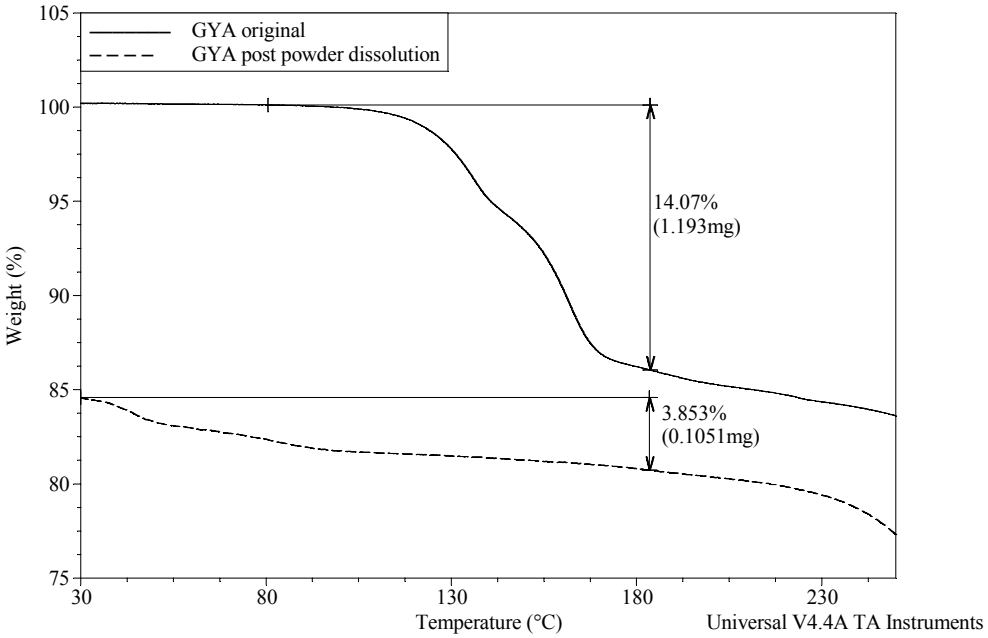

TGA: No cocrytsl remaining, 3.8% likely **FBC**

GYA (cont.)

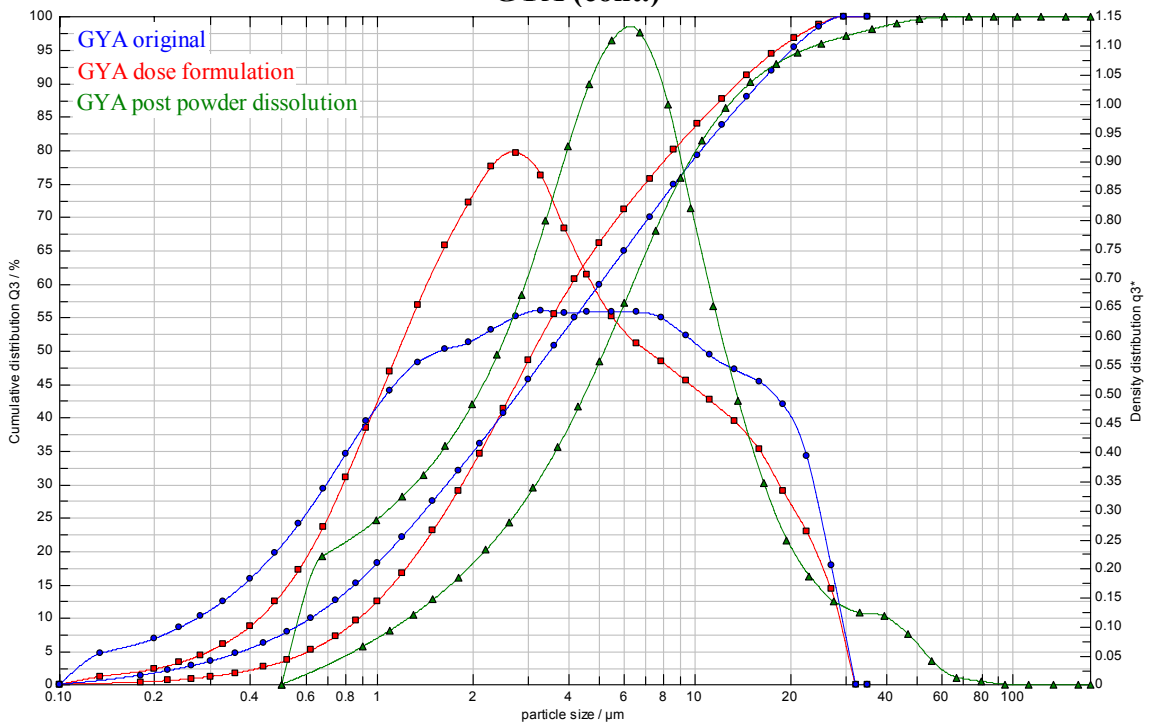

Particle Size Distributions

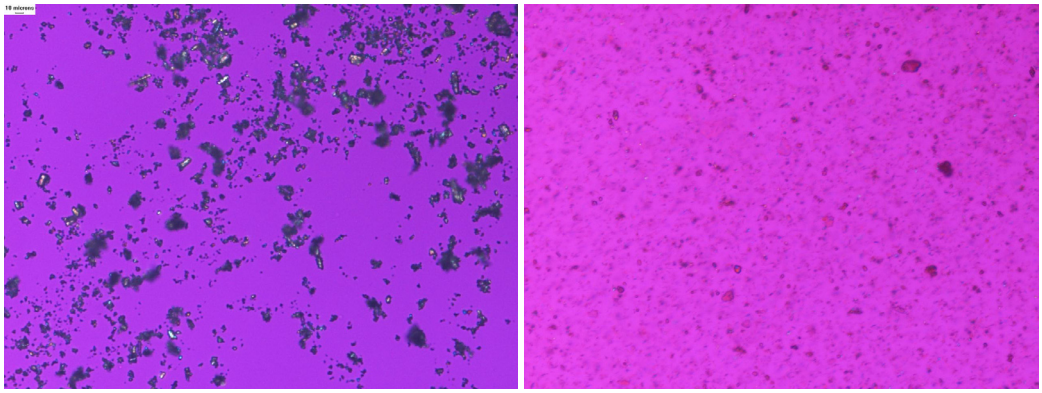

PLM: 200x original powder (left) post powder dissolution (right)

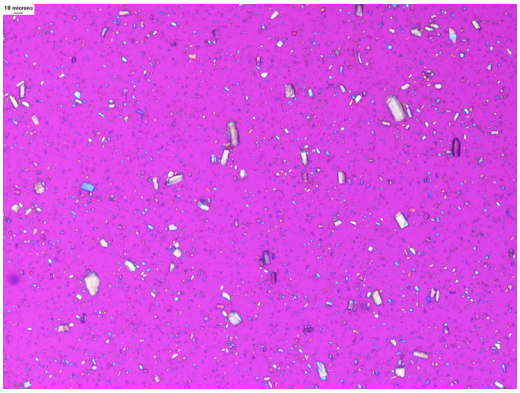

PLM: 200x post dose formulation

GYA (cont.)

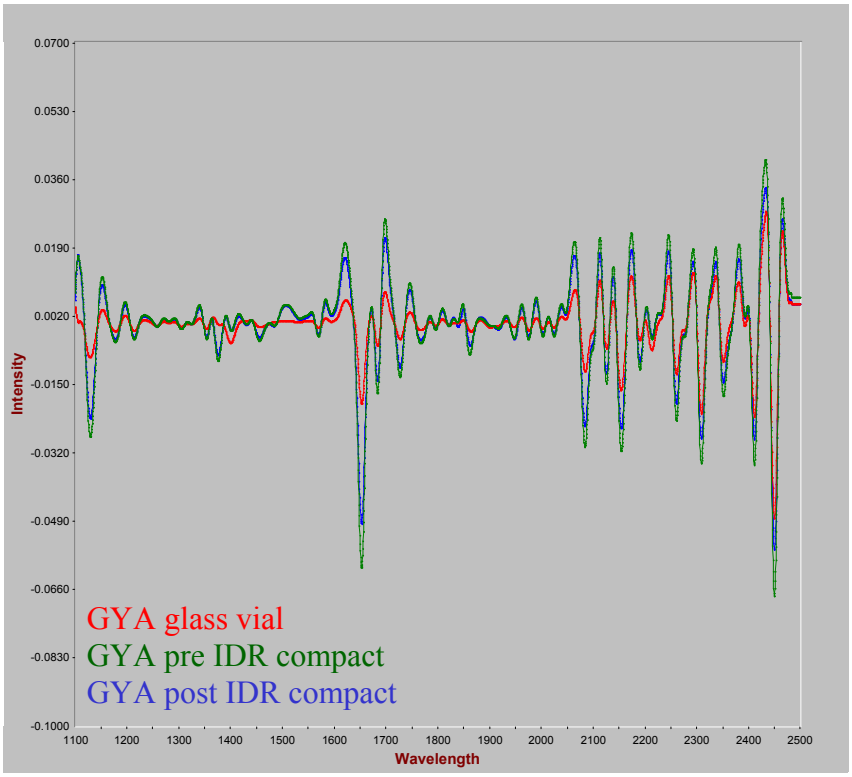

NIR: No change

HXA

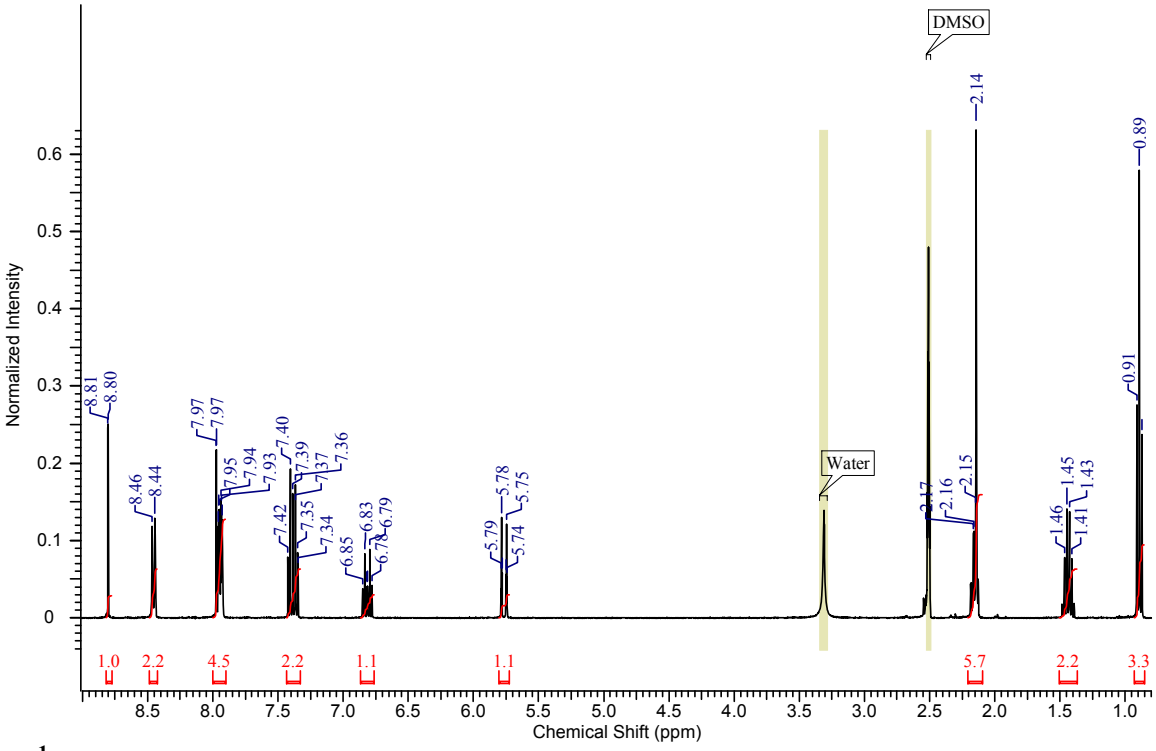

^{1}H NMR: 1.0 eq acid; CH 6.83 and 5.78ppm, CH_2 2.16 and 1.45ppm, CH_3 0.91ppm

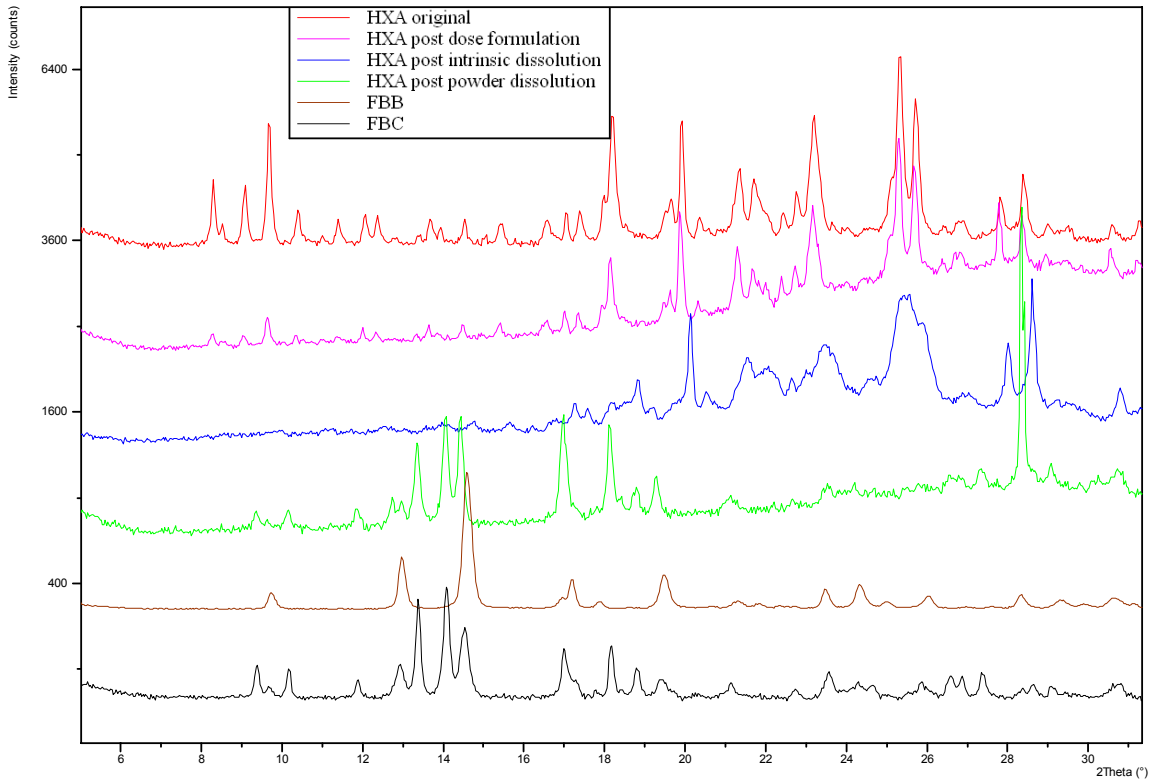

XRPD: FBC post powder dissolution

HXA (cont.)

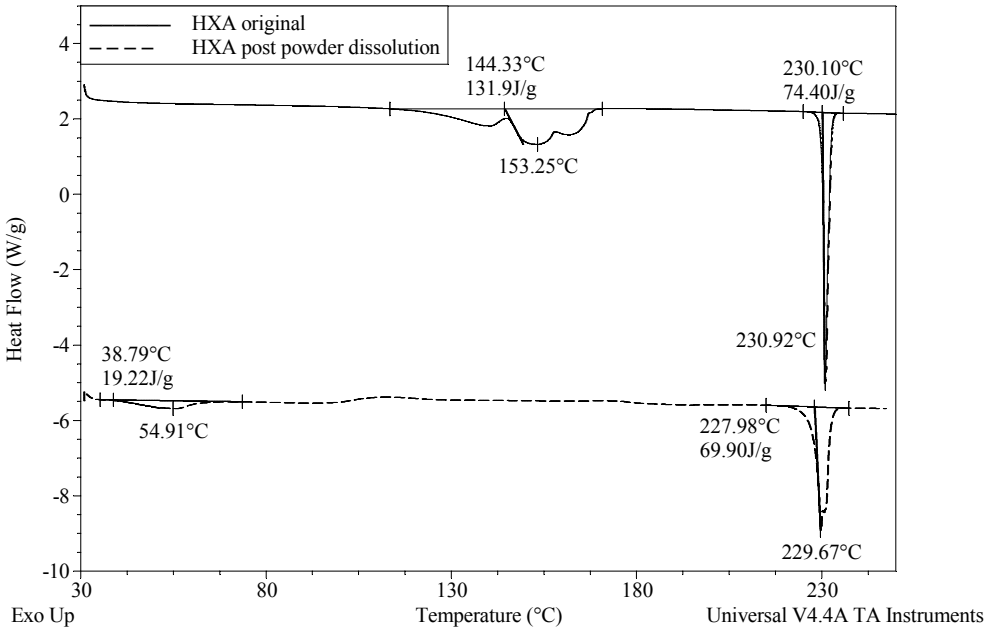

DSC: No cocrystal remaining, early endotherm likely **FBC**

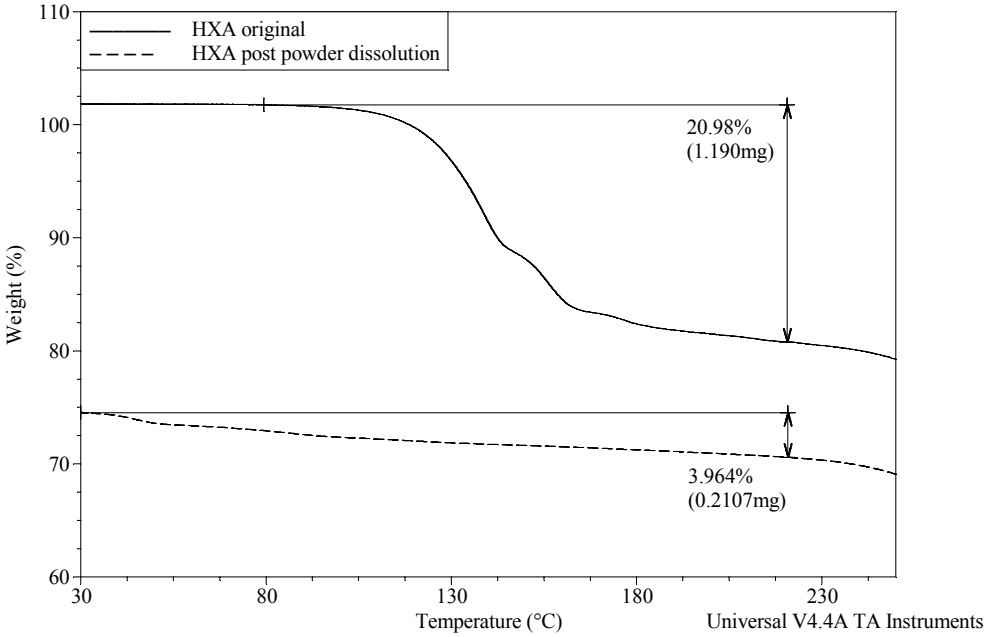

TGA: No cocrytsl remaining, 3.9% likely **FBC**

HXA (cont.)

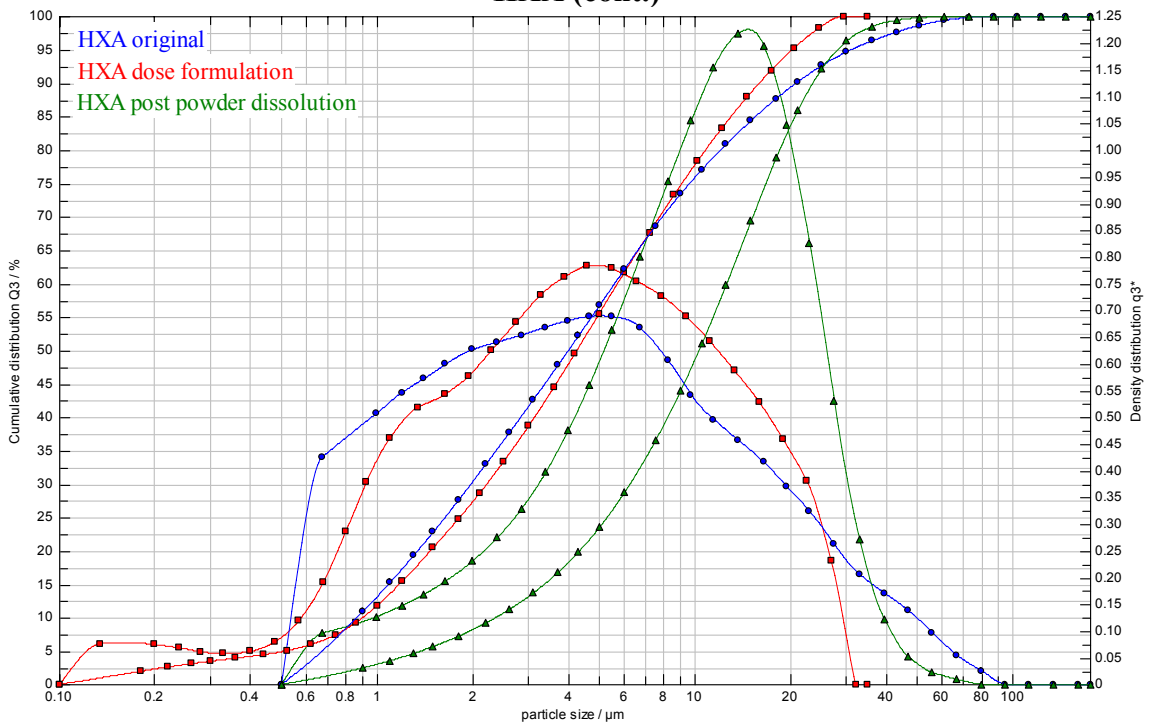

Particle Size Distributions

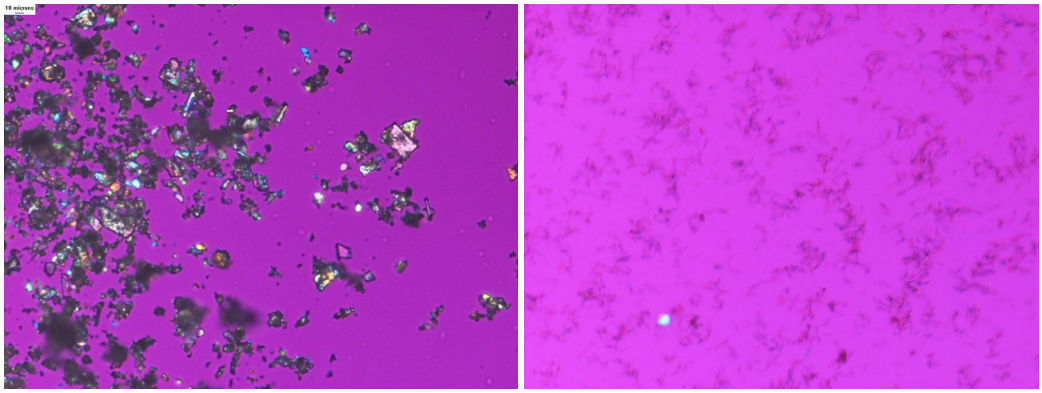

PLM: 200x original powder (left) post powder dissolution (right)

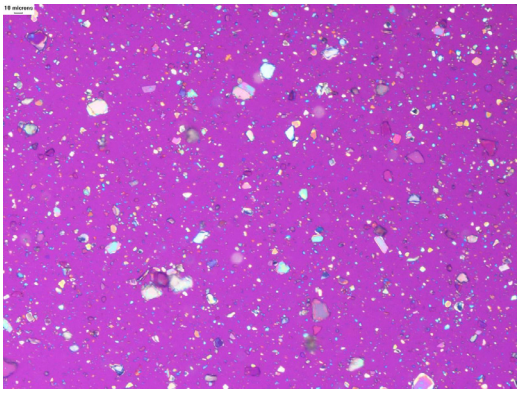

PLM: 200x post dose formulation

HXA (cont.)

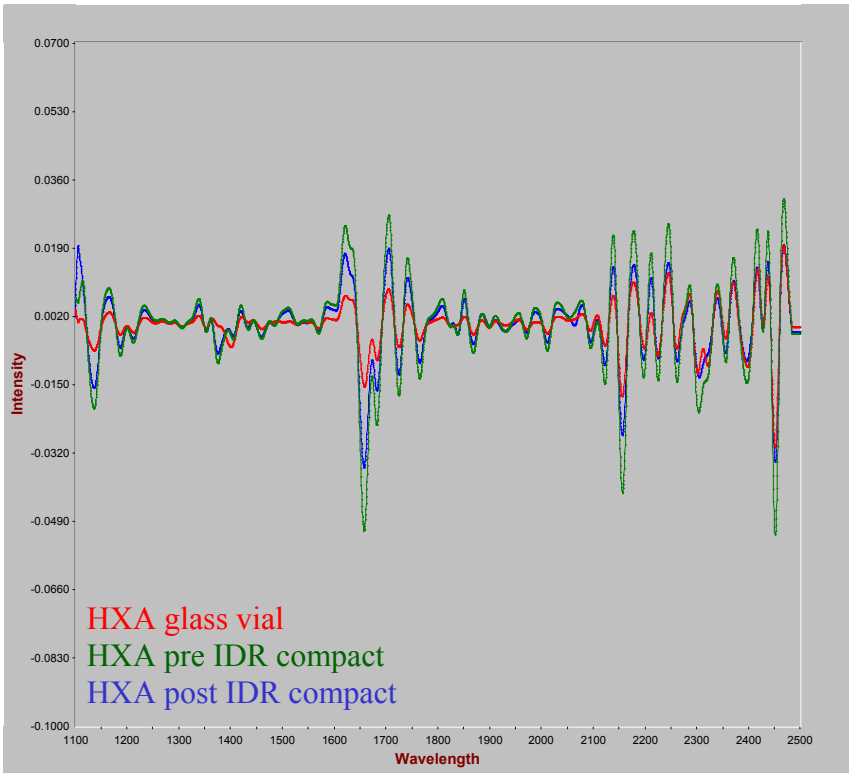

NIR: No change

HCA

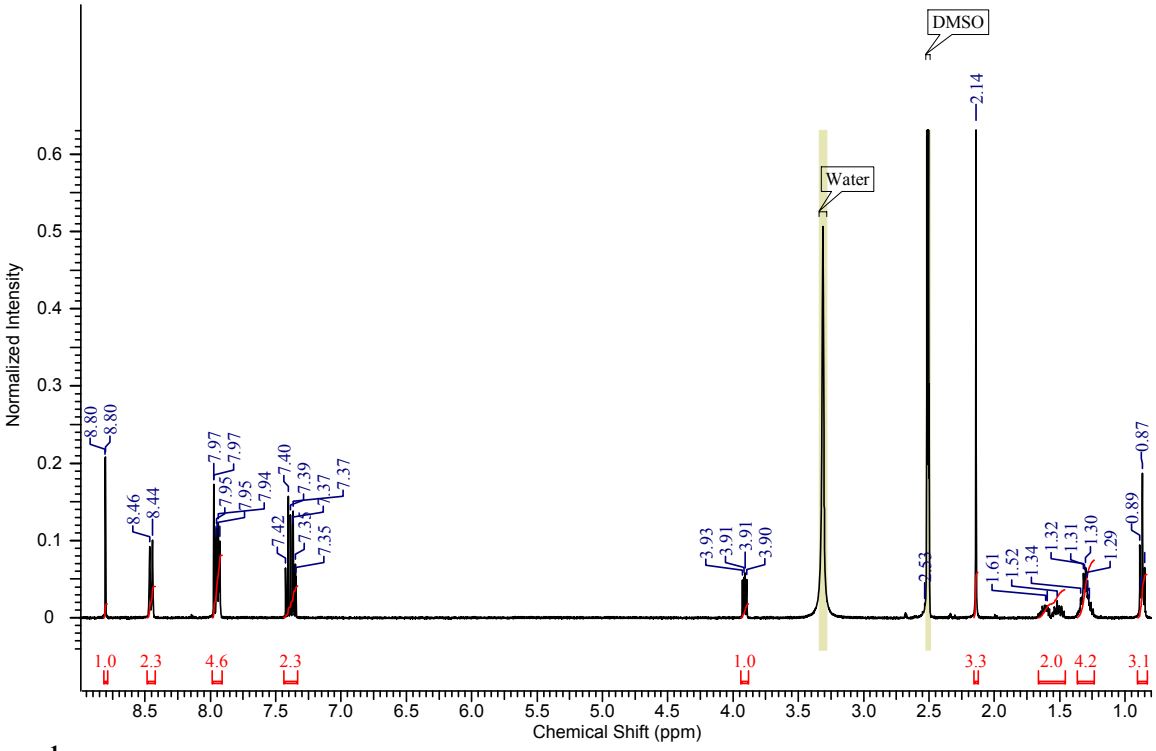

^{1}H NMR: 1.0 eq acid; CH 3.91ppm, CH_2 1.52ppm, 2(CH_2) 1.3ppm, CH_3 0.87ppm

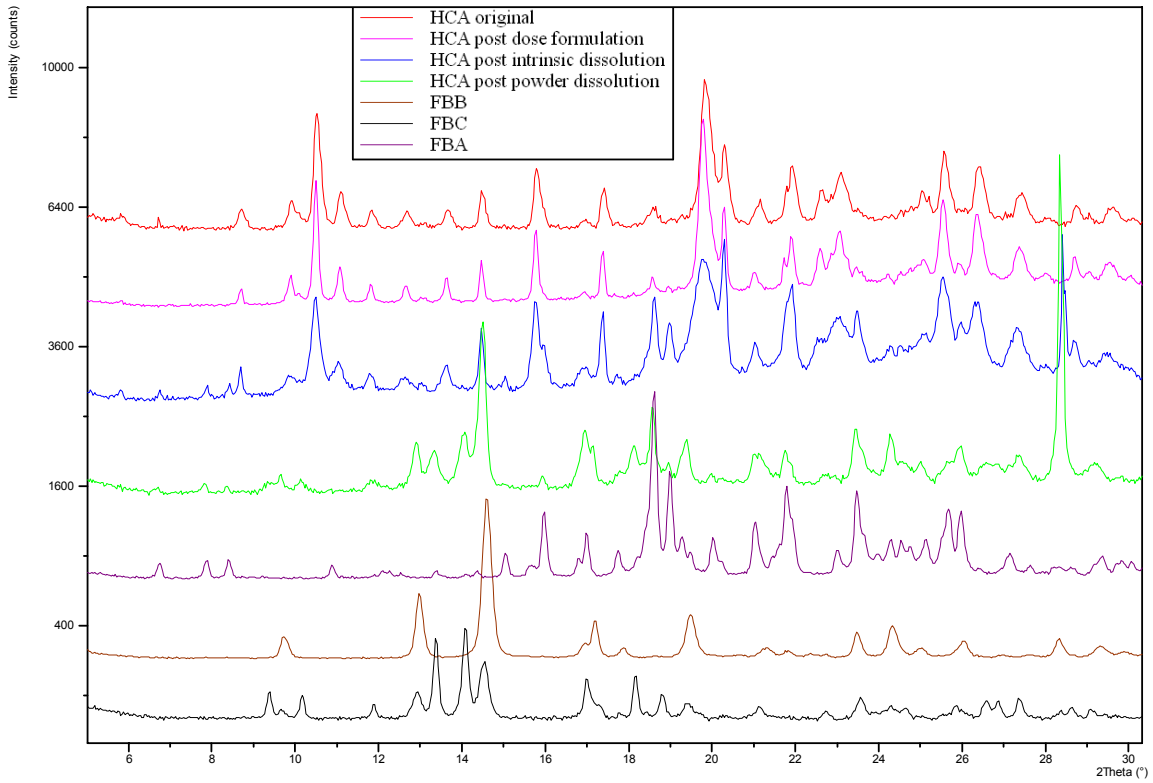

XRPD: FBC/FBA post powder dissolution, **HCA/FBA** post intrinsic dissolution

HCA (cont.)

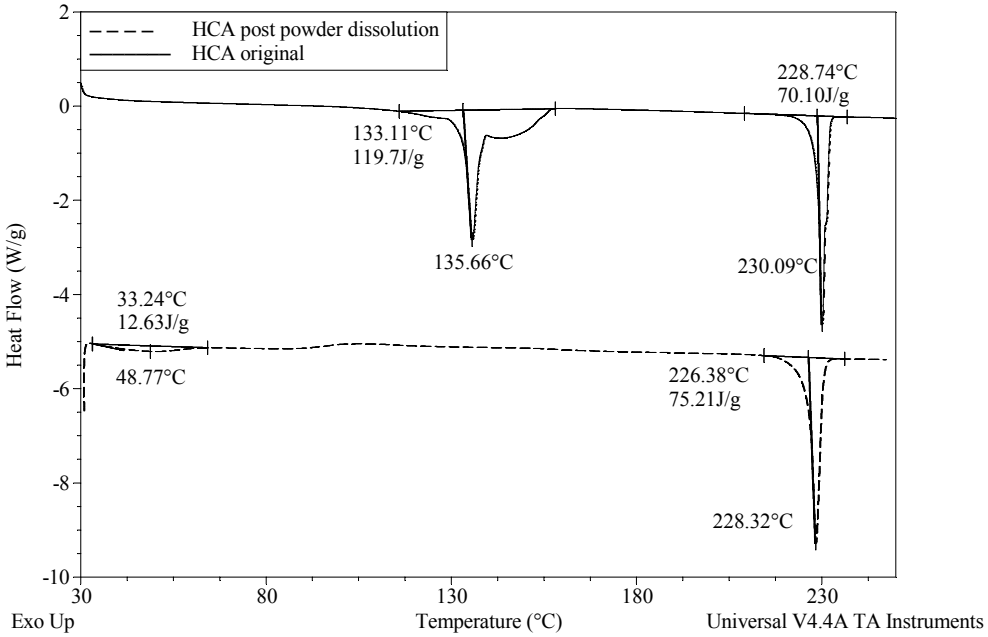

DSC: No cocrystal remaining, early endotherm likely **FBC**

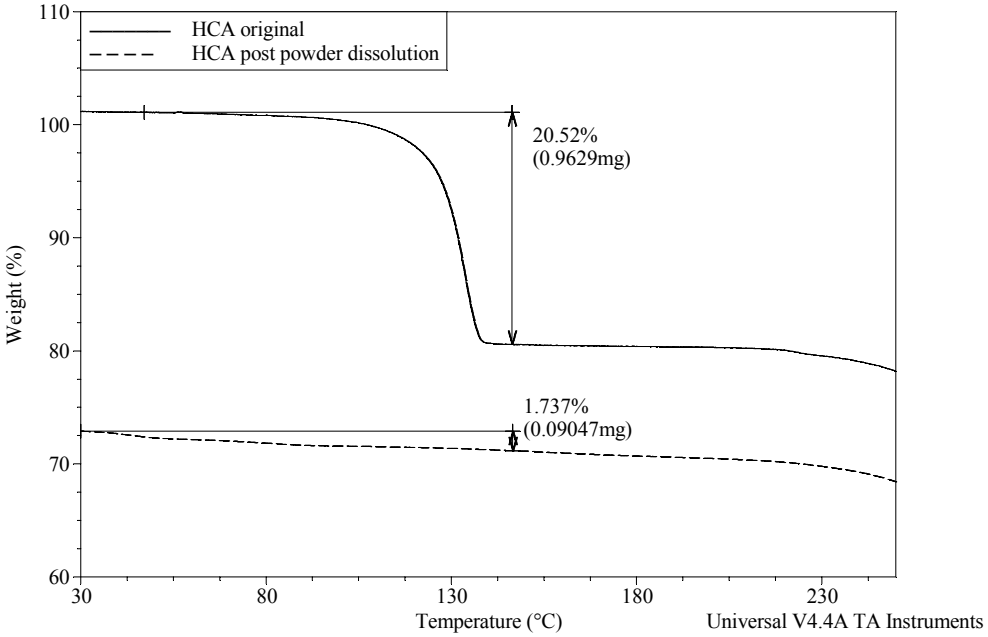

TGA: No cocrytsl remaining, 1.7% likely **FBC**

HCA (cont.)

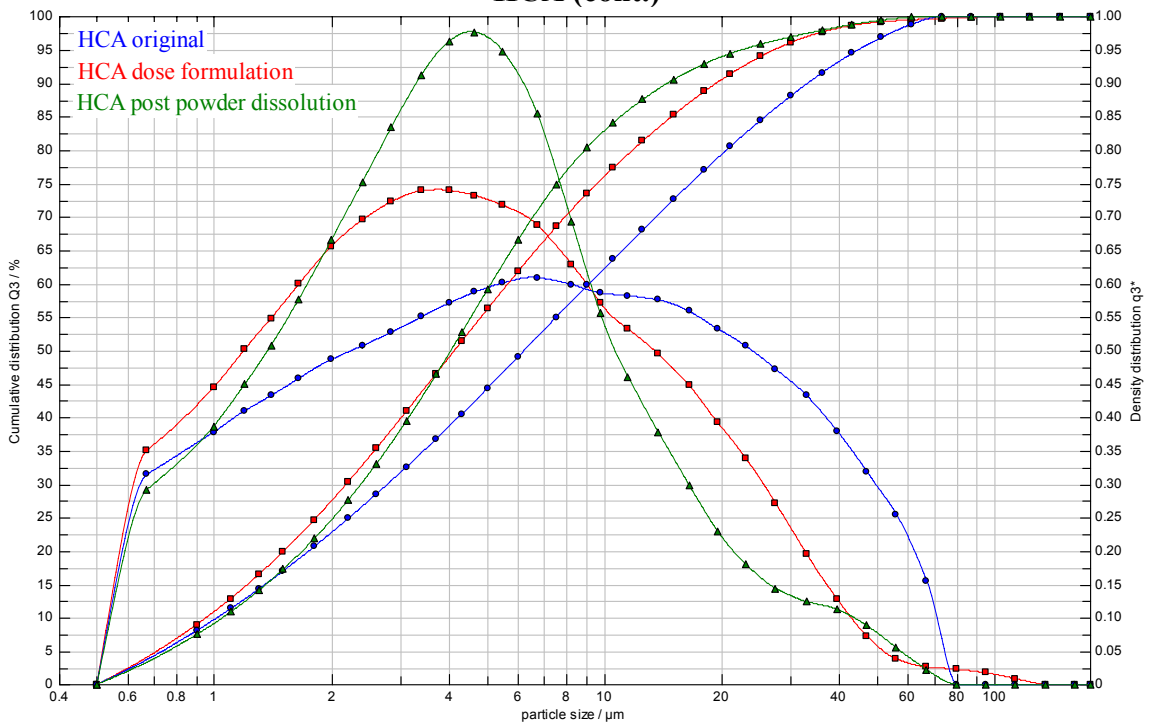

Particle Size Distributions

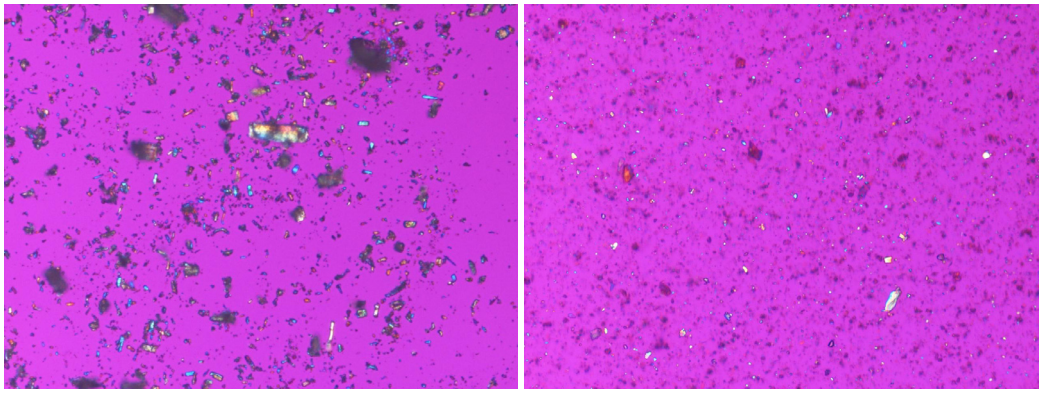

PLM: 200x original powder (left) post powder dissolution (right)

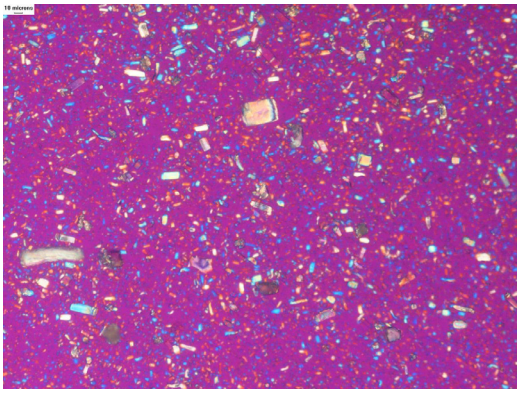

PLM: 200x post dose formulation

HCA (cont.)

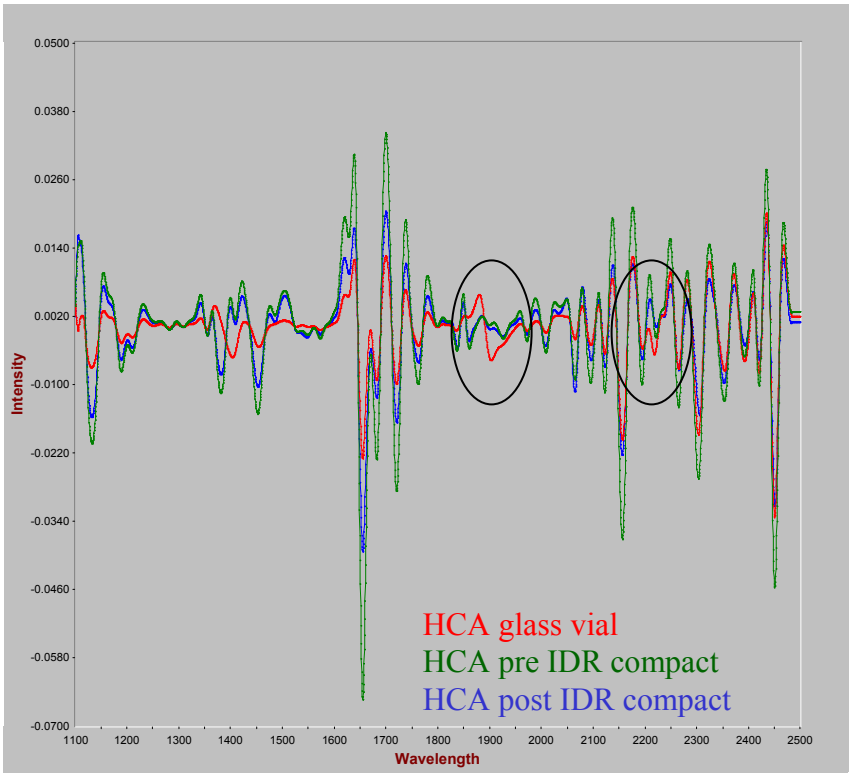

NIR: Changes at 1901 & 2220nm post compaction

LCA

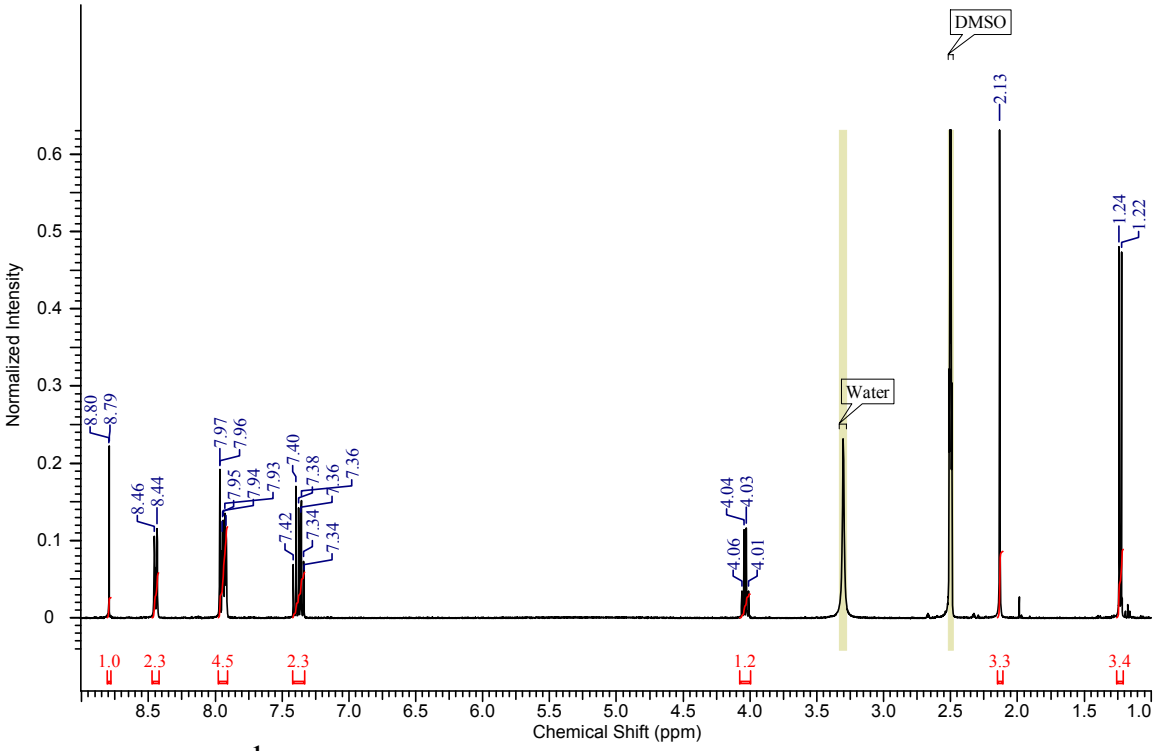

^{1}H NMR: 1.0 eq acid; CH 4.03ppm, CH_3 1.24ppm

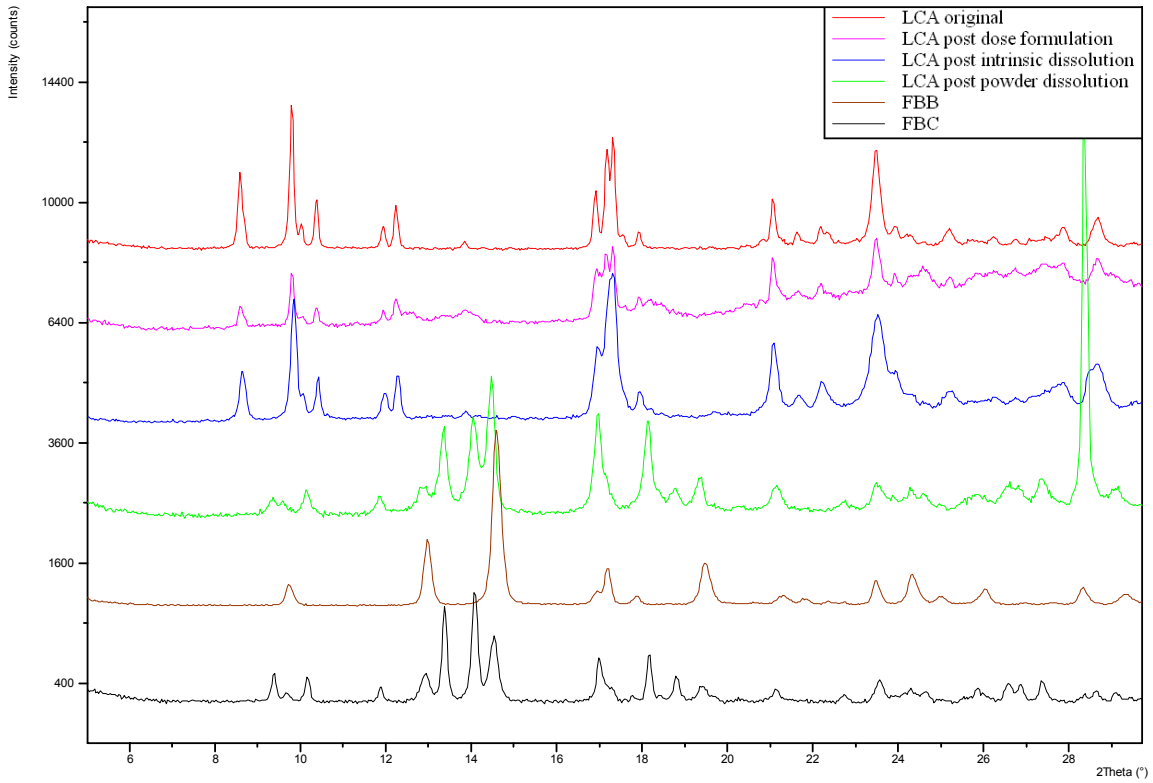

XRPD: FBC post powder dissolution

LCA (cont.)

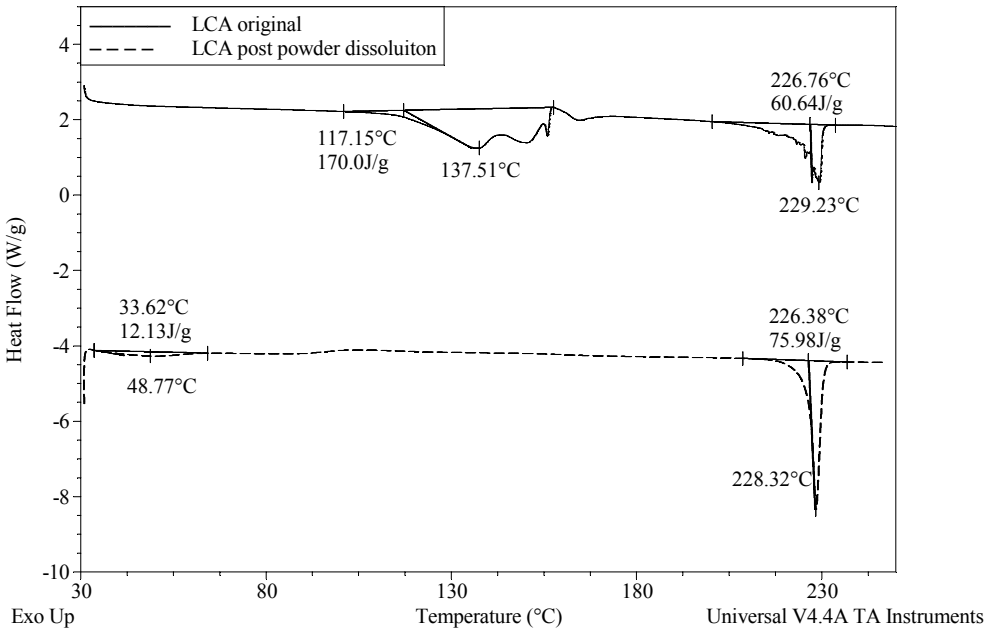

DSC: No cocrystal remaining, early endotherm likely **FBC**

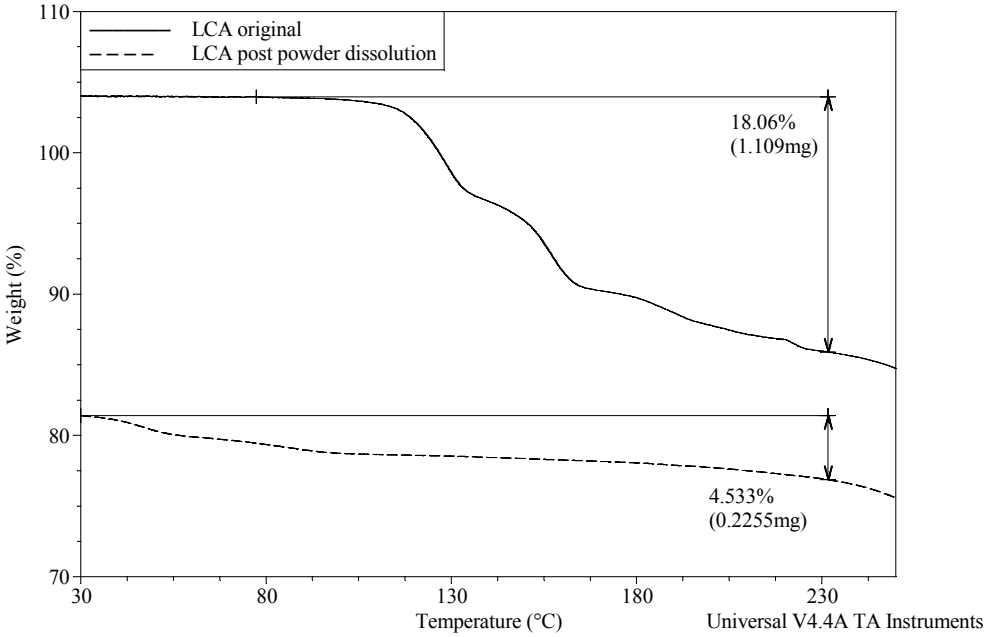

TGA: No cocrytsl remaining, 4.5% likely **FBC**

LCA (cont.)

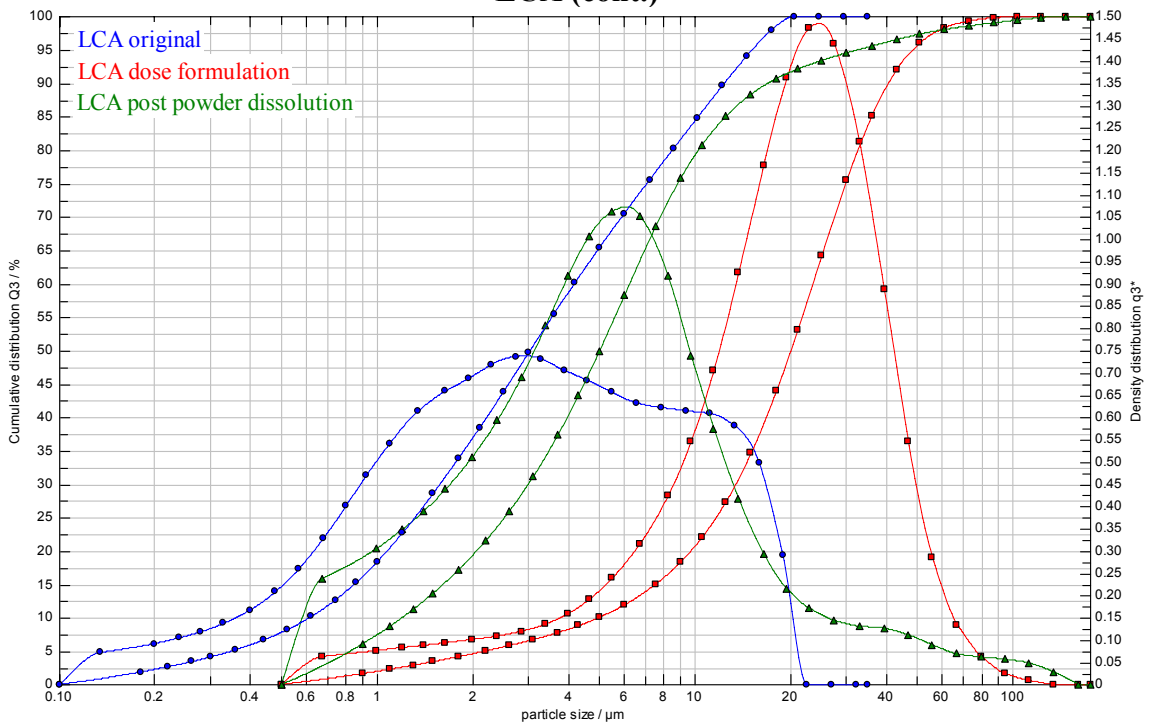

Particle Size Distributions

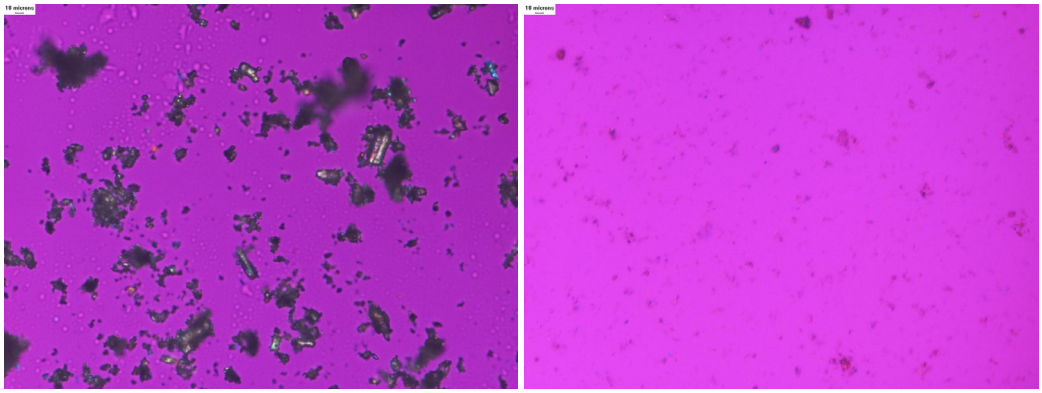

PLM: 200x original powder (left) post powder dissolution (right)

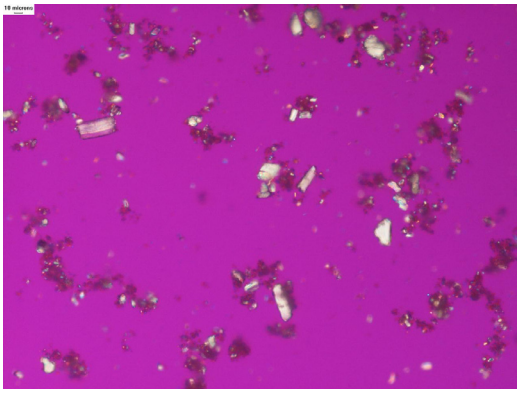

PLM: 200x post dose formulation

LCA (cont.)

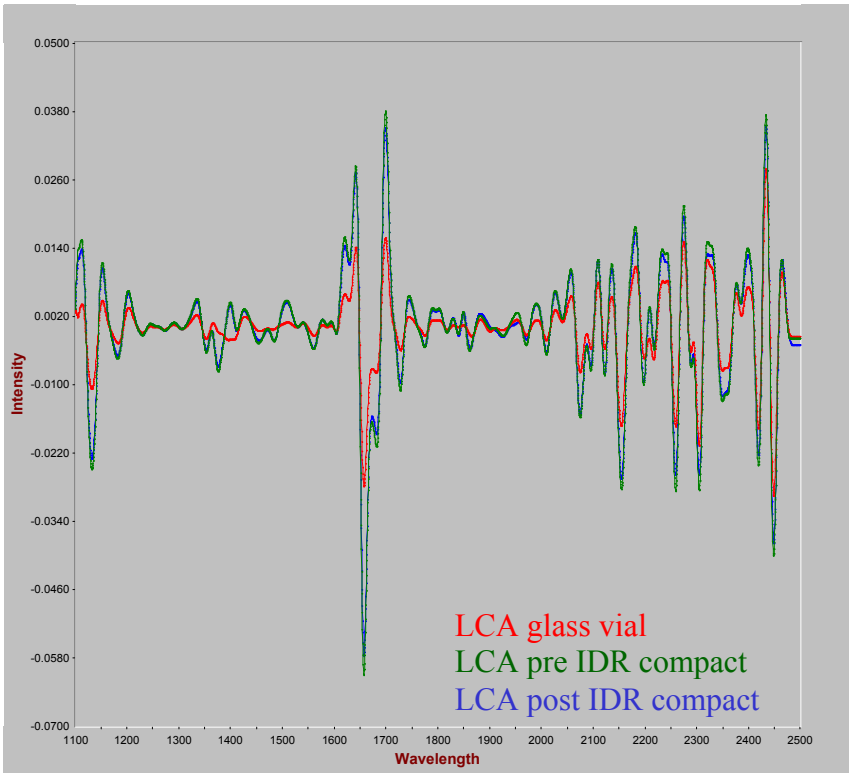

NIR: No change

MEA

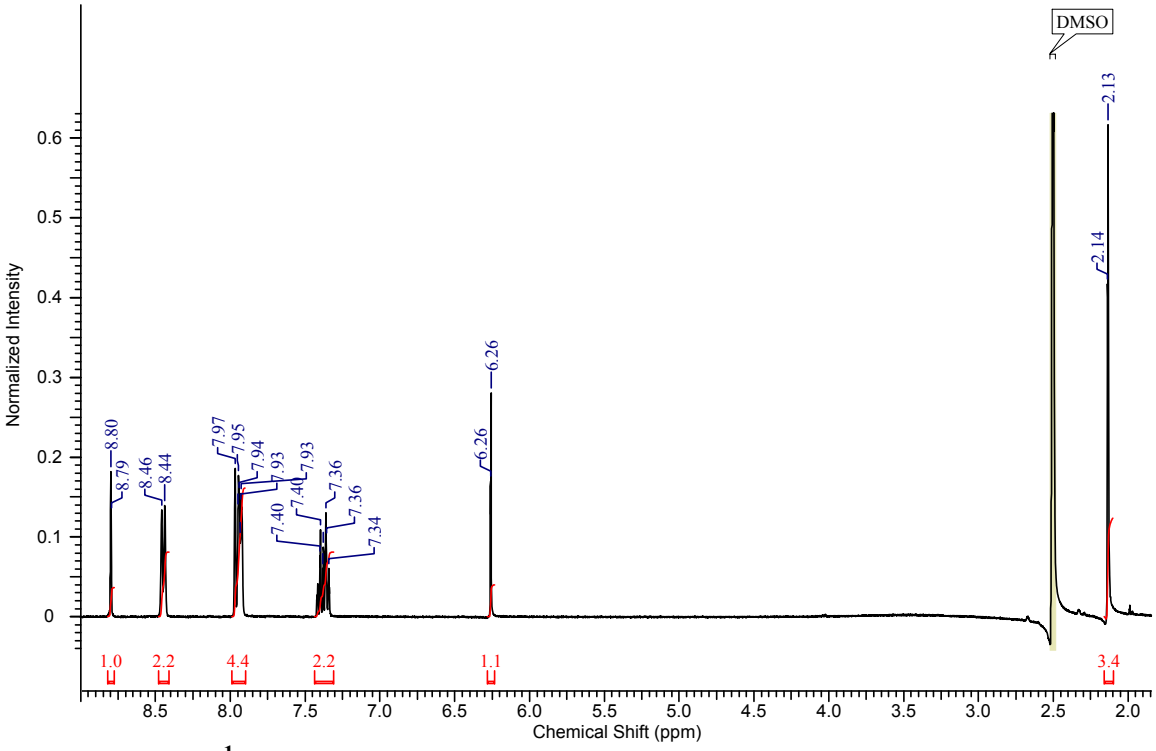

^{1}H NMR: 0.5 eq acid; 2(CH) integrate as 1 at 6.26ppm

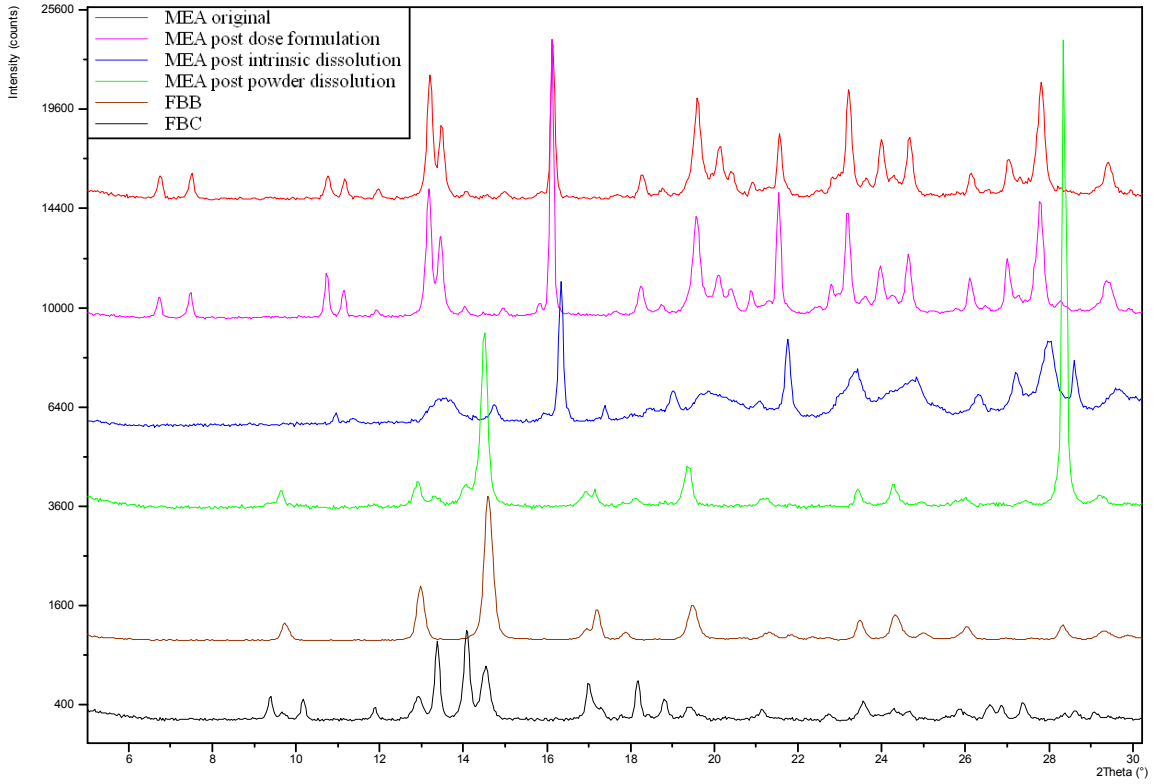

XRPD: FBB/FBC post powder dissolution

MEA (cont.)

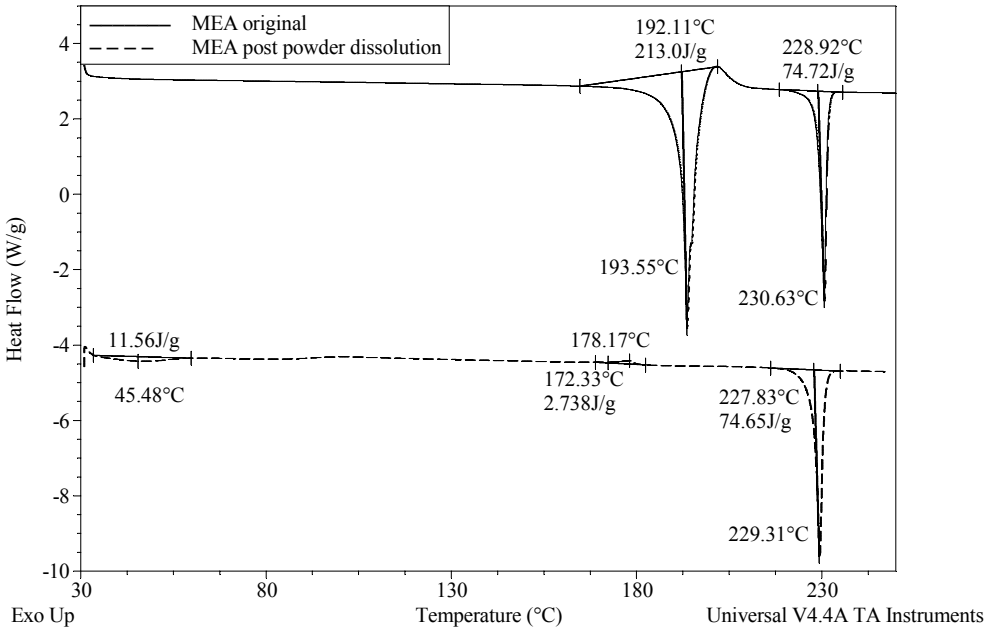

DSC: No cocrystal remaining, early endotherm likely **FBC**

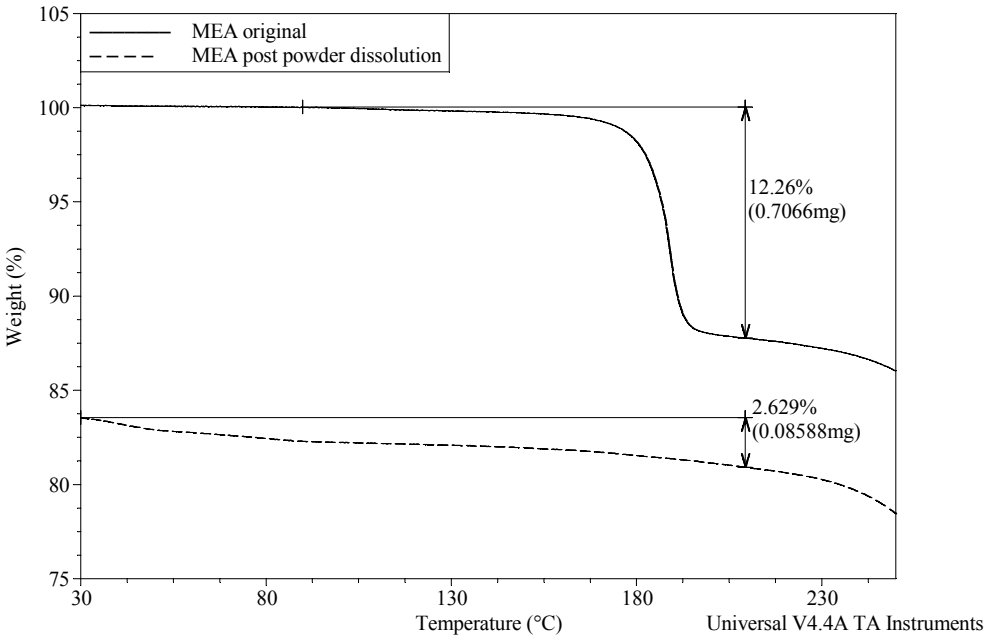

TGA: No cocrytsl remaining, 2.6% likely **FBC**

MEA (cont.)

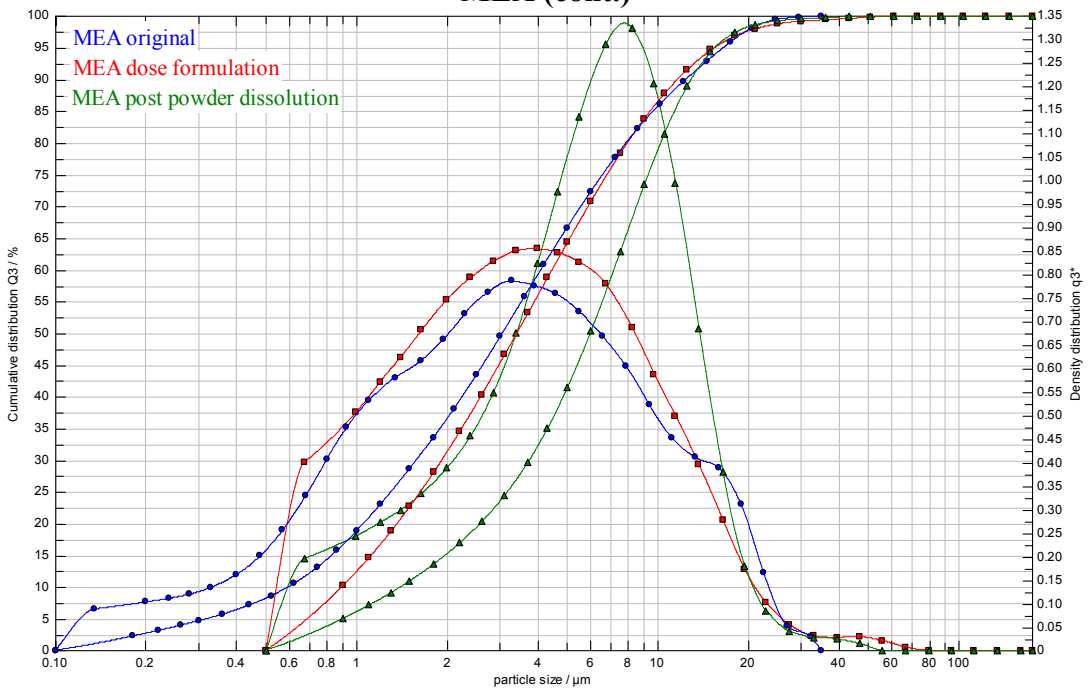

Particle Size Distributions

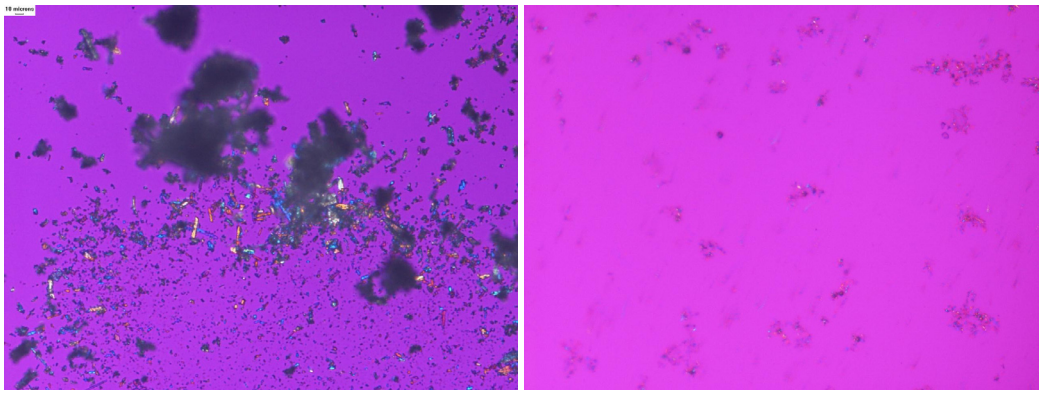

PLM: 200x original powder (left) post powder dissolution (right)

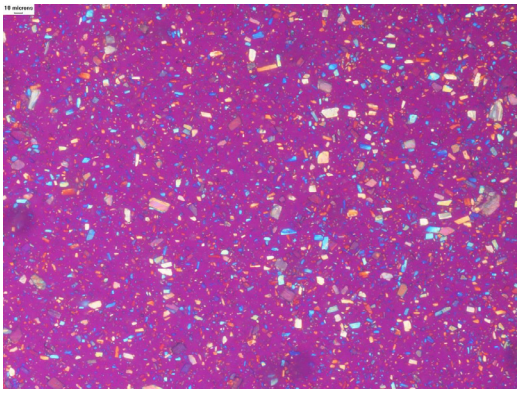

PLM: 200x post dose formulation

MEA (cont.)

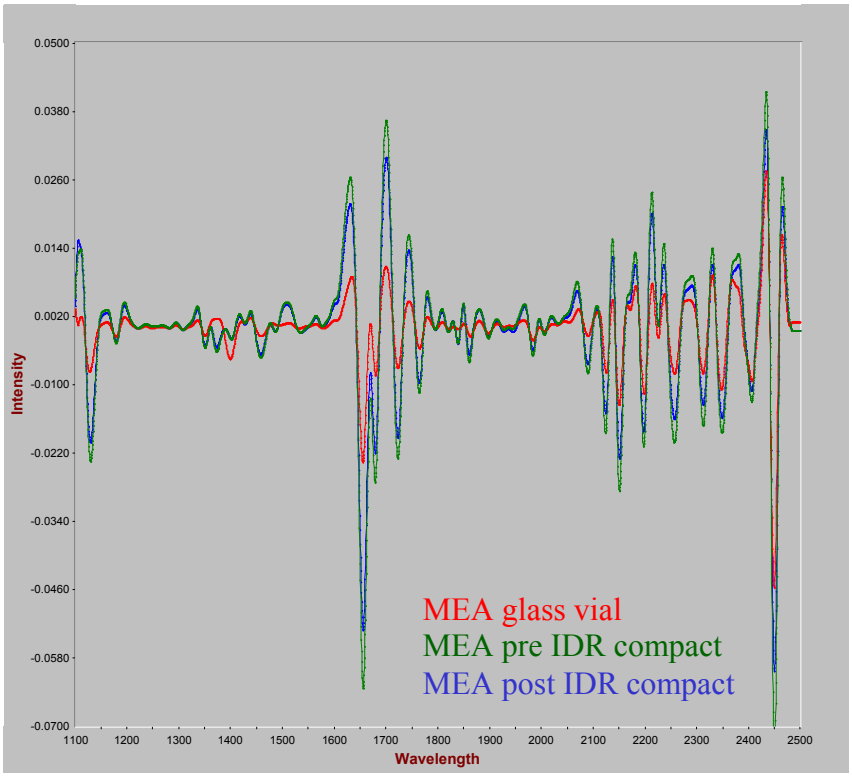

NIR: No change

MIA

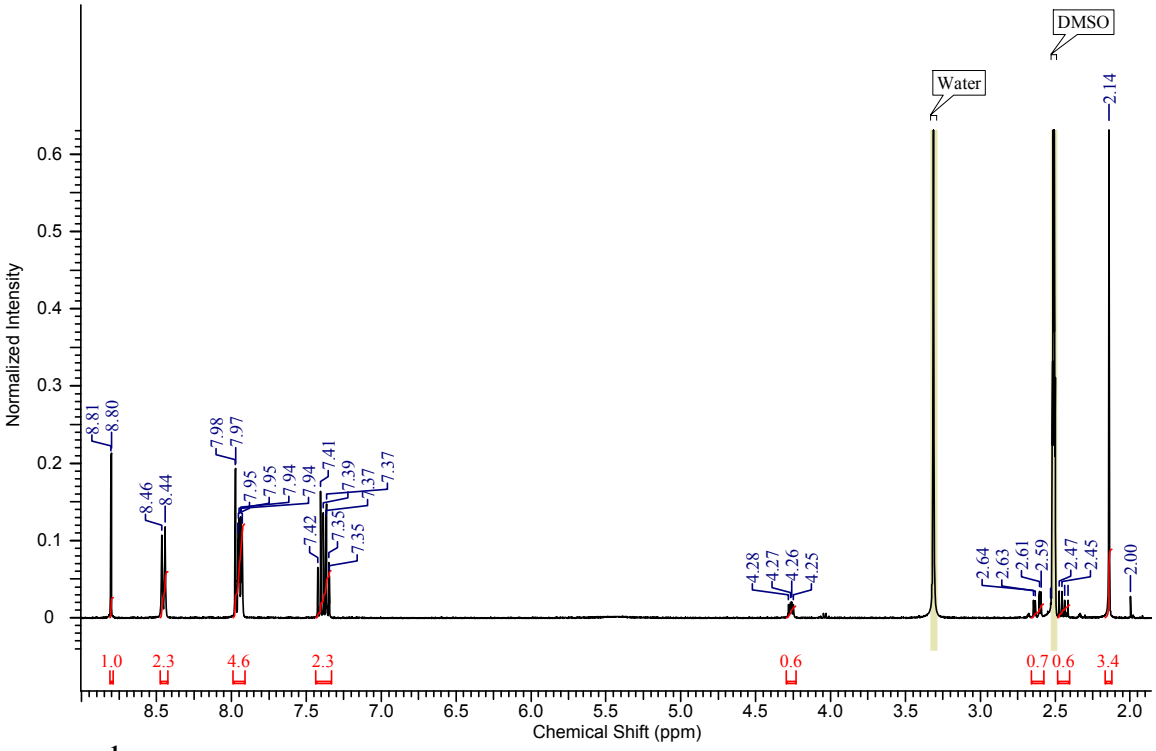

^{1}H NMR: 0.5 eq acid; 3(CH) integrates as 0.5 at 4.26, 2.61 and 2.47ppm

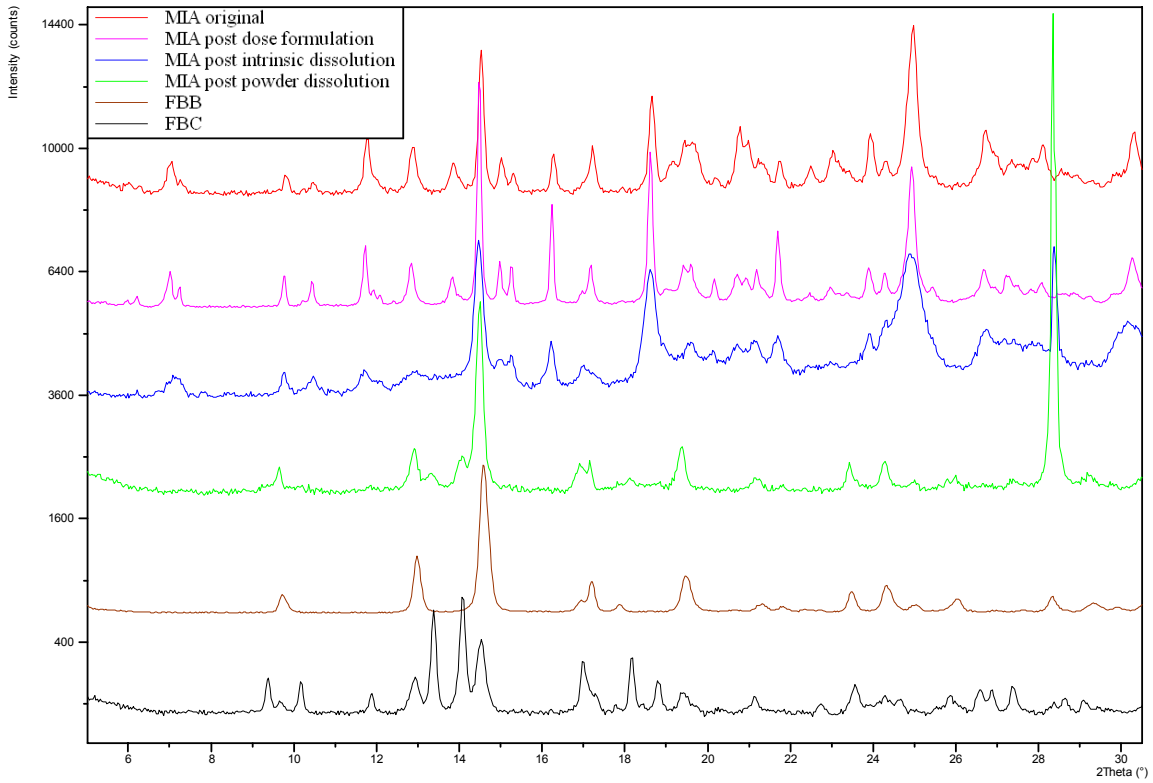

XRPD: FBB/FBC post powder dissolution

MIA (cont.)

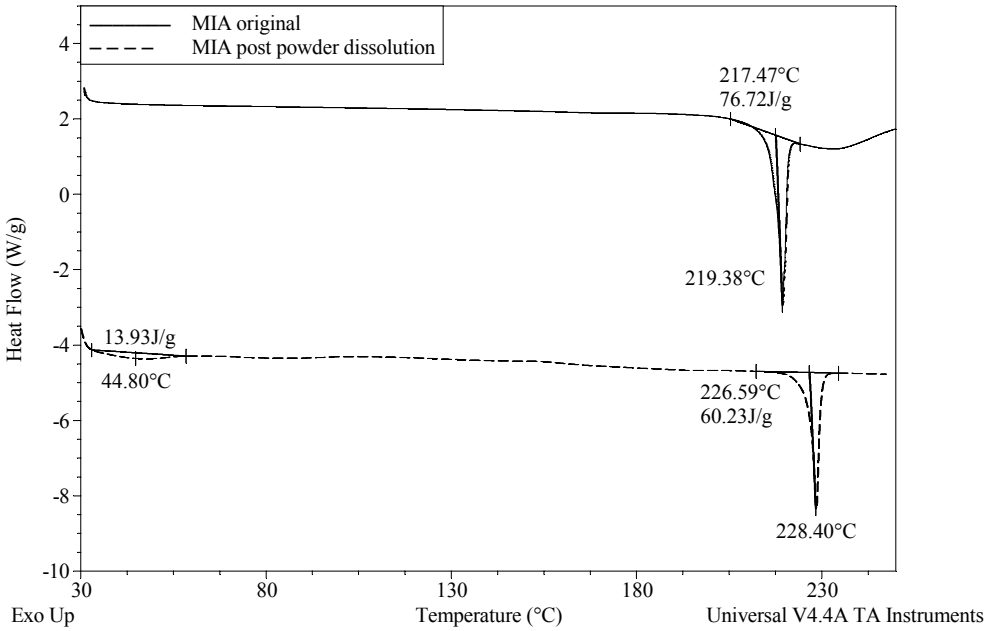

DSC: No cocrystal remaining, early endotherm likely **FBC**

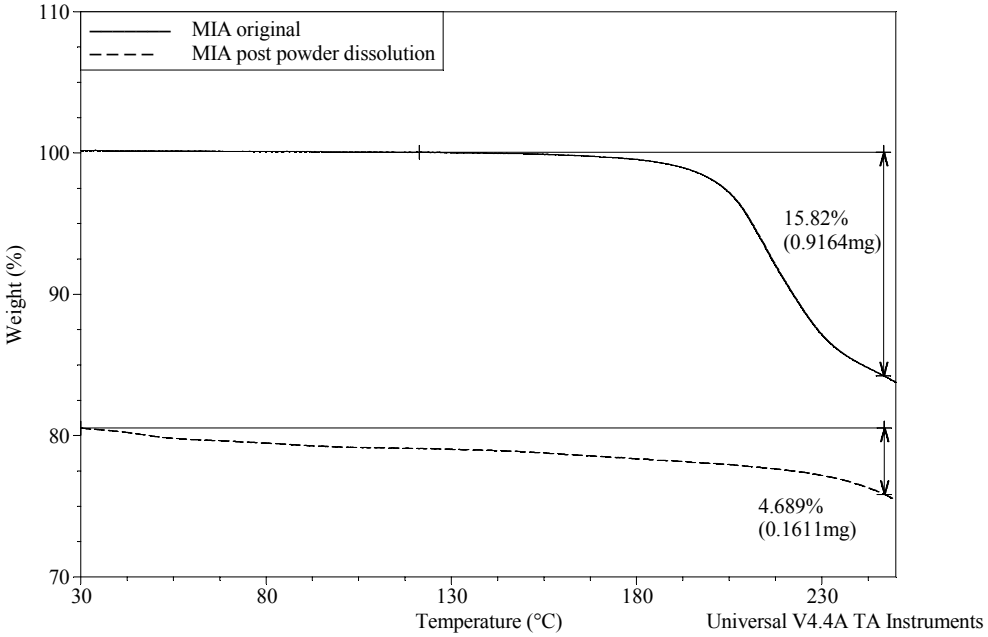

TGA: No cocrytsl remaining, 4.7% likely **FBC**

MIA (cont.)

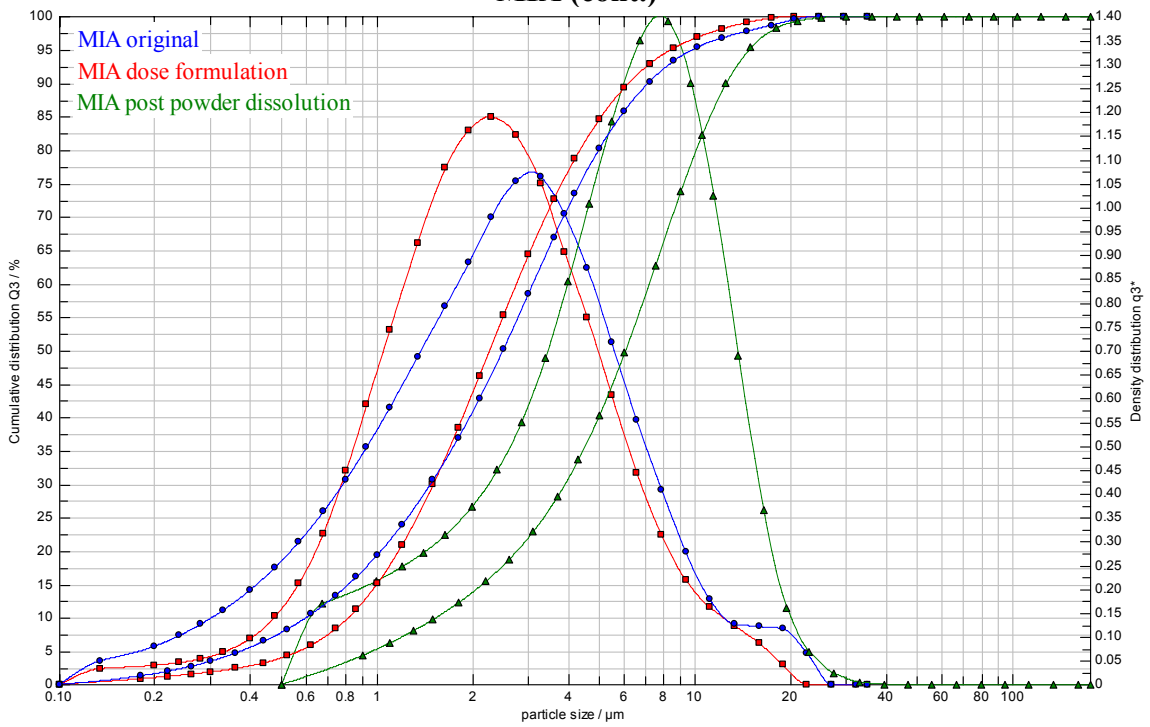

Particle Size Distributions

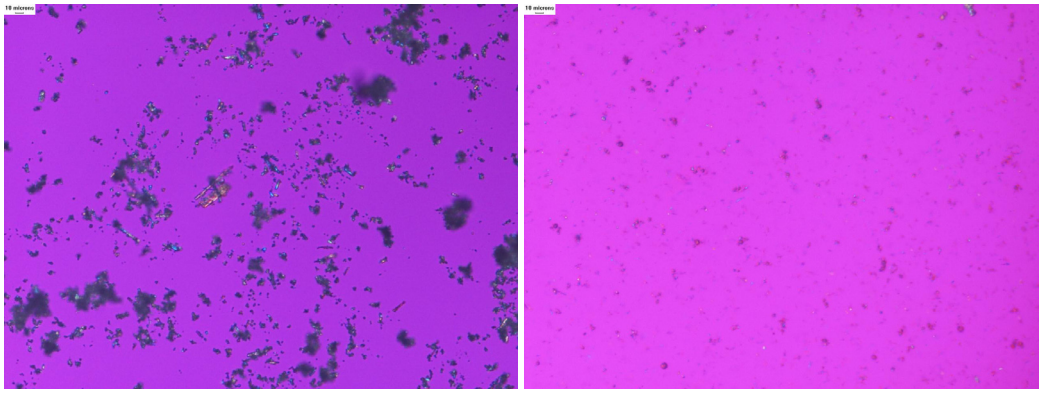

PLM: 200x original powder (left) post powder dissolution (right)

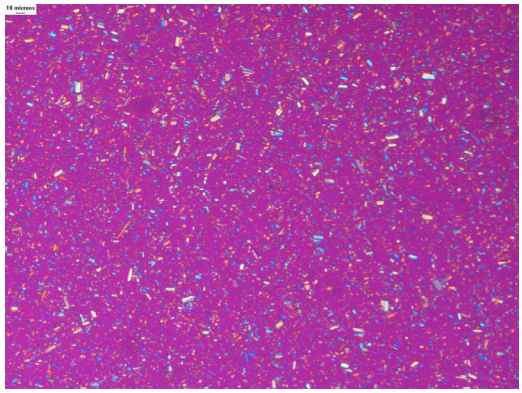

PLM: 200x post dose formulation

MIA (cont.)

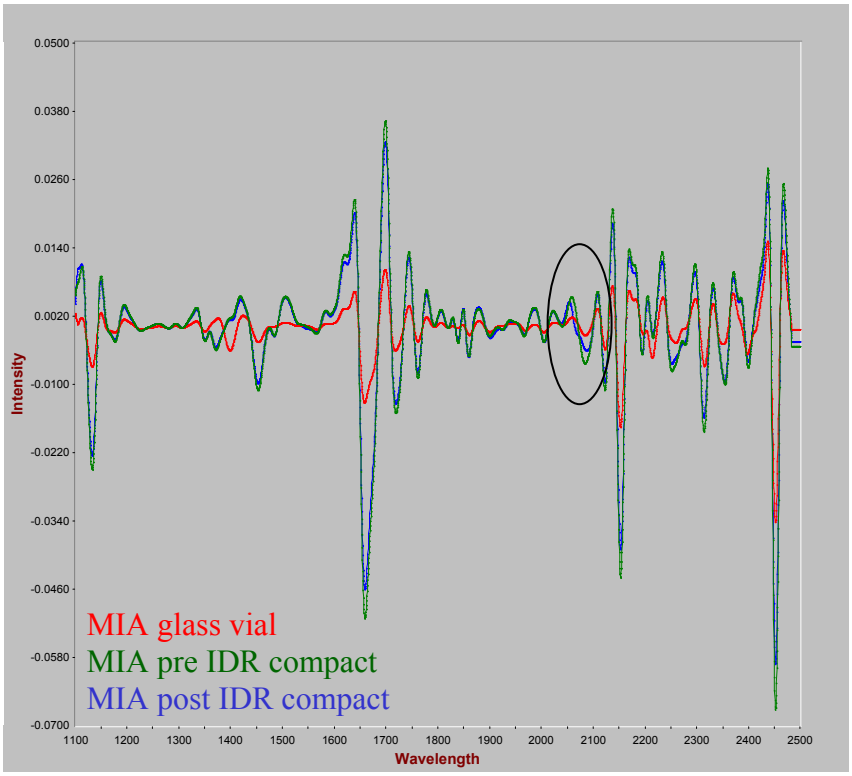

NIR: FBA very minor at 2066nm post intrinsic dissolution

MOA

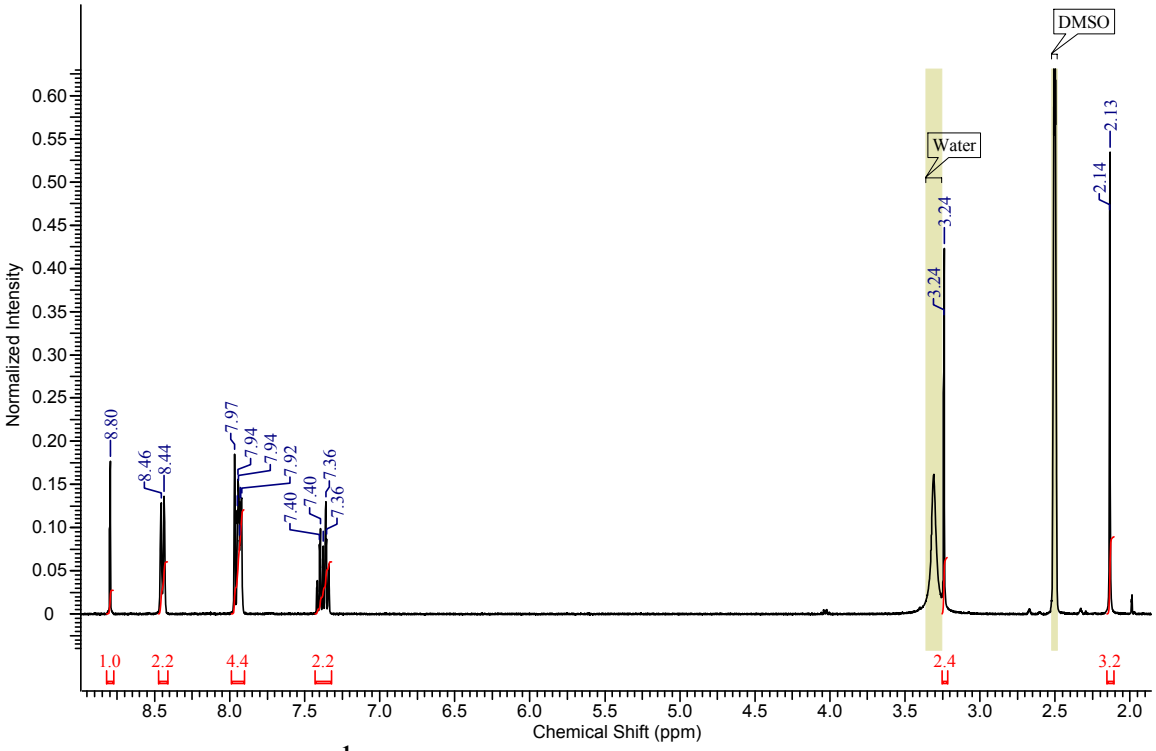

^{1}H NMR: 1.0 eq acid; CH_2 3.24ppm

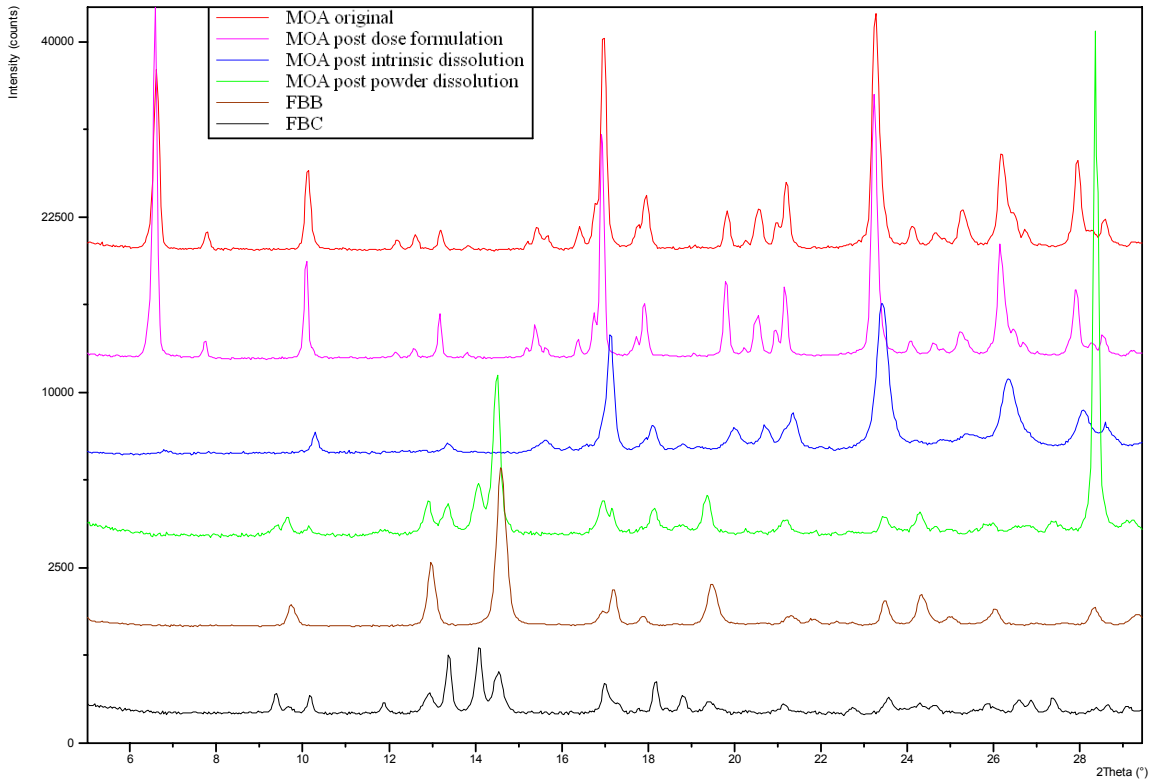

XRPD: FBB/FBC post powder dissolution

MOA (cont.)

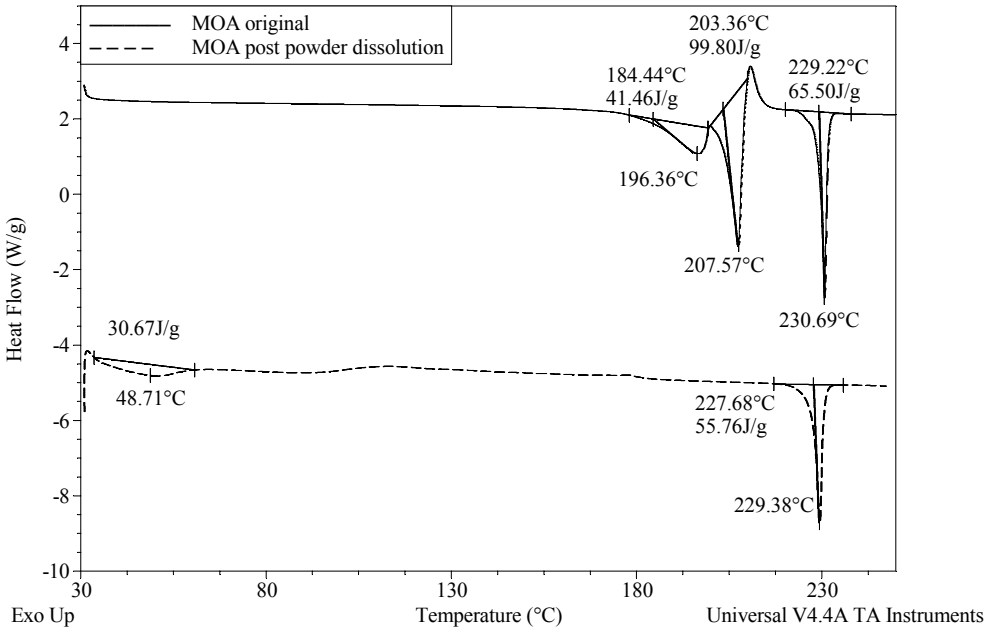

DSC: No cocrystal remaining, early endotherm likely **FBC**

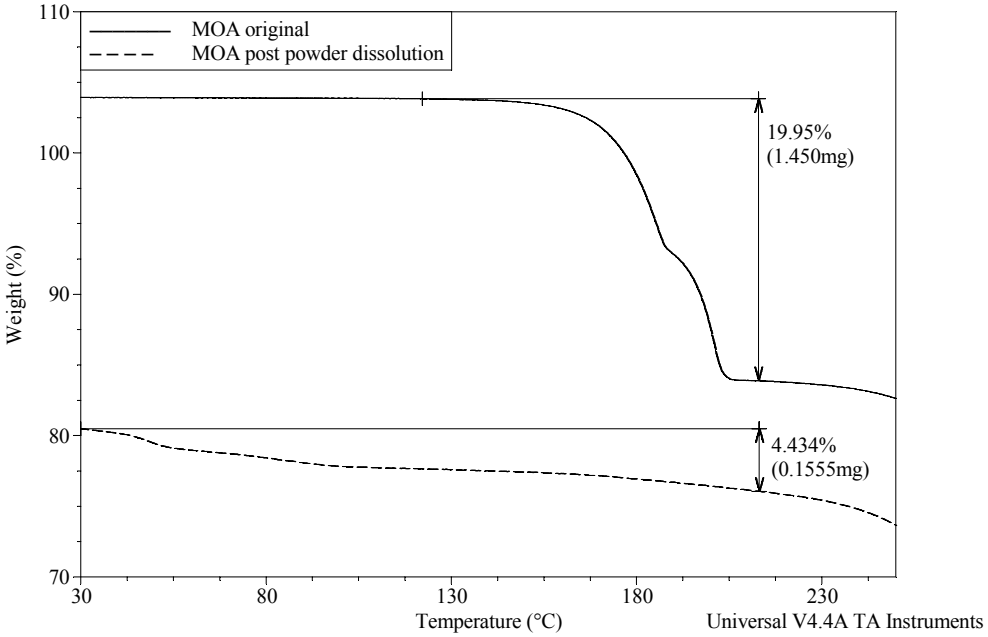

TGA: No cocrytsl remaining, 4.4% likely **FBC**

MOA (cont.)

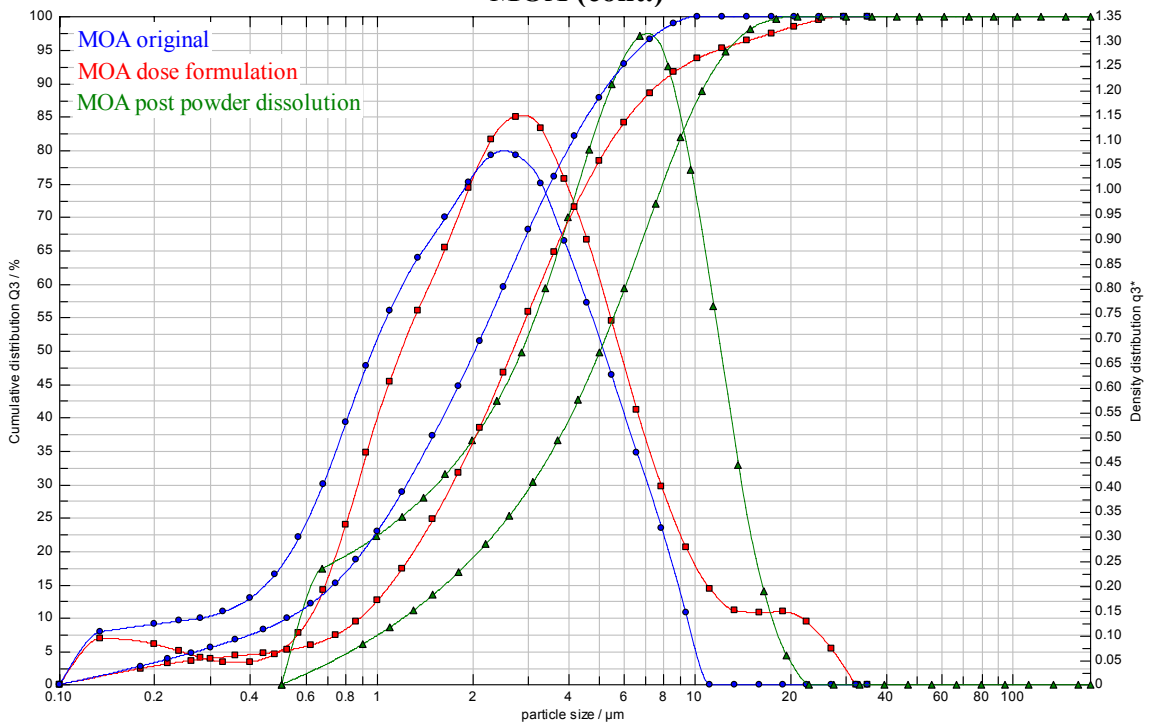

Particle Size Distributions

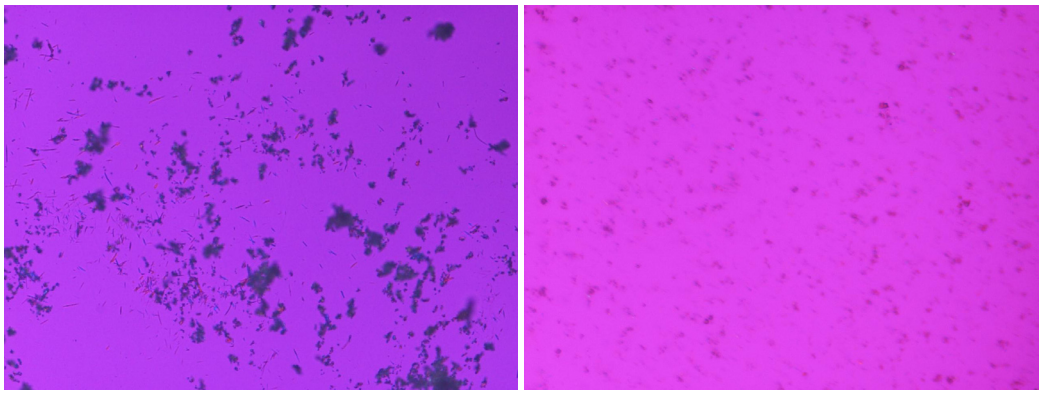

PLM: 200x original powder (left) post powder dissolution (right)

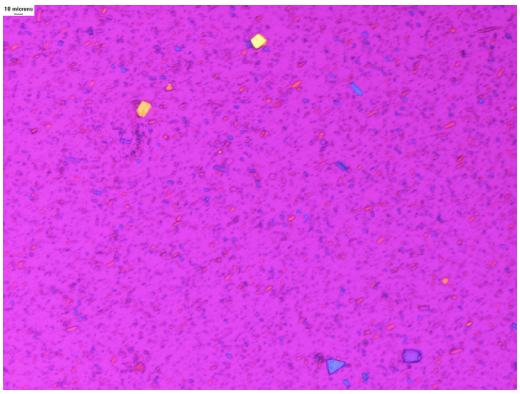

PLM: 200x post dose formulation

MOA (cont.)

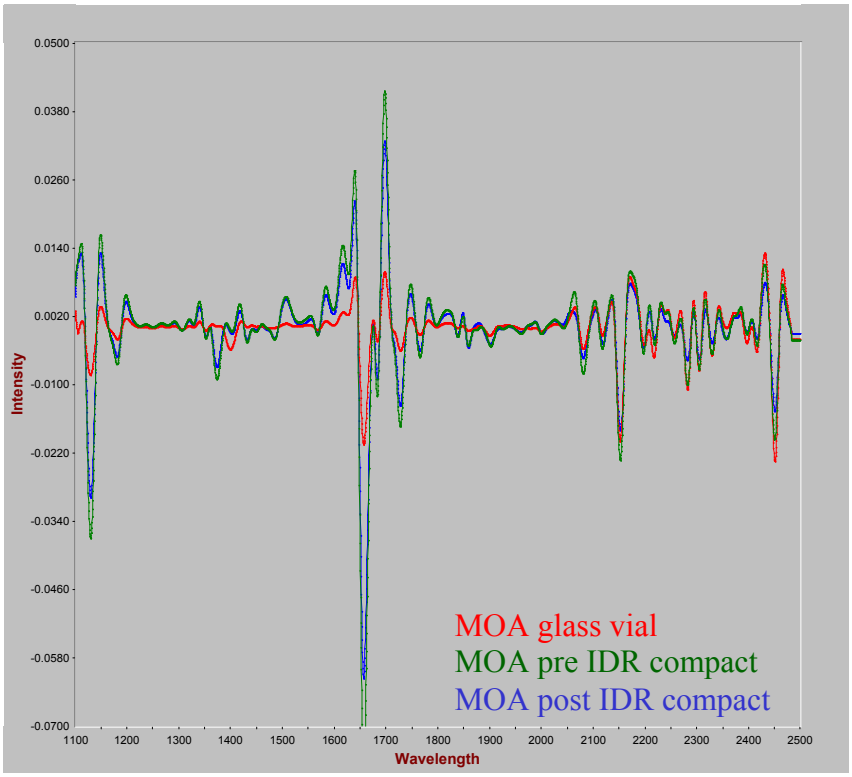

NIR: No change

SRA

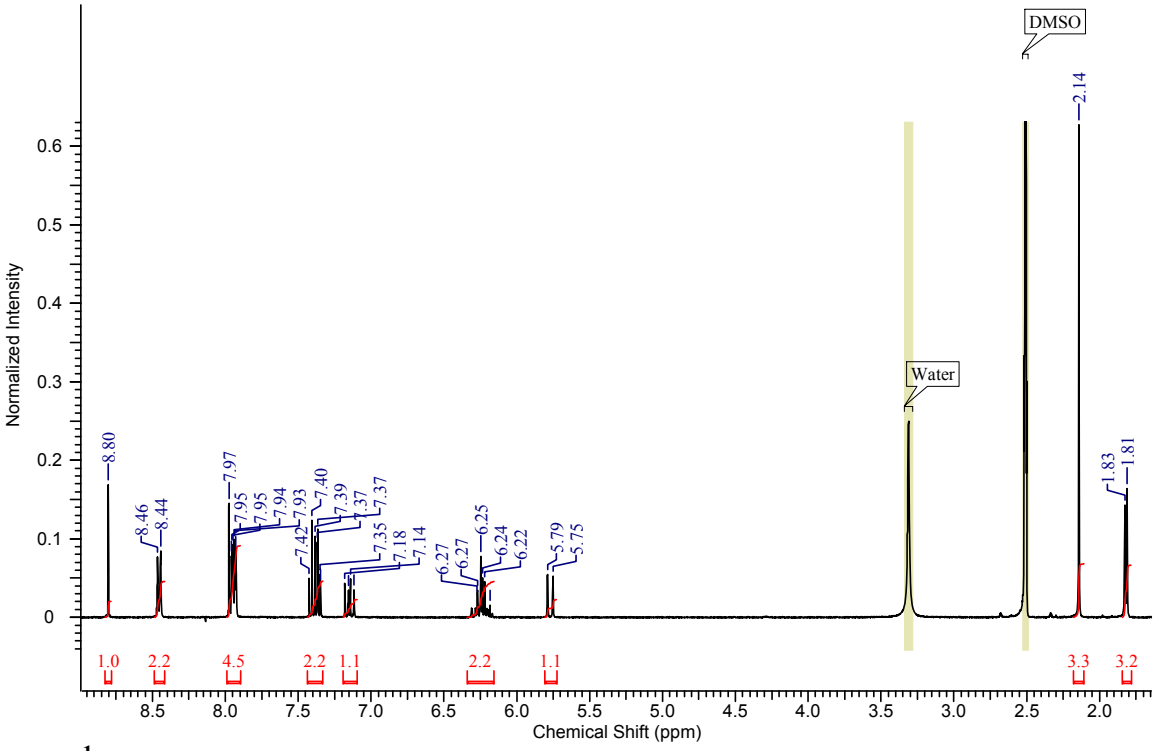

^{1}H NMR: 1.0 eq acid; CH 7.18 and 5.79ppm, 2(CH) 6.25ppm, CH_3 1.83ppm

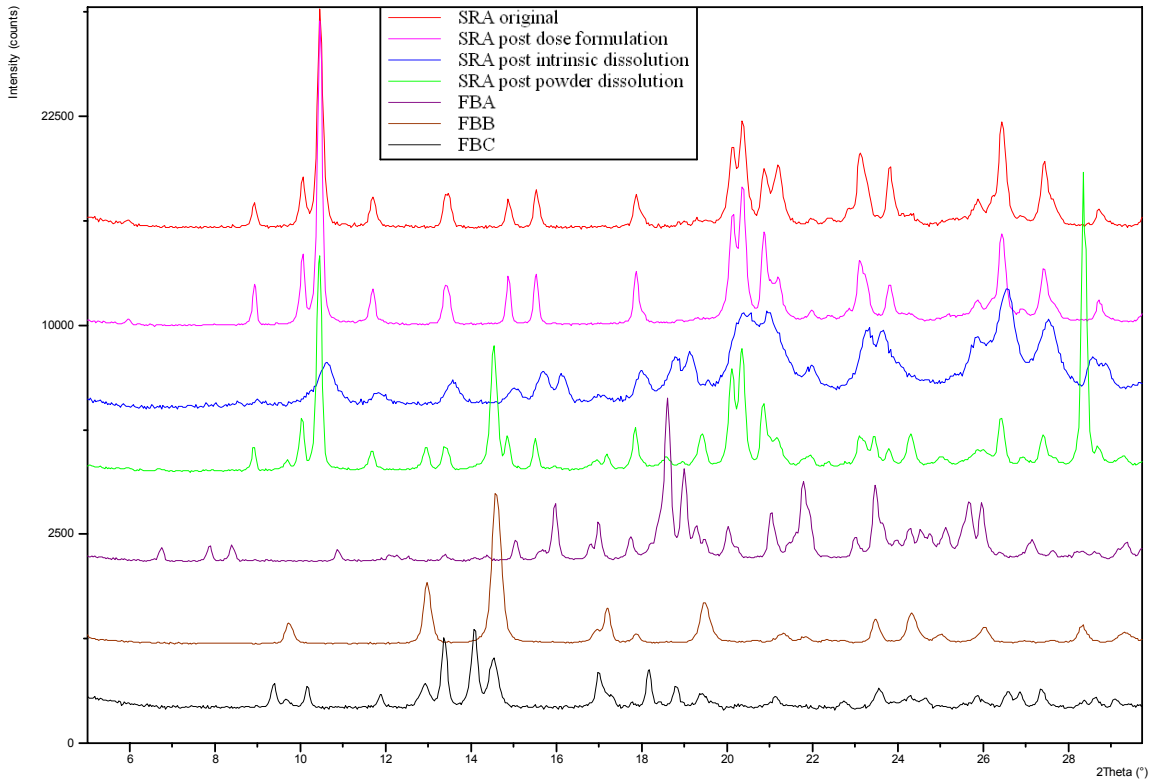

XRPD: SRA/FBB post powder dissolution, **SRA/FBA** post intrinsic dissolution

SRA (cont.)

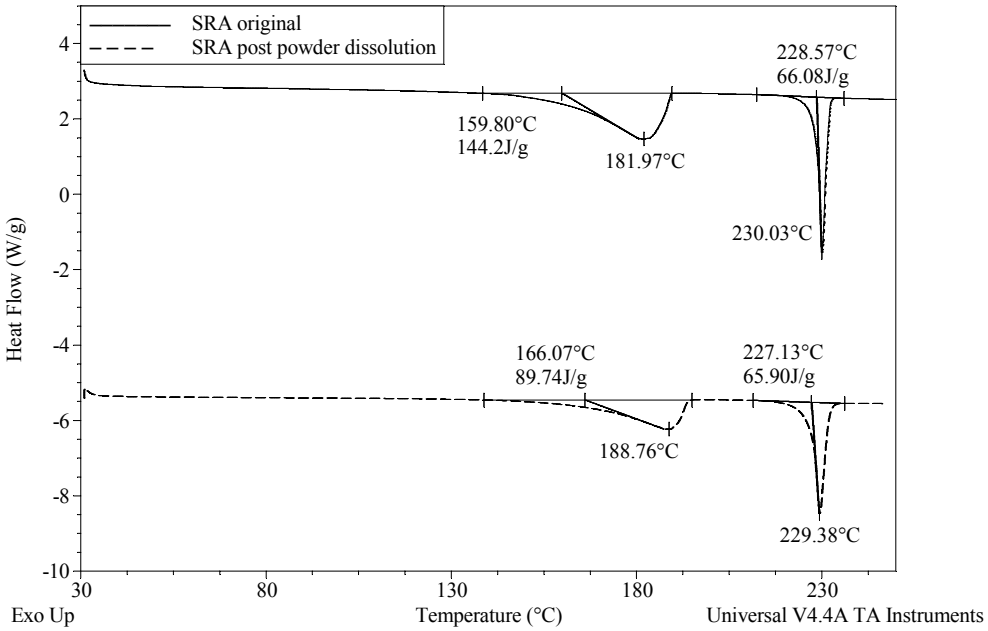

DSC: Mostly cocrystal remaining

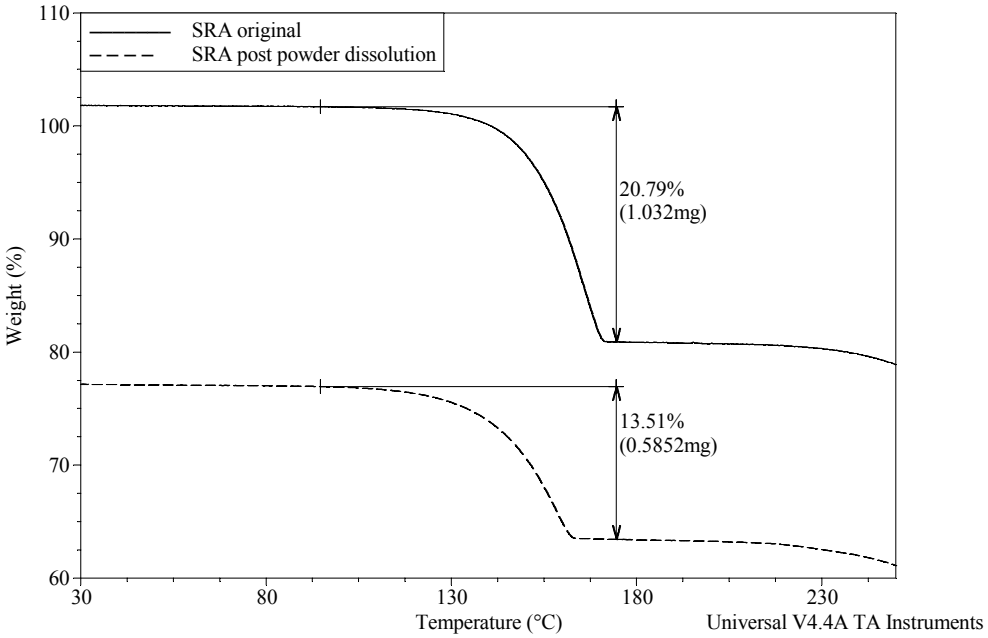

TGA: ~65% cocrystal remaining

SRA (cont.)

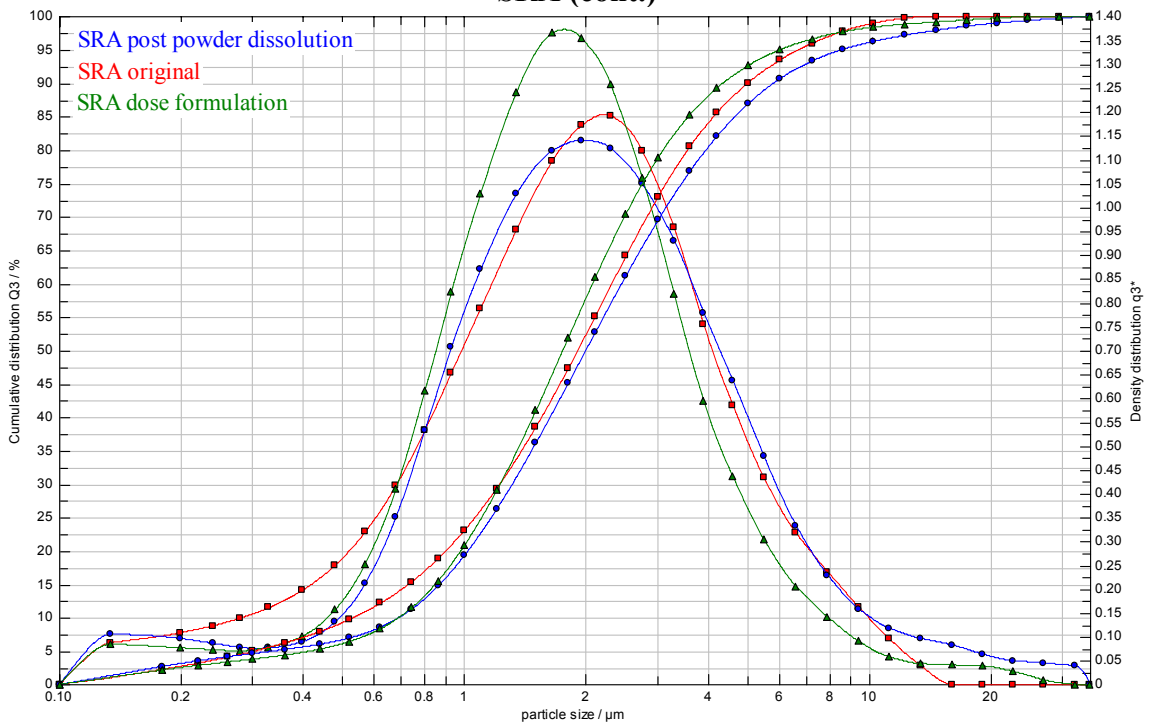

Particle Size Distributions

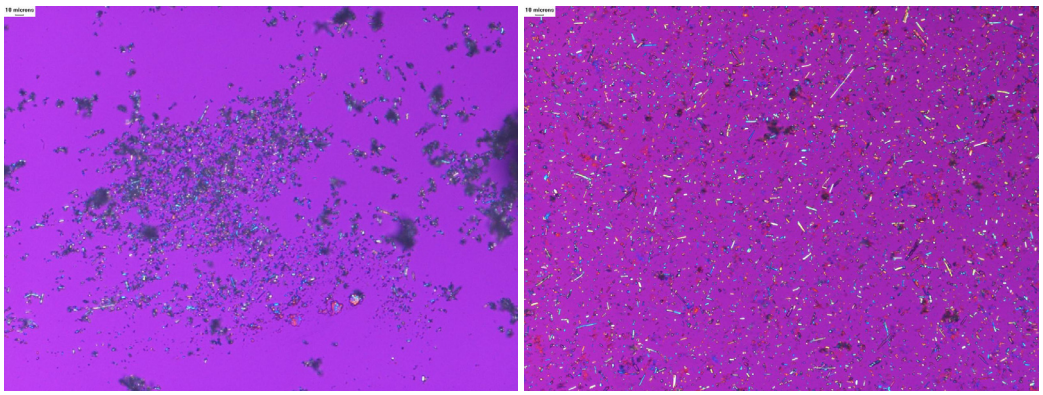

PLM: 200x original powder (left) post powder dissolution (right)

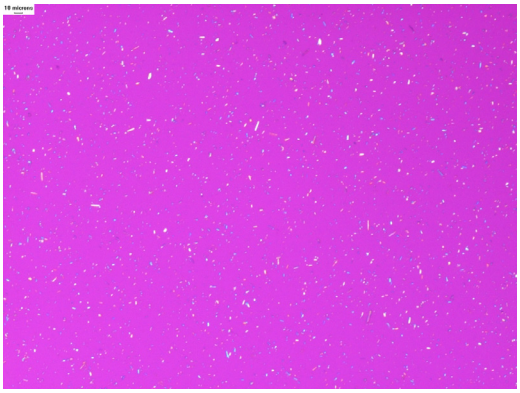

PLM: 200x post dose formulation

SRA (cont.)

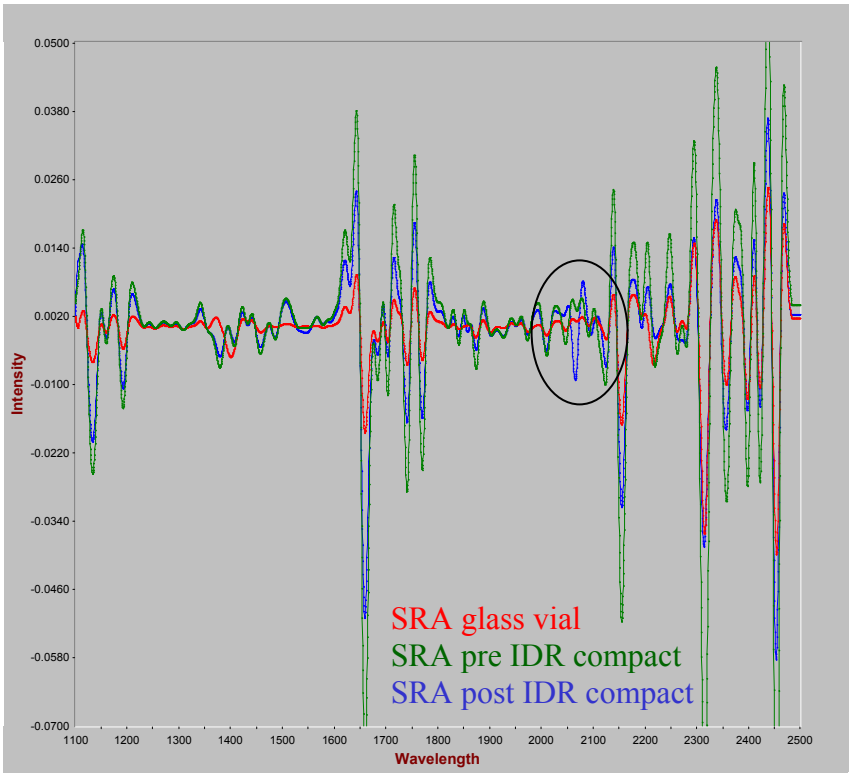

NIR: FBA at 2066nm post intrinsic dissolution

SCA

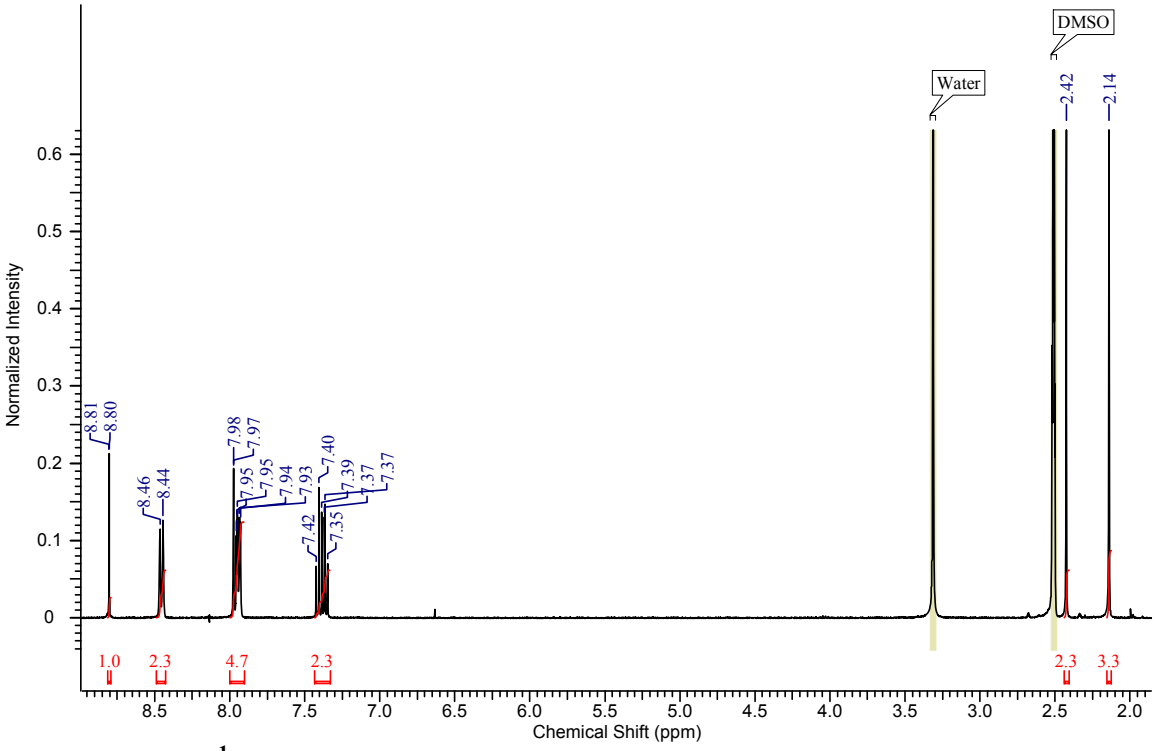

^{1}H NMR: 0.5 eq acid; 2(CH_2) integrate as 2 at 2.42ppm

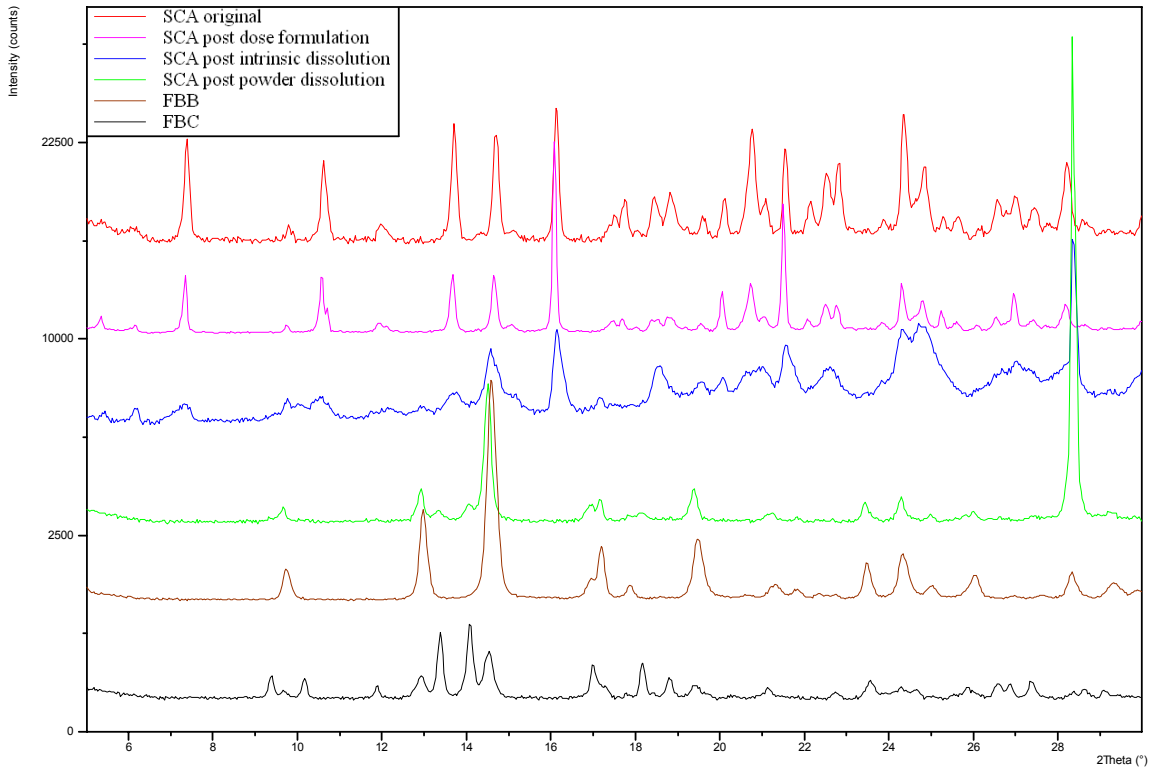

XRPD: FBB/FBC post powder dissolution

SCA (cont.)

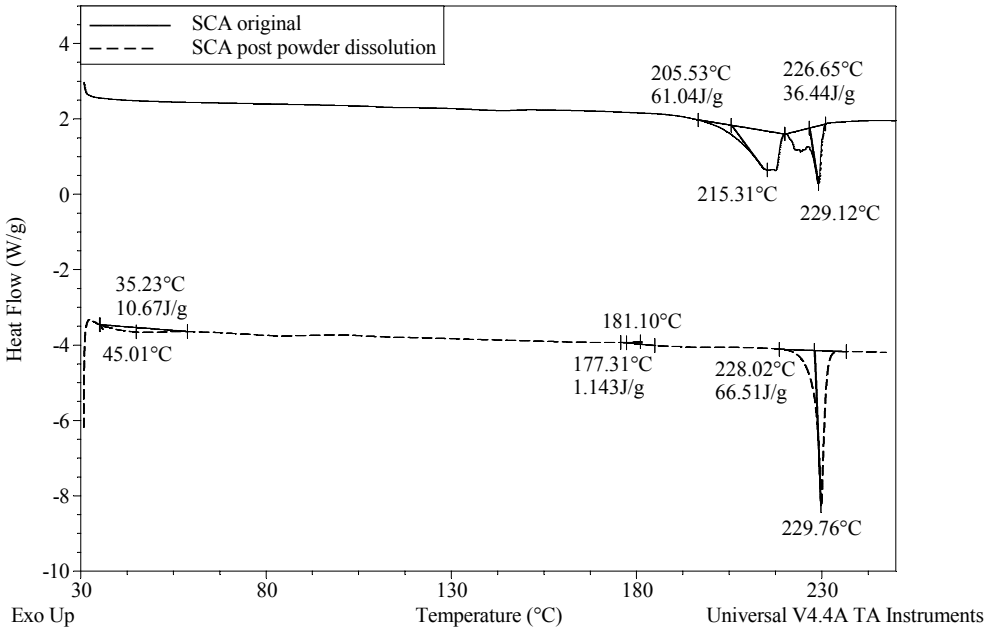

DSC: No cocrystal remaining, early endotherm likely **FBC**

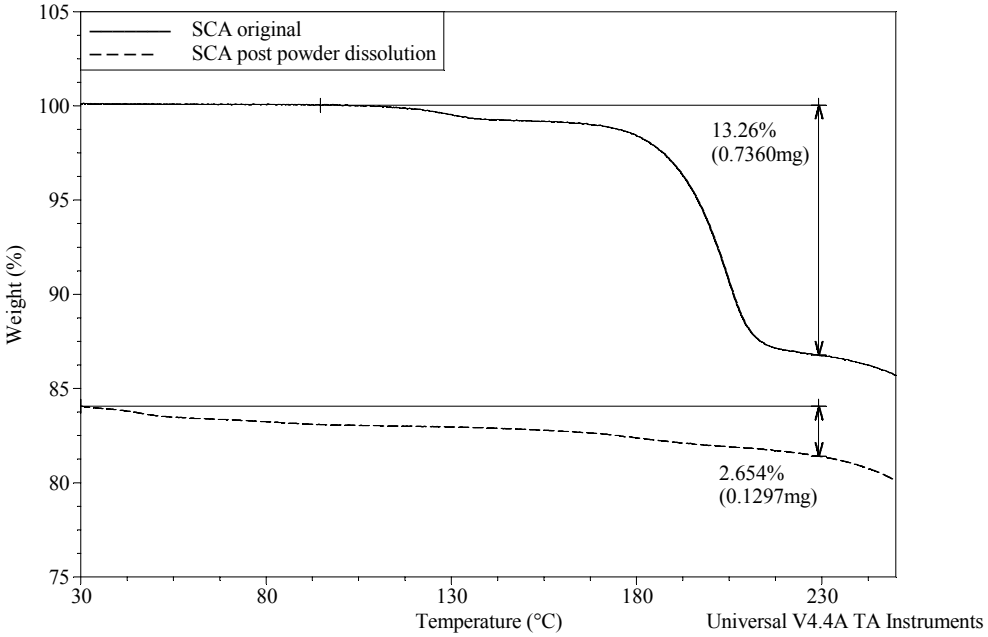

TGA: No cocrytsl remaining, 2.6% likely **FBC**

SCA (cont.)

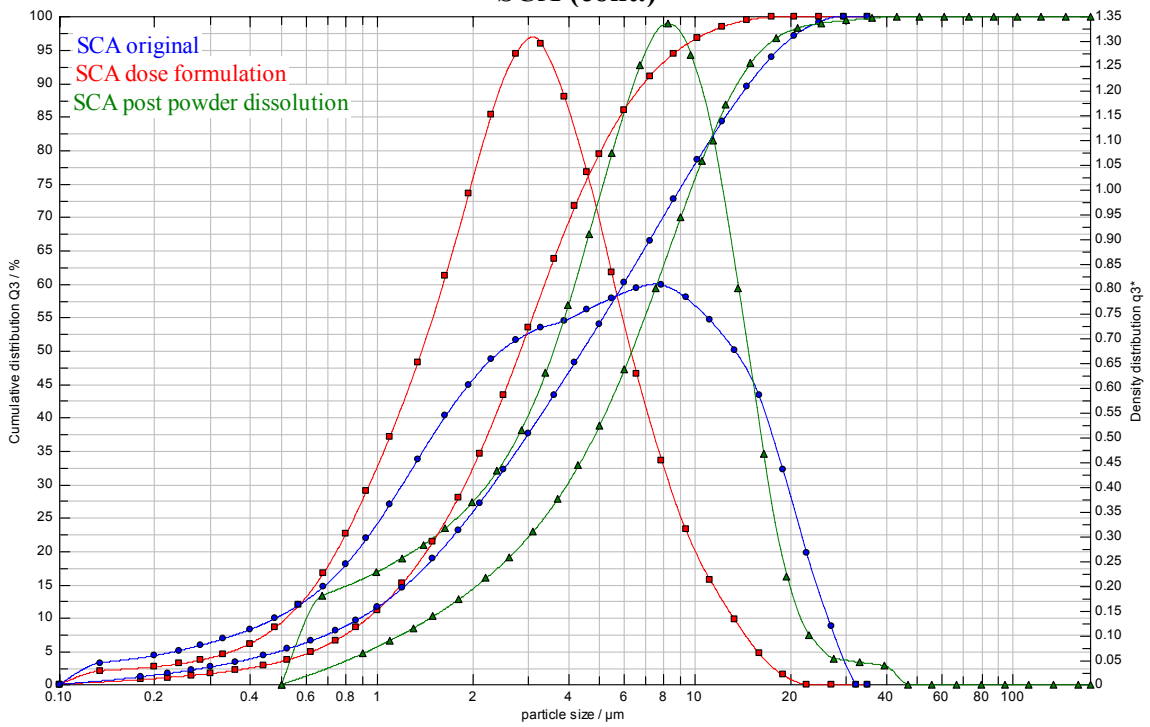

Particle Size Distributions

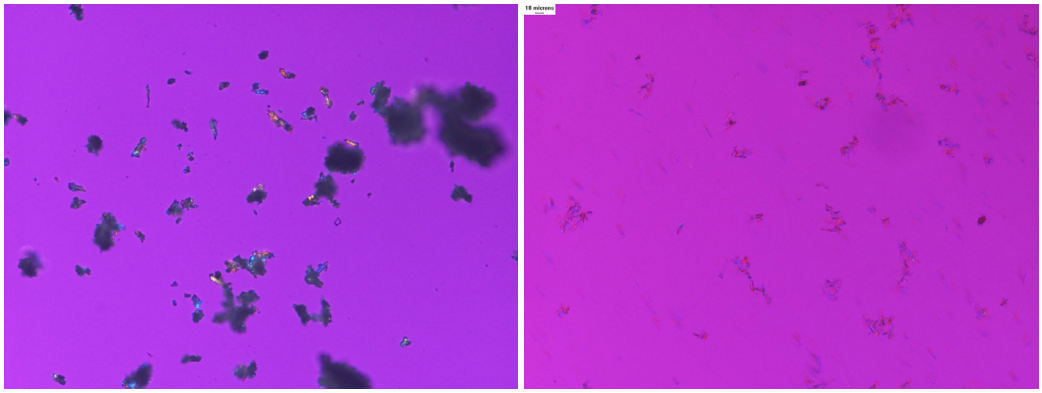

PLM: 200x original powder (left) post powder dissolution (right)

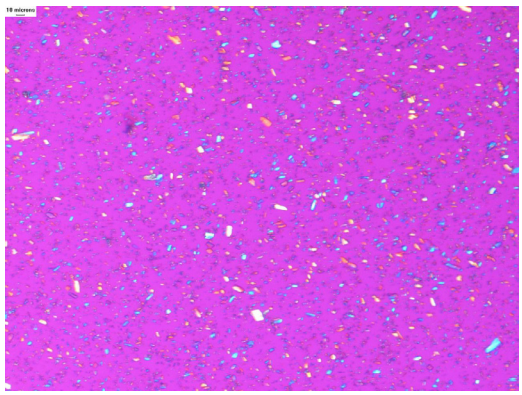

PLM: 200x post dose formulation

SCA (cont.)

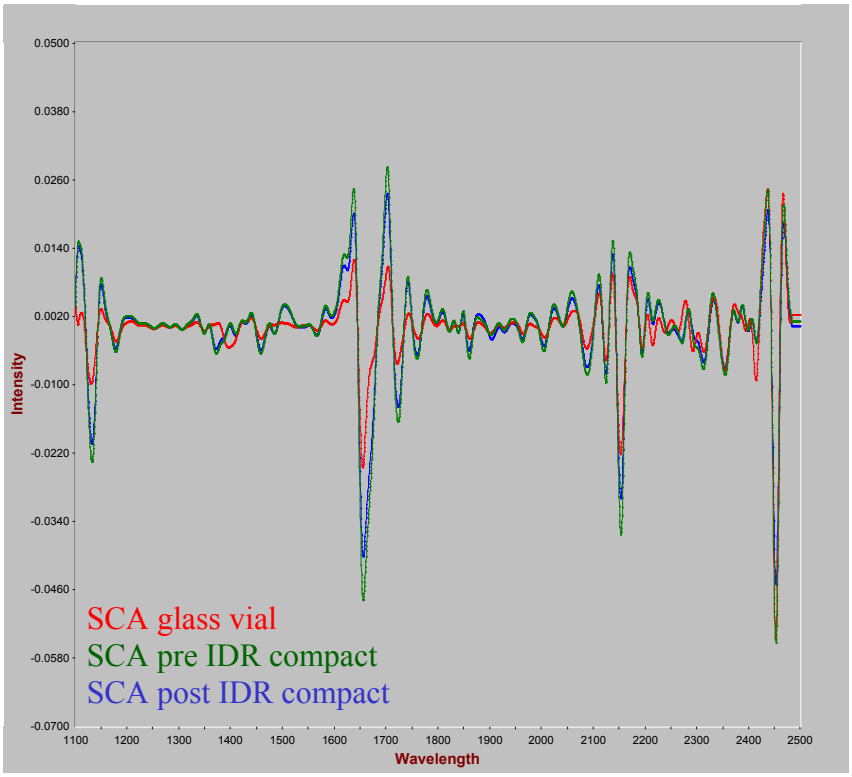

NIR: No change